CAN EXOSOMES BE USED AS DRUG DELIVERY VESICLES?

Fiona Ghina Mary Cooke

A Thesis Submitted for the Degree of PhD
at the
University of St Andrews

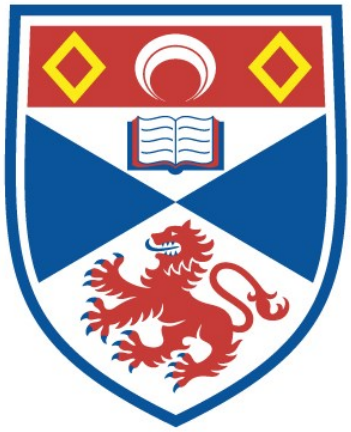

2018

Can Exosomes Be Used as Drug Delivery Vesicles?

Fiona Ghina Mary Cooke

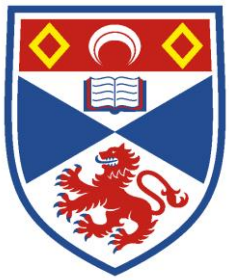

University of
St Andrews

This thesis is submitted in partial fulfilment for the degree of PhD
at the
University of St Andrews

18th January 2018

Abstract

The inflammatory arthritis Ankylosing Spondylitis (AS) is linked to the human leucocyte antigen HLA-B27. HLA-B27 is thought to drive AS because it misfolds during assembly in the endoplasmic reticulum (ER), inducing ER cell stress. Modulating HLA-B27 folding in the ER is therefore a therapeutic target pathway. The recent discovery of polymorphisms in the ER-resident peptidase ERAP1 that can impact on HLA-B27 and AS, makes ERAP1 one such target.

Exosomes are small, typically 50-200 nm sized particles, formed in the endosomal recycling pathway, which can be released into the extracellular environment. Exosomes have a wide range of biological activities depending on the cell type of origin, and on the delivered cargo, which can include bio-active proteins, lipids, mRNA and miRNA. There is interest in the use of exosomes as drug delivery agents. Here, exosomes were studied as a delivery agent to modulate ERAP1, as a potential therapeutic tool for the treatment of AS.

Exosomes, isolated from cell lines including CEM and Jurkat (T cell lineage), Jesthom (B cell lineage), U937 (monocyte lineage) and the epithelial HeLa cell line, were characterized by nanoparticle tracking analysis, flow cytometry and immunoblotting using markers including CD9, CD63, CD81 and TSG101. Differential expression of these markers in the immune cell lines indicated the complexity of defining exosomes.

EVs were then tested using cell penetrating peptides, electroporation, lipid transfection and sonication for their ability to load FITC-siRNA or FITC-antibody as cargo. Significantly, post-loading RNase A or trypsin incubation demonstrated that many techniques do not lead to efficient cargo loading of exosomes. Sonication proved the most effective technique, with up to 30% efficiency. Loading of exosomes with ERAP1-targetted siRNA did not however lead to notable ERAP1 inhibition. The data indicates that external loading of exosomes with cargo remains a significant challenge in developing exosomes as therapeutic tools.

Contents

Table of Figures

Acknowledgements

I would like to first thank my supervisor, Dr Simon Powis, for his continuous support throughout the past 3 years. In particular I would like to thank him for his endless patience and dedicating his time to teaching me. He has encouraged me to develop my career in research and taken time to read and discuss my thesis with me.

I would also like to thank Elaine Campbell for supporting me in those difficult first few months of settling in and sharing her knowledge and expertise with me. In addition, I would like to thank all my current and past lab members. Joao Barbosa, you showed me the drive and dedication a researcher should have. Kelly Rodgers, you never gave up when experiments didn't turn out right and were a constant source of sunshine on those gloomy days. Thanks to all the Project Students who have been a part of our lab at one time or another. It was great experience supervising you and wonderful discussing research with you all.

Thank you to Prof. Elena Batrakova for allowing me to visit her laboratory in North Carolina and supporting me during my visit. My thanks go to all the members of the Batrakova laboratory at the time, in particular Soo Kim. I would have been lost without your guidance both inside and outside the lab. I wish you and Hobbes good luck for the future.

Thank you to Dr Dave Carter, Dr Marcel Ramirez and the whole delegation from the UKEV Forum UK-Brazil collaborative visit. I learned a great deal during this time and forged friendships with future collaborators. Thank you for arranging such a wonderful experience that I will never forget.

A huge thank you to all of the staff, students and fellow PhD students in the School of Medicine. Through one way or another you will have all made me smile or laugh. I have enjoyed my time chatting and working with all of you and I wish you all the best of luck for the future. My special thanks go to Rob Hammond, Sanya Aggarwal, Sophie Ferguson, John Farmer, Fiona McKissock, Scott Millar and Ben Reilly O'Donnell. Both the banter and blood was most appreciated. Thank you Monika Gostic. Even on those days when you were exceptionally busy you made time to chat with me whether it was about experiments or life. Thank you for your friendship.

I would like to send a special kind of thanks to my oldest and wisest friend, Laura Bell. You unwittingly provided the best distractions and procrastinations for me during my PhD. Thank you for not giving up on me and not murdering me when I was singing Mamma Mia whilst we were going through Gatwick, starving, after one particular adventure. Let's never forget the mud and rain of Download and relish the idea of more adventures.

I would collectively like to thank Project Anime, the Pokémon Society, the Fencing Club and the Karate Club. You have all supported me at times and throughout the past 3 years. It has been a joy

getting to know all the new society members and competing with you all. I have dedicated my love and time to these societies and I hope you will go on to blossom and develop.

Special thanks to my Louis. You have met my tiredness and strange moods for the last two years with sympathy and love. You have supported me when times were hard, looked after me and cheered me up on my worst days. Thank you.

Last but not least, I would like to show my thanks to my family. Everyone, thank you for always believing in me and giving me advice. In particular, I would like to thank my mum for putting up with my hectic and occasional weekend visits. You have continued to love and support me throughout and I know that you are always thinking of me. Thank you for all the lovely weekends and supporting me in every way you could. I'm sure Dad would be proud of both of us.

Thesis Declaration

1. Candidate's declarations:

I, Fiona Ghina Mary Cooke hereby certify that this thesis, which is approximately 69301 words in length, has been written by me, and that it is the record of work carried out by me, or principally by myself in collaboration with others as acknowledged, and that it has not been submitted in any previous application for a higher degree.

I was admitted as a research student in November, 2013 and as a candidate for the degree of PhD in November, 2013; the higher study for which this is a record was carried out in the University of St Andrews between 2013 and 2017.

(*If you received assistance in writing from anyone other than your supervisor/s*):
I, …..., received assistance in the writing of this thesis in respect of [language, grammar, spelling or syntax], which was provided by ……

Date: signature of candidate:

2. Supervisor's declaration:

I hereby certify that the candidate has fulfilled the conditions of the Resolution and Regulations appropriate for the degree of PhD in the University of St Andrews and that the candidate is qualified to submit this thesis in application for that degree.

Date: signature of supervisor:

3. Permission for publication: (*to be signed by both candidate and supervisor*)

In submitting this thesis to the University of St Andrews I understand that I am giving permission for it to be made available for use in accordance with the regulations of the University Library for the time being in force, subject to any copyright vested in the work not being affected thereby. I also understand that the title and the abstract will be published, and that a copy of the work may be made and supplied to any bona fide library or research worker, that my thesis will be electronically accessible for personal or research use unless exempt by award of an embargo as requested below, and that the library has the right to migrate my thesis into new electronic forms as required to ensure continued access to the thesis. I have obtained any third-party copyright permissions that may be required in order to allow such access and migration, or have requested the appropriate embargo below.

The following is an agreed request by candidate and supervisor regarding the publication of this thesis:

PRINTED COPY

(a) No embargo on print copy
b) Embargo on all or part of print copy for a period of … years (maximum five) on the following ground(s):
    - Publication would be commercially damaging to the researcher, or to the supervisor, or the University
    - Publication would preclude future publication
    - Publication would be in breach of laws or ethics
c) Permanent or longer term embargo on all or part of print copy for a period of … years (the request will be referred to the Pro-Provost and permission will be granted only in exceptional circumstances).

Supporting statement for printed embargo request:

ELECTRONIC COPY

(a) No embargo on electronic copy
b) Embargo on all or part of electronic copy for a period of … years (maximum five) on the following ground(s):
    - Publication would be commercially damaging to the researcher, or to the supervisor, or the University
    - Publication would preclude future publication
    - Publication would be in breach of law or ethics

c) Permanent or longer term embargo on all or part of electronic copy for a period of … years (the request will be referred to the Pro-Provost and permission will be granted only in exceptional circumstances).

Supporting statement for electronic embargo request:

Date: signature of candidate: signature of supervisor:

Please note initial embargos can be requested for a maximum of five years. An embargo on a thesis submitted to the Faculty of Science or Medicine is rarely granted for more than two years in the first instance, without good justification. The Library will not lift an embargo before confirming with the student and supervisor that they do not intend to request a continuation. In the absence of an agreed response from both student and supervisor, the Head of School will be consulted. Please note that the total period of an embargo, including any continuation, is not expected to exceed ten years.
Where part of a thesis is to be embargoed, please specify the part and the reason.

List of Abbreviations

A
Ab – Antibody
APC – Antigen Presenting Cell
AS - Ankylosing Spondylitis
ASDAS – AS Disease Activity Score
ASQOL – AS Quality of Life
B
BASDAI – Bath AS Disease Activity Index
BASFI – Bath AS Functional Index
BAS-G – Bath AS Global score
BASMI – Bath AS Metrology Index
C
CNT – Carbon Nanotubule
COX – Cyclo-oxygenase
CPP – Cell Penetrating Peptide
CRP – C-Reactive Protein
CXB - Celecoxib
D
ddH_2O – Double Deionised Water
DMARD - Disease Modifying Anti-Rheumatic Drugs
DMC - 2, 5-dimethyl-Celecoxib
E
EDTA - Ethylenediaminetetraacetic acid
ER – Endoplasmic Reticulum
ERAD – ER Associated Degradation
ERAP1 – ER Aminopeptidase 1
ESCRT – Endosomal Sorting Complexes Required for Transport
ESR – Erythrocyte Sedimentation Rate
EV – Extracellular Vesicle
F
FCS – Foetal Calf Serum
FHC – Free Heavy Chain
FSC – Forward Scatter
G
GAPDH - Glyceraldehyde 3-phosphate Dehydrogenase
GRP78 – Glucose Regulated Protein 78
H
HC – Heavy Chain
HCMV – Human Cytomegalovirus
HERP - Homocysteine-inducible ER Protein
HLA – Human Leukocyte Antigen
HUVEC – Human Umbilical Vein Endothelial Cell
I
IBD – Inflammatory Bowel Disease
IFN – Interferon
IL - Interleukin
ILV – Intraluminal Vesicle
M
MHC – Major Histocompatibility Complex
miRNA – Micro RNA
MVB – Multi-Vesicular Body
MWCNT – Multi-Walled CNT
N
NSAID – Non-Steroidal Anti-Inflammatory Drug
NTA – Nanoparticle Tracking Analysis
P
PBS – Phosphate Buffered Saline
PDI – Protein Disulphide Isomerase
PEI - Polyethylenimine
PLC – Protein Loading Complex
PM – Plasma Membrane
R
RISC - RNA Induced Silencing Complex
RME – Receptor Mediated Endocytosis
RNAi – RNA Inhibition Inducer
RT – Room Temperature
S
shRNA – Short Hairpin RNA
siRNA – Small Inhibitory RNA
SSC – Side Scatter
SWCNT – Single-Walled CNT
T
TAP – Transporter Associated with Antigen Processing
TNF – Tumour Necrosis Factor
U
UPR – Unfolded Protein Response
X
XMIR – ERAP1 shRNA XMIRXpress lentivector

Chapter 1: Introduction

1.1 Ankylosing Spondylitis: Disease and Diagnosis

Ankylosing Spondylitis (AS) is an inflammatory disease associated with inflammatory back pain, asymmetrical peripheral oligoarthritis, enthesitis, anterior uveitis, psoriasis and inflammatory bowel disease (IBD)(Robinson & Brown, 2014; Zambrano-Zaragoza, Agraz-Cibrian, González-Reyes, Durán-Avelar, & Vibanco-Pérez, 2013). The National Ankylosing Spondylitis Society (NASS – www.nass.co.uk) indicates that over 200,000 people in the UK currently have a diagnosis of AS. Most current therapies aim just to relieve either pain or general inflammation. As such there are no targeted therapies specific for AS. Therefore there is an unmet clinical need to understand AS at the molecular level to develop novel targeted, AS-specific therapies that can alleviate the burden of this disease.

AS is usually seen from the second decade of life and, somewhat unusually for a condition often described as being autoimmune, is more commonly found in males (2:1, male to female ratio). It is traditionally diagnosed radiographically by a plain X-ray of the lower spine showing sacroiliac sclerosis with evidence of erosion (Reveille, 2015)(Dakwar, Reddy, Vale, & Uribe, 2008). More recently

Figure 1-1: X-rays of the spinal cord showing shiny corners (left) where inflammation is indicated by the black arrow. The X-ray on the right displays fused vertebrae due to prolonged inflammation forming Bamboo Spine.
Images: (Kataria & Brent, 2004)

MRI has been used to detect early disease with the possibility of earlier detection than X-ray (Rudwaleit, van der Heijde, Khan, Braun, & Sieper, 2004). Advanced disease is indicated by fusion of the lower spine or sacroiliac joints; on an X-ray this can be characterised as 'Shiny Corners' (figure 1-1). If Inflammation continues to occur here over a long period, it can manifest as 'Bamboo Spine' or fusion of the vertebrae (Golder & Schachna, 2013). Advanced fusing of the sacroiliac joints occurs in late disease and impacts significantly on normal living and work activities, and may lead to further spinal injury.

1.2 Measuring AS Severity

AS is currently measured by several criteria; Bath AS Functional Index (BASFI), AS Quality of Life (ASQOL), Bath AS Metrology Index (BASMI), Bath AS Global Score (BAS-G), C-reactive protein (CRP), Erythrocyte Sedimentation Rate (ESR), Bath AS Disease Activity Index (BASDAI) (Goh & Samanta, 2009) and AS Disease Activity Score (ASDAS). There are more criteria used to assess the pain, mobility and disease progression of AS patients however these are more rarely used. BASFI, ASDAS, ASQOL, BASDAI and BAS-G all rely on self-report of the patient compared to BASMI which relies on a health care professional's evaluation (Moncur, 2003). Whilst patient opinion can be valuable, it can vary widely between individuals. As such it can produce very confusing and heterogeneous data. Similarly, despite the training completed to carry out the assessment, the opinion of BASMI values may change between health care professionals. However, the same health care professional attending multiple patients will reduce variance. The use of a dichotomous scale for BASFI helps reduce confusion compared to the larger 1-10 choice scale employed in ASQOL, BASDAI and BAS-G. Interestingly ASDAS uses aspects of CRP, BASDAI and global perspective of the patient (J Sieper *et al.,* 2009), forming a chimera of the most useful and best answered questions. ESR is a blood test which determines the time it takes for RBC to sediment in the bottom of a tube. The outcome of this simple test can determine if an inflammatory response is occurring and to what extent. CRP concentration is also a measurement of inflammation and is produced as a non-specific acute phase response (Pepys & Hirschfield, 2003). These are simple and routine tests available for the indication of inflammation however, there appears to be a lack of correlation with disease in most studies (Mei *et al.,* 2011).

1.3 Current Treatment

As stated previously the treatment of AS is mostly based around non-disease specific therapies, involving physiotherapy, Non-Steroidal Anti-Inflammatory Drugs (NSAIDs), Disease Modifying Anti-Rheumatic Drugs (DMARDs) and Tumour Necrosis Factor α (TNFα) inhibitors. Whilst

there are modifications to treatments and several drugs available within each category a few examples will be discussed here.

1.3.1 Physiotherapy

Physiotherapy is the most accessible treatment for AS patients. In a review by Dagfinrud and colleagues, it was concluded that home exercise plans had a beneficial effect for AS patients. However, it was noted that there was no standardised exercise plan between the 11 studies that met their inclusion criteria and that over a period of time patient attendance tended to decline (Dagfinrud, Hagen, & Kvien, 2009). More recently, Giannotti and colleagues describe the essential role of education, support and supervised exercise in AS treatment. Two thirds of the studies analysed showed improvement in both spinal mobility and functional capacity and three fifths of the studies showed a significant improvement in the disease activity index (Giannotti, Trainito, Arioli, Rucco, & Masiero, 2014). Swimming as an alternative to conventional exercise has also been trialled in AS patients. The results suggest that it has a greater influence on symptoms and improving chest mobility, therefore increasing ability to breath (Karapolat *et al.*, 2009). In a preliminary study with a small sample size it was observed that patients undergoing both regular exercise and anti-TNFα treatment experienced a synergistic effect (Dubey, Leeder, & Gaffney, 2008).

1.3.2 NSAID

NSAIDs function by inhibiting prostaglandin production. However, in trials, they have been seen to cause adverse effects or show lack of effectiveness (Dougados *et al.,* 1999). In particular some NSAIDs cause gastrointestinal adverse effects (Wanders *et al.,* 2005). Gastrointestinal problems relating to NSAIDs usually involve their properties as Cyclooxygenase- 1 (COX-1) inhibitors (Dougados *et al.,* 2002). COX-1 inhibitors prevent production of cytoprotective prostaglandins in the gastric mucosa. This can result in minor effects such as dyspepsia and nausea, but also severe effects such as gastric ulcers and related developments in some cases (figure 1-2) (Dougados *et al.*, 2002; Henry *et al.*, 1996). It is now clear that these gastrointestinal adverse effects seen previously are due to the ability of some NSAID's to inhibit COX-1, whereas therapeutic results are seen where the drug selectively inhibits COX-2 (Warner *et al.,* 1999). COX-2 inhibitors prevent prostaglandin production at inflammatory sites where it is usually induced by inflammatory cells (Hinz & Brune, 2002). Examples

of current commonly used NSAIDs include: Celecoxib, Ibuprofen, Naproxen, Diclofenac and Nabumetone (Dougados *et al.*, 2002; Pyrko, Kardosh, & Schönthal, 2008).

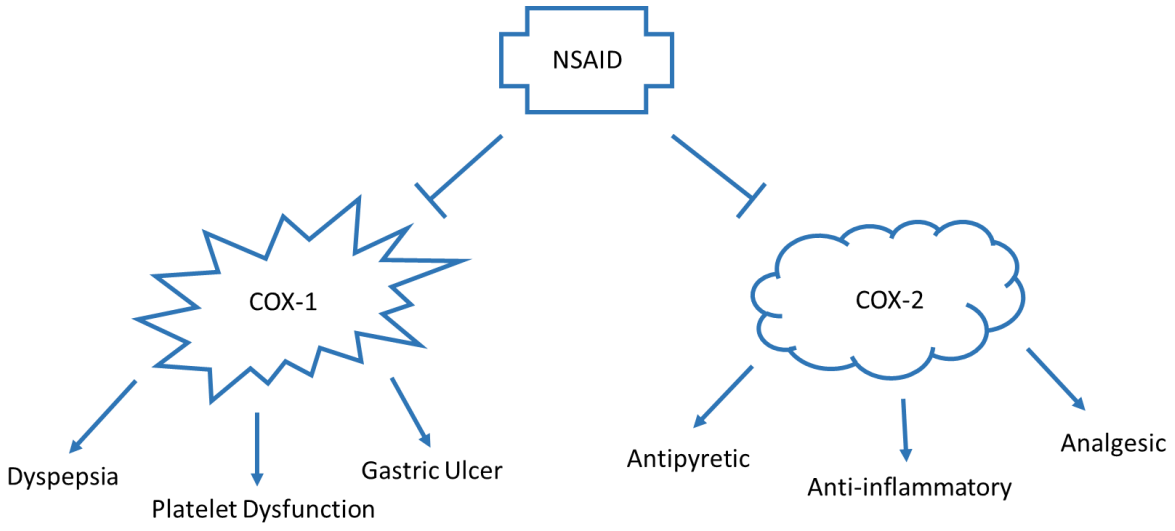

Figure 1-2: NSAIDS are used in AS treatment as inhibitors of COX proteins however if the drug is not specific both minor and serious side effects can develop. Drugs which inhibit the COX family non-specifically have effects from both arms of this diagram. An ideal drug would be one that specifically targets COX-2.

1.3.3 DMARD

For patients who show intolerance or no progress with NSAIDS, the next drug of choice is DMARDs. The term DMARD covers drugs such as gold salts, antimalarial drugs, methotrexate (MTX), D-Penicillamide, sulfasalazine and other immunosuppressant drugs (J. Chen, Liu, & Lin, 2006). MTX has been studied widely in drug trials for its use in AS. Chen and colleagues published a review of three studies looking at the benefits and disadvantages of MTX. They found that the majority of patients in these studies did not show significant improvements in BASFI, BASDI, BASMI, ASAS and other parameters used to monitor disease activity in AS (J. Chen *et al.*, 2006). The most studied DMARD is sulfasalazine. In a study by Chen and colleagues it was shown that there was no significant improvement in the parameters measured when pooled despite some individual studies showing significant results (J. Chen, Lin, & Liu, 2014). In summary, sulfasalazine studies report mixed results with much heterogeneity in their protocol. This suggests that the effectiveness of sulfasalazine as an AS drug cannot be determined. Of significance, DMARDs, whilst showing benefits in cases of AS where peripheral arthritis is presented, do not appear to show any particular benefit in cases demonstrating axial inflammation (Mörck, Pullerits, Geijer, Bremell, & Forsblad-D'Elia, 2013).

1.3.4 TNF-α Inhibitors

Whilst NSAIDs are usually the first therapeutic agents utilised, patients who maintain active disease, are recommended for TNF-α inhibitor treatment. This is measured as a BASDI score of at least 4 and a lack of response to two different NSAIDs over the course of 4 weeks at maximum tolerated dose, (Gulyas *et al.*, 2014). Unfortunately due to the expense of TNF-α inhibitors they have often been available to a more limited number of patients (J. Chen *et al.,* 2006). TNF-α inhibitors show a good level of response in clinical trials, (Goh & Samanta, 2009) however this response is more greatly observed in those with short disease duration (Rudwaleit, Listing, Brandt, Braun, & Sieper, 2004) suggesting that it is less effective in those with structural pathology. Four currently used TNF-α inhibitors are: Infliximab, Golimumab, Etanercept and Adalimumab (Capkin, Karkucak, & Cosar, 2014; Gulyas *et al.*, 2014; Mörck *et al.,* 2013; Joachim Sieper *et al.*, 2012).

1.3.5 Corticosteroid Injection

An alternative and more invasive treatment for AS is injection of corticosteroids into the sacroiliac joint. Maugars and colleagues performed a study on 10 patients where a total of 14 joints were injected; 7 with placebo and 6 with corticosteroids (Maugars, Mathis, Berthelot, Charlier, & Prost, 1996). At 1 month both physician and patient assessment showed good results for 5 patients in the corticosteroid group versus 1 case rated good in the placebo group (Maugars *et al.*, 1996). After this initial result was obtained a further 8 patients were added to the corticosteroid group when follow-up injections were given (Maugars *et al.*, 1996). In total, after 1 month, 85.7 % of patients saw a good or better response. However after 3 months and 6 months the percentage dropped to 62 % and 58 %, respectively, with 2 drop outs by the 6 month assessment (Maugars *et al.*, 1996). Unfortunately, the long term efficacy of this treatment is uncertain and information with regards to it minimal, therefore rendering it with a poor outlook.

1.4 Pathogenesis of AS

Human Leukocyte Antigen B27 (HLA-B27) is used to group a set of MHC class I molecules associated with AS. The role of HLA class I (also known as Major Histocompatibility Complex, MHC class I) is to present proteolytic fragments of intracellular proteins to cells of the immune system. This allows scrutiny of internal components at the cell surface by $CD8^+$ T cells, which upon recognising target antigens, can kill these cells in a highly specific manner. In this manner the immune system can, with extremely high sensitivity, detect the presence of intracellular pathogen infection, typically viruses, and also provide scrutiny for cells showing signs of altered protein production.

The HLA class I system remains one of the most highly polymorphic sets of genes in the human genome. There are three main HLA class I loci, HLA-A, -B and –C, present on chromosome 6, and co-

dominantly expressed, permitting most people to express six different alleles (thus allowing the presentation of many different peptides to T cells). At present there are 3913 HLA-A, 4765 HLA-B and 3510 HLA-C alleles recorded by the EMBL HLA database (http://www.ebi.ac.uk/ipd/imgt/hla/).

Of significance to AS, HLA-B27 was first discovered to be strongly associated with AS in 1973 (Brewerton *et al.,* 1973; Schlosstein, Terasaki, Bluestone, & Pearson, 1973). HLA-B27 has a strong genetic association with AS, however, only 16 out of 105 subtypes have been associated with disease (Khan, 2013) , though this may in part be due to the rarity and lack of data for many of the alleles. At present subtypes HLA-B27:02, HLA-B27:04 and HLA-B27:05 are associated with AS disease whereas HLA-B27:06 and HLA-B27:09 have no disease association (García-Medel *et al.*, 2014; Khan, 2013). Whilst only 5 % of HLA-B27 carriers (5-15 % normal incidence in population) have AS, 90 % of those with AS have the HLA-B27 gene (Golder & Schachna, 2013). In totality AS has a 0.1-1.4 % global prevalence (Dean *et al.,* 2013).

The role HLA-B27 plays in the pathogenesis of AS remains enigmatic, however there are currently 3 main hypotheses; arthritogenic peptides, recognition of non-canonical HLA-B27 and HLA-B27 misfolding (Colbert, Tran, & Layh-Schmitt, 2014).

1.4.1 Arthritogenic Peptide

The arthritogenic peptide hypothesis focusses on the presence of $CD8^+$ T cells in the joints of AS patients. This hypothesis proposes that an antigen derived from a bacterial protein, typically Yersinia or Chlamydia is presented by HLA-B27 and recognised by T Cell Receptors (TCR) on $CD8^+$ T cells as cross-reactive (figure 1-3)(Dakwar *et al.*, 2008). Alternatively an auto-immunogenic $CD8^+$ T cell may recognise the antigen and launch an immune response (Colbert *et al.,* 2014). Through either of these pathways the end result is activation and differentiation of autoreactive T cells into the Th1 and Th17 lineages. However, whilst there is some evidence supporting the arthritogenic peptide hypothesis, there is also a great deal of evidence suggesting that this hypothesis is unlikely, chiefly the occurrence of disease in $CD8^+$ cell depleted HLA-B27 transgenic rats (Colbert, 2000)(Khare, Bull, Hanson, Luthra, & David, 1998).

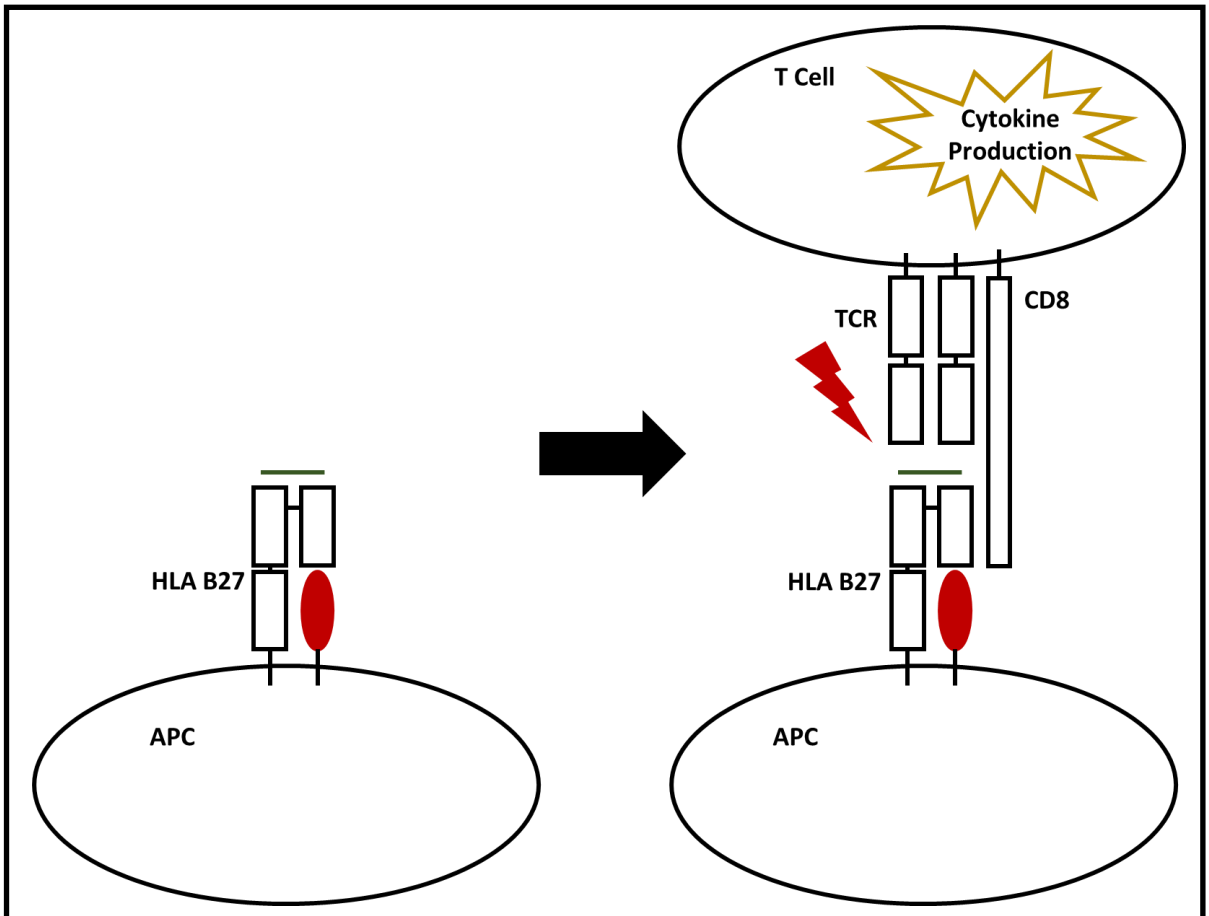

Figure 1-3: diagram of the arthritogenic peptide theory. A peptide (green line) is presented by HLA-B27 on an APC. Eventually this APC will meet a $CD8^+$ T cell. The TCR on the T cell will interact with the peptide presented on the class I molecule. It is theorised that the peptide presented may be cross reactive with tissue found in joints, specifically the sacroiliac joints, therefore activating and expanding T cells. These T cells travel to their associated tissue and cause inflammation via activation and differentiation of macrophages. However, studies have been carried out to examine the population of peptides that HLA-B27 bind and there has so far been no discovery of HLA-B27 presenting a cross-reactive protein.

1.4.2 Non-canonical

The non-canonical HLA-B27 hypothesis suggests that it is the recognition of HLA-B27 homodimers or free heavy chains (FHC) on the cell surface by KIR receptor positive cells that underlies AS (Wong-Baeza *et al.*, 2013). Cells suggested to be involved in this aberrant recognition are NK cells and Th17 cells (Bowness *et al.*, 2011; Zambrano-Zaragoza *et al.,* 2013). These homodimers or FHC are found on the cell surface without their β_2 microglobulin. It is proposed that they are formed from recycled HLA-B27 molecules that have passed through an acidic, unfolding-promoting endocytic compartment (figure 1-4) and then re-expressed at the cell surface (Bird *et al.,* 2003). These homodimers form disulphide bonds through their possession of a cysteine at position 67 (Allen, O'Callaghan, McMichael, & Bowness, 1999) and can be detected on the outside of cells by monoclonal antibody, HC10, and more recently a new reagent generated in vitro called HD6 (Rysnik *et al.*, 2016).

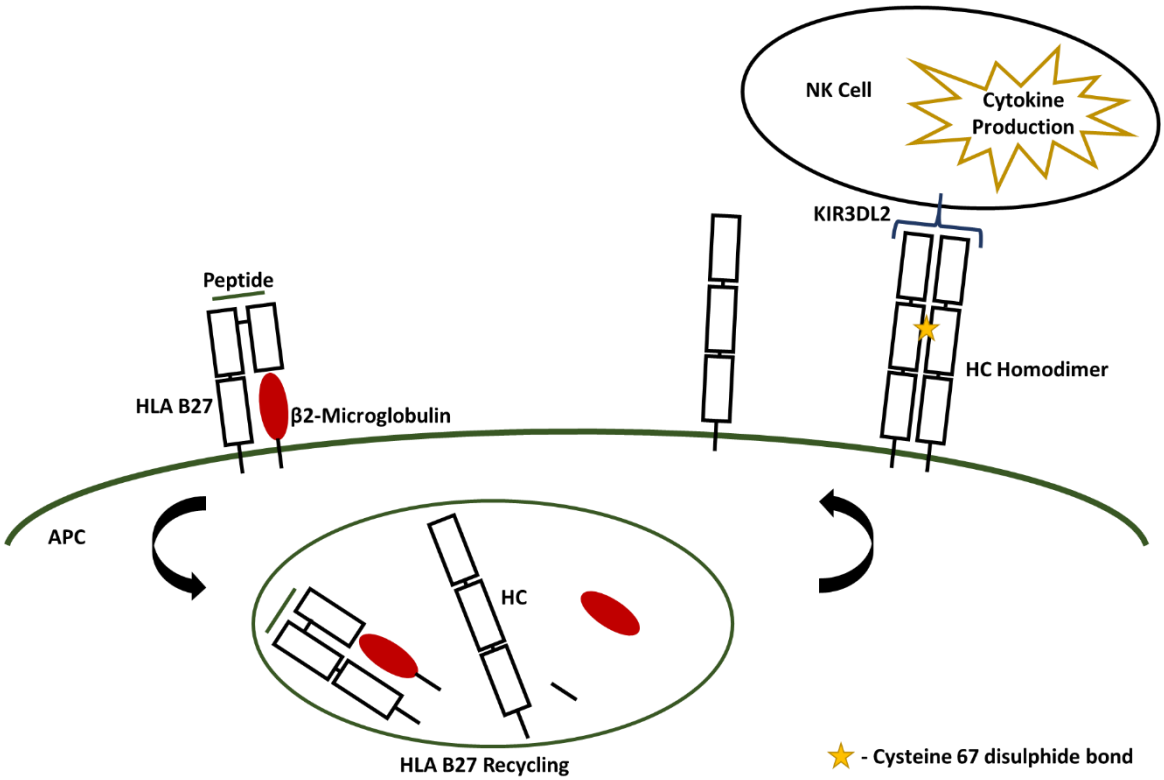

Figure 1-4: diagram describing the non-canonical theory. In this theory it is proposed that when the HLA-B27 molecule is recycled it is able to become partially disassembled. This is due to acidic conditions in the cell compartment, where it can be reduced to components such as heavy chains and β_2 microglobulin. Following this the compartment delivers the molecules with transmembrane domains back to the surface of the cell again. Here heavy chains can interact with proteins and receptors on other cells. In particular, KIR3DL2 on NK cells is able to bind to the partially deconstructed HLA-B27 molecule and causes a chain of cytokine products to be released.

It should be noted that HC10 does not exclusively recognise dimers, it also recognises unfolded and partially folded HLA-B27 monomeric HCs. The cysteine 67 disulphide bond is necessary for homodimer expression at the cell surface (Bird *et al.,* 2003) as without it a decrease in homodimers is seen on the cell surface and an increase in FHC is detected. These homodimers are recognised by leukocyte

receptors such as KIR3DL2. They promote survival of the leukocytes and divert the production of cytokines to promote the Th17 pathway (Wong-Baeza *et al.*, 2013).

1.4.3 Misfolded Protein

HLA-B27 misfolding proposes that HLA-B27 is prone to undergoing misfolding events within the environment of the ER early in its normal assembly pathway, which prevents it from being exported to the plasma membrane (figure 1-5). Instead, excessive production and lack of clearance of these misfolded proteins causes the induction and/or engagement of a suite of cellular responses that have evolved to cope with unfolded proteins, such as the ER-associated Degradation pathway (ERAD) and the Unfolded Protein Response (UPR). The UPR is stimulated by a change in the ratio of free to bound GRP78 in the ER which causes downstream activation of either reparation or apoptosis pathways. A study by Mear and colleagues suggests that the presence of a unique feature in HLA-B27, essentially the residues lining the B-pocket of the peptide-binding groove, is responsible for the build-up of misfolded protein in the ER (Mear *et al.,* 1999). Specifically, the forming of homodimers inside of the ER, via disulphide bonding of cysteine 67, inside of this B pocket (Dangoria *et al.,* 2002). It is hypothesised that the net effect of the misfolding and UPR pathway engagement is the production of pro-inflammatory cytokines in key immune cells.

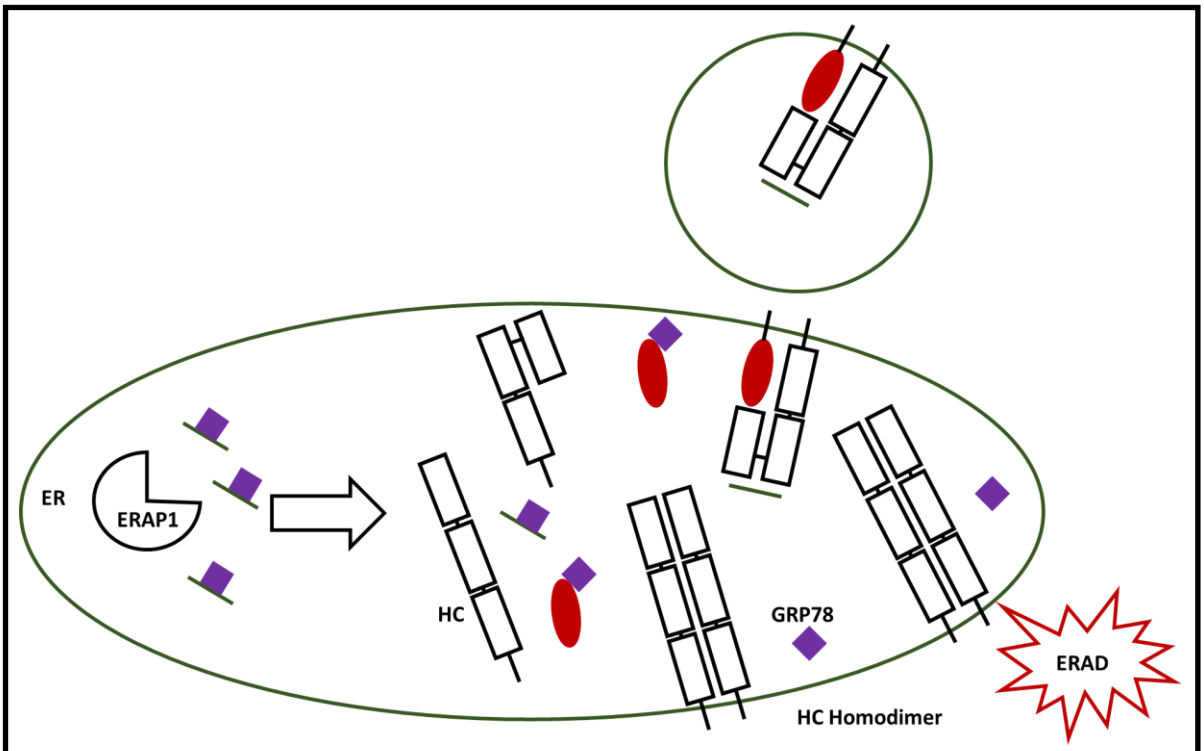

Figure 1-5: diagram displaying the events leading to the misfolding of HLA-B27 for the third hypothesis. ERAP1 cuts the peptides to size to be incorporated into the HLA-B27 complex however mutations in the HLA-B27 complex mean that it does not fold correctly. This enables the HCs to bind to other HCs and for parts of the complex such as the peptide or β_2-microglobulin to not be incorporated. This causes changes in the expression of ER chaperones and ERAD or UPR happens.

In the rat model of AS it has been observed that macrophages undergoing UPR produced IL-23 (DeLay *et al.*, 2009). IL-23 encourages differentiation of T cells into the Th17 lineage which produces IL-17 (Aggarwal, Ghilardi, Xie, De Sauvage, & Gurney, 2003). Furthermore there is evidence of increased expression of IL-17 both in the joints of patients with inflammatory diseases such as IBD, and the relevant rat model (Iwakura & Ishigame, 2006). Taken together, this information gives a strong argument that the latter hypothesis plays a role in initiating and driving AS.

1.4.4 ERAP1

MHC class I assembly occurs in the ER. Assembly is a chaperone mediated event involving peptides generated by the cytosolic proteasome, which are then transported into the ER by the TAP peptide transporter. A significant number of the TAP-supplied peptides are longer than the preferred 9-11 mers that are bound by MHC class I alleles, and as such require trimming to the correct length by enzymes within the ER. Of key significance, one enzyme that has drawn particular attention for its role in AS, due to its detection in GWAS studies (WTCCC & TASC, 2007), is the Endoplasmic Reticulum Aminopeptidase 1 (ERAP1). ERAP1 is an aminopeptidase which cleaves longer peptides into smaller lengths suitable for MHC class I binding (Alvarez-Navarro & López de Castro, 2014). Various mutations in ERAP1 have been described to associate the enzyme with AS (Martín-Esteban, Gómez-Molina, Sanz-Bravo, & López de Castro, 2013). For ERAP1 there appears to be two recurring mutations that associate it with AS; K/R528 (lysine to arginine) and Q/E730 (glutamine to glutamic acid) (Yousaf *et al.*, 2015). As ERAP1 is involved in N-terminal and peptide trimming, mutations could cause the P1 of the resulting peptide pool to be less optimal for HLA-B27 folding. Alternatively, the enzymatic activity of the aminopeptidase could be slowed or hastened. In the case of a mutation near the catalytic domain this would result in a possible deficit of suitable peptides, preventing efficient folding of the HLA-B27 molecule (García-Medel *et al.,* 2012). Problems associated with peptide loading could lead into either the non-canonical or misfolded protein hypothesis mentioned above. ERAP1 could lead to the formation of non-canonical HLA-B27 by producing a protein with suboptimal binding to the peptide-binding groove, which could result in a non-thermodynamically stable structure. This structure could achieve cell surface expression, but then unfold prematurely and lose either the peptide or β_2 microglobulin. Alternatively, the enhanced loss of components during recycling may result in excess FHCs present on the PM (figure 1-4). With respect to the misfolded hypothesis, the production of sub-optimal peptides or over-digestion of peptides could lead to the chaperones being unable to load the

peptides or associate with the MHC. The complexes would then be subject to the strict quality control measures for MHC class I molecules in the ER (figure 1-6).

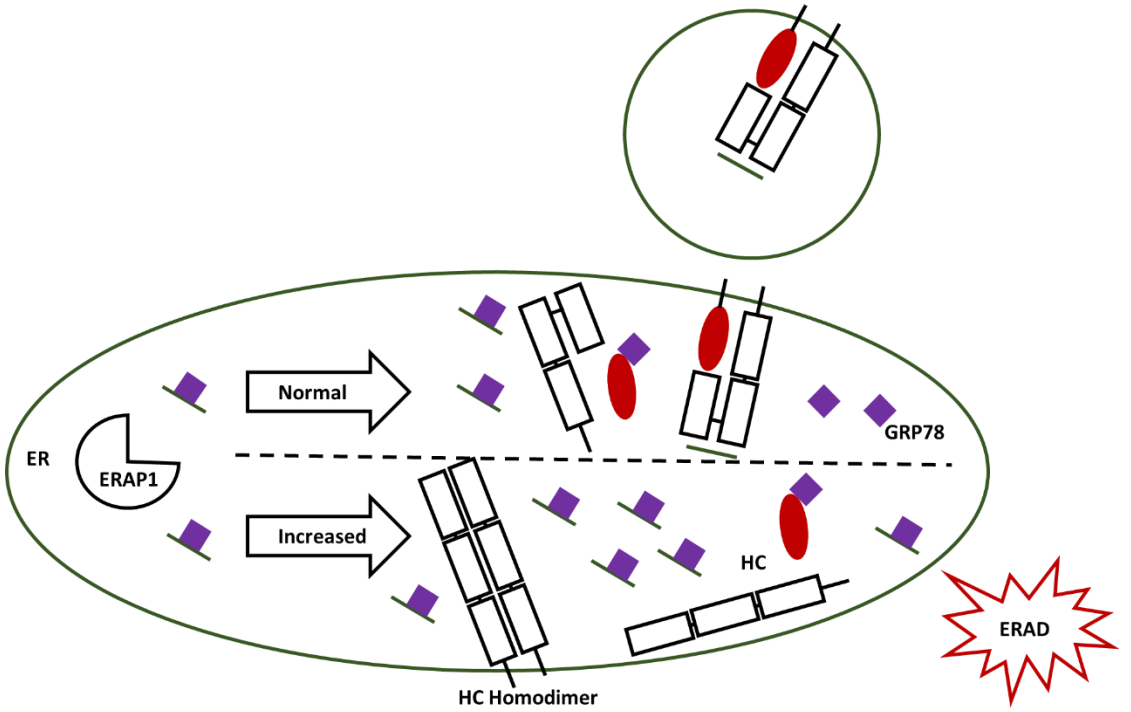

Figure 1-6: diagram of the effects when ERAP1 is mutated. During normal peptide production, ERAP1 cuts up peptides at a regular pace and the peptides are delivered as the protein is folded. If ERAP1 has a mutation that causes it to produce peptides too quickly it can over-produce peptides to a level where there are too many and the chaperone expression is upregulated in order to deal with the high production rate leading to ERAD. Alternatively, a mutation in ERAP1 may also cause it to produce suboptimal peptides that either partially bind or do not bind at all to the HLA-B27. This leaves a population of unfinished HLA-B27 molecules in the ER which builds up and causes an UPR.

1.5 MHC Class I ER Associated Proteins

As previously mentioned, in order for a peptide to reach a HLA class I molecule it must first be transported into the ER by the ATP dependent transporter associated with antigen processing (TAP) (Schumacher *et al.,* 1994). The peptides are then cut to optimal length for MHC class I presentation by ERAP1 or other aminopeptidases. Following this the peptides are chaperoned by components of the protein loading complex (PLC) (Reeves, Elliott, James, Edwards, & Edwards, 2014). Invaluable roles are also played by other chaperone proteins and enzymes in the ER during this process. Without individual and combinations of these proteins in the ER HLA class I misfolding will occur (Guiliano *et al.,* 2016). In this next section I will discuss several of the key components.

1.5.1 Chaperones

Chaperones are proteins in the ER which aid in formation of polypeptides, including MHC class I. They can do this in a number of ways; by holding proteins in close proximity, delivering subunits

together or by promoting correct folding. The most well characterised chaperone associated with this role is GRP78 (BiP). GRP78 aids HLA Class I by transiently binding to the newly synthesised heavy chain, where it remains until β_2 microglobulin binds. As such GRP78 may hold the key to modulation of the earlier events in the assembly of HLA-B27, where deficits in the process may occur. A deeper understanding of these early events could hold novel therapeutic advances in the future. GRP78 binds to exposed hydrophobic regions of proteins. It also binds to oxidised proteins and has been observed to extend its binding time in the case of proteins joined by a disulphide bond (Maurizio Molinari, Galli, Piccaluga, Pieren, & Paganetti, 2002). GRP78 is involved in ERAD and is a marker of acute UPR along with Protein Disulphide Isomerase (PDI) (Colbert *et al.,* 2014). During ERAD, GRP78 expression is upregulated in order to compensate for the GRP78 sequestered by misfolded proteins (Hori *et al.,* 2004). Its ability to engage and regulate the UPR is because normally GRP78 is bound and sequestered in the ER by the transcription proteins IRE1, PERK and ATF6 (Colbert *et al.,* 2014). When GRP78 dissociates, due to increased presence of misfolded proteins, these UPR activators are freed to act. This results in a number of responses including the upregulation of UPR proteins and overall downregulation of transcription, to limit the production of new unfolded proteins (Hiramatsu, Chiang, Kurt, Sigurdson, & Lin, 2015). This ultimately leads to apoptosis if cell homeostasis is not restored.

For MHC class I assembly, calnexin and calreticulin are key chaperones. This pair of chaperones quality control the glycosylation and de-glucosylation processes in the ER (Vassilakos, Cohen-doyle, Peterson, Jackson, & Williams, 1996). In fact, upon transport into the ER the first chaperone that a protein can come into contact with can be either GRP78 or calnexin, depending on the position of the protein's glycans (M Molinari & Helenius, 2000). In the case of calnexin interactions, the glycans are usually N-terminally positioned (Parodi, 2000). The function of calnexin during protein folding is to prevent incorrect folding or inappropriate interactions between subunits.

Calnexin binds first with the heavy chain of the MHC class I, but then is displaced by the β_2 microglobulin subunit, which permits the association of calreticulin with the complex (Sadasivan, Lehner, Ortmann, Spies, & Cresswell, 1996). Calreticulin maintains this association and forms the Peptide Loading Complex (PLC), which comprises of MHC class I tapasin, calreticulin, the oxidoreductase ERp57 and TAP (Sadasivan *et al.,* 1996). At this early stage it is thought that relatively low affinity peptides are bound in the MHC class I peptide groove awaiting a, still unclear, editing process involving primarily tapasin. This allows high affinity peptide binding, dissociation of the class I molecule from the PLC and egression to the cell surface.

1.5.2 Other Molecules Relevant to the MHC Class I Pathway and its Degradation

The chaperone Protein Disulphide Isomerase (PDI) initially binds to proteins to prevent misfolding but it also has the ability to form and re-arrange disulphide bonds (Xiao *et al.,* 2004). Normally PDI works with the GRP78 pathway as opposed to the calnexin/calreticulin pathway.

However, it is known to also interact with MHC class I in the PLC (Turano *et al.,* 2002). PDI is one of the most abundant proteins in cells and it also prevents protein aggregation in the ER (Zeeshan, Lee, Kim, & Chae, 2016). During the UPR PDI is not only upregulated to prevent protein aggregation but also to attempt to correct misfolded proteins or reduce the disulphide bonds resulting in recycling or reordering, relieving ER stress. Upregulation of PDI occurs via ATF4 which is produced from downstream effects of PERK (Halperin, Jung, & Michalak, 2014). PERK, as previously mentioned, is a transcription factor sequestered by GRP78, hence PDIs link with the GRP78 pathway.

Homocysteine-inducible ER Protein (HERP) is a further ATF6-dependent gene therefore, in a similar manner to PDI upregulation, the majority of HERP appears during ERAD (Hori *et al.,* 2004). As a membrane component with both N and C termini facing the cytosolic side of the ER, it is unlikely that HERP possesses chaperone responsibilities like the other proteins mentioned here (Kokame, Agarwal, Kato, & Miyata, 2000). HERP is needed for the destruction of proteins and is also required to form a larger retrotranslocation complex with other ER proteins; HRD1, Derlin-1, VIMP and ATPase p97 (McLaughlin *et al.,* 2010). Furthermore, it has been suggested that HERP is involved in the delivery of proteins to the proteasome for degradation during ERAD (Okuda-Shimizu & Hendershot, 2007).

Hrd1 is recruited to the ER by HERP. In cells where HERP is downregulated, Hrd1 does not localise to the ERAD (Leitman *et al.,* 2014). Hrd1 is an E3 ubiquitin ligase and forms part of the HRD1 complex with other proteins (Denic, Quan, & Weissman, 2006). The core of HRD1 is formed by Hrd1 and Der3 (Kostova, Tsai, & Weissman, 2007). This simple core is stabilised by Hrd3 which is necessary for ERAD activity (Gardner *et al.,* 2000). Furthermore, initial recognition of misfolded proteins is associated with this subunit as well as recruitment of other essential complexes such as Yos9 (Gauss, Jarosch, Sommer, & Hirsch, 2006). It has been suggested that HRD1 is important in the clearance of HLA-B27 complexes during ERAD (Burr *et al.,* 2011).

1.6 Localisation of AS pathogenesis

One of the key mysteries of AS is why the damage appears localised primarily to the vertebrae. Therefore, whilst the molecular mechanisms behind AS are the primary focus of research, the reasons behind the localisation of AS to the lower back and its related effects should also be discussed. As mentioned earlier, AS is often localised to the Sacroiliac joints (SIJ) which are located close to the lower back (figure 1-7). The SIJ is thought to play a role in relieving stress on the pelvic girdle when force is applied during movement (Southerst, Dufton, & Stern, 2012). Therefore it is reasonable to suggest that the SIJ undergoes a great deal of stress. Furthermore, this can lead to agitation and subsequent IBP (inflammatory back pain). AS is diagnosed most commonly in the second decade of life, this coincides with adolescent development involving the SIJ. However there is little literature to provide a reason associated with this. The most obvious change during adolescent development is the production of hormones. A literature search for terms related to this topic uncovers very little, relatively outdated information, usually by 2-4 decades (A T Masi & Medsger, 1979). More research is required into the subject in order to suggest any correlation with any particular aspect of adolescence and AS onset.

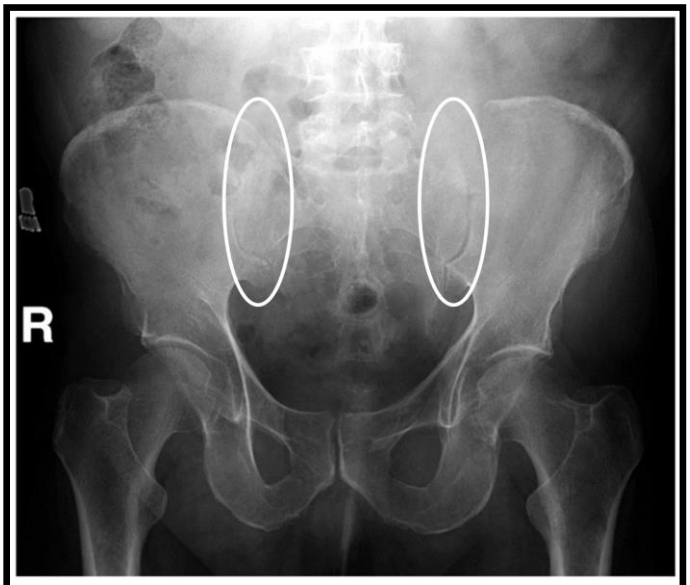

Figure 1-7: x-ray of human lower spine and hip area. Sacroiliac joints are circled on each side with a white oval. Image: (Southerst et al., 2012)

In addition, the ratio of female to males diagnosed also indicates the possibility of a role for hormones in the onset of AS. Decreased levels of oestrogen have been associated with a more active AS phenotype (Jimenez-Balderas, Tapia-Serrano, Madero-Cervera, Murrieta, & Mintz, 1990). It was suggested that pregnancy in particular may be related to AS in women however no conclusive results have been shown (Dudley Hart & Robinson, 1959; Förger, Villiger, & Ostensen, 2009; Giltay, Van Schaardenburg, Gooren, Popp-Snijders, & Dijkmans, 1999; Ostensen, Romberg, & Husby, 1982). Again there is frequent reliance on older literature.

Of particular interest is the association of AS with other co-occurring diseases such as Uveitis, Psoriasis and IBD. These pathologies localise to very different sites of the body, namely the eye, skin and GI tract, respectively. A logical link between these sites would be the activation of immune cells elsewhere that then travel to designated areas. The immunologically privileged status of the eye

suggests that further cell communication would need to occur at the site of inflammation (Zhou, Horai, Mattapallil, & Caspi, 2011). It has been suggested that Uveitis is activated by commensal microbiota (Agrawal, Rukkannagari, & Kethu, 2007; Horai *et al.,* 2017). This provides an interesting theory for the link between IBS, Uveitis and other inflammatory reactions coinciding with AS (Turkcapar *et al.,* 2006). However Uveitis and IBD not always preceding AS suggests that this is not always the case *(Brophy et al.,* 2001). It has been suggested that the biomechanical stress that these areas experience unites them and therefore allows the upregulation of inflammatory cytokines such as TNFα during AS (McGonagle, Stockwin, & Isaac, 2001). Mechanical stress on cells can cause the induction of cell stress molecules such as NALP3 and prostaglandin E2 which lead to inflammatory cytokine production (Alfonse T. Masi *et al.,* 2011). BMP is one such cytokine which drives the formation of new bone (Lories, Luyten, & de Vlam, 2009). Another family of proteins called WNT are also able to drive osteoblastogenesis (Wang *et al.,* 2014). These two families of proteins are able to work together to promote osteoblast differentiation which results in new bone formation seen in AS.

It has also been suggested that an imbalance of cytokines and T cells subsets plays a role in the pathogenesis of AS (Mei *et al.,* 2011; Szanto *et al.,* 2008). In particular IL-17 producing cells known as Th17 cells have been implicated in autoimmune diseases and RA (Miossec, 2009). Fibroblast and macrophage cytokine production are influenced by IL-17 (Jethwa & Bowness, 2016). Th17 cell differentiation, expansion and survival was originally thought to be influenced by TGFβ, IL-6 and IL-23 (Volpe *et al.,* 2008). However, more recent human research has shown that Th17 cells are able to differentiate in a pro-inflammatory environment using IL-1β, IL-6 and IL-23 (Pourgholaminejad, Aghdami, Baharvand, & Moazzeni, 2016). TGFβ, on the other hand, was shown to cause reduction in IL-17 and IL-22 production and proliferate the differentiation of Th17 suppressive T regulatory (Treg) cells (Pourgholaminejad *et al.,* 2016).

There has also been evidence of IL-17 involvement in synovial joint inflammation (Iwakura & Ishigame, 2006). IL-17 is produced by a subset of differentiated $CD4^+$ T cells called Th17 cells. Th17 cells also induce the production of cytokines IL-1 and TNF α by macrophages (Jovanovic *et al.,* 1998). The combination of these three cytokines acts synergistically and activates NFκB. In turn this activates enzymes, and other cytokines such as IFN β in a positive feedback loop (Chabaud & Miossec, 2001). The release of IL-1, IFN β and TNF α cytokines during inflammation causes the activation of osteoclasts and matrix metalloproteinases (Smith, Märker-Hermann, & Colbert, 2006). These can cause the bone degradation and fusion seen during sacroiliac sclerosis and erosion.

Stimulation of a T cell through its TCR results in anergy of the cell and suppression of any effector T cells potentially responsive to the detected antigen (Corthay, 2009; Liao, Lin, Tsai, & Chou, 2015). Of note, an imbalance between Th17 and Treg ratio can result in autoimmune diseases which

otherwise would have been prevented by the suppression of the Th17 cells (Hoe *et al.,* 2017). The production of Th17 differentiating cytokines links back to the three hypotheses of AS pathology. Macrophages undergoing UPR, induced by HLA-B27 misfolding and LPS or chemical stimulation, show an increased expression of IL-23 (DeLay *et al.,* 2009). Experimental mouse models lacking IL-23 have been shown to resist inflammatory autoimmune diseases, in particular EAE and IBD (Wilson et al., 2007). IL-23 is produced by T cells, dendritic cells and macrophages, suggesting roles for both the adaptive and innate immune system (Stoll, 2011). Th17 cells produce other inflammatory cytokines such as IL-22, IL-21, IL-6 and TNFγ (Volpe *et al.,* 2008). IL-22 is known to influence synovial fibroblast proliferation and cytokine production however Th1 cells have also been shown to produce IL-22 (Shen, Goodall, & Hill Gaston, 2009). In addition to Th17 cells there are other cells that are able to produce IL-17, suggesting that there may be other inducers of osteoblast and osteoclast differentiation (Rossini *et al.,* 2016). Altogether this information shows a complex cellular pathology pathway relating to AS. Potentially the origin of AS could lie with Treg problems, IL-23 polymorphisms, HLA-B27 UPR or another, as yet undiscovered, mechanism.

1.7 The HLA-B27 Transgenic Rat Model

Moderate insight into AS has been provided by the AS rat model. Whilst mouse models have also been produced, they appear not to replicate the human disease. In order to produce the rat model, rat embryos were transfected with restriction endonuclease cut DNA fragments of HLA-B27:05 (mentioned earlier) or human β2 microglobulin (Hammer, Maika, Richardson, Tang, & Taurog, 1990). Spontaneous disease in this model is characterised by inflammation of the peripheral and axial joints accompanied by inflammation of the gut, male genital tract, nails, skin and heart (Hammer *et al.,* 1990). These characteristics bear a close resemblance to the symptoms associated with AS. Studies have used both transgenic rats and their cells to analyse the interactions of T cells, cytokines and proteins associated with AS (Breban *et al.*, 1996; DeLay *et al.*, 2009; Fert *et al.*, 2014; Tran *et al.*, 2004; Turner *et al.*, 2005). Of significant note however, of the several transgenic rat lines produced, those with a relatively low HLA-B27 copy number are not prone to disease, only those lines with high copy number develop the pathology. Interestingly rats with a similar high copy number of control HLA-B7 are not disease prone, indicating there is still HLA-B27 specificity in this rat model (Fert *et al.,* 2008).

1.8 Gene Therapy

Gene therapy is an emerging, important technique in the treatment of, primarily, genetic diseases. As such it may have a future role in treating AS. Gene therapy is either the *ex vivo* transfection of a cell which is then replaced in a patient as a graft, or *in vivo* recombination of genetic

information to replace the deleterious gene. A recent aspect of gene therapy is the development of RNA interference. This alters the expression or translation of mRNA in the target cell. If gene therapy could be used to insert a gene that produces RNA interference inducers (RNAi) into the HLA-B27 pathway, then it could be possible to reduce the inflammation and pathology seen in AS. Micro Ribonucleic Acid (miRNA), Small Interfering Ribonucleic Acid (siRNA) and Short Hairpin Ribonucleic Acid (shRNA) are all potential RNAi. siRNA functions directly upon introduction into cells whilst miRNA and shRNA require processing. miRNA is formed initially from primary miRNA (Pri-mRNA) endogenously expressed transcripts (figure 1-8). It is then transcribed by RNA polymerases and cleaved by Drosha (a nuclear RNase III enzyme) to produce precursor miRNA (Pre-mRNA) (Zeng, Yi, & Cullen, 2005). The precursor miRNA is then transported out of the nucleus by Exportin-5 and into the cytoplasm (Bohnsack, Czaplinski, & Gorlich, 2004). Here it is cleaved by Dicer into 21-22 nucleotide long dsRNA fragments (Provost *et al.,* 2002) and then incorporated into a RNA Induced Silencing Complex (RISC) (Fernández-Messina, Gutiérrez-Vázquez, Rivas-García, Sánchez-Madrid, & de la Fuente, 2015). The RNAi duplexes are separated and used to complementary base pair with mRNA from the nucleus which RISC subsequently cleaves (Nakanishi, 2016). In the case of miRNA, RISC binds and causes either translational repression or cleaves mRNA, like siRNA induced silencing. There are studies, recently published, describing the use of ERAP1 siRNA to downregulate the production of

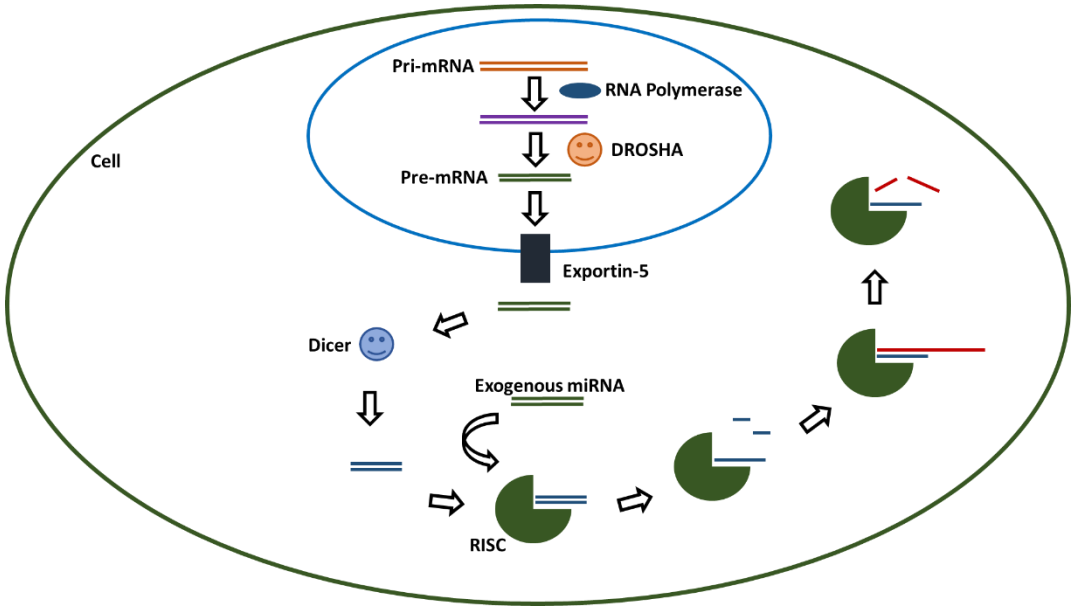

Figure 1-8: diagram describing the role of miRNA as an inhibitory RNA. miRNA is initially formed from Primary mRNA. RNA polymerase then proceeds to transcribe it and DROSHA cleaves the introns to form Pre-mRNA. Pre-mRNA is transported out of the nucleus by Exportin-5 to the cytosol where it is cleaved by Dicer to shorter dsRNA fragments. A fragment may now be incorporated into the RISC complex where the dsRNA is separated and one strand retained to complementary base pair with the mRNA of the protein that requires downregulating. It does this by binding and then digesting the complementary bound mRNA molecule. Exogenous miRNA may also act to downregulate proteins by binding to the RISC complex and directing translational repression.

ERAP1 in HeLa.B27 and C1R.B27 cells, which resulted in reduced expression of HLA-B27 free heavy chain (FHC) on the cell surfaces (L. Chen *et al.,* 2015). Whilst on a cell culture level this has proven to be successful, it must be kept in mind that in order to use siRNA on a treatment level an efficient drug delivery method will be required. Delivery of siRNA in small vesicles known as exosomes is the method under analysis in this thesis, to be discussed in detail later.

1.9 Celecoxib and its Use in AS

Celecoxib (CXB) is an NSAID member of the Cyclooxygenase (COX) inhibitor family. It selectively inhibits COX-2 and as such presents itself as a useful drug to combat inflammation in AS (Warner *et al.,* 1999). However recently, CXB used at higher concentrations has been reported to have additional effects including anti-tumorigenic properties (Huang *et al.,* 2012). Pyrko *et al.* have shown that CXB downregulates cyclin D synthesis, inhibits eIF2α and induces GRP78 and CHOP (Pyrko *et al.,* 2008). Of particular interest to us is CXBs role as an inducer of GRP78 and CHOP (figure 1-9). CHOP is normally kept at low cellular levels until ER stress occurs, playing an opposite roll to GRP78. CHOP is

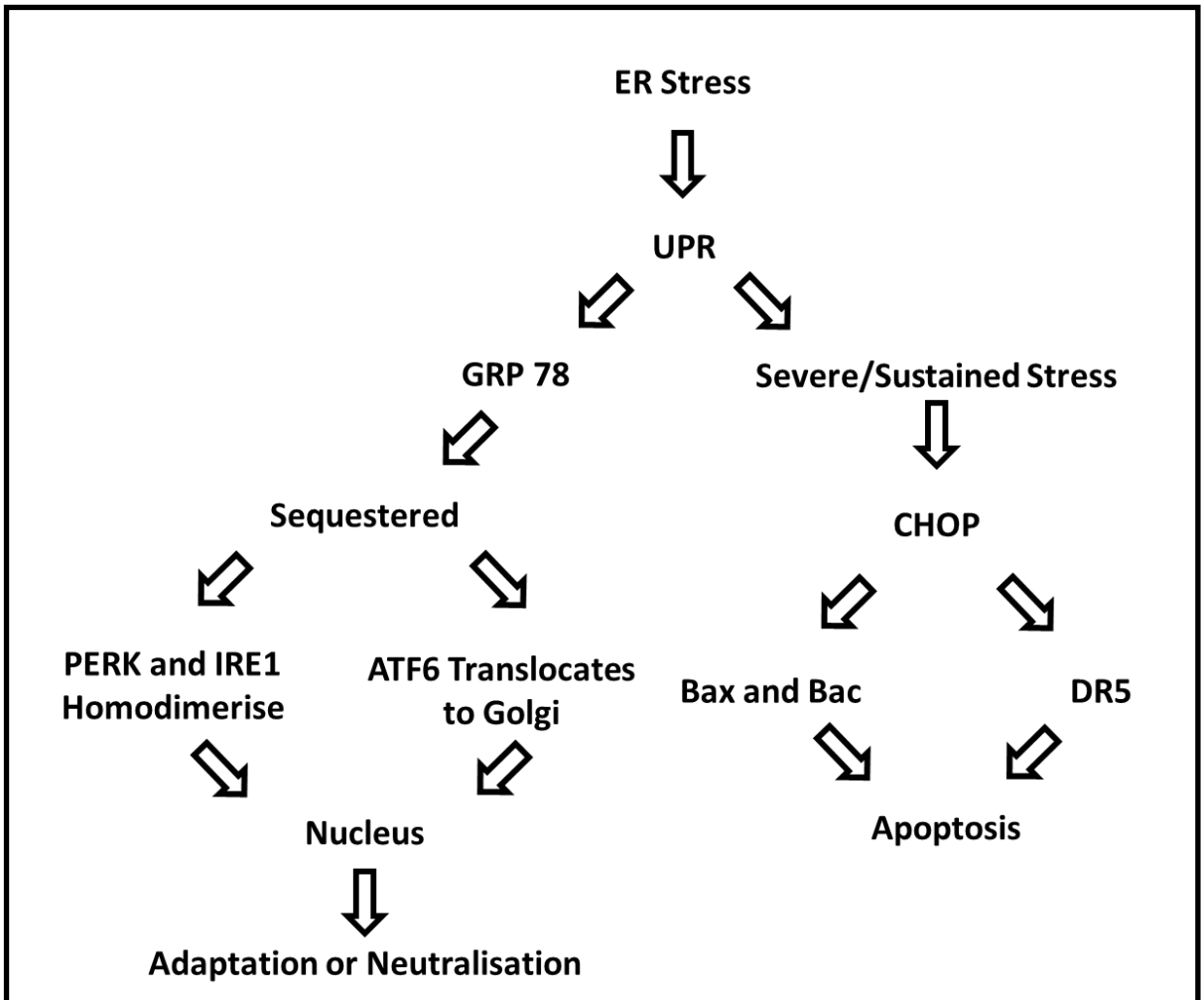

Figure 1-9: flow diagram showing the pathway that UPR leads to with its two outcomes.

strongly induced by IRE1, PERK and ATF6 but does not exert its full apoptotic potential unless the concentration of unfolded protein in the ER remains high over a period of time. Once this threshold has been met, CHOP can induce expression of Bim and Death Receptor 5 (DR5) leading to cell sensitisation and apoptosis (Schönthal, 2012). CXB therefore induces cellular mechanisms that aid in clearance of unfolded protein. When combined with the AS hypotheses this suggests a potential mechanism for clearance of misfolded proteins in order to prevent inflammation. A variant of CXB, which has no COX-2 inhibitory capacity, but induces ER stress is 2, 5-dimethyl-Celecoxib (DMC). DMC is currently under investigation in anti-tumour therapies (Schönthal, 2006; Sobolewski *et al.*, 2015) due to its ability to inhibit cell cycle progression without CXB side effects. DMC downregulates NFκB and cyclins and induces an increase in intracellular calcium levels. This suggests that DMC may reduce inflammation in a manner useful in the study of AS.

1.10 Viral Vectors

Owed to the ability of certain viruses to incorporate themselves into the DNA of cells, viruses are considered powerful tools for gene manipulation. Viral vector delivery research expanded in the 1990s with Adenosine deaminase (ADA) severe combined immunodeficiency disease (SCID) (Blaese *et al.*, 1995). However, initial success was short lived after a study involving 18 participants who were being treated with Adenoviral vectors for Ornithine Transcarbamylase Deficiency experienced failure. One patient initially demonstrated Acute Respiratory Distress Syndrome (ARDS) followed by multiple organ failure. After 98 hours they were removed from oxygenation apparatus, and subsequently died (Raper *et al.,* 2003). Further studies using retroviral vectors have demonstrated more problems with using these vectors. Hacein-Bey-Abina and colleagues used retroviral vectors in their clinical trial for

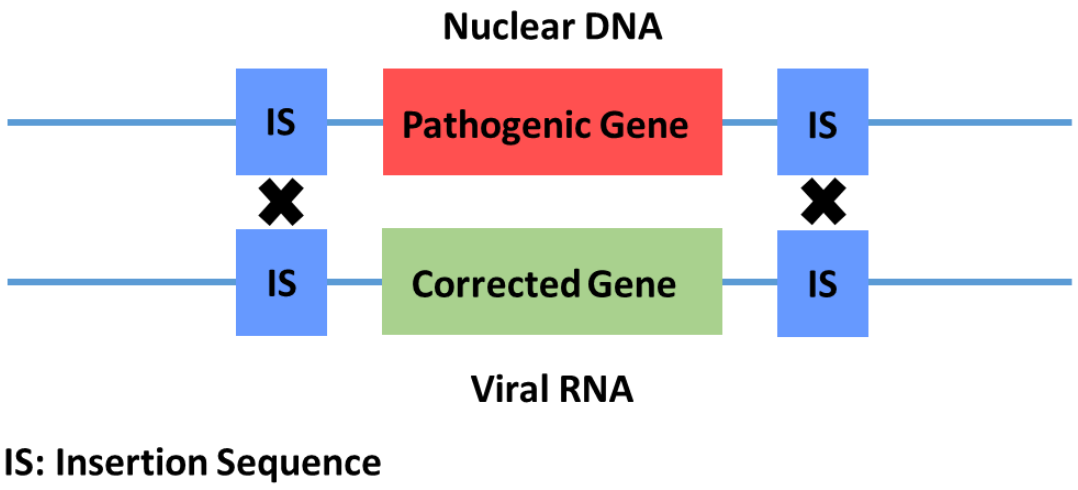

Figure 1-10: diagram describing the exchange of genes via insertion sequences that some viruses use. This can be used to correct mutated genes however the risk of mutagenesis when using viruses occasionally causes problems.

X-linked SCID resulting in 2 of their subjects developing Leukaemia (Hacein-Bey-Abina *et al.,* 2004). These failures in treatment demonstrate the dangers involved in using viral vectors. The clinical trials mentioned above aimed to use viral vectors to recombine cDNA into target cells, however, the risk in this method is that the virus may insert the gene in to a random sequence or with a random mutagenesis (figure 1-10). While both *in vivo* and *ex vivo* gene therapy using viral vectors initially has had its setbacks, more recent *ex vivo* gene therapy seems to have had more successes with treating ADA-SCID patients without them developing leukaemia (Herzog, Cao, & Srivastava, 2010). The most recently used viral vectors tend to be HIV lentiviral vectors with all HIV virulent genes removed. Kaiser and colleagues (Kaiser, 2009) demonstrated the success of using retroviral vectors for β-thalassemia gene therapy clinical trials. However, the same risks of insertion mutagenesis still plague this vector. Overall this type of therapy remains potentially dangerous and very expensive.

1.11 Non-viral Vectors

Nanoparticles and nanoparticle-like structures represent a group of varying synthetic delivery vehicles. A well-documented synthetic vehicle, classed as a member of the nanoparticle group, for gene therapy is liposomes. Liposomes are close relatives to extracellular vesicles (EVs), having a spherical structure. They vary largely in size and can be manufactured to contain specific receptors or proteins on their surface. Unlike viral vectors, liposomes have the benefit of not causing such adverse reactions, though they have been observed aggregating in specific non-target organs such as the liver and spleen (Poste *et al.,* 1982). Basic liposomes are composed of egg-phosphatidylcholine, 1,2-dioleoyl-sn-glycero-3-phosphoethanolamine, 1,2-dioleoyl-3-trimethylammonium-propane and 3β-[N-(N',N'-dimethylaminoethane)-carbamoyl]cholesterol. Depending on the ratios, this can result in differences in liposome size, zeta potential and ionic charge (Soema, Willems, Jiskoot, Amorij, & Kersten, 2015). Ideally a liposome should be cationic to optimally interact with the anionic outer cell membrane. Unfortunately liposomes in circulation are targeted by complement as they lack the necessary proteins to identify as part of the body (Szebeni, Muggia, Gabizon, & Barenholz, 2011). This leads to a quick clearance by the innate immune system and renders them therapeutically unusable. To counter this, the compound polyethylene glycol (PEG) can be added to liposomes to increase the circulation time of drug in the blood before being cleared by the liver and spleen (Romberg, Hennink, & Storm, 2008). Characteristics like this can help target blood parasites, however PEG also has the ability to form steric stabilization. This prevents blood components from binding to the PEG coated liposome. Whilst this protects against complement binding and the innate immune system, it leaves liposomes at a disadvantage with regards to targeting blood-born parasites and red blood cells (RBC). On the other hand, it gives liposomes a prolonged suspension time to bind to potential target sites.

1.11.1 Carbon Nanotubes

Carbon nanotubes (CNT) are elongated nanoparticles in a tubular shape. They have a diameter of 1-2 nm and length of 50 nm to 1 cm. They come in two types; single-walled CNT (SWCNT) or multi-walled CNT (MWCNT) (Draz *et al.*, 2014). Both are used in biological applications, however, SWCNTs seem to be favoured due to their single wall, reduced cytotoxicity and lack of complexity. These features make them ideal as nano-sized needles and give them an advantage in penetrating cellular barriers. Furthermore, the exposed carbon molecules can easily be bound to or drugs can be carried inside of the tube and be protected from immune detection and clearance. Zhang and colleagues have shown that CNT can be used to reduce tumour size in a nude mouse model when telomerase reverse transcriptase siRNA is delivered to the tumour in CNTs (Zhang *et al.,* 2006). Other groups have also shown successes in cell culture and animal models with the use of CNT (Gupta *et al.,* 2015)(Kam, O'Connell, Wisdom, & Dai, 2005). The field of Light Triggered Nanotheranostics (LTN) seems to be advancing in conjunction with CNTs. Materials possessing LTN properties are those which can be triggered by light to exert radiation in a specific area. Kam and colleagues used the LTN properties of SWCNTs to excite them with a near infra-red laser which caused selective cell death (Kam *et al.,* 2005). The characteristic of specific cell targeting, along with other characteristics such as imaging and lack of resistance make CNTs interesting vehicles. However, there have also been studies looking into the toxicity of CNTs both during manufacture and as a potential drug. Sun and colleagues found that CNTs, whilst not directly cytotoxic themselves, promoted lymphocyte toxicity by increasing the expression of NF-κB (Sun *et al.,* 2011). In contrast, Fujita and colleagues performed a study of the effect of CNT on those working to produce them. They found that both SWCNTs and MWCNTs caused inflammation in and around the lungs (Fujita *et al.,* 2016). Currently CNTs have many studies with contrasting results and suppositions which result in confusion over the cytotoxicity of these vehicles. Whether indirect or over time, evidence of toxicity associated with CNTs suggests that their synthesis and manufacturing protocol still need to be developed further.

1.11.2 Magnetic Nanoparticles

Recent studies have considered the use of magnetic nanoparticles for use in oncology despite the technology being available since 1979 (Widder, Senyei, & Ranney, 1979). The main attraction of magnetic particles is that the particles can be localised to a specific area using magnetic fields for an allotted time. So far magnetic nanoparticles have been approved for use in imaging with MRI and as such have a promising characteristic for tracking treatment in an animal model or clinical trials. The majority of magnetic nanoparticles are composed of iron, nickel or cobalt with manganese being the unusual exception (Bondi, Oyler, Ke, Schiffer, & Schaak, 2009). Of further interest is the manufacture of superparamagnetic iron oxide nanoparticles (SPIONs). These 10-100 nm diameter particles possess superparamagnetism, which means that they are not magnetic until an external magnetic field is

applied to them (Wahajuddin & Arora, 2012). SPIONs can be injected into a site and then focussed on an area using a magnetic field. Furthermore, once the magnetic field is turned off, the SPIONs should readily disperse. Whilst there have been many studies looking at the use of SPIONs as drug delivery vesicles, so far none have been successful in clinical trials. Wu and colleagues found that iron oxide nanoparticles caused a decrease in HUVEC viability and furthermore inhibited their differentiation on Matrigel (Wu, Tan, Mao, & Zhang, 2010). It has also been proposed that, over a period of time, iron free radicals may be formed which would cause DNA damage, cellular redox problems and immune inhibition (Singh, Jenkins, Asadi, & Doak, 2010; Toyokuni, 1996). The toxicities so far reported with regards to magnetic nanoparticles may render them unusable as drug vehicles despite their ideal features. However, research into these nanoparticles is still in its infancy and it is expected that there will eventually be a way to overcome the adverse effects.

1.11.3 Extracellular Vesicles

Extracellular Vesicle (EV) is an umbrella term used to cover the collection of vesicles both secreted and budded from cells. There are 3 main types of EVs; exosomes, microvesicles and apoptotic bodies. These EVs are categorised by their cellular origin as opposed to their protein markers. It was previously thought that exosomes could be defined by the presence of CD63, CD9 and CD81 however these tetraspanins have also been identified on microvesicles and apoptotic bodies (Buzas *et al.,* 2015). In the relevant literature, TSG101 is still used with CD63 and CD9 to confirm the enrichment of exosomes (Shahabipour *et al.,* 2017). Identification of the 3 main vesicle types therefore depends on an initial enrichment in associated tetraspanins but then further evidence of vesicle size and morphology, the latter usually attained via Electron Microscopy (EM). Exosomes are vesicles in the range of 50-200 nm that have a cup shaped morphology on EM. They differ from the other two types as they are specifically produced inside of the cell and then released into the extracellular environment. Exosomes start off as Intraluminal Vesicles (ILVs) formed from the budding of the membrane of an early endosome to create a Multi Vesicular Body (MVB) (figure 1-11). Microvesicles bud-off from the plasma membrane (figure 1-12) whilst apoptotic bodies are formed as dead cells bleb and break down. The size range of microvesicles is 50 nm to 1 µm and 50 nm to 5 µm for apoptotic

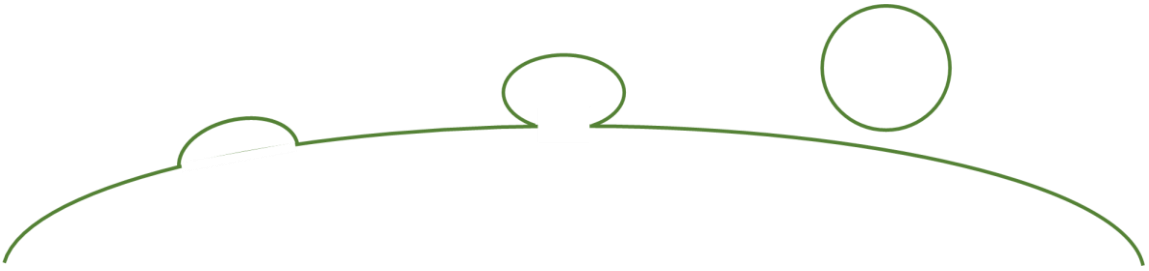

Figure 1-11: diagram of a plasma membrane budding off to form microvesicles.

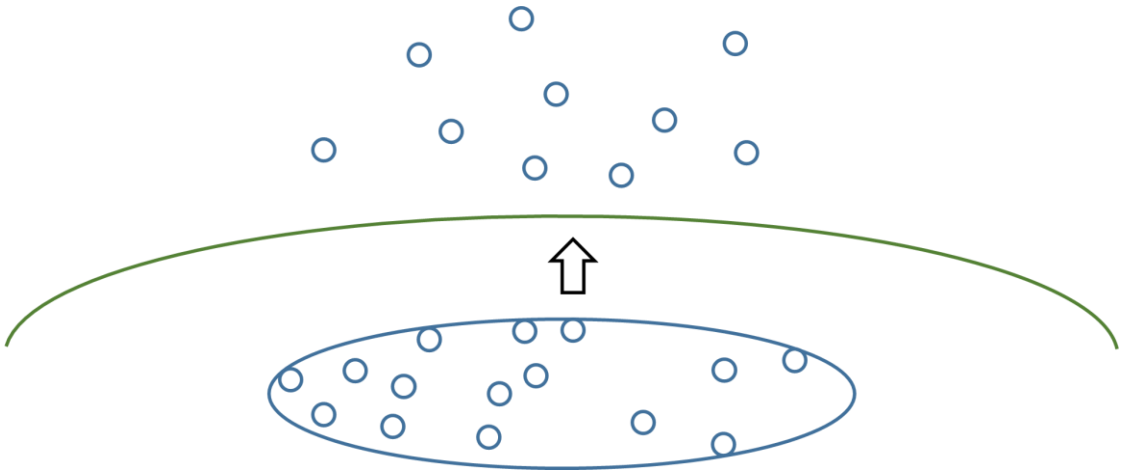

Figure 1-12: diagram of a MVB with ILVs inside. When these vesicles are released from the MVB past the plasma membrane they are termed exosomes as they were not directly budded from the plasma membrane.

bodies. As the sizes of these vesicles overlap it is important that morphology is also confirmed. It is difficult to come to a consensus for the definition of an exosome therefore recently it is preferred to refer to the population as a whole with the term extracellular vesicles.

1.11.4 Exosome Formation

A set of proteins called ESCRT proteins work to allow the early endosome to bud in on itself. This effectively forms ILVs with molecules such as MHC correctly orientated to the outside of the vesicle. There are 4 distinct ESCRT machinery components: ESCRT-0, ESCRT-1, ESCRT-2 and ESCRT-3. Each of these machinery components are formed by their own set of subunits with ESCRT-0, 1 and 2 being the smallest complexes and ESCRT-3 forming a large multimeric lattice. The ESCRT machinery assembles due to its preference for lipids and proteins which are present on the endosomal membrane. ESCRT-0, 1 and 2 all play a role in the sorting of cargo to endosomes as they interact with ubiquitin labelled molecules (figure 1-13). This ubiquitin label is subsequently removed from cargo by ESCRT-3 associated de

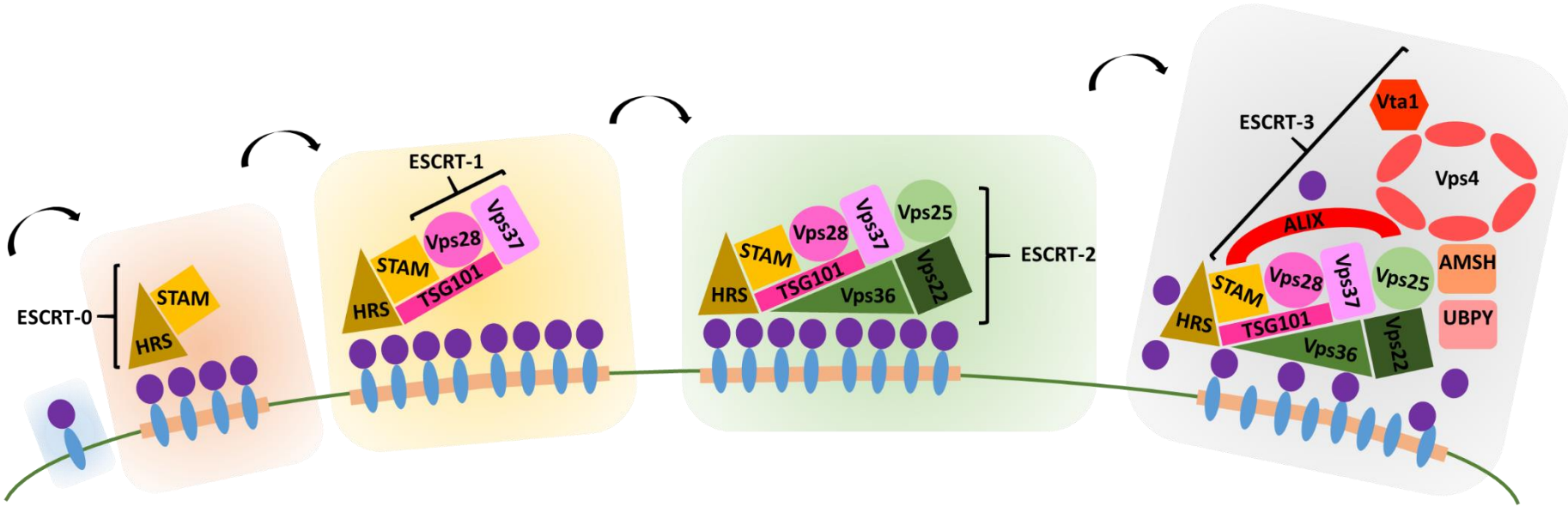

Figure 1-13: diagram describing the formation of ESCRT complexes. Red boxed area: first ESCRT-0 is recruited to the membrane by phosphatidylinositol-3-phosphate (Robbins & Morelli, 2014). Yellow boxed area: here ESCRT-0 is able to bind ubiquitinated membrane proteins and use its HRS subunit to interact with the TSG101 subunit of ESCRT-1. Furthermore, ESCRT-0 is able to gather ESCRT-1 complexes by recruiting clathrin locally. Green boxed area: ESCRT-1 goes on to recruit ESCRT-2 which interacts with the ubiquitinated cargo via its GLUE domain present on Vps 36 subunit. Grey boxed area: the ALIX subunit of ESCRT-3 is recruited by ESCRT-2 and binds to ESCRT-1 which in turn recruits UBPY and AMSH in order to deubiquitinate the membrane proteins. Once this has occurred the ESCRT machinery is disassembled by Vps4 aided by Vta1.Vps4 disbands the clathrin area and forms a ring in the ER membrane to transport the ESCRT subunits out into the cytoplasm.

ubiquitination enzymes before loading into the ILV (Williams & Urbé, 2007). ESCRT-0, 1 and 2 begin the process of ILV formation by interacting first with the phosphatidylinositol in the endosomal membrane and then interacting with ubiquitinated cargo and each other (Williams & Urbé, 2007). The subunits that each ESCRT is composed of help with this task; HRS and STAM for ESCRT-0 (Mizuno, Kawahata, Okamoto, Kitamura, & Komada, 2004); TSG101, Vps28 and Vps37 for ESCRT-1 *(Stuchell et al.,* 2004); Vps22, Vps25 and Vps36 for ESCRT-2 (Babst, Katzmann, Snyder, Wendland, & Emr, 2002); ESCRT-3 is similarly a multi-component structure. ESCRT-0 also plays a further role in gathering the ESCRT-1 complexes. This occurs by recruiting clathrin to the endosome and forming clathrin rich areas. In turn this increases the interaction with ESCRT-1 and gathers ubiquitinated cargo in a specific area (Clague, 2002). The TSG101 subunit of ESCRT-1 interacts with the HRS subunit of ESCRT-0 (Bache, Brech, Mehlum, & Stenmark, 2003). ESCRT-2 has a special GLUE domain formed from a protruding Vps36 subunit which aids in its binding to ubiquitinated cargo (Slagsvold *et al.,* 2005). However, to date, there has been no distinct subunit in mammalian cells, as there is in yeast cells, to cause an interaction between ESCRT-1 and 2. Instead there is a theory that these ESCRTs co-assemble with clusters of ubiquitinated cargo (Hurley, 2008). The addition of ESCRT-3 to the early endosomal membrane machinery is more straight forward; the ALIX subunit of ESCRT-3 is recruited by ESCRT-2 and interacts with the subunits of ESCRT-1 (Odorizzi, 2006). In order to signal the internalisation of the cargo it must now be deubiquitinated and released. The components of the complex are transported into the ILV or freed to move in the outer membrane of the ILV. This is accomplished by UBPY and AMSH, two deubiquiting enzymes recruited by ESCRT-3 (Agromayor & Martin-Serrano, 2006). The next role of ESCRT-3 is to disassemble the ESCRT complex. It initiates this with the Vps4 subunit. The Vps4 subunit is an AAA^{+} ATPase which disassembles the clathrin bilayer where the ubiquitinated cargo was clustered around the other ESCRT complexes (Sachse, Strous, & Klumperman, 2004). Another protein, Vta1, complexes with Vps4 in order to accelerate the ATPase activity of Vps4 (Lottridge, Flannery, Vincelli, & Stevens, 2006) and promote the assembly of Vps4 in to a ring structure. This ring structure is thought to use the energy generated by the ATPase to transport the remaining ESCRT machinery out in to the cytosol (Scott *et al.,* 2005). Alongside sorting of cargo it is suspected that ESCRT-3, along with tetraspanins, play a role in the self-invagination of the endosomal membrane and pinching off to form the ILV which form the MVB (Piper & Katzmann, 2007). More specifically, the induction of a curvature enhancing molecule to the endosomal membrane in the ILV neck encourages the formation of ILVs (Williams & Urbé, 2007).

1.11.5 Exosome Release

The MVB, upon appropriate signalling, will travel via actin filaments to the surface of the cell. Here it releases the ILVs to the extracellular environment. The ILVs are then termed exosomes.

Exosomes are further identified by characteristic vesicle markers. These include TSG101 and the tetraspanins CD63, CD9 and CD81. However, the absolute presence of any one of these markers may vary depending on the cell type the vesicles are collected from. For both microvesicles and apoptotic bodies the method of formation from the cell is budding from the plasma membrane. Generally speaking, the size range of microvesicles goes up to 1000 nm whereas the size of apoptotic bodies can be beyond this. The protein marker content of microvesicles is very similar to the protein expression on the plasma membrane of the parent cell with the exception that some protein can be specifically included or excluded (Cocucci, Racchetti, Podini, & Meldolesi, 2007) and it has been described that lipid raft specificity can help identify microvesicles (Van Dommelen *et al.*, 2012). As apoptotic bodies are a sign of cell death it was expected that a minimal percentage of EVs isolated would be apoptotic bodies. It is important to state that unless a population of EVs is enriched for vesicles with a specific marker it is most likely that the population will not be purely any one of the above mentioned vesicle types and as such the population of vesicles used in this research will be referred to as EVs.

Further identifiers of EVs may be their cargo. The contents of an EV will directly relate back to the activity of its parent cell as it contains a sample of the cytoplasm. Online information banks such as Exocarta (http://www.exocarta.org/) and Vesiclepaedia (http://www.microvesicles.org/) have emerged over the past few years summarising information related to EV contents and composition in comparison to cell type used in the study recorded (Kalra *et al.,* 2012; Mathivanan & Simpson, 2009). Cargo of particular interest in RNA interference research are the micro RNA (miRNA) reported to be associated with EVs. Mittelbrunn and colleagues have published on the unidirectional movement of EVs containing miRNA across the immunological synapse of T cells to APC when stimulated (Mittelbrunn *et al.,* 2011). The work of Momen-Heravi and colleagues also suggests that cells can be manipulated to segregate induced miRNA to EVs. Thus, upon activation, cells such as B cells may release EVs in a controlled manner to deliver miRNA to a targeted cell type such as macrophages (Momen-Heravi, Bala, Bukong, & Szabo, 2014). Altogether it is reasonable to suggest that EVs would make an effective new generation of drug delivery vesicles.

1.12 EV Delivery Pathways

1.12.1 EV Cargo Loading

Before discussing the uptake of EVs the primary routes by which exosomes and microvesicles are loaded *in vitro* and *ex vitro* must be identified. *In vitro* refers to the cell of origin performing the loading. The least specific route for this is overexpression. In this instance the cargo is overexpressed in the cell therefore causing it to be present in excess in the cytosol or other subcellular compartment. As microvesicles form or bud off, taking a sample of the cytosol for example with them, it is presumed that a representative sample of the overexpressed cargo will be present. Similarly, for exosomes, as

the ILV is budded from the cytosol it should also take a sample of the overexpressed cargo. A second method for *in vitro* EV loading that is more controlled and specifically targeted to exosomes involves transfection. This has been most successful *ex vivo* so far. To give an example a plasmid encoding a miRNA, siRNA or shRNA would be transfected with targeting to the exosome pathway made optimal. Villarroya-Beltri and colleagues found the EXOmotif (a motif specific for guiding miRNA cargo to exosomes) GGAG in both T cells and Jurkat cells (Villarroya-Beltri *et al.,* 2013). They also found a motif specific for delivery of the miRNA to the cell. Therefore, they found that when the miRNA sequence was cloned into viral vectors and directed mutagenesis performed to switch its delivery motif with the delivery motif of an miRNA destined to be delivered to the cytosol, the exosome delivery motif labelled miRNA were delivered at a higher ratio to the exosomes rather than the cytosol and vice versa for the miRNA that underwent directed mutagenesis to be tagged with the cytosol delivery motif (Villarroya-Beltri *et al.*, 2013).

1.12.2 EV Uptake by Cells

Whilst the mechanisms of how EVs are formed are partially understood, the route by which they cross the plasma membrane (PM) of a cell and move to the desired cellular compartment has yet to be fully elucidated. EVs can carry signals to other cells. Therefore, they must first attach to the surface of the PM and cause a conformational or structural change to allow passage into the cytosol. This means a specific reaction must happen first and that the receptors of a cell or of the EV must bind. Examples of receptor protein target pairs are; LFA-1 and ICAM-1; MFGE8 or TIM4 and phosphatidylserine (PS); ICAM-1 and α4 integrin; CD169 and α2, 3-sialic acid (Miyanishi *et al.*, 2007; Morelli *et al.*, 2004; Saunderson, Dunn, Crocker, & McLellan, 2014; Segura, Guerin, Hogg, Amigorena, & Thery, 2007). In the case of specific receptor binding this may be enough to promote a change in the PM and the EV can be internalised however there are other pathways for EVs to cross the PM. Morelli and colleagues suggest that receptor mediated endocytosis (RME) may play a role in this (Morelli *et al.,* 2004). During RME (figure 1-14) the area where the receptor has been bound on the PM is pinched in and forms a vesicle inside of the cell. The act of the PM folding in on itself is due to

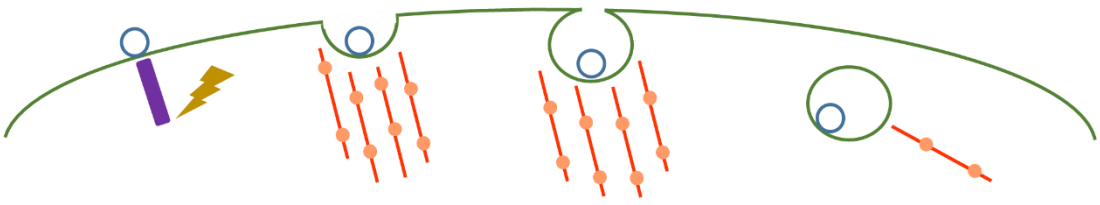

Figure 1-14: diagram showing the process of vesicle absorption via RME. First the vesicle binds to a receptor on the outside of the cell which causes a chain reaction of protein phosphorylation and activation resulting in the activation of actin and transport proteins. Actin works to pull the membrane into the cytosol forming an invagination which seals itself off forming a membrane around the vesicle.

the receptor being associated with a tyrosine kinase. This triggers a phosphorylation chain eventually activating transport regulating proteins such as Actins. Another mode of transport across the membrane is through clathrin dependent endocytosis (CDE). In the case of CDE, an area called a clathrin coated pit is used to bind groups of proteins to be endocytosed as a group. In a similar manner to RME, the clathrin coated pit will bud in on itself and the PM will fuse to produce a clathrin coated vesicle in the cytoplasm with the EV inside (Mousavi, Malerød, Berg, & Kjeken, 2004).

1.12.3 Clathrin Independent Pathways

Alternatively, there are several clathrin independent pathways for EVs to enter cells depending on the cell type; phagocytosis, macropinocytosis and lipid raft mediated endocytosis. Phagocytosis, perhaps one of the best known methods for cellular uptake of extracellular material, is a characteristic of phagocytic cells such as macrophages. Phagocytosis is receptor mediated therefore it requires the binding of a ligand to a receptor before actin polymerisation is activated. This allows formation of an invagination around the associated extracellular fluid. Phagocytosis was initially thought to internalise larger structures, mainly apoptotic bodies, however particles as small as 85 nm have been taken up via this method (Mulcahy, Pink, & Carter, 2014). Feng and colleagues showed in their study that PI3K and actin are essential in the phagocytic pathway and that EVs co-localise to phagolysosomes (Feng *et al.,* 2010). Furthermore, they also showed that EVs may be taken up by a PS receptor as TIM-4 (an endogenous phagocytic cell receptor present on apoptotic bodies) antibody partially reduced the phagocytosis of EVs (Feng *et al.,* 2010).

Macropinocytosis, similar to phagocytosis, uses membrane ruffles of the PM to encompass part of the extracellular fluid and anything attached to the membrane (figure 1-15). This results in the formation of a macropinosome once the ruffles have merged with themselves or the PM. Macropinocytosis differs from phagocytosis as direct contact through receptors or cargo with the

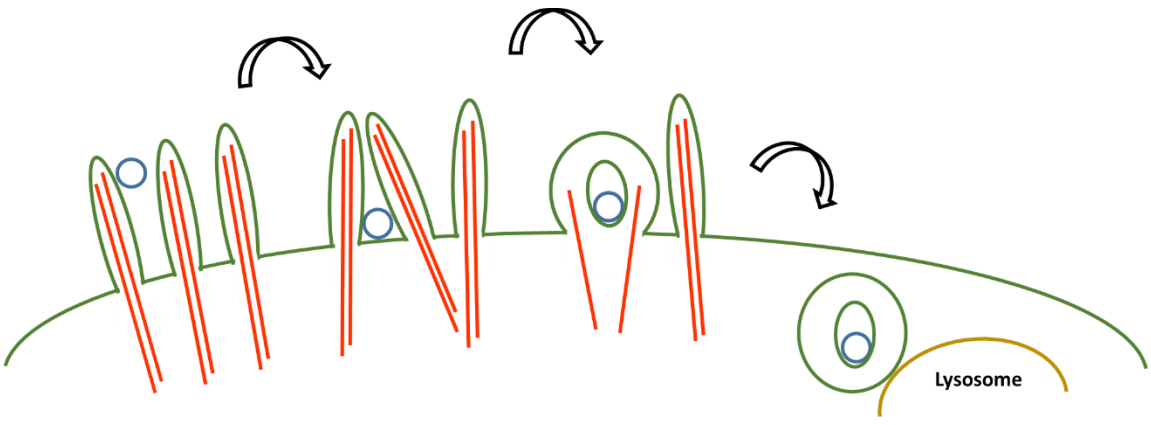

Figure 1-15: diagram demonstrating the use of ruffles to capture material from the outside of a cell. First the vesicle interacts with the ruffles, but does not bind to a receptor on the cell surface. This causes the ruffles to join together and entrap the receptor bound material. Via the use of actin and transport proteins the macropinosome formed is pulled into the cytoplasm where it can join a lysosome amongst other fates.

membrane is not required to cause the ruffles to retract (Kirkham & Parton, 2005). Macropinocytosis relies on receptor tyrosine kinases to increase actin ruffling and therefore increase the amount of macropinocytosis occurring at the PM (Kerr & Teasdale, 2009). The retraction of the ruffles can be cholesterol-dependent or promoted by PI3K (Mulcahy *et al.,* 2014). Normally in macrophages the macropinosomes will be targeted toward the late endosomal or lysosomal system where the contents will be either broken down or transported to other sites of the cell. It is most likely that EV uptake via macropinocytosis is coincidental rather than a purposeful action. Studies by Feng and colleagues and Christianson and colleagues have demonstrated through the use of inhibitors that the majority of EVs are still taken up into cells by phagocytosis and receptor-dependent endocytosis (Christianson, Svensson, van Kuppevelt, Li, & Belting, 2013; Feng *et al.,* 2010). Recently Heusermann and colleagues showed that EVs surf along filopodia to endocytosis hotspots at their base (Heusermann *et al.,* 2016). The EVs appear to 'surf' by taking advantage of the F-actin retrograde flow of the filopodia. A decrease in EV uptake is seen when actin polymerisation is inhibited (Heusermann *et al.,* 2016). Movement of poly-D-lysine coated beads along lamellapodia has also been observed (Nobezawa, Ikeda, Wada, Nagano, & Miyata, 2017).

Lipid raft-mediated endocytosis revolves around the lipid raft structure. The lipid raft is composed of tightly packed protein receptors and sphingolipids. This results in the lipid raft forming its own free moving domain in the PM (Simons & Ehehalt, 2002). These rafts are usually enriched in cholesterol and therefore able to influence membrane fluidity. A wide range of inhibitors have been used to test the validity of lipid rafts as an EV uptake route and the majority show a promising outcome for lipid raft dependent endocytosis (Mulcahy *et al.,* 2014).

1.13 EV Targeting

In order to perform gene therapy successfully with EVs, the EV must be tailored to deliver the cargo accurately. For example, if the EV contains DNA for recombination of genes it must be able to deliver its cargo to the nucleus. Alternatively, if the cargo of the EV is for RNA interference it must be delivered to the RISK complex in the cytosol of the cell (Guo & Huang, 2013). There have been multiple successful attempts to target various sites of animal models and humans (Ohno *et al.*, 2013). Alvarez-Erviti and colleagues took advantage of the Lamp2b protein found in the membrane of EVs and made two fusion proteins that would target two different areas in a mouse. The first fusion protein inserted was Rabies Viral Glycoprotein (RVG); this was to target neurones as RVG specifically targets Acetylcholine Receptors. The second fusion protein was made with Muscle Specific Peptide (MSP) which targets muscle cells. Both muscle and neuronal cells were significantly targeted in this experiment with the RVG EVs passing through the blood brain barrier (BBB) to reach their target. This

suggests that EVs are able to pass through into immunologically exclusive sites. Furthermore BACE1 knockdown occurred when RVG fused EVs were loaded with BACE1 siRNA, demonstrating a role for these EVs in treating Alzheimer's Disease (AD) (Alvarez-Erviti *et al.,* 2011). Liu and colleagues also successfully used the Lamp2b RVG fusion protein in their study of delivering Mu siRNA to treat Morphine relapse. This emphasizes the effectiveness of RVG fusion targeted EVs (Liu *et al.,* 2015). Furthermore, the cell of origin of the EVs can be used to target a specific area. For example, Mesenchymal Stem cells (MSC) have been used to produce MiR-9 loaded EVs in order to target Glioblastoma Multiforme (a cancer of the central nervous system) and reduce the expression of P-glycoprotein (Munoz *et al.,* 2013). Judging by the positive results of the studies mentioned above, EVs can be easily manipulated to deliver cargo to a target area in the body and more specifically a target cell type.

1.14 External Cargo Loading

The second main method of loading cargo into EVs is *ex vitro*. In method, EVs are first isolated from cell media by a variety of techniques. The current most widely used method, because of its lack of expense and time, is ultracentrifugation. Other methods include sucrose cushion density grade ultracentrifugation, filtration, size exclusion chromatography and chemical commercial methods which are sold as kits and usually involve precipitating out the EVs. Sucrose cushion density grade ultracentrifugation is considered the most clinically clean method, enriching samples in exosomes rather than other EVs. Once the EVs have been isolated and characterised, they can be stored at -80 °C over long periods with minimal changes to vesicle size and number, at -20 °C with small structural changes or at 4°C or room temperature overnight without loss of function (Lőrincz *et al.,* 2014). However, it is recommended that fresh isolations are used whenever possible to reduce the risk of losing function or the characteristics of EVs changing. External loading of the EVs can now be attempted by several methodologies.

1.14.1 Electroporation

Electroporation is one such method where EVs are suspended in fluid between two conducting plates (figure 1-16) and an electrical potential applied. The electrical potential, in an attempt to conduct through the fluid and to the opposite conducting plate, presumably punches a hole in the outer membrane allowing the movement of particles into the EV. If the concentration of cargo around the EVs at the time of electroporation is high, then theoretically a sample of the cargo should enter the EV. Once the EVs have resealed some of them should contain cargo. Due to the nature of electroporation there will likely be a proportion of EVs that do not reseal or a population of EVs that have increased in size due to fusion. There has been a high profile study claiming the successful integration of siRNA by electroporation into EVs (Alvarez-Erviti *et al.,* 2011). In contrast to the claims of success, there has been a study published looking at the effects of electroporation on siRNA which indicates that siRNA aggregates to form large particles rather than be loaded into EVs (Kooijmans *et al., 2013)*. Whilst a study preventing the aggregation of EVs during electroporation has been published (Hood, Scott, & Wickline, 2013), there is yet to be an answer to preventing siRNA aggregation.

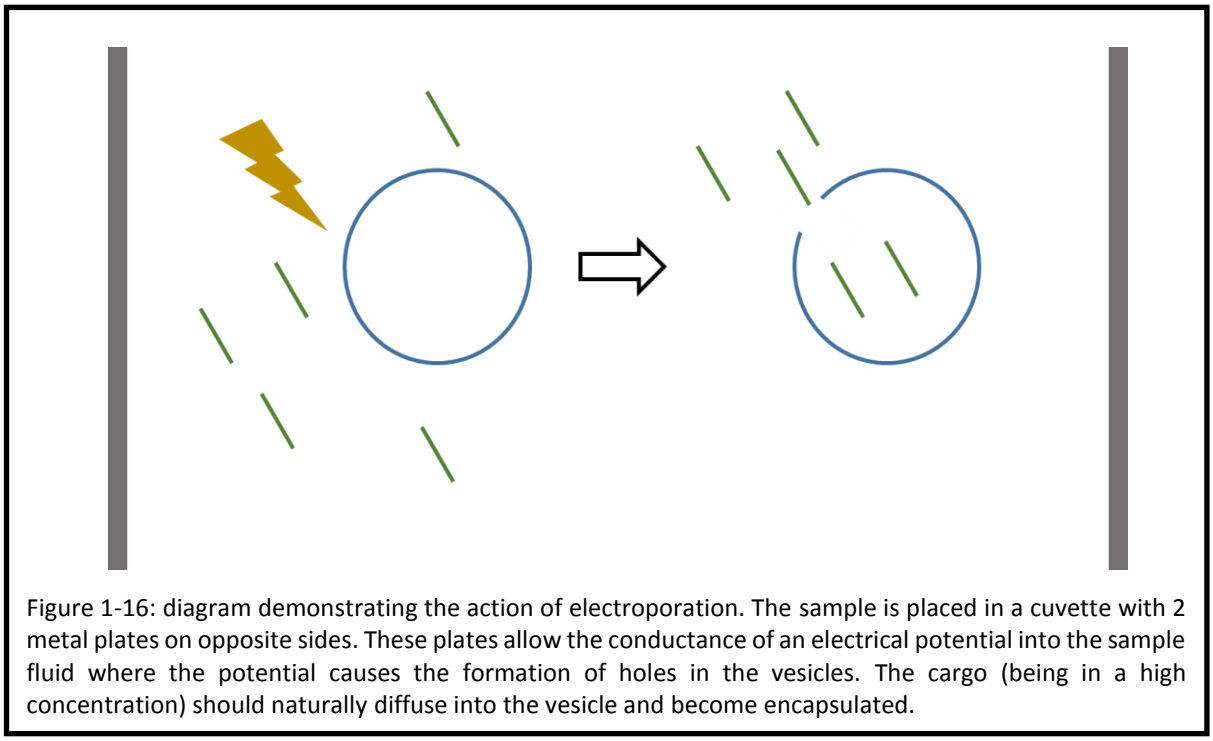

Figure 1-16: diagram demonstrating the action of electroporation. The sample is placed in a cuvette with 2 metal plates on opposite sides. These plates allow the conductance of an electrical potential into the sample fluid where the potential causes the formation of holes in the vesicles. The cargo (being in a high concentration) should naturally diffuse into the vesicle and become encapsulated.

1.14.2 Sonication

A second method for *ex vitro* loading of EVs is sonication. Sonication is perhaps even more destructive than electroporation, however more success has been seen with this method. During sonication, the sample is once again suspended in a small volume of fluid with a high concentration of the cargo of choice. A probe is used to transmit ultrasound energy waves and focus them on a point in the fluid (figure 1-17). Microbubbles are formed during the energy transfer which both expand and collapse causing extremely high pressures and temperatures inside of the microbubbles (Gong, 1998). These extreme conditions cause vapour to be formed inside the microbubbles and the release of free radicals to occur for use in chemical synthesis reactions (Gong, 1998). However, for cargo loading, interest lies not in the free radicals but the cavitation to damage and tear open the EVs. Theoretically if EVs can be sonicated at a low enough energy transfer level then minimal damage can be applied to the EVs, also encouraging the formation of inlets in the EV structure. This is very similar to the method of loading during electroporation where the concentration gradient encourages the movement of cargo into the EV before the EV reforms. Sonication has been successfully reported to load both nanoparticles and EVs (Haney *et al.,* 2015; Sharma, Yusuf, & Pathak, 2014). Haney *et al*. loaded EVs via several methods of which sonication was observed to be the most effective *(*Haney *et al.,* 2015). They

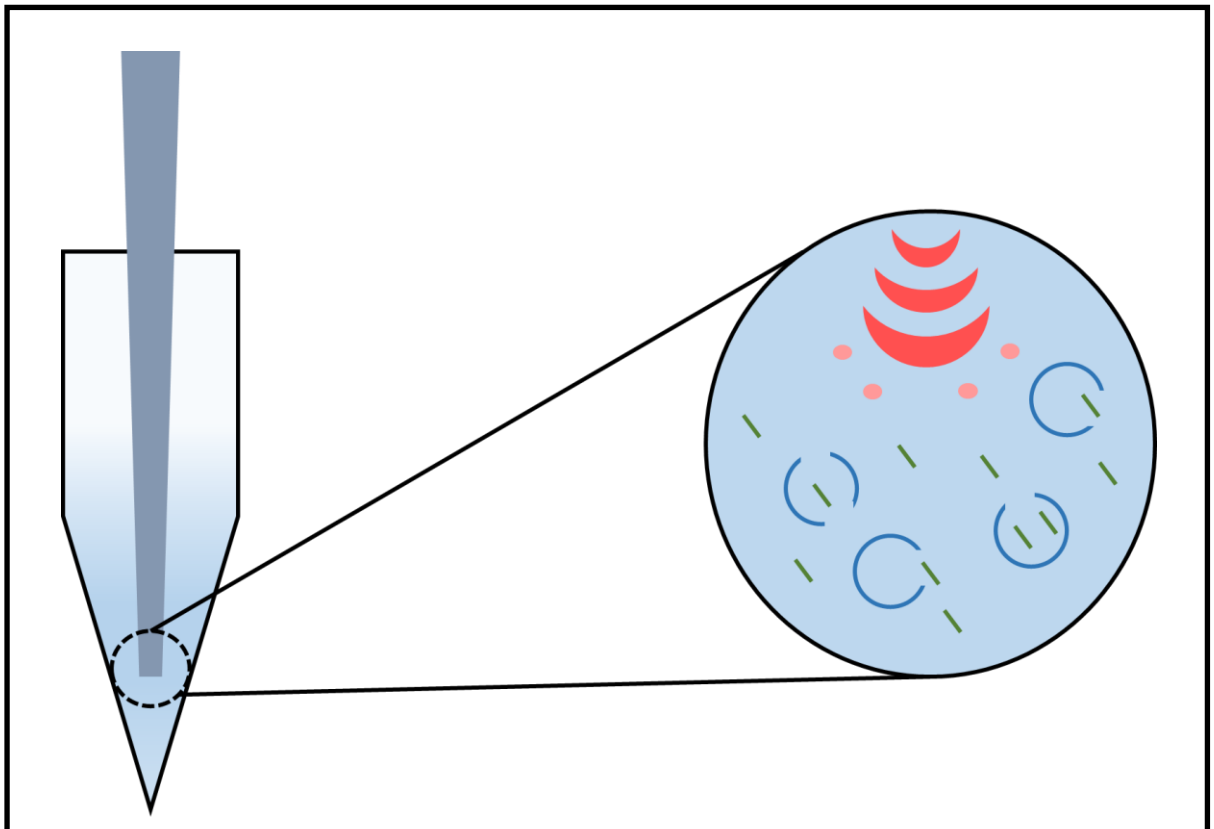

Figure 1-17: diagram showing the action of sonication and how it disrupts vesicles. Energy waves are emitted from the probe in the liquid. This causes cavitation to occur which disrupts the vesicles. Also in the liquid is a high concentration of cargo which should naturally transfer into the vesicles before they repair and reform.

loaded a large protein called catalase therefore a similar method can be used to load cargo of the same size or smaller.

1.14.3 Cell Penetrating Peptides

Other methods that could be of potential use loading EVs *ex vitro* include cell penetrating peptides (CPPs) (figure 1-18). CPPs are a family of natural or synthetic proteins which contain domains that allow passage of cargo proteins through the PM. CPPs can be cationic, amphipathic or hydrophobic molecules capable of binding cargoes and transporting them to the inside of cells (Mussbach, Franke, Zoch, Schaefer, & Reissmann, 2011). Cationic peptides rely on their high positive charge to associate with the anionic cell membrane and glycocalix. CPPs can bind either covalently or non-covalently with their cargo. The advantage of using non-covalent bonds over covalent bonds is the lack of change in the cargoes structure or sequence upon binding. Using a non-covalent bond also means that the cargo can theoretically dissociate from the CPP and be released into the cell unchanged. This is particularly useful if the CPP used incorporates itself into the PM. Whilst some CPPs rely on a covalent bond formation with their cargo, the CPPs that will be discussed in this research were used to form non-covalent bonds. This is because the cargo destination is the nucleus. Studies have also shown that depending on the CPP used and method of penetration into the cell, that CPPs can incite the PM repair response therefore preventing any residual damage (Palm-Apergi, Lorents, Padari, Pooga, & Hällbrink, 2009). With many of the older generation CPPs it was found that they struggled with delivery of nucleic acid cargoes to the nucleus. The incorporation of Nuclear Localisation Sequences (NLS) into CPPs has shown promising results with linear DNA (Cartier & Reszka, 2002). A further challenge was also seen in the delivery of nucleic acids in general as they are anionic,

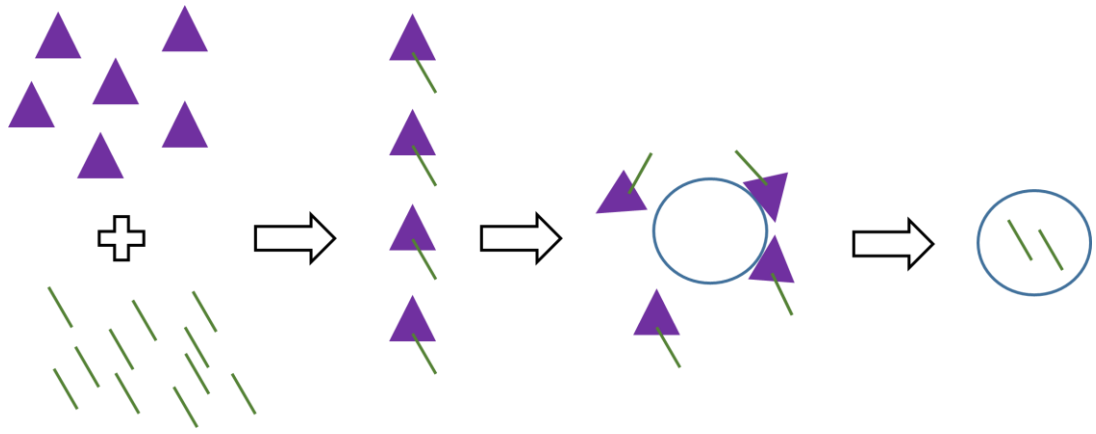

Figure 1-18: diagram showing the process of CPP complex formation and delivery of cargo into the cell or vesicle. The CPP initially interacts with the cargo through ionic bonds due to the difference in charge between the cargo and CPP. The complex then interacts ionically with the membrane of a cell or vesicle but does not bind to a receptor. The CPP, using its structure, charge and hydrophobicity disrupts the membrane through which the cargo is delivered.

the same as the PM. However, this has been overcome by synthesising highly cationic CPPs such as CADY. There have only been a couple of studies that looked at the toxicity of CPPs. CPP cytotoxicity is caused by perturbation of the PM where the cell does not repair or is not able to repair quickly the disturbance in the PM where the CPP has bound. Saar and colleagues found that MAP and Transportan-10, out of the selection of CPPs that they tested for cytotoxicity, were the most cytotoxic (Saar *et al.,* 2005). However, there are uses for cytotoxic CPPs such as treating cancerous cells. Many CPPs have been synthesised, here I will talk about the three concerned in this research; MPGα, CADY and JBS Nucleoducin.

MPGα is an amphipathic peptide. It is a chimeric protein made from a combination of the fusion sequence of HIV gp41 and the NLS of SV40 T-antigen (M. C. Morris, Vidal, Chaloin, Heitz, & Divita, 1997). As such it is able to deliver oligonucleotides into cells. As mentioned above, MPGα is a non-covalent linking CPP which gives it the advantage of not having to go through a chemical bonding process prior to use. Simeoni and colleagues have shown in their study that the MPGα action of penetration is endocytosis independent. This is because MPGα can deliver siRNA to the nucleus when endosomal pathway inhibitors are co-administered (Simeoni, Morris, Heitz, & Divita, 2003). Thus there is less chance of cargo being degraded or sent to the wrong organelle. Furthermore, upon binding siRNA as a cargo, MPGα changes its structure to a more stable helical form (Konate *et al.,* 2010). MPGα has shown success in embryonic stem cell studies (Zeineddine *et al.,* 2006).

CADY, similar to MPGα, is also an amphipathic molecule. It is able to spontaneously insert into the membrane and undergoes a helical conformation change upon interaction with siRNA cargo. The helical conformation allows the exposure of certain residues to form three domains; tryptophan, charged residues and hydrophobic. It has been found that CADY is one of the most hydrophobic and therefore most stable CPPs (Keller *et al.,* 2013). This means that in an aqueous environment it will readily bind itself to the PM and reduce the time it takes for the CPP to come into initial contact with the cell. CADY is a synthetic peptide made from a combination of PPTG1 peptide, Tryptophan and charged amino acids (Laurence Crombez *et al.,* 2009). Incubation times as short as 30 minutes were seen for CADY uptake with an siRNA cargo where target knockdown was successful (Laurence Crombez *et al.,* 2009).

JBS-Nucleoducin is a cocktail of CPPs rather than a homogenous population. This allows for coverage of different cargoes and allows multiple cell type delivery. Whilst the composition of CPP cocktails remains a secret with the manufacturer, they are usually either hydrophilic or hydrophobic.

1.15 Aims

The aim of this thesis was to test the suitability of various methods to load EVs with ERAP1 siRNA.

First it was necessary to characterise the EVs to be used in experiments and prove their presence. To do this NTA, flow cytometry and western blotting were used.

Next a list of ten well-known methods and novel methods, some adapted, were compiled based on the literature (Alvarez-Erviti *et al.*, 2011; Canatella, Karr, Petros, & Prausnitz, 2001; Laurence Crombez *et al.*, 2009; Haney *et al.*, 2015; Kim *et al.*, 2011; Mohr, De Pablo, & Palecek, 2006; Momen-Heravi *et al.*, 2014). These methods were then scrutinised through repetition according to established methods and alterations made in order to optimise aspects. Analysis of EV loading was carried out by flow cytometry, fluorescence detection, NTA or western blotting. If methods suggested successful loading, the method was used to deliver cargo to cells in a cell assay.

As the use of ERAP1 siRNA is based around the downregulation of inflammation in AS. The EV loading method that appeared most successful was used to load two drugs, Celecoxib and 2, 5-dimethyl-Celecoxib, suggested in the literature to upregulate the unfolded protein response. This may aid inflammatory downregulation in AS.

Chapter 2: Methods and Materials

2.1 Materials

2.1.1 Cell Culture

Material	Details
RPMI 1640	Gibco, Life Technologies
0.25 % Trypsin/EDTA	Gibco, Life Technologies
Kanamycin	Gibco, Life Technologies
FCS	Gibco, Life Technologies
24-well plate	Thermo Scientific
12-well plate	Thermo Scientific
6-well plate	Thermo Scientific, cat no. 140 675
Hygromycin B	Invitrogen (used at 0.1 mg/ml)
G-418	(used at 0.5 to 1 mg/ml)
96-well plate (flat bottomed)	Thermo Scientific
96-well plate (round bottomed)	Thermo Scientific
T25 Flasks	Easy Flask Filtered 25, Thermo Scientific
T75 Flasks	Easy Flask Filtered 75, Thermo Scientific
Puromycin	Sigma (used at 1 µg/ml)

Cell Line	Growth Media	Details
HeLa	5-R-K (see section 2.2.1 for definition)	Adherent (Human epithelial cell line)
HeLa.B27	5-R-K + 0.1 mg/ml Hygromycin	Adherent (as above, stably transfected with HLA-B*27:05)
HUVEC hTERT	2.5-R-K	Adherent (hTERT immortalised human umbilical cell line)
CEM	5-R-K	Non-Adherent (Human T lymphoblastoid cell line)
CEM sh2 (ERAP1 shRNA2)	5-R-K + 0.1 mg/ml Puromycin	Non-Adherent (as above, stably transfected with ERAP1 shRNA)

CEM NEG (neg control shRNA)	5-R-K + 0.1 mg/ml Puromycin	Non-Adherent (as above, stable transfected with control scrambled shRNA)
CEM.B27	5-R-K + 1 mg/ml G418	Non-Adherent (as above, stably transfected with HLA-B*27:05)
Jurkat	5-R-K	Non-Adherent (Human T cell leukaemia line)
Jesthom	5-R-K	Non-Adherent (Human EBV transformed B cell line)
U937	5-R-K	Non-Adherent (Human monocytic cell line)
C58.B27	RPMI + 1 mg/ml G418	Non-Adherent (Rat T cell line stably transfected with HLA-B*27:05)

2.1.2 Flow Cytometry Antibodies

Material	Details
FITC anti-CD9	AbD Serotec, FITC, MCA2656F
FITC anti-CD123	eBiosciences, FITC, 6HC
FITC anti-CD80	eBiosciences, FITC, 2D10.4
AF488 anti-CD63	Santa Cruz, AF488, SC-5275
Anti-Me1	Powis laboratory stocks
Anti- HLA-B and -C (HC10)	Powis laboratory stocks

2.1.3 Western Blot Antibodies

Material	Details	Concentration
Anti-GAPDH	Santa Cruz (mouse mAb IgG1, sc-47724, lot no: L2010	1:13000 (i.e. 1µl in 13 ml)
Anti-HRD1 (Synoviolin)	Santa Cruz (rabbit polyclonal Ab IgG1, sc-130889, lot no: A0313)	1:13000
Anti-GRP78 (BiP)	St Johns Laboratory (lot no: B0801, cat no: STJ97526)	2:13000

Anti-PDI	Santa Cruz (mouse mAb IgG1, sc-376370, lot no: A1314)	1:13000
Anti-HERP(UD1)	Abcam (rabbit mAb, ab150424)	1:13000
Anti-Calnexin	Stressgen (SPA-860)	1:13000
Anti-Calreticulin	Stressgen (SPA-600)	1:13000
Anti- HLA-B and -C (HC10)	Powis Laboratory Stocks	4:13000
Anti-ERAP1	Santa Cruz (rabbit polyclonal IgG1, sc-98254, lot no: A0109	4:13000
Anti-ERAP1 (ARTS1)	Abcam (mouse mAb, ab65162-100, lot: 507220)	4:13000
Anti-ERAP1	R&D Systems (mouse mAb IgG1, clone 6119, cat no. MAB2334, lot no. CBKI0108111)	4:13000
Anti-β Actin	Santa Cruz	1:13000
HRP anti-mouse	Novex Rabbit anti mouse IgG HRP (A16166)	1:13000
HRP anti-rabbit	Sigma goat anti-rabbit IgG HRP (A0545)	1:13000
800CW goat anti-mouse	Li-cor (Lot no. C40528-02)	1:13000
800CW goat anti-rabbit	Li-cor (Lot no. C40325-02)	1:13000
Exosome-anti-CD9 (Ts9)	Invitrogen (mouse mAb IgG1, 10626D, lot no. DAP-PF140424T2) (non-reduced)	3:13000
Anti-ALIX	Santa Cruz (mouse mAb IgG1, sc-53538, lot no. J2406)	3:13000
Anti-TSG101	Santa Cruz (mouse mAb IgG2a, sc-7964, lot no. G0207)	3:13000
Exosome-anti-CD63 (Ts63)	Invitrogen (10628D, mouse mAb IgG1, lot no: DAQ-PF150624) (non-reduced)	3:13000
Exosome-anti-CD81 (M38)	Invitrogen (10630D, mouse mAb IgG1, lot no: 521514) (non-reduced)	3:13000

2.1.4 Plasmids

Material	Details
pSuperRetro miR-US4-1	Kwaesong Ahn (South Korea)

Suresilencing ERAP1 shRNA Plasmid	Qiagen (cat no. 336314 KH01107P)

2.1.5 siRNA

Material	Details
GAPDH siRNA	Qiagen (cat no. SI02653266, lot no. 195522409)
Allstars siRNA	Qiagen (batch nos. 186182780, 194531115, 182224853, 213959180)
ERAP1 siRNA	Qiagen, flexitube (cat no. SI04955419)
ERAP1 siRNA	R&D (details not found)
ERAP1 siRNA	Santa Cruz (details not found)
ERAP1 siRNA	Thermo Fisher (details not found)

2.1.6 Hardware

Material	Details
NAP-10 Columns Sephadex G-25, DNA Grade	Illustra, GE Healthcare (cat no. 17-0854-01)
Black Optics 96-well Flat Bottom Plate	Perkin Elmar
Cell Culture Centrifuge	Wifug 500E
Floor Centrifuge	Jouan CR312 floor centrifuge
Bench-top Centrifuge	Eppendorf, centrifuge 5417R
Ultracentrifuge	Beckman Coulter, Optima L-100 XP
Incubator	Galaxy S, CO_2 Incubator, Wolf Laboratories
Microscope	CK, Olympus Tokyo
1.5 ml Microtubes	Axygen
Western Blot Equipment	Bio-Rad
Bio-Rad Power Pac 300	Bio-Rad
Chromatography Paper	Whatman 3MM chromatography paper
Nitrocellulose	Amersham Protran 0.45 um nitrocellulose membrane, GE Healthcare Life Sciences
RT Shaker	Stuart Scientific Platform Shaker STR6
Cold Room Rocker	Stuart See-saw Rocker SSL4
Chemiluminescent Detector, LAS-3000	Fujifilm
Li-cor Odyssey CLx	Li-cor
15 ml Falcon Tubes	Cellstar, Greiner Bio-one, cat no. 188271
50 ml Falcon tubes	Cellstar, Greiner Bio-one, cat no. 227261
0.22 µm Filters	PES 0.2 um, 33 mm, Milles-GP filter unit
Amicon Ultra 0.5 ml filters	Merck Millipore

Ultraclear Ultracentrifuge tubes	Beckman Coulter, Ultraclear centrifuge tubes, 25 x 89 mm
Needles (25G and 30G)	BD Microlance 3
Syringes (1 ml and 20 ml)	Terumo
Nanosight LM-10, 640 nm red laser	Nanosight (now Malvern Instruments)
Temp Probe for NTA	Omega HH804
Flow Cytometer	Millipore Guava Easycyte 8HT
Water Sonicator	Camlab CamSonix C080T
BioRad Gene Pulser	BioRad
Cuvettes	BTX, Electroporation Plus Cuvettes
Sonicator	QSonica Q700 Sonicator
Orbital Incubator	Stuart Scientific Orbital Incubator SI 50
UV Light Box	Herolab UVT-20M
ChemiDoc (Iberose Gel Reader)	BioRad Molecular Imager ChemiDoc XRS+
Axiovert	Axiovert 40 CFL, Zeiss
0.2 µm Pore Transwells	Corning
Spectrophotometer	DYNEX Technologies MRX
Fluorimeter	BMG Labtech FLUOstar Microplate Reader
Sw32Ti Rotor and Buckets	Beckman Coulter, S/N: 10U 2562
Sw55Ti Rotor and Buckets	Beckman Coulter, S/N: 10E 0316
Balance	Ohaus Precision Plus
DNA Gel Tank and Casting Chamber	Peqlab Perfect Blue horizontal midi gel

2.1.7 Reagents

Material	Details
peqGOLD Protein Marker III	Peqlab (lot no.178767)
RNase A	Qiagen
XL10-Gold Ultracompetent cells	Stratagene (cat no. 200315)
Mini plasmid purification kit	Qiagen
Midi plasmid purification kit	Qiagen
Maxi plasmid purification kit	Qiagen
100 nm beads	Malvern Instruments
200 nm beads	Malvern Instruments
400 nm beads	Malvern Instruments

EcoR1 restriction endonuclease	promega
HindIII restriction endonuclease	promega
4 % W/V Latex Beads	Invitrogen, Life Technologies (A37304, lot. no. 51938A)
Lipofectamine 2000	Invitrogen, Life Technologies (cat no. 11668-027)
Anti-CD63 magnetic beads	Invitrogen
Alamar Blue	Invitrogen
BCA protein estimation kit	Thermo Scientific
Celecoxib	Sigma-Aldrich
25 kDa, LMW, linear PEI	Polysciences Inc.
Phosphate Buffered Saline (PBS)	Stocks made up in 1L ddH_2O at 10 x PBS : 79.4 g NaCl, 2 g KCl, 2 g KH_2PO_4, 7.7 g $Na_2HPO_2.2H_2O$, pH7.4
NaCl	Fisher Scientific
KCl	VWR International LTD
KH_2PO_4	BDH Chemicals LTD
$Na_2HPO_2.2H_2O$	Acros Organics
Lysis Buffer	1 % NP40, 150 mM NaCl, 10 mM Tris pH 7.6, 100mM NEM and 1 mM PMSF
NP40	Sigma Aldrich
NEM	Sigma E3876
PMSF	Sigma
Running Buffer	0.3 % w/v Tris, 1.4 %w/v Glycine and 0.1 %w/v SDS
Tris	Sigma
Glycine	Acros
SDS	Sigma
2,5-di-methyl Celecoxib	Sigma-Aldrich
Ponceau Red	Sigma
Milk Powder	Tesco instant dried skimmed milk powder
CADY	Jena Biosciences Germany
PFN	PBS, 2 % FCS and 0.1 % N_3^-

MPGα	Jena Biosciences Germany
JBS Nucleoducin	Jena Biosciences Germany
IFNγ	Immunotools (11343534)
XL-10 Ultracompetent Cells	XL-10 Gold, Stratagene
Luria Broth (LB) Granules	Fisher Scientific
Iberose agarose	Web Scientific, lot no. W-090025
LB Amp Plates	In house generated, 100 µg/ml amp
BCA	Thermo Scientific, Pierce BCA Protein Assay
BSA (for BCA)	Thermo Scientific Albumin Standard
Reducing Sample Buffer (RSB)	50 mM Tris.Cl, 100 mM Dithiothreitol (DTT), 2 % SDS, 0.1 % Bromophenol Blue and 10 % glycerol
Non-RSB	50 mM Tris.Cl, 2 % SDS, 0.1 % Bromophenol Blue and 10 % glycerol
Bradford assay	Sigma
Tris Acetate EDTA (TAE)	pH8, 242 g Tris, 18.6 g EDTA, 57.1 ml Glacial Acid
Safeview DNA stain	NBS Biologics LTD
DNA Ladder	Generuler 1kb DNA Ladder, Thermo Scientific
Triton X-100	Sigma Aldrich
Transfer Buffer	0.3 % w/v Tris and 1.44 % w/v glycine
PBS TWEEN	1 x PBS + 0.1 % TWEEN 20
TWEEN 20	Sigma
Supersignal West Femto Kit	Thermo Scientific

2.2 Methods

2.2.1 Routine Cell Culture

Cell Lines were maintained in appropriate cell culture media (see table 2.1.1 above) at 37 °C and 5 % CO_2. A 6-well stock plate (Thermo Scientific, cat no. 140 675) of all cell lines under use at the time was constantly maintained. Upon reaching confluency in the 6-well plate, cells were harvested (approx. 90 %) and a fraction of the cells returned to fresh media. In the case of adherent cells, the cells were first gently trypsinised and the remainder replenished with fresh media.

Adherent cells for experiments were prepared beforehand by seeding a 6-well plate from the stock plate and allowing it to grow to confluency. Non-adherent cells were prepared beforehand by seeding cells from the stock well into a T25 flask (Easy Flask Filtered 25, Thermo Scientific) and adding 5-10 ml of media.

In preparation for EV Isolation, non-adherent cells were seeded into a T75 flask with 20 ml of 5-R-K (5 % FCS (Gibco), RPMI medium 1640 + GlutaMAX (Gibco) and 100 µg/ml Kanamycin (Gibco)). When the 5-R-K indicated that the cell media was becoming acidic an additional 20 ml of 5-R-K was added. When the 5-R-K indicated acidity a second time cells were centrifuged for 5 minutes at 300 x*g* (Wifug 500E), the supernatant discarded and the cells re-suspended in a clean T75 (Easy Flask Filtered 75, Thermo Scientific) flask containing 20 ml RPMI with no serum (see EV Isolation, section 2.2.4).

To prepare adherent cells for EV isolation, the stock well was trypsinised by removing cell media, adding 3 drops of 0.25 % trypsin-EDTA (Gibco, Life Technologies) and returning the plate to the incubator (Galaxy S, CO_2 Incubator, Wolf Laboratories) (37 °C and 5 % CO_2) for 2 minutes. Once the cells had detached from the culture plate they were divided evenly between 6 x T75 flasks with 20 ml 5-R-K. If media indicated acidity before cells reached confluency an extra 20 ml 5-R-K was added. Once cells were confluent the 5-R-K was removed from the T75 and replaced with 20 ml RPMI without serum (see EV Isolation section).

2.2.2 Protein Concentration Measurement

This was done with a BCA microplate assay (Pierce BCA Protein Assay, Thermo Scientific). Lysates intended for western blot were diluted 1 in 100 and 1 in 10 in 1 x PBS in a clean 1.5 ml microtube and 50 µl added in triplicate to a flat bottom 96-well plate. A BSA concentration gradient was made by diluting stock BSA (Thermo Scientific Albumin Standard) in 1ml PBS to a starting concentration of 1mg/ml. This was then diluted down a 1 in 3 concentration gradient 5 times by transferring 100 µl of the previous concentration into a clean 1.5 ml microtube with 200 µl PBS inside. 50µl of the concentration gradient was then pipetted in to the 96-well plate in triplicate. A 50 µl blank of PBS was also added in triplicate. BCA solution was then prepared as instructed by the manufacturer and 50 µl of this added to each well in use. The plate was left to shake at 50 rpm, 37 °C for 20 min. After incubation, the 96-well plate was loaded into a Spectrophotometer (Dynex Technologies MRX) and the optical density measured at 570 nm. End calculations were incorporated to account for the dilutions of the starting sample. This allowed the western blot wells to be loaded equally according to protein content.

For samples of EVs diluted in Triton-X100, the protein content was measured by BCA as above except using triton-X100 instead of PBS.

The concentration of proteins that had not been exposed to reducing agents or detergents such as the concentration of protein seen in EV samples was measured by Bradford assay. 50µl ddH_2O

was pipetted into the first 6 wells of a flat bottom 96-well plate in triplicate. 50 µl of Bradford reagent (Sigma) was then added to all water wells and pipetted gently to mix. BSA was diluted down to 0.1 mg/ml and 10, 8, 6, 4 and 2 µl added to the first 5 wells. The 6th well remained a blank control. Then 1 µl of sample was added to each sample well and optical density measured at 600 nm. For samples where 1 µl was too concentrated, samples were first diluted 1 in 10 or 1 in 100 before being read. Dilutions were corrected for during calculations.

2.2.3 Sephadex Enrichment

PD-10 columns (PD-10 Desalting Columns, GE Healthcare) were initially used to enrich the EV samples after cargo encapsulation or complexation in order to remove unbound cargo. Later NAP-10 columns (Illustra NAP-10 Columns, Sephadex G-25, DNA Grade, GE Healthcare) were used. First the column was washed with 15 ml 1 x PBS or RPMI (Gibco), then 0.5 ml of sample added to the column followed by a further 0.5 ml PBS or RPMI. A maximum of 1 ml of sample could be added to the column with no additional buffer added. Once this had entered the column bed completely, 1.2-1.5 ml elution buffer (in the case of NAP-10 columns) was added and the eluate collected in a clean 15 ml falcon tube.

2.2.4 Fluorimetry

Fluorescence of Allstars siRNA was assessed by a BMG Labtech FLUOstar Microplate Reader. A fluorescence concentration gradient was assembled by diluting half the sample input concentration of Allstars siRNA into 1 ml 1 x PBS or Triton X-100 in a clean 1.5 ml microtube. This was then diluted 1 in 3, five times by taking 100 µl of the previous concentration and adding it to 200 µl of 1 x PBS or Triton X-100 in a clean 1.5 ml microtube. This made a total of 200 µl per concentration value with 900 µl in the first and 300 µl in the last concentrations. 50 µl of gradient was pipetted in triplicate into a black, flat clear bottomed 96-well plate (Perkin Elmar). 50 µl of blank PBS or Triton X-100 was also added in triplicate. 50 µl of enriched samples were diluted 1 in 4 into 150 µl of either PBS or Triton X-100 and added in triplicate to the plate. The plate was covered in foil to avoid exposure to light whilst in transit to the plate reader. The concentration gradient was used to construct a curve in order to calculate the concentration of Allstars siRNA present in the well and therefore present inside of EVs. Dilutions were also taken into account in these calculations.

2.2.5 Cell Lysis

Adherent cell line lysis was performed on the following cell lines: HeLa, HeLa.B27 and HUVEC hTERT.

A 6-well plate (Thermo Scientific, cat no. 140 675) of confluent adherent cells were first incubated with 3 drops of 0.25 % trypsin-EDTA incubated for 2 minutes at 37 °C in 5 % CO_2. 1 ml 5-R-K was then added to dilute the trypsin and all fluid transferred from the plate in to a 1.5 ml clear microtube. Microtubes were then centrifuged (Wifug 500E) at 300 x*g*, the supernatant discarded and

cells re-suspended in 200 µl cold PBS. Cells were then washed 3 times by centrifuging at 300 x*g* (Jouan CR312 floor centrifuge), discarding supernatant and re-suspending cells in 100 µl cold 1 x PBS. After the last wash step, cells were re-suspended in Lysis buffer (1 % NP40, 150 mM NaCl, 10 mM Tris pH 7.6, 100mM NEM and 1 mM PMSF) and left on ice for 3 minutes. Next, lysates were centrifuged (Eppendorf, centrifuge 5417R) at 20200 x*g* for 10 minutes at 4 °C. The top 90 % of the supernatant was decanted into a 1.5 ml microtube and stored for western blot.

A second method was also used. First the 6 well plate was placed on ice, all cell media was removed from each well, the well washed with 0.5 ml 1 x PBS and 100 µl lysis buffer (1 % NP40, 150 mM NaCl, 10 mM Tris pH 7.6, 100mM NEM and 1 mM PMSF) added. The wide end of a yellow pipette tip (i.e. upside down) was then used to scrape the well of cells for 5 seconds in both circular and linear motions. The cells were then left to incubate in the lysis buffer for 3 minutes on ice. Next, cells were centrifuged (Eppendorf, centrifuge 5417R) at 20200 x*g* for 10 minutes at 4 °C in a clean 1.5 ml microtube. The top 90 % of the supernatant was decanted into a clean 1.5 ml microtube and stored for western blot.

Non-adherent cell line lysis was performed on the following cell lines: CEM, CEM.B27, CEM sh2, CEM NEG, Jurkat, Jesthom and U937.

In the case of non-adherent cells, cells were re-suspended by pipetting and transferred into a clean 1.5 ml microtube. Microtubes were then centrifuged (Wifug 500E) at 300 x*g*, the supernatant discarded and the cells re-suspended in 200 µl cold PBS. Cells were then washed 3 times by centrifuging (Jouan CR312 floor centrifuge) at 300 x*g*, discarding supernatant and re-suspending cells in 100 µl cold 1 x PBS. After the last wash step, cells were re-suspended in lysis buffer, instead of PBS, and left on ice for 3 minutes. Next, cells were centrifuged (Eppendorf, centrifuge 5417R) at 20200 x*g* for 10 minutes at 4 °C. The top 90 % of the supernatant was decanted into a clean 1.5 ml microtube and stored for western blot.

2.2.6 Western Blot

Polyacrylamide Gel Construction

Bio-rad western blot equipment was used to carry out all western blots. A polyacrylamide gel was made by constructing a Bio-rad gel cast with 2 glass plates, a Bio-rad chamber, 2 spacers and a spacing guide card. The complete gel cast was then set into a holder to seal the bottom of the cast. 8, 10 or 12 % polyacrylamide gel (main gel) was then mixed according to the table below and 7 ml pipetted into the cast chamber. 1 ml of H_2O was carefully pipetted on top of the main gel so as to form an even layer between the surfaces. The gel was left to set for 20-30 minutes. Solidity of the gel was signalled by a clear line between the gel and the water pipetted on top. Next the stacking gel was mixed (according to the table below). The top layer of H_2O was removed from the main gel and stacking gel pipetted up to the top of the glass plates. A 15-well comb was inserted in the top of the

chamber, displacing some of the stacking gel and the gel left for 15 minutes to set. Once set the combs were removed, gel casts clipped into a gasket and placed into the gel tank. Running buffer (0.3 % w/v Tris, 1.4 % w/v Glycine and 0.1 % w/v SDS) was added to the tub to cover the bottom black gel cast screws and the inner chamber of the gasket filled.

Polyacrylamide Gel Electrophoresis

A 1:1 ratio of cell lysate and either reduced or non-reduced sample buffer (maximum total 20 µl per sample) was heated at 80 °C for 45 seconds in a 1.5 ml microtube before being pipetted into the corresponding gel well. The gel was set to run at 150 V using a Bio-rad Powerpac 300 and stopped once the sample buffer dye front had reached the bottom of the gasket. To transfer the blot, cassettes (Bio-rad) were prepared with sponges, chromatography paper (Whatman 3mm chromatography paper) and nitrocellulose transfer paper (Amersham Protran 0.45 µm nitrocellulose membrane, GE Healthcare Life Sciences). The gel was sandwiched between the nitrocellulose paper and the blotting paper inside the cassette and the cassettes placed in a tub. An ice container was slotted into the tub and transfer buffer (0.3 % w/v Tris and 1.44 % w/v glycine) was added to fill the tub. The transfer was ran at 100 V for 30 minutes on a Bio-rad Powerpac 300. After 30 minutes the nitrocellulose was removed from the cassette and placed in a container of distilled H_2O on a Stuart Scientific Platform Shaker STR6 at 30 rev/minute. H_2O was removed and 10 ml Ponceau red (Sigma) was added to assess the blot for protein transfer or transfer defects. The Ponceau red was left on for 10 seconds and then poured back into the bottle and residual dye washed off with water. Blocking solution (approximately

Gel Percentage →	**8% (10ml)**	**10% (10ml)**	**12% (10ml)**	**Stack**
H2O (ml)	4.6	4.0	3.3	5
30% Acrylamide (ml)	2.7	3.3	4.0	1
1.5 M Tris (pH8.8) (ml)	2.5	2.5	2.5	2.5 (Tris pH6.8)
10% SDS (ml)	0.1	0.1	0.1	0.1
10% AMPS (ml)	0.1	0.1	0.1	0.1
TEMED (ml)	0.006	0.004	0.004	0.01

1-2 g Tesco instant dried skimmed milk powder and 40 ml PBS TWEEN) was added and the blot left on the shaker for 15 minutes. Next the primary Ab was added (for dilutions please see Western Blot Antibody table) to PBS TWEEN and the blocking solution replaced by the primary Ab solution. The nitrocellulose was then left in this solution overnight in the cold room on a rocker (Stuart See-saw rocker SSL4) at 13 oscillations/minute before replacing the solution with secondary Ab solution.

Primarily anti-mouse or anti-rabbit horseradish peroxidase (HRP) secondary antibody and a Fujifilm Photobox was used to study the western blots however the laboratory later adopted Licor

fluorescence imaging technology and Licor secondary fluorescent Ab. In the case of the HRP method, the secondary anti-mouse HRP Ab was diluted into 15 ml PBS-TWEEN and left on the nitrocellulose for 15 minutes at RT on the shaker before removal, three 1 x PBS-TWEEN washes and the addition of developing solution (Thermo Scientific Supersignal West Femto Kit). The developing solution was left on for 1 minute before excess being absorbed off the side of the blot with white roll (Wypal L20). The nitrocellulose was then sandwiched between 2 acetate sheets and viewed in the Fujifilm Photobox using Precision, Manual, Standard/High, 1 minute and Chemiluminescent settings.

For the Li-cor secondary Ab, either Li-cor 800CW goat anti mouse (Lot no. C40528-02) or Li-cor 800CW goat anti rabbit (Lot no. C40325-02) Ab was added 1 in 13000 in PBS-TWEEN to the nitrocellulose membrane and left covered for 1 hour at RT. The nitrocellulose was then washed 3 times in PBS TWEEN and 3 times in PBS (5 minutes for each wash), and left to dry for at least 30 minutes in a dark environment. The nitrocellulose was then viewed and analysed on the Licor Odyssey CLx.

2.2.7 EV Isolation

EVs were isolated from cell culture media (see cell culture table for media specific to cells). Two days previous to media collection, normal cell media contained in a T75 flask (Thermo Scientific, Easy Flask 75 filtered) was replaced by 20 ml of serum free RPMI. Cells were then incubated at 37 °C, 5 % CO_2 for 48 hours. Cell media was decanted into 50 ml falcon tubes (Cellstar, Greiner Bio-one, cat no. 227261) and centrifuged (Wifug 500E) at 300 x*g* for 5 minutes. The supernatant was then decanted into a clean 50 ml falcon tube and filtered through a 0.2 µm filter (PES 0.2 µm, 33 mm, Milles-GP filter unit) into another clean 50 ml falcon tube. Buckets for a sw32Ti (Beckman Coulter, S/N: 10U 2562) or sw55Ti (Beckman Coulter, S/N: 10E 0316) ultracentrifuge rotor were cleaned and placed on a balance (Ohaus Precision Plus) with the corresponding lid. An Ultraclear (Beckman Coulter, Ultraclear centrifuge tubes, 25 x 89 mm) ultracentrifuge tube was inserted into the rotor bucket and approximately 45-50ml filtrate added for the sw32Ti and 4 ml for the sw55Ti. The balance was then zeroed and buckets removed. Balancing rotor buckets were placed on the balance and assembled with Ultraclear tubes and filtrate to return the balance to zero. Rotor buckets were then inserted in to their corresponding rotor and placed inside of the ultracentrifuge (Beckman Coulter, Optima L-100 XP). The Ultracentrifuge was ran at 100000 x*g* for 2 hours to pellet the EVs. After ultracentrifugation, Ultraclear tubes were carefully removed from the buckets and the supernatant carefully discarded without disturbing the pellet. The pellet was re-suspended in 50-100 µl 1 x PBS. EV concentration and protein concentration were then checked by NTA (Malvern Instruments) and GE NanoVue, respectively. Where EVs were not used fresh they were either stored at -20 °C, for long term use, or 4 °C for overnight use.

2.2.8 Nanosight Tracking Analysis (NTA)

NTA (Malvern Instruments) was used to view EV size and concentration. NTA can view and analyse 10-2000 nm (according to the manufacturer) spherical particles in both a homogenous and heterogeneous population sample. A maximum sample volume of 0.5 ml was used to load the chamber. First the chamber was washed with 1 ml ddH_2O from a 1 ml syringe and loaded with ddH_2O to ensure that there were no visible particles. The syringe was removed and used to pass air through the chamber, pushing out the residual ddH_2O in the chamber. Then the chamber was opened, wiped dry and closed. Sample was then loaded into a 1 ml syringe and gently pushed into the chamber via the input port. To prevent cross-contamination of samples the chamber was washed between samples. To wash the chamber, first the sample was pulled back out via the input port by retracting the syringe and the syringe removed and sample expelled back into the 1.5 ml microtube. Next the chamber was opened and wiped dry. The chamber was then closed again and a 1 ml syringe used to push ddH_2O through the chamber. The ddH_2O was absorbed onto white roll from the output port and the syringe again removed and reused to push air through the chamber, clearing residual ddH_2O. The chamber was again opened, dried with white roll and closed ready for the next sample. The camera level was set between 9 and 11, the particles loaded to measure 40-100 particles over a time period of 30 seconds and the detection threshold set to between 4 and 6. A temperature probe (Omega HH804) was used to determine the temperature of the sample and the viscosity of samples was set to that of water. Videos were recorded in triplicate by gently pushing through a small amount of the sample after each video and recording another video.

2.2.9 Flow Cytometry

A Guava 8HT with InCyte software was used to analyse the changes in characteristics of EVs, EVs attached to beads and cells. To analyse EVs the sensitivity was lowered to 1 FSC and the side scatter and forward scatter measured on a logarithmic scale. To analyse cells, magnetic beads and latex beads, the sensitivity was set to 100 FSC and side scatter and forward scatter measured on a linear scale. The sensitivity of the side scatter, forward scatter and fluorescence were either set to optimal settings using a control well prior to each experiment or reused where appropriate.

Data was analysed by setting a gate to a control well and using the software to calculate the percentage of events or fluorescent events outside of the gate.

2.2.10 Latex Beads

EVs were attached to latex beads (Invitrogen, A37304, lot. no. 51938A). This allowed the EVs to be detected by flow cytometry (Millipore Guava Easycyte 8HT) more easily and allowed the EVs to be washed and labelled without the use of an ultracentrifuge. The latex beads were 4 μm in size. 20 μg of U937 EVs or samples containing EVs were mixed with 4 x 10^6 4 % W/V Latex beads in 1.5 ml microtubes and left to incubate at room temperature for 15 minutes. For EV characterisation, 2

additional dilutions of latex beads were also mixed with 20 µg EVs to optimise bead coating. Following this they were incubated on ice for 1 hour. The beads were then washed 3 times with either 100 µl 1 x PBS or PFN (1 x PBS + 2 % FCS + 0.1 % N_3^-) by centrifugation (Jouan CR312) at 300 x*g* for 5 minutes at RT. The supernatant was discarded and the beads re-suspended in 200 µl PFN before analysis by flow cytometer (Millipore Guava Easycyte 8HT).

2.2.11 EV Antibody Characterisation

20 µg of CEM, HeLa, Jesthom, Jurkat and U937 EVs were associated with either 2 x 10^6, 1 x 10^6 or 0.5 x 10^6 latex beads (Invitrogen) in a total of 250 µl PBS. 250 µl of beads and EVs were split into 5 wells per EV type (for a total of 75 wells with 50 µl in each well) in a round bottom 96-well plate. To clarify, there were three concentrations of latex beads used for every antibody for each EV type. This meant there were 15 samples in total for each EV type and each well contained 4 µg EVs. Anti-CD63 (Santa Cruz, AF488, SC-5275), anti-CD9 (AbD Serotec, FITC, MCA2656F), anti-CD123 (eBiosciences, FITC, 6HC), anti-CD80 (eBiosciences, FITC, 2D10.4) or no antibody were added to their corresponding well at a concentration of 1 in 10 and left, covered, for 20 minutes on ice. Next, EV-beads were washed 3 times with PFN by centrifuging at 300 x*g* for 5 minutes. Each time the supernatant was discarded before re-suspension of the beads in 100 µl PFN and the final pellet was re-suspended in 200 µl PFN. Before analysis by flow cytometer (Millipore Guava Easycyte 8HT) samples were transferred into a 96-well flat bottom plate.

2.2.12 EV Extrusion

Samples containing either EVs with or without siRNA were diluted into 1 ml PBS in a 1.5 ml microtube. U937 EVs were used at the following values: 50 µg, 75 µg and 150 µg. Allstars siRNA (Qiagen) was used at the following two concentration ranges: 0.01-0.05 µM and 0.1-0.5 µM. Sample was taken up into a 1 ml syringe (Terumo) and either a 25 or 30 G needle (BD Microlance 3) fitted to the end of the syringe. The needle cap was removed and sample forcefully expelled through the needle and back into the 1.5 ml microtube before a 5 µl aliquot was taken and diluted into 1 ml PBS in a clean 1.5 ml microtube. The extrusion was repeated by recapping the needle, removing the needle from the syringe, pulling up sample in to the 1 ml syringe and reattaching the needle. The needle cap was then removed again and a similar amount of force applied again to expel the sample through the needle and back into the original 1.5 ml microtube. Samples were extruded a total of 5 times and 5 µl aliquots taken after each extrusion. For analysis by NTA, the aliquots were diluted 1 in 200 in 1 x PBS in a clean 1.5 ml microtube.

For cell assays 50 µg EVs were diluted into 1 ml RPMI. Then either Allstars siRNA or ERAP1 siRNA were added in the range of 0.1-0.3 µM. Samples were extruded 5 times, as above, and the 30 G needle flushed with RPMI 3 times between each sample. Samples were then incubated at 37 °C for 30 minutes before adding 2 µl RNase A. Another 30 minute incubation at 37 °C followed this. NAP-10

columns were prepared and samples enriched through the columns. U937 cells were counted using a haemocytometer and 1 x 10^6 cells placed in a 12 well plate. For IFNγ activation experiments 10 ng of IFNγ was added to the cell line before adding the enriched sample. Cells were then incubated in 5 % CO_2, 37 °C for 3 hours. Following this cells were lysed and western blotted. This process was performed under sterile conditions.

2.2.13 CPP and PEI Complexation (Basic Method)

Either 0.5, 1, 2 or 4 µg of PEI or CPP were mixed in a 1.5 ml microtube in either 0.5 ml of RPMI, 0.5 ml 1 x PBS or 0.5 ml 300 x*g* centrifuged HeLa cell supernatant, where EVs were required. Samples were left to incubate for 30 minutes at RT, unless specified, before replacing cell line media or being analysed by a flow cytometer (Millipore Guava Easycyte 8HT) or fluorimeter (BMG Labtech FLUOstar). As experiments progressed cell media ultracentrifuged with a 0.2 µm pre-ultracentrifugation filtration step was used instead of centrifuged cell supernatant.

2.2.14 CPP and PEI Complexation (Stage Method)

0.5, 1 or 2 µg PEI or CPP and cargo were incubated in 50 µl 1 x PBS or 50 µl RPMI at 37 °C for 30 minutes in a 1.5 ml microtube. Samples were then vortexed, 5-150 µg EVs in 50 µl 1 x PBS or 50 µl RPMI added and incubated again for a further 30 minutes at 37 °C, unless specified. In the case of a time course, samples were prepared and incubated according to the staggered starting times. Samples were then either analysed or used for further experiments. In the case of a cell assay, samples were prepared and incubated in sterile conditions before being added to a cell line.

2.2.15 CADY Motion and Temperature Experiments

Samples of CADY and FITC Ab were prepared by incubating 2 µg CADY in 10 µl PBS in a 1.5 ml microtube for 5 minutes at RT and then mixing it with a dilution of 0.02 µM FITC Ab in 10 µl PBS. This mixture was covered and incubated either on the bench, on a Stuart Scientific Platform Shaker STR6 at RT or at 4 °C (cold room) for 1, 10, 20 and 30 minutes. Samples were then analysed by flow cytometer (Millipore Guava Easycyte 8HT).

2.2.16 CADY Complex Time Intervals

CADY was incubated at different time points to observe complex formation. Primarily, complexation times were 30 minutes, 1 hour and 2 hours. For these time points complexation time was staggered and all samples analysed by flow cytometry (Millipore Guava Easycyte 8HT) together however for the 5 minute time intervals all the samples were set up at the same time and their fluorescence measured on the flow cytometer every 5 minutes.

2.2.17 Complex Centrifugation

Samples of pre-complexed CPP and cargo were centrifuged at 20200 x*g* in 1.5 ml microtubes for 5 minutes at 4 °C in order to pellet out larger aggregates. The supernatant was then decanted into a clean 1.5 ml microtube and either incubated with EVs or analysed on NTA (Malvern Instruments) or

by flow cytometry (Millipore Guava Easycyte 8HT). Centrifugation of CADY before complex formation also occurred in order to centrifuge out pre-formed aggregates. 1, 2 or 4 µg CADY was diluted into 100 µl 1 x PBS in a 1.5 ml microtube and centrifuged (Eppendorf, centrifuge 5417R) for 5 minutes at 20200 x*g* before analysis or addition of other components.

2.2.18 Water Sonication

Water sonication was performed on samples of CADY in order to reduce the size of aggregates. 1, 2 or 4 µg CADY and 100 µl 1 x PBS were placed in a polystyrene holder to float them on the water of the sonication chamber. The water sonicator (Camlab CamSonix C080T) was set to infinite and sonication timed for 30 seconds. Samples were then analysed by flow cytometry (Millipore Guava Easycyte 8HT) or NTA (Malvern Instruments).

2.2.19 Amicon Ultra Filtration

Amicon Ultra 0.5 ml filters (Merck Millipore) were first pre-rinsed with RPMI at 20200 x*g* (Eppendorf, centrifuge 5417R) for 10 minutes. Then 0.5 ml of sample was added immediately to the filter unit before being centrifuged at 20200 x*g* (Eppendorf, centrifuge 5417R) for 20 minutes. This was followed by elution of the remaining sample into a clean 1.5 ml microtube by centrifuging the inverted filter at 1000 x*g* (Eppendorf, centrifuge 5417R) for 2 minutes. Filtered samples were then analysed by flow cytometry (Millipore Guava Easycyte 8HT).

2.2.20 RNase A wash

100 µl samples of latex beads incubated with 2 µg EVs and 0.05 µM Allstars siRNA electroporated or sonicated, PEI or CPP samples containing 50-150 µg U937 EVs and 0.01 – 0.3 µM siRNA diluted in 1 ml PBS or RPMI had 10 µg RNase A (Qiagen) added and incubated at 37 °C for 30 minutes or 1 hour. In the case of EVs associated with latex beads, samples were centrifuged (Jouan, CR312) at 300 x*g* for 5 minutes. After centrifugation, the supernatant was discarded and the pellet re-suspended in 100 µl PFN. Samples were washed three times in PFN in this way. After the final wash the pellet was re-suspended in 200 µl PFN. In the case of diluted EV samples, the samples were enriched through a NAP-10 column (Illustra NAP-10 columns, Sephadex G-25, DNA Grade, GE Healthcare) instead of centrifugation and PFN washes.

2.2.21 PEI Cell Transfection

2 µg PEI and 0.02 µM ERAP1 siRNA were added to 2 x 10^5 Jesthom cells in duplicate in a 12 well plate. Allstars siRNA was also transfected in duplicate at the same concentrations as a positive control. Duplicate wells of Jesthom cells were cultured as negative controls. All cells were incubated at 37 °C, 5 % CO_2 O.N. After 24 hours the ERAP1 transfected cells were lysed and western blotted (see Cell Lysis and Western Blot sections) to analyse their ERAP1 and β Actin or GAPDH expression. The Allstars siRNA transfected cells were analysed for their fluorescence.

2.2.22 Electroporation

Samples were electroporated in a BioRad Gene Pulser Xcell Electroporation system. Settings were programmed to use the exponential mode or timed mode with 300-1200 V and 25-50 µF. 0.2 ml samples were prepared in either 100 mM sucrose, PBS or 50 mM trehalose with either 1, 2 or 4 mM EDTA in 1.5 ml microtubes. 0.5 ml of each sample was pipetted into a corresponding 2 mm or 4 mm cuvette (BTX Electroporation Cuvettes Plus) and placed on ice. The cuvettes were inserted into the BioRad Gene Pulser Xcell and each electroporated in turn at the pre-agreed settings. Samples were then pipetted out of the cuvette and into a clean 1.5 ml microtube. The microtube was then placed on ice until all samples had been electroporated. 200 µl of sample was then pipetted into a 96 well, clear, round-bottom plate (Thermo Scientific) and analysed by flow cytometer (Millipore Guava Easycyte 8HT).

2.2.23 Electroporation Multiple Pulse Method

The original method of electroporation was altered to incorporate multiple pulses. 100 µl of 50 mM trehalose with either 2 or 4 mM EDTA and EVs or Allstars siRNA was added to a 4 mm cuvette (BTX Electroporation Cuvettes Plus) on ice. The electroporation settings were set to Pulse and 1 to 5 pulses were administered in succession. Following this samples were kept on ice and decanted to a 1.5 ml microtube before analysis.

2.2.24 Electroporation Cell Assay

Samples of 0.01 µM GAPDH siRNA and 2 µg EVs were prepared in 50 mM trehalose with 2 mM EDTA under sterile conditions and electroporated in 2 mm cuvettes with either 1 pulse or 4 pulses at 400 V and 25 µF. Electroporation conditions were kept as sterile as possible. Samples were then returned to a sterile environment and 10 µg RNase A added. Samples were then incubated at 37 °C, 5 % CO_2 for 30 minutes before being added to a plate of confluent HeLa cells. Cells were then incubated at 37 °C, 5 % CO_2 for 48 hours before lysis and western blotting analysis.

2.2.25 Trypsin wash

Cells in media (for cell and media type please refer to Cell and Media Table) or EVs incubated with latex beads were centrifuged (Jouan, CR312) at 300 x*g* and the supernatant discarded. The cell pellet was then re-suspended in 200 µl cold 1 x PBS and centrifuged (Jouan, CR312) at 300 x*g* again for 5 minutes. The supernatant was discarded and the pellet re-suspended in 0.1 mg/ml trypsin-EDTA and incubated at 37 °C for 30 min. Another 100 µl of cold 1 x PBS was added and the cells centrifuged (Jouan, CR312) at 300 x*g* for 5 minutes at RT. The supernatant was discarded and the pellet re-suspended in 100 µl PBS followed by three 100 µl 1 x PBS washes. The supernatant was discarded, and the pellet re-suspended in 200 µl PFN. Samples were then analysed by flow cytometry.

2.2.26 Acid Wash

100 or 200 mM glycine acid, from laboratory stocks, was added to 1.5 ml microtube samples containing 5 µg EVs and 0.01 µM FITC Ab and left to incubate at RT for 30 minutes. Samples were then associated with latex beads (see Latex Beads section) and washed in 100 µl PFN. The supernatant was discarded and the beads re-suspended in 200 µl PFN. 200 µl of sample was transferred to a round bottom 96-well plate and analysed by flow cytometer (Millipore Guava Easycyte 8HT).

2.2.27 Dissolving pSuperRetro miR-US4-1 Plasmid

pSuperRetro miR-US4-1 was generously sent to us from the laboratory of Kwaesong Ahn and reconstituted by soaking the blotting paper containing the plasmid in ddH_2O in a 1.5 ml microtube for 5 minutes and then centrifuging (Jouan, CR312) at 300 x*g* for 30 seconds before transferring the supernatant to a clean 1.5 ml microtube on ice. This stock was immediately used with heat shock to transform competent bacteria.

2.2.28 Heat-shock

50 µl ultracompetent bacteria (XL-10 Gold, Stratagene) were mixed with 2 µl of re-hydrated pSuperRetro miR-US4-1 plasmid in a 1.5 ml microtube and incubated for 15 minutes on ice. They were then immediately transferred to a heating block at 42 °C for 30 seconds then immediately put back on ice for 2 minutes. Afterwards the mixture was added to 50 µl of Luria Broth (LB) in a clean 1.5 ml microtube and incubated at 37 °C for 30 minutes. The LB bacteria mixture was then plated out onto 100 µg/ml Ampicillin (Sigma) LB plates and incubated at 37 °C overnight. An ultracompetent bacteria negative control was also produced in this way without plasmid.

2.2.29 pSuperRetro miR-US4-1 Expansion and Selection

After following the Heat-shock protocol, colonies of bacteria that had been selected on the Ampicillin agar plates were picked with a yellow pipette tip and the pipette tip ejected into 4 ml LB broth with 100 µg/ml Ampicillin and left to incubate O.N at 37 °C at 200 rev min^{-1} in a shaking incubator (Stuart Scientific Orbital Incubator SI 50). In order to expand the cultures, a miniprep kit (Qiagen) was used to enrich the plasmid. Following this 10 µl of enriched plasmid was ran on a 1 % Iberose (Web Scientific, lot no. W-090025) gel (see Plasmid Detection on Iberose). Once it was confirmed that the plasmid was the correct size (approx. 6kb), 200 µl of the bacterial culture was diluted into 100 ml LB with 50 µg/ml Ampicillin in a 200 ml glass conical flask with double foil covering the opening. Midiprep or Maxiprep (as directed by the kit instructions) was then performed to enrich the plasmid and 1 µl plasmid ran on a 1 % Iberose gel again to confirm plasmid size.

2.2.30 Plasmid Detection on 1 % Iberose Gel

pSuperRetro miR-US4-1 bacterial colonies were picked and expanded into 4 ml of 100 µg/ml Ampicillin LB and left on a shaker at 37 °C overnight. A mini-prep was performed on the overnight culture, as instructed by Qiagen Mini-prep kit. Following this, 1-5 µl plasmid (depending on the use of

mini or maxi prep stock) was added to 1 µl multicore, 0.5 µl of either EcoR1 or HindIII restriction enzyme endonucleases and the volume made up to 10 µl with ddH_2O. Samples were heated at 37 °C for 30 minutes before 5 µl DNA loading buffer was added. A 1 % Iberose gel was made by dissolving Iberose into TAE. This was done by heating the mixture in a glass bottle in a microwave until all Iberose was dissolved. The molten gel was then cooled by running cold water over the bottle while moving the gel. Once the bottle was cool enough to touch, 3 µl Safeview (NBS Biologics LTD) was mixed into the gel. The gel was then poured into a casting chamber (Peqlab Perfect Blue horizontal midi gel) and bubbles removed. Once the gel was set, end plates and combs were removed before placing the gel and holder into the gel tank (Peqlab Perfect Blue horizontal midi gel). The gel tank was filled to the fill line with TAE. Samples and DNA Ladder (Generuler 1kb DNA Ladder, Thermo Scientific) were then pipetted into a 1 % Iberose gel (Web Scientific, lot no. W-090025) and ran for 90 minutes at 150 V. The gel sample movement was checked on a UV light box (Herolab UVT-20M) after 30 minutes and 90 minutes. The gel was imaged on a BioRad Molecular Imager ChemiDoc XRS+.

2.2.31 Plasmid Transfection of Cells

3 µl Lipofectamine 2000 was diluted into 50 µl RPMI in a 1.5 ml microtube and incubated for 5 minutes at RT. 1 or 2 µl of stock pSuperRetro miR-US4-1 plasmid was then added with 50 µl RPMI to the Lipofectamine dilution and left to complex at RT for 20 minutes. Next the old media was removed from the 12-well culture plates of confluent HeLa cells and 1 ml RPMI and the Lipofectamine mixture added. These were left to incubate O.N at 37 °C and the following day 1 ml of 1 µg/ml Puromycin in 5-R-K added to begin the selection process.

2.2.32 Transfected Cell Selection

Cells that had been transfected by plasmids underwent initial drug selection. Following this the transfected cells were lysed and western blotted for their ERAP1 expression (see Cell Lysis and Western Blot sections). In the case of the plasmid producing a fluorophore, the cells were observed in culture for fluorescence. An Axiovert inverted microscope (Zeiss) and flow cytometry (Millipore Guava Easycyte 8HT) were also used to detect fluorescence.

2.2.33 Lentivector Transfection and Selection

2 wells of HeLa and 2 wells of HeLa.B27 cells were grown to confluency in a 6-well plate. 8 µl Peqfect was added to 200 µl RPMI and 4 µg XMIR lentivector plasmid was added to 200 µl RPMI and both were incubated at RT for 5 minutes. These solutions were then mixed together and incubated at RT for 20 mins. Then 100 µl of the mixture was added to each well of cells and the plate of cells incubated overnight at 37 °C, 5 % CO_2. The next day transfected cells were selected by removing cell media and adding 1 ml of 5-R-K supplemented with 1 µg/ml Puromycin. Cells were checked with the Axiovert inverted microscope for fluorescence and 2 fluorescent colonies from each cell line picked.

Once the colonies reached confluency, cells were analysed for ERAP1 expression by western blot and transfection levels by flow cytometry (see XMIR Me1 and HC10 flow cytometry section).

2.2.34 XMIR Me1 and HC10 Flow Cytometry

Fluorescent HeLa cells were trypsinised and removed from a confluent plate. Next cells were washed three times in PBS then split in to a 96-well plate. 50 µl of anti-HC10 antibody and 4 µl of anti-Me1 antibody in PBS were added to the cells and left covered on ice for 20 minutes. Cells were then washed three times in PFN before re-suspension in 200 µl PFN and analysis on the flow cytometer.

2.2.35 Cell Co-Culture Assays

Three types of Co-Culture were performed during this research; cell-cell, layering and trans-well.

The cell-cell co-culture was performed with 6 non-adherent cell lines: CEM, CEM sh2, CEM NEG, Jesthom, Jurkat and U937. Two cell lines were both grown to confluency, counted and then the same number of each cell line seeded together in a clean 6-well plate with fresh cell media containing 5 % FCS, RPMI and Kanamycin (Gibco). The cells were incubated at 37 °C and 5 % CO_2 together overnight and all cells removed from the plate the next day to be lysed and western blotted (see Cell Lysis and Western Blot sections).

In the case of the cell layering assay, an adherent cell line such as HeLa or HUVEC hTERT was grown to confluency in a 6-well culture plate and 1-2 x 10^6 cells of a non-adherent cell line such as CEM, CEM sh2, CEM NEG, Jurkat or Jesthom was added to sit as a layer in contact with the adherent cells. Again, the cell lines were incubated together overnight at 37 °C with 5 % CO_2. The non-adherent cells were then pipetted off and each well gently washed with PBS prior to the adherent layer being lysed and western blotted (see Cell Lysis and Western Blotting sections).

As EVs are able to move through a 0.2 µm trans-well membrane, trans-wells (Corning) were used as a filter to differentiate between a cell directly causing a downregulation in ERAP1 and cytokines or EVs causing it. HeLa.B27 or HUVEC hTERT cells were grown to confluency in a 6-well plate. Non-adherent cells such as CEM, CEM sh2, CEM NEG, Jesthom, Jurkat and U937 were grown in a separate plate, counted and then 1-2 x 10^6 cells placed inside the trans-wells and 5-R-K cell culture media added to cover all cells and the trans-well membrane. The cells were incubated together at 37 °C, 5 % CO_2 overnight and the trans-well removed the next day so that the adherent bottom layer of cells could be lysed and western blotted (see Cell Lysis and Western Blotting Sections).

2.2.36 IFN Activation Assay

HeLa.B27 cells were grown in a 6-well cell culture plate to confluency. Following this, CEM and CEM shRNA2 cells were counted and 2 x 10^6 cells added to the corresponding wells of the 6-well plate. Either 10 ng or 50 ng of IFN γ were also added as controls to HeLa.B27 wells both with and without CEM or CEM shRNA2 cells present. The cytokines were incubated with the cells overnight at 37 °C and

5 % CO_2. The next day the co-culture wells were washed by discarding all non-adherent cells and cell media and adding 1 ml sterile PBS (Gibco). The PBS was pipetted gently around the well before also being discarded. The HeLa.B27 cells were removed, as described in the Cell Lysis section, then lysed and western blotted (see Western Blot section) for ERAP1 and GAPDH expression.

2.2.37 siRNA Detection on Agarose

Samples containing siRNA and EVs were ran on a 1 % Iberose gel in order to determine if siRNA had been encapsulated inside EVs. 1 % Iberose was dissolved by heating in TAE (pH8, 242 g Tris, 18.6 g EDTA, 57.1 ml Glacial Acid) then left to cool before adding 3 µl Safeview and set in the gel chamber. 10 µl of sample was directly loaded into the gel wells and ran for 1 hour. Afterwards the gel was viewed on a BioRad Geldoc Gel Imager.

2.2.38 Sonication

Samples were sonicated in 0.5 ml PBS or RPMI (Gibco) using the QSonica Q700 Sonicator. Settings were set at 20 % amplitude, on for 4 seconds, off for 2 seconds and this was programmed to repeat 6 times over a 36 second time period. Samples were then incubated on ice for 1 minute and then the sonication procedure repeated (Haney *et al.,* 2015). In a later experiment the amplitude was set to 40 %. Samples were then analysed by flow cytometry.

The updated method from the Batrakova laboratory visit used Triton X-100 (Sigma Aldrich) instead of PBS and, post-sonication, the samples were left at 37 °C, 5 % CO_2 for 30 minutes before enrichment on a NAP-10 column (Illustra, NAP-10 Columns, Sephadex G-25, DNA Grade, GE Healthcare) and analysis using a BCA assay (see Protein Concentration Measurement section) to measure protein content and a fluorimeter (see Fluorimetry section) to measure sample fluorescence. Two modifications included were the addition of a 10 µg RNase A (Qiagen) incubation at 37 °C for 30 minutes after the post-sonication incubation and the use of NTA (Malvern Instruments) to monitor EV size and concentration. Optimising sonication involved the trial of 40 % amplitude. For this experiment protocol was as above except with 40 % amplitude instead of 20 %.

2.2.39 Anti-CD63 Magnetic Beads

0.005 µM Allstars siRNA and 5.7 µg EVs were sonicated in PBS as described in the sonication section. Post sonication samples were incubated with 20 µl anti-CD63 magnetic beads at RT for 1 hour with mixing every 15 minutes. The mixture was then washed 3 times by sitting the microtube in a magnet for 2 minutes and re-suspending the pellet in 500 µl PBS. Beads were re-suspended in a final volume of 200 µl PBS in a 96-well plate before analysis by flow cytometer.

2.2.40 ERAP1 Sonication and Cell Transfection

75 µg EVs and 0.2 µM ERAP1 siRNA (Qiagen) were first mixed together in a 1.5 ml microtube and then sonicated using a QSonica Q700 sonicator with 6.4 mm tip. Standard settings used (unless stated) were 20 % amplitude, 2 seconds on, 4 seconds off and set to repeat 6 times. Microtubes were

then left on ice for 2 mins before repeating the protocol. Samples were then returned to the ice until all samples had been processed. Microtubes containing sample were left at 37 °C and 5 % CO_2 for 30 minutes. EV encapsulation was assessed by either flow cytometry (Millipore Guava Easycyte 8HT), fluorescence assay (BMG Labtech FLUOstar) or cell assay (see Flow Cytometry and Fluorimetry sections).

In the case of the cell assay, samples were prepared in a sterile tissue culture hood and sonicated with as little exposure to contaminants as possible. Sample was directly added to the cell line of choice. The cells were then incubated for 2 hours before checking cell viability by microscopy and further left overnight at 37 °C. Cells were lysed and western blotted for ERAP1 and GAPDH expression the following day.

In the case of EVs sent for flow cytometric (Millipore Guava Easycyte 8HT) analysis, sample was incubated with latex beads on ice for 20 minutes. The mixture was then washed 3 times in PBS before being re-suspended in 200 µl PFN and transferred into a 96-well plate. The plate was then inserted into the flow cytometer. The flow cytometer was set to count either 5000 or 10000 particles over a time period of 3 minutes. In order to observe the beads, the FSC was set to 100.

2.2.41 Cell Viability Assay

Vitality of cells following CXB or DMC (Sigma-Aldrich) drug experiments was assessed by Alamar Blue (Invitrogen DAL 1025). After the samples underwent an O.N incubation (see Celecoxib Drug Titrations and Celecoxib Time Course sections), one set of sample wells was removed for lysis (see Cell Lysis section). Then a 1 in 200 dilution of Alamar Blue was added to the remaining duplicate wells of the 12 or 24-well plate and the cells returned to 37 °C, 5 % CO_2 for 30 mins to allow the Resazurin to be reduced to Resorufin. 100 µl of cell media was pipetted into a clear, flat bottom, black 96-well plate (Perkin Elmar) and serial dilutions of 1 in 2 performed down the plate by pipetting 50 µl ddH_2O into all wells and then using a multichannel pipette (Labsystems, Finnpipette Digital Multichannel) to take 50 µl cell media from the top wells and mix it into the wells below. This was repeated down the plate using clean pipette tips for each dilution. Colour change was then assessed by Spectrophotometry (Dynex Technologies MRX) or fluorimetry (see Fluorimetry section).

2.2.42 Celecoxib Drug Titrations

Both CXB and DMC (Sigma-Aldrich) drug titration experiments were carried out together in a 12-well or 24-well culture plate. First the HeLa.B27 cells were cultured to confluency then cell media was replaced before the addition of 1, 10, 25 or 50 µM CXB or DMC. Immediately after the addition of drug to each well the cell media and drug were thoroughly pipetted together. This was to prevent the DMSO or the drug from pooling in one area of the well and causing apoptosis. The cells were then incubated at 37 °C, 5 % CO_2 overnight before lysis and western blotting (see Cell Lysis and Western

Blotting sections). In the case where a cell viability assay (see Cell Viability Assay section) was also carried out, all wells were duplicated.

2.2.43 Celecoxib Time Course

The time course for CXB and DMC (Sigma-Aldrich) was carried out with either 25 µM CXB or 10 µM DMC over a 12-hour time period. Wells of HeLa.B27 cells were grown to confluency in a 12 or 24-well plate (Thermo Scientific, cat no. 150628, cat no. 142475). RPMI and drug were added at time 0 (12 hours), after 4 hours (8 hours), after 8 hours (4 hours), after 10 hours (2 hour) and after 11 hours (1 hour). After 12 hours cell viability was measured (see Cell Viability Assay section) and cells were lysed and western blotted (see Cell Lysis and Western Blotting sections).

2.2.44 FCS Titration

To set up an FCS titration assay for CXB and DMC, first a 24-well plate (Thermo Scientific, cat no. 142475) of C58.B27 cells were grown to confluency and divided into four 15 ml falcon tubes. The falcon tubes were then centrifuged (Wifug 500E) at 300 x*g* for 5 minutes, their supernatant discarded and the cell pellet re-suspended in 18.5 ml of RPMI with either 0, 2.5, 5 or 10 % FCS. 1 ml of cell media was added to each well of a 24-well plate. Next, either 0, 1, 10, 25 or 50 µM CXB was added and thoroughly pipetted into the media. 100 µl from each well was then pipetted into a 96-well plate in duplicate and incubated at 37 °C, 5 % CO_2 for 5 hours before cell viability was checked (see Cell Viability Assay section).

2.2.45 CXB and DMC Sonication and Cell Assay

1 ml RPMI, 150 µg EVs and 1 mM of either CXB or DMC were sonicated as described in the sonication section and incubated at 37 °C for 60 minutes. Next samples were kept on ice when possible and enriched through a NAP-10 size exclusion column as described in the sephadex enrichment section. 0.6 ml (half of the eluate) was pipetted into a 24 well plate of confluent HeLa.B27 cells and the other half into a duplicate well below for cell viability assessment. Cells were incubated at 37 °C, 5 % CO_2 for 1 hour. Cell media was then discarded and replaced with 5-R-K supplemented with 0.1 mg/ml Hygromycin B. Cells were incubated for a further 24 hours before lysis and analysis.

Chapter 3: Characterising EVs

In this first chapter a characterisation is undertaken of the pool of exosomes from several cell lines that will be used for functional studies in the rest of the thesis. As recommended by the International Society of Extracellular Vesicles (ISEV), the minimal number of techniques to characterise EVs should be two (Gardiner *et al.,* 2016). Here, three methods are utilised to compare the exosomes isolates; NTA, flow cytometry with fluorochrome labelled antibodies, and 'Western' immunoblotting of cell and EV isolates.

3.1 NTA

Nanoparticle Tracking Analysis (NTA) involves the analysis of EVs whilst in suspension, either in the form of prepared tissue culture supernatant or post-enrichment, typically after ultracentrifugation. Diluted samples of EVs are injected into a chamber through which a laser beam (red, 638 nm LM10 unit) is passed. Light reflected from the EVs is detected by a microscope objective and recorded on a CCD device as a video for typically 30 to 60 secs depending on the sample concentration. Tracking software then uses the principle of Brownian motion to calculate the size of the spheres depending on the speed of motion and temperature of the apparatus. Of significant note, motion of particles in this nanometre size range is essentially independent of particle density, thus NTA can be used on both solid and vesicle-like particles.

To characterise EV diameter CEM, HeLa, Jesthom, Jurkat and U937 cell media from cells grown for 24 to 48 hours in serum-free tissue culture medium was analysed. Supernatants were spun at 300 x*g*, 0.2 µm filtered and ultracentrifuged at 100000 x*g* for 2 hours. Three videos of each sample were recorded with the dilution moved between videos to record a different set of EVs. CEM EVs had a mean diameter of 240 nm, HeLa EVs had a mean diameter of 129 nm, Jesthom EVs had a mean diameter of 199 nm, Jurkat EVs had a mean diameter of 188 nm and U937 EVs had a mean diameter of 196 nm (figure 3-1). This places some of the samples at the upper limit of the stated exosome range, suggesting the population is composed of a mixture of exosomes and other microvesicles. Interestingly HeLa cells, which have been used in many prototypical exosome studies produced a vesicle size comparable to that expected of exosomes. However, the possibility of some exosome aggregation induced after sample re-suspension and storage of EVs cannot be excluded. The data clearly demonstrates how more than one technique should be used to characterise the sample of interest.

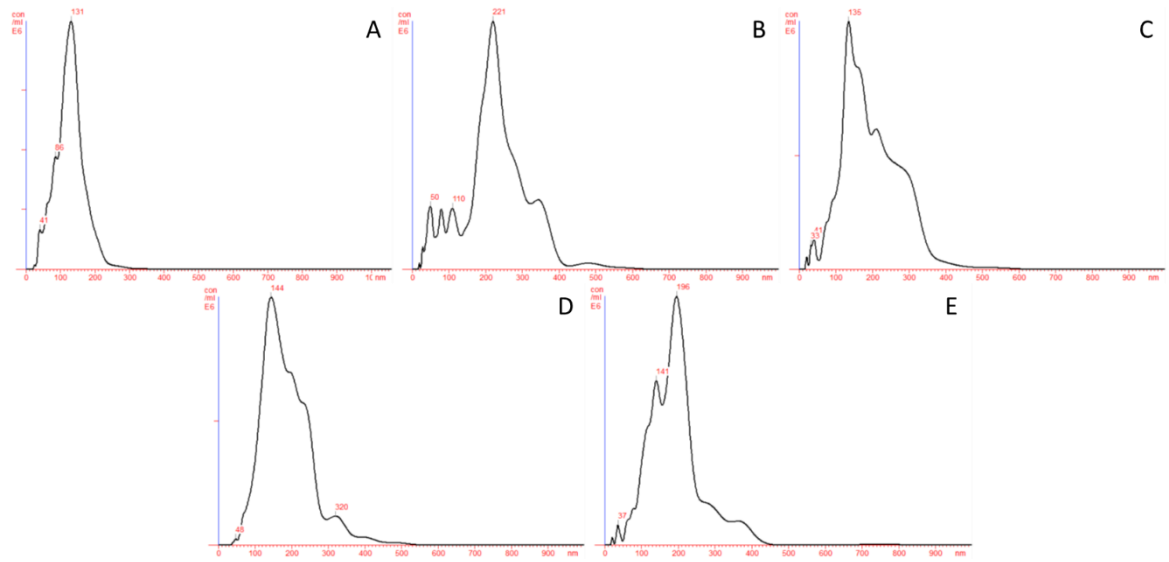

Figure 3-1: NTA of Jesthom, Jurkat and U937 EVs.
A: HeLa EVs, mean diameter = 129 nm. B: CEM EVs, mean diameter = 240 nm. C: Jestom EVs, mean diameter = 199 nm. D: Jurkat EVs, mean diameter = 188 nm. E: U937 EVs, mean diameter = 196 nm.

3.2 Flow Cytometry

Flow cytometry also uses lasers to detect objects, typically cells. In this system cells, often labelled with fluorochrome-tagged antibodies (or also internal markers in the case of permeabilised cells), pass one or more laser beam in a column of fluid. Reflected/scattered light and flashes of fluorescent light are recorded by detectors placed around the flow chamber. The advantage of flow cytometry is in its high flow rates and ability to use multiple wavelengths of light tailored to specific fluorochromes. Whether flow cytometry in most standard machines can be used to detect EVs remains somewhat controversial. In practice, flow cytometry requires specially adapted machines, such as imaging flow cytometers, to easily detect EVs, or careful control with latex beads of known sizes to obtain useful information.

Typically EVs are adsorbed on to latex beads in order to analyse them in the range of a standard flow cytometer. In this way multiple EVs can bind to beads providing multiple epitopes to enhance signal detection.

The typical proteins used as exosome indicators are: CD9, CD63, CD81 and TSG101 (Schey, Luther, & Rose, 2016). CD63, CD9 and CD81 are tetraspanins specifically upregulated in exosomes. Tetraspanins usually function by inducing cell mobility, fusion and signalling events (Hemler, 2005). Typically tetraspanins have four transmembrane domains and 2 extracellular loops (Boucheix *et al.,* 1991).

CD9 is a 21-24 kDa ubiquitous member of the tetraspanin family. More specifically it has been associated with gamete fusion, cell motility and interactions with integrins (Kaji & Kudo, 2004). CD9 is able to accomplish multiple functions thanks to its ability to form heterodimers, particularly with CD63 and CD81, the latter with palmytolation (Stephanie Charrin *et al.,* 2002; Pols & Klumperman, 2009). CD9 is also an important indicator in the invasiveness of cancerous cells which actively downregulate it in order to promote motility (Todeschini & Hakomori, 2008).

CD63 is a major 30-60 kDa component of the lysosomal membrane and limiting membranes of MVBs which is different to most other tetraspanins (Hořejši & Vlček, 1991; Mazurov, Barbashova, & Filatov, 2013). Like CD9 it is ubiquitous across cell lines (Hořejši & Vlček, 1991) and it makes a good protein marker as it is highly enriched in exosomes (Escola *et al.,* 1998). Its association with AP-2 involves it in clatherin mediated endocytosis at the plasma membrane, allowing cellular uptake of exosomes (Mains, Sulston, & Wood, 1990).

CD81 is mostly associated with immune cells such as B and T cells. Upon formation of an immune synapse, it is rapidly recruited to complexes (Mittelbrunn, Yáñez-Mó, Sancho, Ursa, & Sánchez-Madrid, 2002). CD81 negative mice show a decrease in a B cell subset and it has been shown that it is required for an efficient Th2 response (Deng *et al.,* 2000; Miyazaki, Müller, & Campbell, 1997).

In the brain CD81 is associated with suppression of astrocyte and microglia proliferation (Kelić, Levy, Suarez, & Weinstein, 2001). CD81 is approximately 27.5 kDa (Escola *et al.,* 1998). Its wide variety of functions are thought to depend on its heterodimer or complexing partners.

TSG101 (though inside the vesicles, and not used for flow cytometry, but discussed here for completeness) is a component of the ESCRT machinery associated with exosome packaging and formation. TSG101 has a molecular weight of approximately 49 kDa (Yuana *et al.,* 2017). As mentioned in the introduction TSG101 interacts with the HRS subunit of ESCRT-0 (Bache *et al.,* 2003). A function outside of vesicle formation and trafficking for these proteins is cytokinesis and abscission during mitosis (Baietti *et al.,* 2012; Fujii, Hurley, & Freed, 2007; Schorey & Bhatnagar, 2008).

The markers chosen for flow cytometry here were CD9, CD63 and CD123. CD9 and CD63 are frequently enriched in exosomes while CD123 (IL3 receptor chain) is used as a negative control. EVs, enriched by ultracentrifugation, were incubated with 3 different concentrations of latex beads. This allowed optimisation of the number of EVs coating the beads. FITC or AF488 tagged antibodies were used based on the study by Lotvall and colleagues (Lötvall *et al.,* 2014). The three different concentrations of latex beads chosen to optimise the ratio of EVs to beads were 0.5×10^6, 1×10^6 and 2×10^6 (initial studies indicated 4×10^6 beads was too high, data not shown). Bead-bound EVs were then analysed by flow cytometry (Figure 3-2). The data indicated that HeLa EVs were clearly positive for CD9 and CD63. CEM EVs were weakly positive for CD63 but not CD9. Jesthom EVs were weakly positive for CD9 and CD63. Jurkat EVs were very weakly positive for CD9 and CD63. U937 EVs were positive for CD63 but negative for CD9. This lack of expression confirms published literature where CEM and U937 cells show no cell surface CD9 expression and Jurkat cells show very low expression (Stéphanie Charrin *et al.,* 2001; Jolly & Sattentau, 2007). CD123 was negative on all EVs tested.

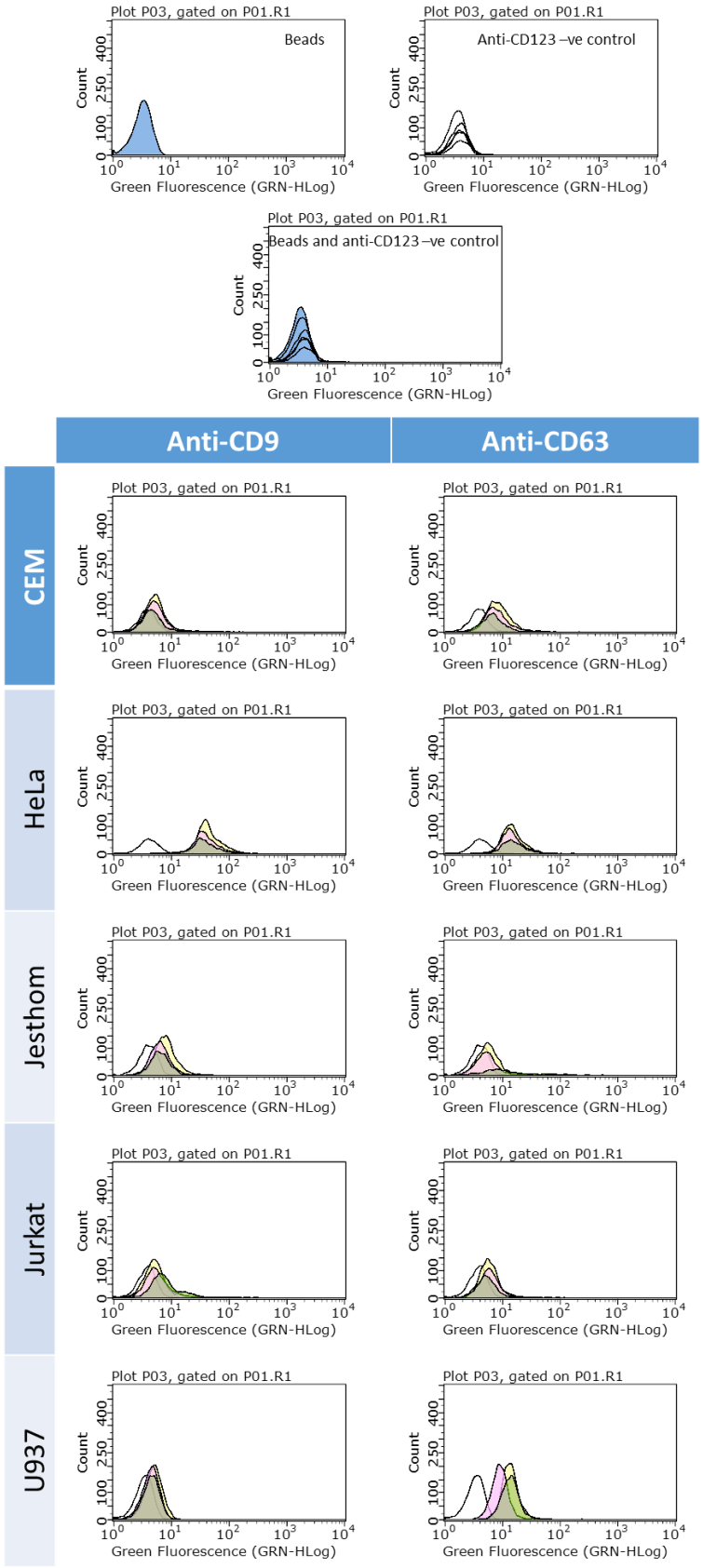

Figure 3-2: fluorescent intensity histograms showing the levels of EV markers, CD9 and CD63, present on the membrane surface. The 4 different peaks represent the following: the clear peak is the anti-CD123 negative control, the green peak signifies the use of 0.25 µl latex beads, the pink peak represents 0.5 µl latex beads and the yellow peak represents 1 µl latex beads used. n=1.

3.3 Western Blot

To further analyse the EVs for the presence of classical exosome markers, TSG101, CD9 and CD63 antibodies were used to perform a western blot on both EV and cell lysates. Calnexin (ER marker) expression was also tested as a negative control. BCA assays were used to determine the concentrations of both the cell lysates and EV samples and 5 µg of protein loaded per well. Blots were incubated with the relevant primary and secondary antibodies and then analysed using a Licor Odyssey ClX. As shown in Figure 3-3, none of the EVs from CEM, HeLa, Jesthom, Jurkat or U937 cells contained notable levels of calnexin, as expected, indicating no significant contribution from cell debris in the preparations. CEM EVs were positive for TSG101, CD63 and CD81, but not CD9, matching the flow cytometry data. Hela EVs were positive for TSG101, CD63, CD9 and CD81, matching the flow cytometry data. Jesthom EVs were positive for CD63 (weakly), CD9 and CD81, but not TSG101 (again matching flow cytometry data). Jurkat EVs were positive for TSG101, CD63 (weakly) and CD81, but not CD9. This is not an exact match for the flow cytometry, where some CD9 signal is seen (but may be background contamination). U937 EVs were positive for TSG101 and CD63, but not CD9 or CD81, matching the flow cytometry observations.

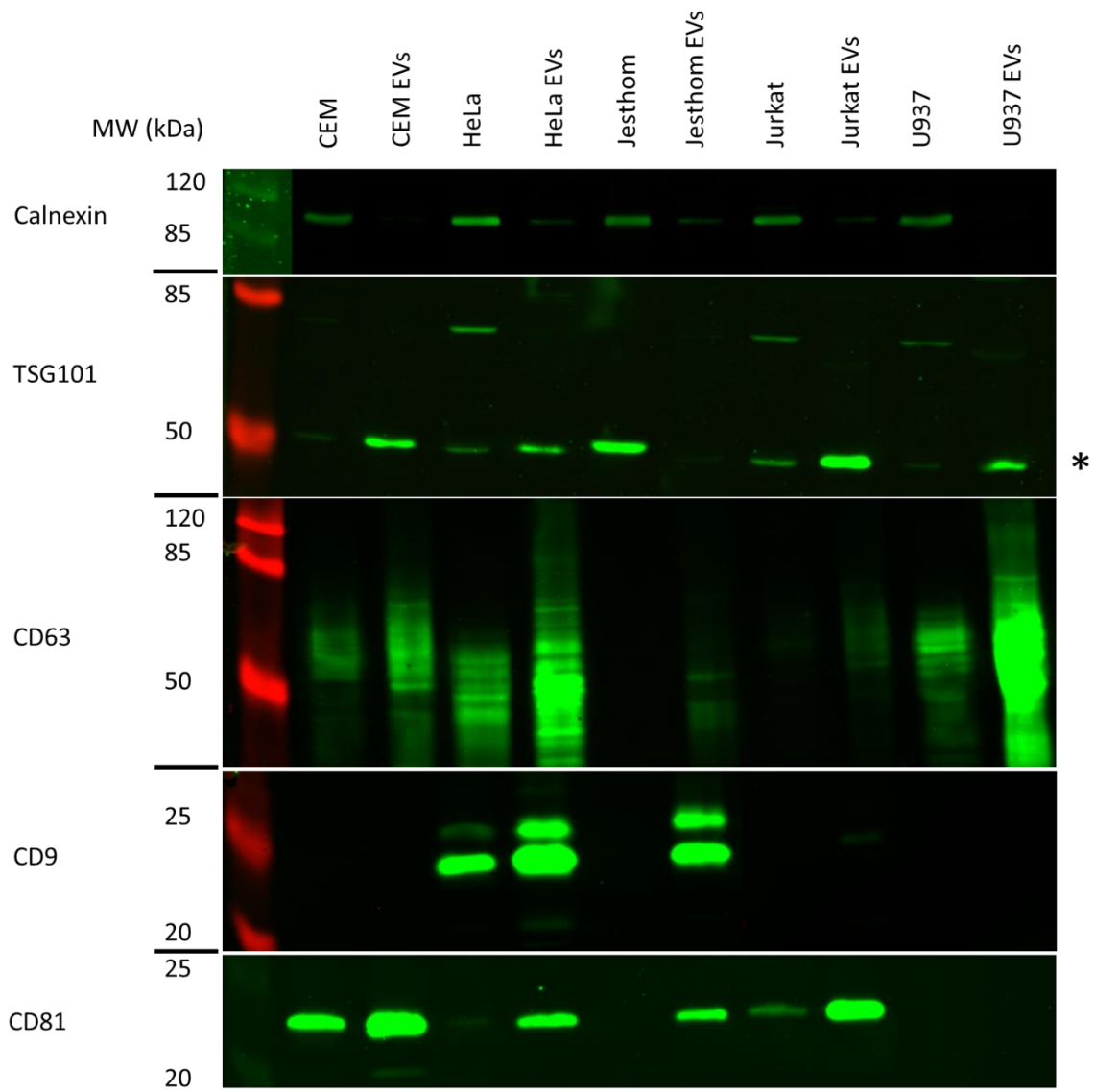

Figure 3-3: western blot of parent cell line and corresponding EV protein expression for typical EV protein markers. * indicates TSG101 band, the second larger protein detected is an unknown artefact. n=1.

3.5 Discussion

The basis of this chapter was to provide evidence that suggested the presence of exosomes in media from the chosen sample of cell lines. It is not enough to show that exosome markers are present by one method. Ideally there should be a requirement to show the presence of multiple protein markers over more than one method. In 2014 the International Society of Extracellular Vesicles (ISEV) published a paper discussing the collective framework required to suggest that exosomes are present in a sample. They first suggest that the amount of 3 or more proteins be reported in at least a semi-quantitative manner (Lötvall *et al.,* 2014). Some of these proteins should be positive in EVs but also negative testing proteins should also be used. It was also mentioned that the protein expression of the EV samples should be compared to the secreting cell.

The data presented in this chapter uses the three methods of NTA, flow cytometry and immunoblotting to characterise the EV population derived from HeLa, CEM, Jurkat, Jesthom and U937 cells. One of the most striking observations is that whilst the prototypical epithelial cell line HeLa produced vesicles of an appropriate size and with the expected classical markers of TSG101, CD9, CD63 and CD81, in marked contrast the cell lines representing cells of the immune system lineage displayed heterogeneity in their expression of some of the markers. This is despite the origin of all these cells as haematopoetic stem cells (though it is appreciated that cell lines might not fully represent normal blood immune cells). In fact of all the markers tested, only CD63 showed commonality between the immune EVs, and even their expression levels were highly variable. This data therefore provides a very clear example of how the use of multiple methods and multiple markers is an absolute requirement in the characterisation of the proposed EV/exosome population under study. Reliance on a restricted method or marker set could easily mislead an investigator as to the nature of the samples.

Another widely used technique for EV characterisation, in addition to the techniques used in this chapter, is Electron Microscopy (EM). EM is used to detect gold tagged structures to determine the morphology of an EV. As EVs are spherical in nature they appear to have a cup shaped morphology on EM due to sample dehydration. Unfortunately EM is an expensive method of characterisation making it less accessible. EM would be an interesting addition to this chapter as it may also give an indication of the extent of EV aggregation.

Given the above caveats, together this data confirms the existence of an enriched population of exosomes in the EV samples utilised in this thesis. Of note, alongside almost all the techniques currently in use, it does not give a precise indication of the exact ratio of exosomes versus other vesicles in the population, as it analyses bulk samples for markers rather than individual vesicles. However, the presence of typical exosome markers in these samples is proven.

Chapter 4: Extrusion

Extrusion is a method that is commonly used in the preparation of vesicle and multi-lamellar substrates using lipid film formulations. The ability to utilise such a relatively simple and cheap technique would be a significant advantage in the exosome and EV field. Specific commercial extrusion machines are available, but in this study an initial test using small gauge syringe needles, which can disrupt cells into vesicle like preparations was assessed. The method involves forcing a sample through a small aperture or pore which usually results in a monodispersed population (So & Lodge, 2016). Furthermore, as extrusion does not involve extraneous solvents or chemicals it is also less likely to affect the natural contents of EVs. 25 G and 30 G needles (nominal diameter of 0.26 mm and 0.159 mm, respectively) were used as a readily available substitute for a commercial extruder. The diameter of these needles is of course significantly larger than the expected diameter of an exosome, however enough pressure may potentially be produced to damage the EVs. Damage to the EVs will provide opportunity for cargo, at a high concentration, to diffuse into the EV before the vesicle is able to reform.

4.1 Results

Studies of extrusion were initiated by comparing the use of a 25 G needle (nominal diameter of 0.26 mm) to a 30 G needle (nominal diameter 0.159 mm) and extruding RPMI containing 50 µg U937 EVs (isolated by filtration and ultracentrifugation) by passage through the needle aperture five times. At the start and after each extrusion pass, a 5 µl aliquot of sample was diluted 1 in 200 in PBS and analysed by NTA. The EVs used with the 25G needle started with mean diameters of 213 and 174 nm (figure 4-1A). No meaningful alterations in mean diameter were observed after each pass. The mean diameter recorded for the RPMI samples reflects a few particles seen at a very low concentration in the RPMI. The experiment was repeated with a 30 G needle with initial mean EV diameters of 205 and 216 nm (figure 4-1B). Again, no meaningful alterations in mean diameter were observed after each pass. EV diameters therefore remain similar to un-extruded EVs, suggesting that no significant disruption to the EVs had occurred.

Figure 4-1A: bar chart showing the changes in particle size when 50 µg U937 EVs are extruded with a 25 G needle 5 times. The orange bars represent the first extrusion experiment and the blue bars represent the second experiment. There was a very small concentration of particles detected in the RPMI for the first experiment. Each of the samples were measured immediately after they were extruded and before the next extrusion. n=2

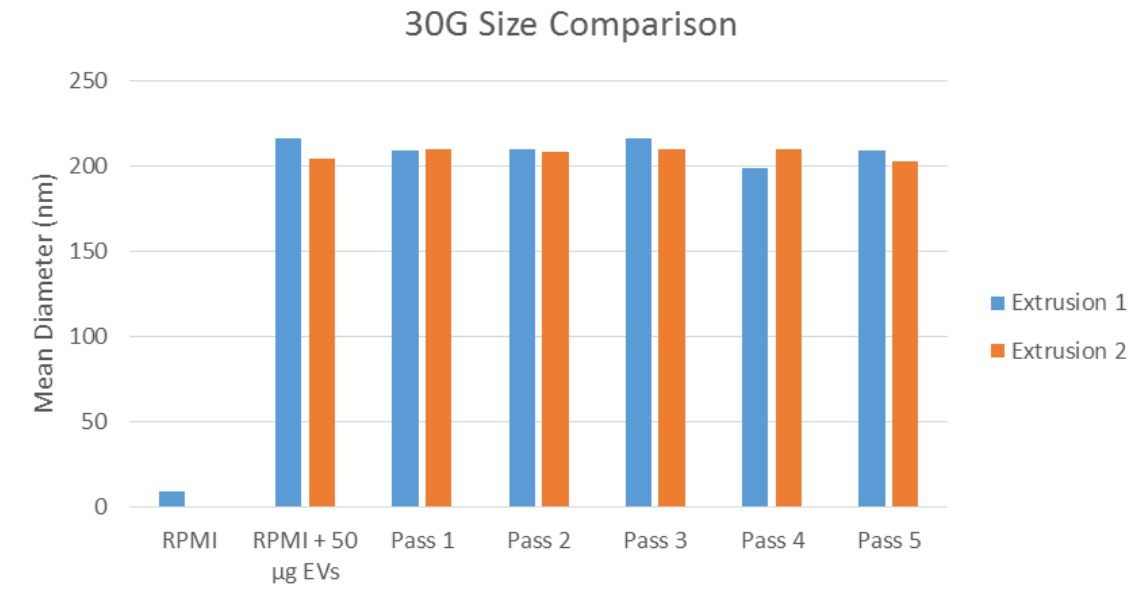

Figure 4-1B: bar chart showing the changes in particle size when 50 µg U937 EVs are extruded through a 30 G needle. The blue bar is the first experiment and the orange bars are the results for the second experiment. n=2. There was a low concentration of small particles seen in the RPMI.

To determine if the initial data above, which clearly suggested no modification to the EVs, also resulted in no loading of cargo into the EVs, an experiment was performed using a model fluorescent cargo. Allstars siRNA is a 21 nucleotide (nt) long siRNA conjugated to a 488 nm fluorophore available from Qiagen. 0.3 µM siRNA was incubated with 50 µg U937 EVs and passaged through a 30 G needle as before. After extrusion the sample was split in two. One half was incubated with RNase A for 30 minutes at 37 °C. Following this both samples were enriched by NAP-10 column and the eluate collected for analysis of fluorescent content. Allstars siRNA retention was calculated by creating a fluorescence concentration gradient of the Allstars siRNA. The gradient was fitted with a line of best fit and the equation for the line calculated. The equation was then used to calculate the concentration of Allstars siRNA remaining in the extruded sample and a percentage worked out based on the starting concentration of Allstars siRNA. Figure 4-2 shows that without the RNase A incubation, 26 % of the input Allstars siRNA is present in the eluate. However, with the addition of RNase A there is a decrease in retention to 2 % suggesting superficial association of the siRNA with the EVs.

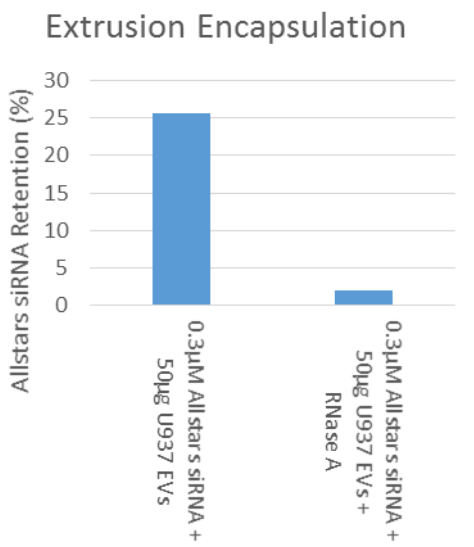

Figure 4-2: bar chart showing the changes in Allstars siRNA retention in samples for extrusion of 0.3 µM Allstars siRNA and 50 µg U937 EVs with a 30 G needle. The left bar is sample without an RNase A incubation stage and the right bar when RNase A is added. n=1.

To attempt to improve encapsulation the experiment was repeated and the extruded sample was incubated at 37 °C for 30 minutes to allow EVs more time to reform (if any disruption had taken place). After this additional reform time the sample was halved and processed as previously. The percentage of Allstars siRNA input concentration remaining was calculated again as previously. Figure 4-3 shows an apparent improvement in the percentage of Allstars siRNA associated and encapsulated when the extra reformation step is applied. Without an RNase A incubation 46 % of the input Allstars siRNA remains associated with the EVs. This percentage decreases to 16 % when an RNase A incubation is applied, an increase of 14 % on the original 2 % observed in the initial experiment. This suggests that 37 °C promotes EV reconstitution or association and encapsulation of Allstars siRNA.

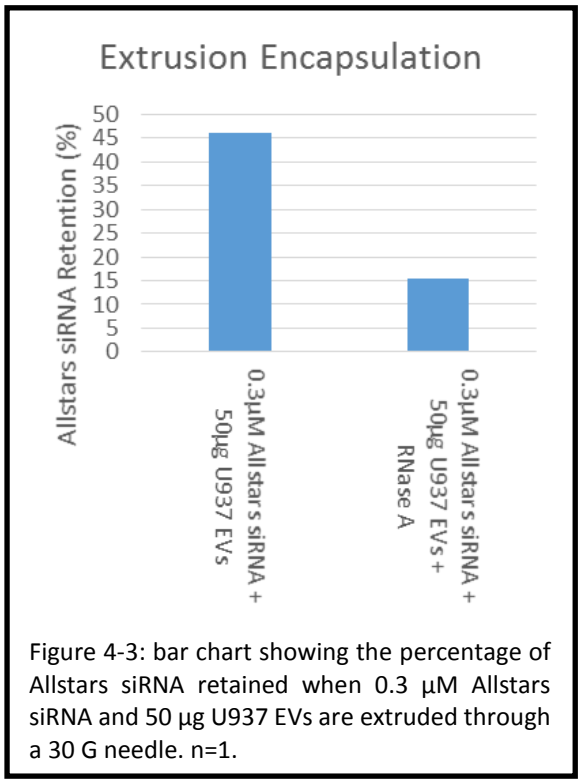

Figure 4-3: bar chart showing the percentage of Allstars siRNA retained when 0.3 µM Allstars siRNA and 50 µg U937 EVs are extruded through a 30 G needle. n=1.

Given the previous experiment suggested some uptake of siRNA cargo, an experiment was performed using a validated siRNA targeted against ERAP1. A concentration of 0.3 µM ERAP1 siRNA was extruded with 50 µg U937 EVs. These EVs were then treated as previously with the addition of RNase A and column separation before being added to U937 cells. Cells were incubated for 3 hours before lysis and western blot. This experiment was repeated twice and each set of lysates western blotted 3 times. ERAP1 expression was first normalised using the GAPDH expression of each lysate (figure 4-4B). The percentage of ERAP1 expression was then calculated using the value of the U937 cell lysate (negative control) as 100 %. As can be seen in figure 4-4A and 4-4B, there was no consistent inhibition of expression of ERAP1, and an actual increase in ERAP1 apparent expression in most samples.

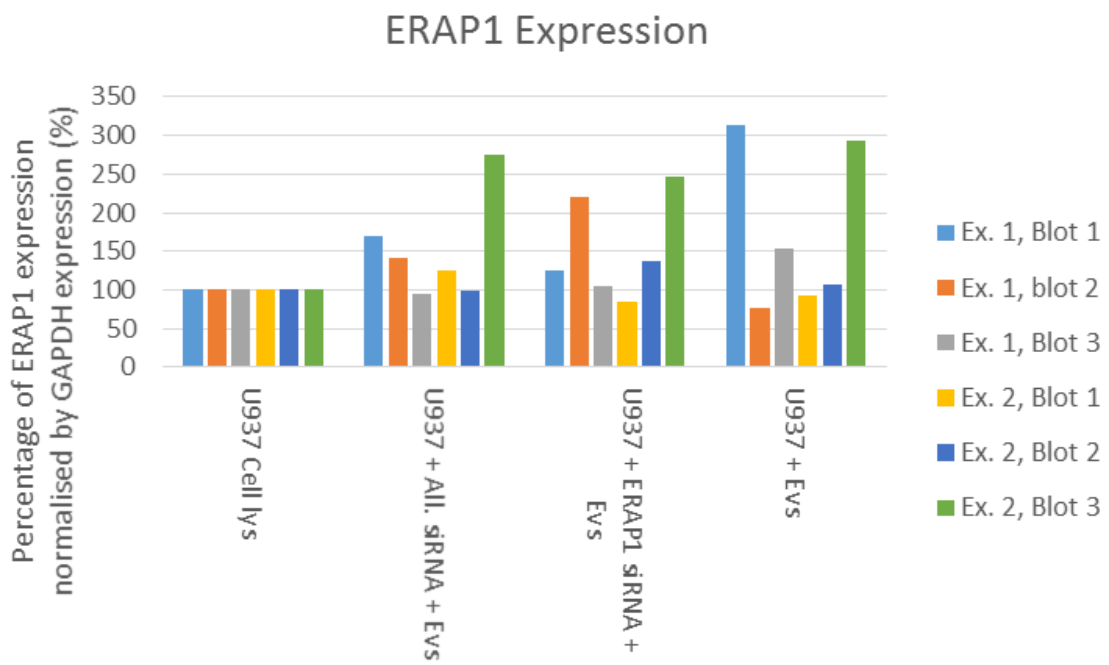

Figure 4-4A: bar chart showing ERAP1 expression when extruded 0.3 µM ERAP1 siRNA and 50 µg U937 EVs are incubated with U937 cells. The U937 cell lysate is used as the negative control and all ERAP1 expression related to this in the form of a percentage. This experiment was carried out twice (Ex.1 and Ex2.) and each set of cell lysates western blotted 3 times (blot 1-3).

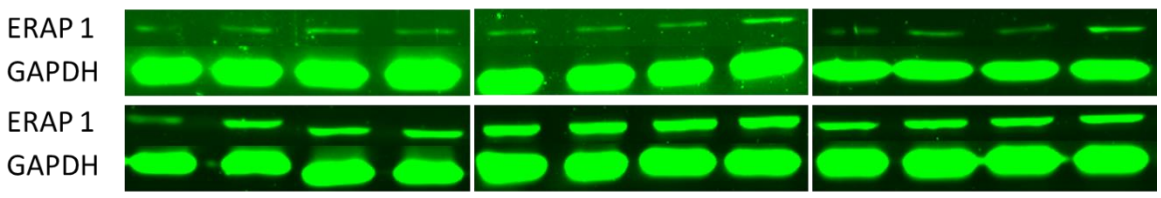

Figure 4-4B: western blots showing ERAP1 expression when extruded ERAP1 siRNA and EVs are incubated with U937 cells. The GAPDH expression of each sample lysate was use to normalise the sample. Each group of 4 are arranged in the same order as the bar chart above (figure 4-4A).

To check if ERAP1 siRNA related ERAP1 expression reduction was being hidden by an upregulation in HLA class I and therefore ERAP1, 10 ng/ml IFNγ was also added to the cells with the extruded siRNA and EVs. Cells were incubated, lysed and western blotted as previously (Figure 4-5A and 4-5B). The percentage of ERAP1 expression was calculated as previously. Once again only one blot of the lysates showed a decrease in ERAP1 expression compared to the negative control whilst the other blots all show a decrease in ERAP1 expression compared to the positive controls (figure 4-5A). Overall the results of the western blots demonstrate no agreement whether the presence of ERAP1 siRNA decreases or increases ERAP1 expression.

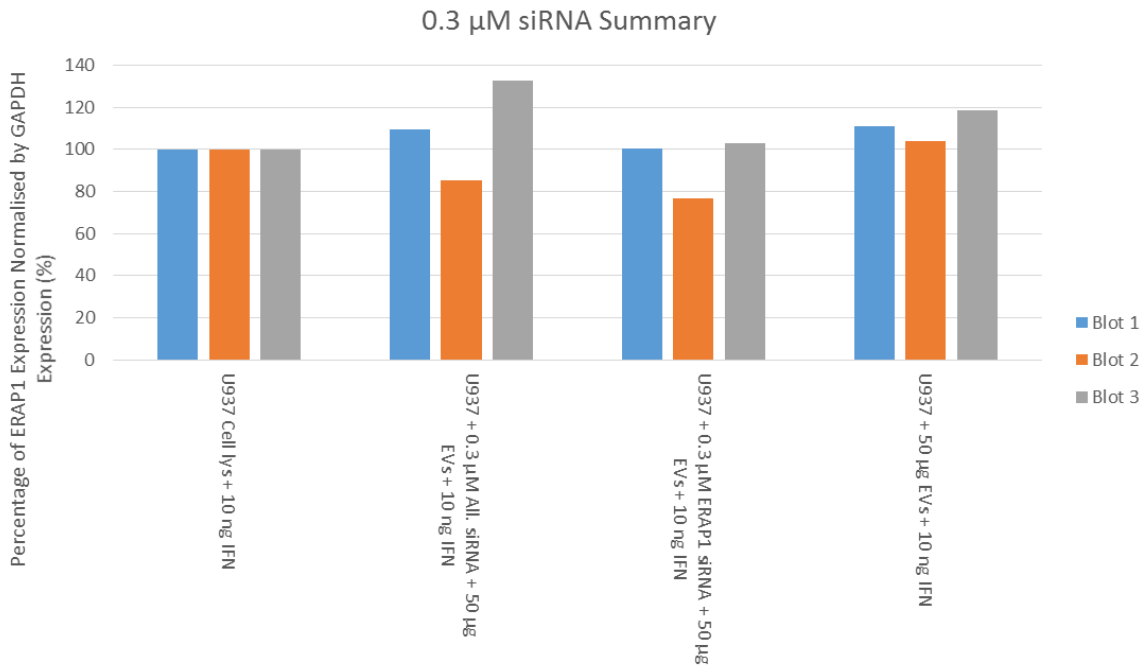

Figure 4-5A: bar chart showing ERAP1 expression when extruded 0.3 µM ERAP1 siRNA and 50 µg U937 EVs are incubated with IFNγ and U937 cells. The percentage of ERAP1 expressed was calculated using the U937 cell lysate negative control. Experiment was performed once and the lysates western blotted three times.

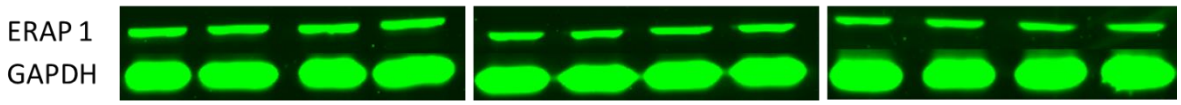

Figure 4-5B: western blot showing ERAP1 expression when extruded ERAP1 siRNA and EVs are incubated with IFNγ and U937 cells. The GAPDH expression of each sample lysate was used to normalise the sample. Each group of 4 are arranged in the same order as figure 4-5A.

Two other concentrations of siRNA were also used with the same protocol as the IFN γ experiments. The concentrations used were 0.1 µM (figure 4-6A) and 0.2 µM (figure 4-7A). As seen in figure 4-6A and figure 4-6B, all ERAP1 siRNA samples show a decrease in ERAP1 expression compared to the negative and positive controls. However, as seen in figure 4-7A an increase in siRNA concentration to 0.2 µM causes the ERAP1 expression levels to again disagree.

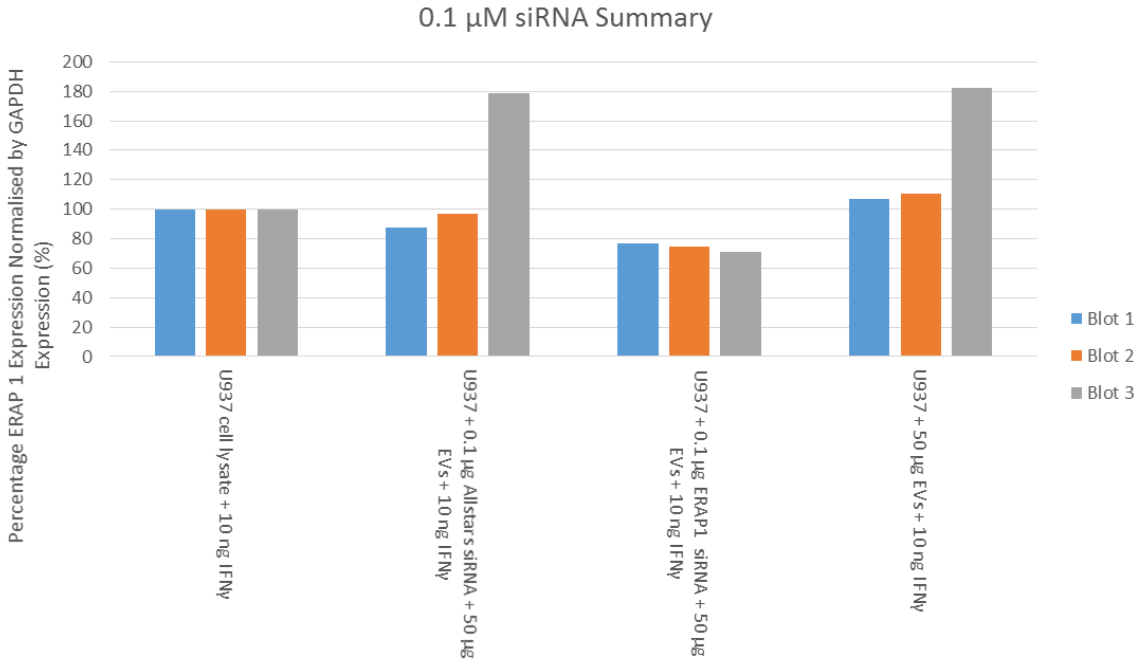

Figure 4-6A: bar chart showing ERAP1 expression when extruded 0.1 µM ERAP1 siRNA and 50 µg EVs are incubated with IFNγ and U937 cells. ERAP1 expression was calculated using the U937 cell lysate (negative control) as 100 %. Experiment was performed once and the lysates western blotted three times.

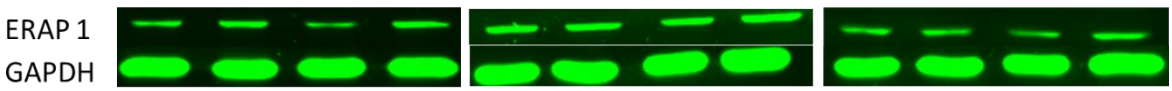

Figure 4-6B: western blot showing ERAP1 expression when extruded ERAP1 siRNA and EVs are incubated with IFNγ and U937 cells. GAPDH expression was used to normalise ERAP1 expression. Each group of 4 samples were arranged in the same order as figure 4-6A.

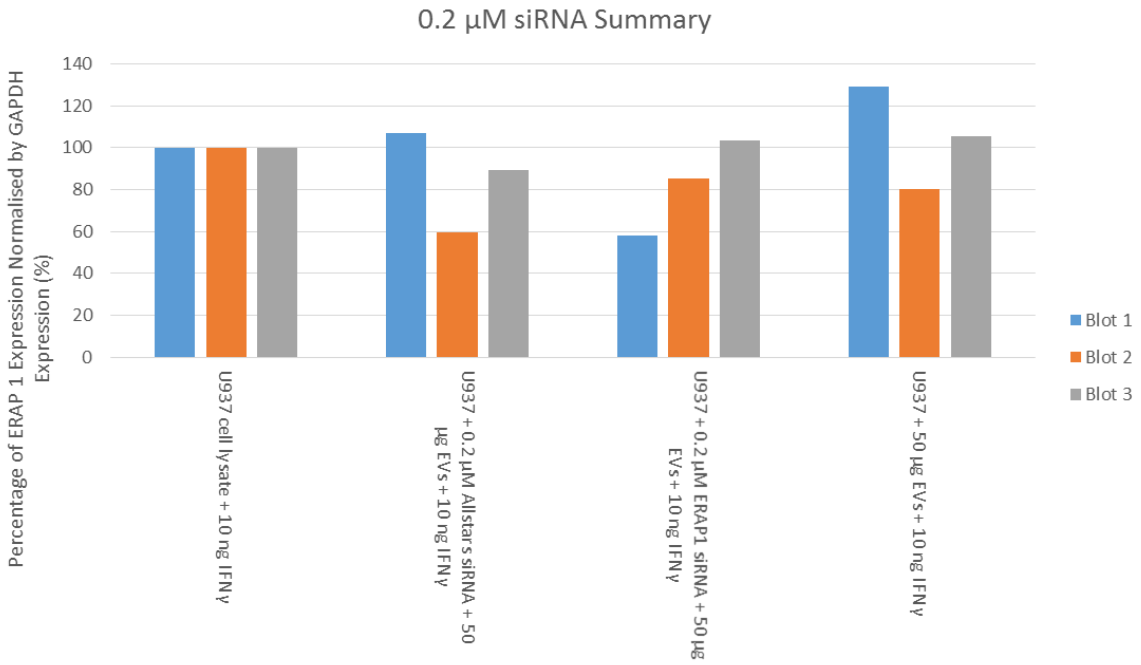

Figure 4-7A: bar chart showing ERAP1 expression when extruded 0.2 µM ERAP1 siRNA and 50 µg U937 EVs are incubated with IFNγ and U937 cells. Percentage of ERAP1 expression was calculated relative to the U937 cell lysate (negative control). Experiment was performed once and cell lysates western blotted 3 times.

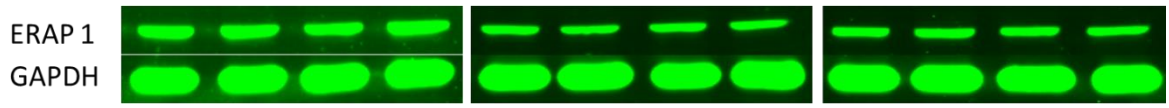

Figure 4-7B: western blot showing ERAP1 expression when extruded ERAP1 siRNA and EVs are incubated with IFNγ and U937 cells. ERAP1 expression was normalised by GAPDH expression. Each group of 4 samples were arranged in the same order as figure 4-7A.

A summary of all siRNA concentrations used with IFN γ (figure 4-8) shows that overall 50 % of western blots showed a decrease in ERAP1 expression compared to the controls. Whether 0.2 µM or 0.3 µM ERAP1 siRNA causes a decrease in ERAP1 expression is inconclusive. Somewhat suprisingly the 0.1 µM siRNA data suggests a concentration which is more likely to cause a decrease in ERAP1 expression.

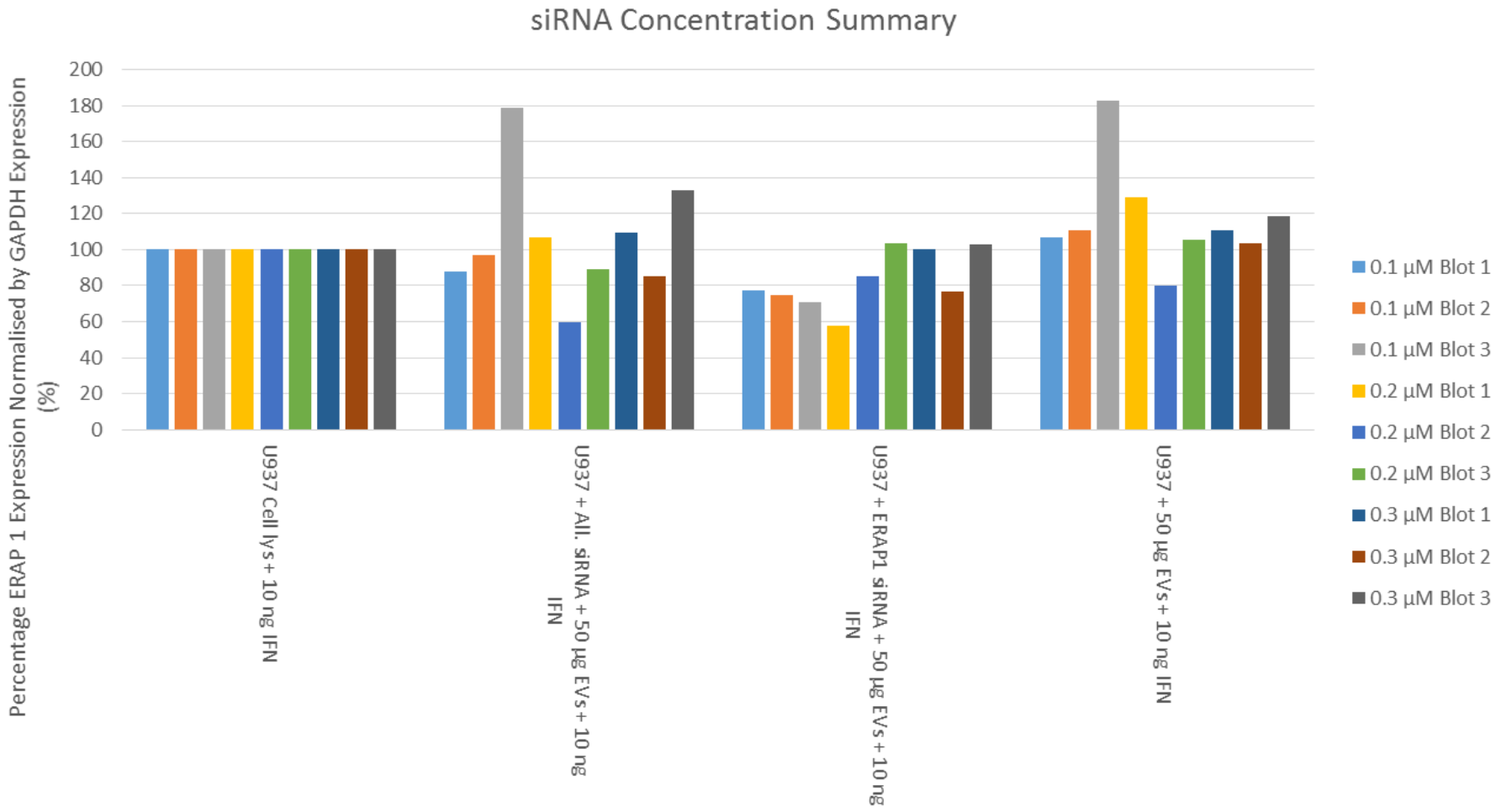

Figure 4-8: bar chart summarising ERAP1 expression when increasing concentrations of siRNA and 50 µg EVs are incubated with IFNγ and U937 cells. Experiment was performed 3 times at increasing concentrations of siRNA and cell lysates were western blotted 3 times. For western blots see individual figures.

4.2 Discussion

Upon comparison of basic extrusion size experiments there was no obvious change in vesicle size. This was probably due to the size of the needles as the larger needle used (25 G) had an inner diameter of 260 µm and the smallest needle available (30 G) had an inner diameter of 159 µm. Whilst significant force was required to extrude the samples through the barrel of the needle, it is evident that this had very little effect on the mean size of the EVs observed on NTA. However despite this some association and encapsulation of siRNA cargo was observed with the use of the 30 G needle. This suggests that, although encapsulation is happening, the EVs apparently do not change in size. Potentially, EV disruption was being induced, but EV reformation was so rapid that damage and alterations were simply not detected.

The force exerted during extrusion is impossible to keep precise between experiments as it was performed manually. Whilst care was taken to apply a similar force, it is possible that a small change in pressure could affect the success of extrusion. For example the extrusion of the 0.1 µM siRNA may have appeared more successful than the higher concentrations due to a different application of force. As the earlier results in this chapter suggest that siRNA encapsulation may not be due to the diameter of the needle, finding a way to maintain the same force between experiments would remove a varying factor.

An important result of this chapter was obtained at the start; the extruded EVs do not greatly change in diameter. Whilst a change in diameter could indicate that EVs have collapsed and reformed, it also influences the way that the EVs may be taken up by cells. This is not a problem for fluorescence studies but would influence a cell assay. Furthermore, altering the EVs in such a way may affect their therapeutic abilities for a clinical application. RME and phagocytosis are the most common uptake pathways for EVs. Reform of the EV may result in a lower percentage of ligands presented on the EV surface. In the case of RME, this would reduce the likelihood of binding and endocytosis which may include the endocytosis of other EVs in the membrane region.

Extrusion is currently used most effectively in the formation of synthetic vesicles (Eiríksdóttir, Konate, Langel, Divita, & Deshayes, 2010; Jo *et al.,* 2014; Papadia, Markoutsa, & Antimisiaris, 2016; Parolini *et al.,* 2009; Simonsen, 2015; Urbano *et al.,* 2015; Van der Meel *et al.,* 2014). Of note, the most commonly formed vesicles by extrusion are unilamellar liposomes. These vesicles are prepared from a lipid film composed of specific lipids depending on the function of the liposomes. A further variation in vesicles formed by extrusion are EVs. By mixing the right combination of phospholipids in suspension it is possible to form a homogenous population of EVs. Specifically, the lipids that EVs are composed from are extruded repetitively through a membrane with pore size 30-200 nm. A more recent development is the extrusion of cells through smaller pores to form nanovesicles composed of

the PM of the cell. The advantage to forming vesicles from a lipid film is being able to choose specific components. For example, if vesicles need to be a specific charge to interact with a cargo it is possible to alter or add in a lipid component. Furthermore, the exact composition of the vesicles is known. However, composing a vesicle by extrusion and enriching a vesicle from cell media are two very different methods. Whilst an enriched EV may be produced under conditions of chemical stress, an extruded EV is produced under physical stress. Another important feature of cell enriched EVs is their contents. This is influenced by the cell type and can result in the packaging of miRNA, tetraspanins and various proteins. An EV produced by extrusion will not possess these proteins which may prove to be an advantage or disadvantage.

More relevant to this research, the extrusion of cargo into vesicles has been previously reported (Fuhrmann, Serio, Mazo, Nair, & Stevens, 2014; Haney *et al.,* 2015). Fuhrmann and colleagues recorded that they extruded their EVs with drug 31 times through 400 nm pores whereas Haney *et al.* recorded that they extruded 10 times through 200 nm pores. Similarly, in this research encapsulation of cargo with 5 extrusions through a single 159 µm pore has been observed. However neither of these experiments employed a wash step to degrade any unbound cargo. Fuhrmann and colleagues report their loading efficiency in terms of drug molecule per vesicle however they do not specify the position of the drug in relation to the vesicle. Haney and colleagues specify that they enriched EVs loaded with 22.2 % catalase from free cargo by gel filtration chromatography. However, as seen in this chapter, it is possible for cargo to remain associated with the outside of EVs. Fuhrmann and colleagues do not mention enrichment after extrusion. Together this suggests that some of the encapsulation seen in the literature could be cargo associated with the outside of EVs as well as encapsulation. In this current research it has been shown that the effects seen in the cell assays are likely due to siRNA encapsulated by vesicles, due to the use of an RNase A incubation step.

Given the initial data in this chapter, future research into this area could make use of more specific vesicle extrusion devices available commercially, especially those used in the generation of liposomes, that have membrane pore sizes as low as 0.03 µm. One such example, used by both Fuhrmann *et al.* (Fuhrmann *et al.,* 2014) and Haney *et al.* (Haney *et al.,* 2015) is the Avanti Lipid extruder. An analysis using such equipment based on the preliminary data shown here could yet provide a simple extrusion method for EV loading.

Chapter 5: Electroporation

Electroporation is a well-established technique for the brief generation of holes in the surface membrane of cells. This allows the uptake of cargo such as proteins or more frequently siRNA or DNA for transient or stable transfection of cells. Electroporation uses an electrical potential to punch holes in the membrane in order to allow passage of material into the cell. Considering the similarity of the EV membrane to the plasma membrane, it was hypothesised that it would be possible to create holes in EVs by which siRNA or other cargo would be able to enter. Furthermore, a high profile exosome paper used electroporation for similar siRNA loading with the settings being chosen to start this study based on that paper (Alvarez-Erviti *et al.,* 2011), where targeted EVs were used to deliver BACE1 siRNA to the mouse brain in order to study an Alzheimer's Disease (AD) model.

5.1 Results

These studies began with the analysis of the changes in events detected by the flow cytometer when the EVs were added to and electroporated in the chosen media. EVs were electroporated in either sucrose dissolved in double distilled water (ddH_2O) to a concentration of 100 mM or PBS in a range of 400 – 750 V at 50 µF. The post-electroporation samples were analysed by flow cytometry. Care was taken to notice the background pattern inherent for the flow cytometer with PBS alone. Percentages of events were calculated by gating around the un-electroporated PBS control sample. The value obtained was subtracted from 100 to attain the percentage of events occurring outside of the background area. This allowed the assessment of increases in either or both side scatter (SSC) and forward scatter (FSC) for the events detected. Essentially an increase in FSC or SSC may be due to an increase in size or granularity of the events detected suggesting the presence of EVs. As can be seen in figure 5-1, both PBS and sucrose show a base value of <3 % of events outside of the gated area (light blue bars). Upon electroporation there is an increase of at least 76 % for all samples containing PBS. Alternatively, all the samples containing only sucrose dissolved in ddH_2O showed an increase of 2-4 % maximum after electroporation. Of significant interest, there are increases in events outside the gate for sucrose dissolved in ddH_2O with EVs. For 400 V (orange bars) and 500 V (grey bars) samples there is an increase of 59 % and 63 %, respectively, when compared to the non-electroporated control. This

then decreases for 600 V (yellow bars) and 750 V (dark blue bars) to an increase of 7 % and 6 %, respectively. The data suggest sucrose as a preferred electroporation medium compared to PBS.

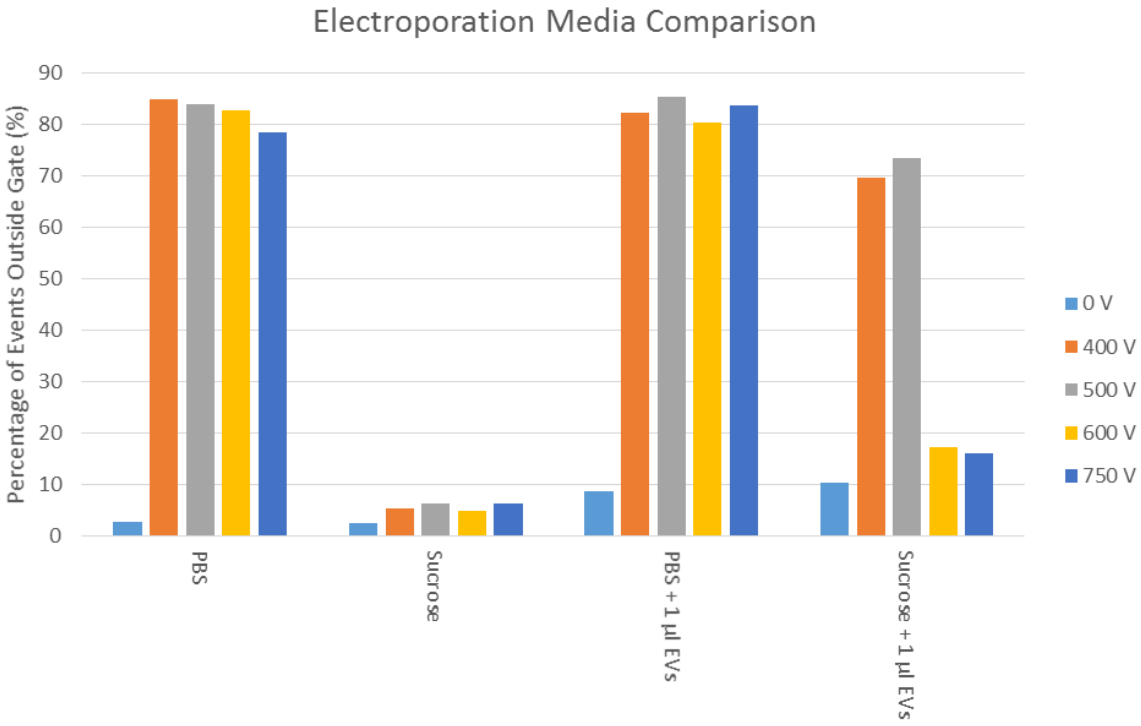

Figure 5-1: bar chart comparing the position of events recorded on a SSC vs. FSC dot plot. The control PBS at 0 V was used to set a gate. Here the use of specific electroporation media is compared. n=1.

Next the range of voltages trialled was increased. Again the electroporated sucrose in ddH_2O had a low background at all voltages similar to the un-electroporated (lightest blue bars) control (figure 5-2) and with the addition of EVs an increase in events outside of the set gate is seen across all voltages. In the bottom bar chart of figure 5-2 there is an increase of 11-19 % when samples containing EVs are electroporated. In the top bar chart there is an increase of 1-21 % when the EV control is electroporated. This data and the previous data together show that the EVs increase in either or both size and granularity when electroporated, particularly at lower voltages such as 400 V (orange bars) and 500 V (grey bars). This suggests that the EVs may be aggregating. Of note, at voltages of 600 V and above there is a lower percentage increase in events outside of the set gate.

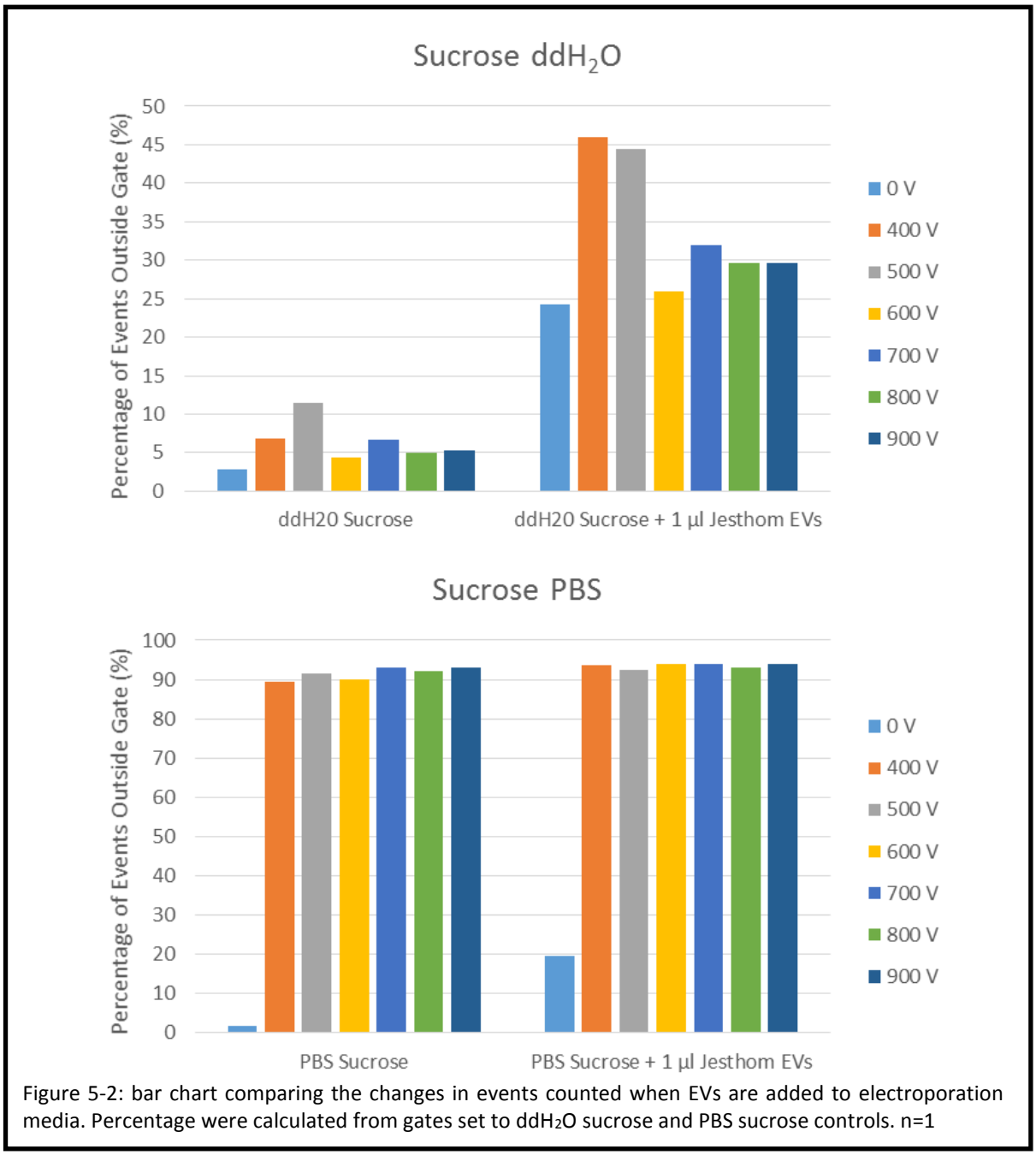

Figure 5-2: bar chart comparing the changes in events counted when EVs are added to electroporation media. Percentage were calculated from gates set to ddH_2O sucrose and PBS sucrose controls. n=1

To check the samples for aggregates the experiment was performed again at 300, 600 and 1200 V, according to Hood *et al.,* and then the samples observed on both NTA and flow cytometer (Hood *et al.,* 2013). This time sucrose diluted in PBS was used rather than sucrose diluted in water. In the literature the use of PBS (or a similar mixture) is favoured over ddH_2O (Dad Abu-Bonsrah, Zhang, & Newgreen, 2016; Fuhrmann *et al.,* 2014; Hood *et al.,* 2013). This may be because the ions in PBS help the conductance of the electrical potential or form a more hospitable environment for membrane recovery. In figure 5-3A there is an observed increase in concentration of particles from 0.26×10^8 particles per ml to a minimum of 4.47×10^8 particles per ml in the sucrose in PBS control. This information confirms that aggregates form in the electroporation media even without the presence of EVs. Most surprisingly, the mean diameters of the particles formed during electroporation of sucrose PBS without EVs are in the size range of EVs. This means that the events observed outside the gated area from the flow cytometry analysis may be aggregates. When sucrose PBS was electroporated with EVs present there was only an increase of 3.94×10^8 particles per ml for 600V whilst the other voltages show a decrease in concentration of particles compared to the non-electroporated control. However the 600 V sample with EVs present also had an increase in mean particle diameter. Together this suggests that post electroporation samples containing EVs may also still contain aggregates however the majority of particles are most likely EVs. To ensure that stock sucrose PBS was not contaminated it was filtered with a 0.22 µm filter. This would filter out any particles present above 220 nm. The results of this can be seen in figure 5-3B. For either PBS or sucrose PBS unelectroporated controls (light blue bars), the number of events outside the gate was less than 7 % and 9 %, respectively. When EVs were added to these media the events outside the gate increased to 16 % and 17 %, respectively. However when all 4 samples were electroporated a large increase in events outside the gate was observed. This confirmed that it was not electroporation media contamination but electroporation itself that causes an increase in events outside the gated area. It was also noted that sucrose PBS samples compared to PBS samples showed a smaller increase in events outside the gate. This suggests that the presence of sucrose prevents some of the aggregation formed during electroporation.

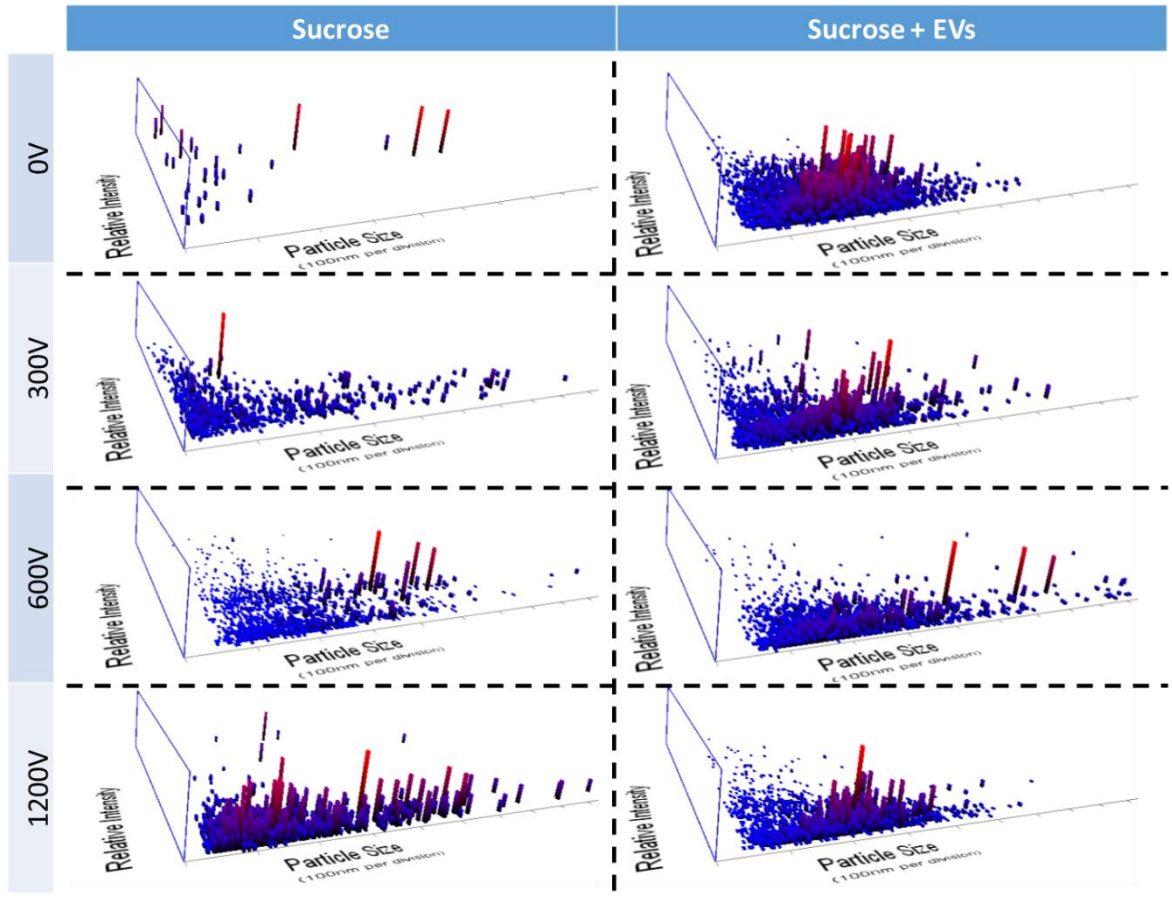

Voltage (V)	Sucrose		Sucrose + EVs	
	Mean Diameter (nm)	Concentration (10^8 particles/ml)	Mean Diameter (nm)	Concentration (10^8 particles/ml)
0	264	0.26	212	15.96
300	170	4.97	196	10.35
600	297	10.06	278	18.02
1200	231	4.47	220	10.46

Figure 5-3A: relative Intensity vs. particle size bar charts. When a voltage is applied to either 100mM sucrose dissolved in PBS or 100mM Sucrose dissolved in PBS with Jesthom EVs added, there are changes in the concentration and size of the particles analysed.

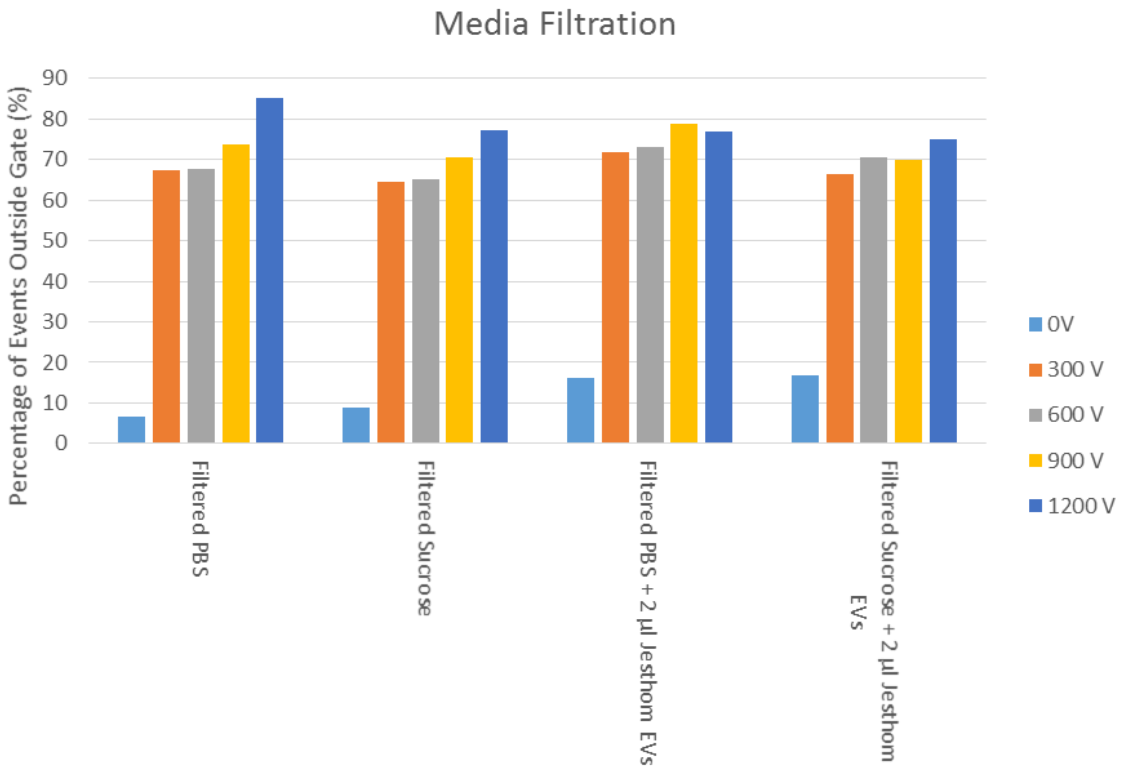

Figure 5-3B: bar chart comparing electroporation media. A gate was set around the filtered PBS control and the number of events measured and compared to the gate for each sample. n=1

To further reduce the aggregation seen post-electroporation other electroporation media compositions were researched. Traditionally electroporation media contains EDTA as a metal chelator for free ions that detach from the cuvette plates. Therefore, 100mM sucrose in PBS was electroporated with either 1 mM EDTA or 2 mM EDTA. Samples were prepared as previously and electroporated at voltages between 500 V and 900 V before analysis by flow cytometry. In figure 5-4, the addition of EDTA at either concentration causes a decrease in the number of events seen outside the set gate at every electroporation voltage except 600 V. Furthermore the use of 2 mM EDTA shows a decrease again in 3 of the 5 electroporation voltages. This decrease in events outside of the gate however varies between 1 % and 20 %. As 2 mM EDTA shows a decrease in possible aggregation, it was included in further experiments.

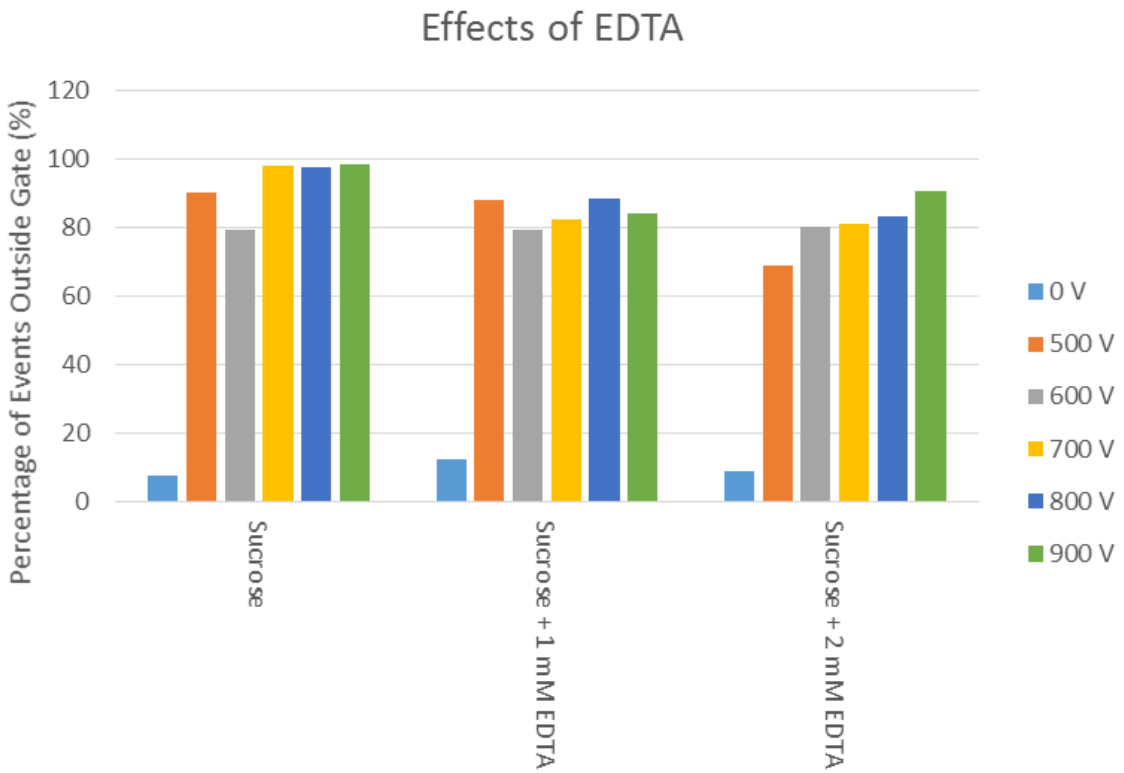

Figure 5-4: bar charts comparing the effects of two concentrations of EDTA on electroporation media. A gate was set to the PBS at 0 V control and samples compared. n=1.

Whilst conducting this research a paper was published describing the use of Trehalose as a pulse field medium for electroporation (Hood *et al.,* 2013). Trehalose is a disaccharide capable of protecting cells during stress in extreme conditions. It is commonly used in medicine and biotechnology as a cryopreserving agent (G. Chen *et al.,* 2016; López, Bollag, Yu, Isales, & Eroglu, 2016; Payton, Wempe, Xu, & Anchordoquy, 2014). Trehalose is described as a tool to disperse EVs post electroporation and therefore may reduce aggregation further. 50 mM trehalose was trialled as an electroporation media with and without 2 mM EDTA. For comparison, sucrose, also with and without 2 mM EDTA, was electroporated alongside the trehalose samples. The samples of sucrose and trehalose with EDTA both show fewer events outside the gated area than their counterparts without EDTA (figure 5-5) and both show very similar results. The sucrose and EDTA showed more reduction than trehalose and EDTA for 3 out of 5 voltages. Trehalose was chosen as the next media due to its advantages in the literature however as this chapter continues it will continue to be compared to sucrose controls.

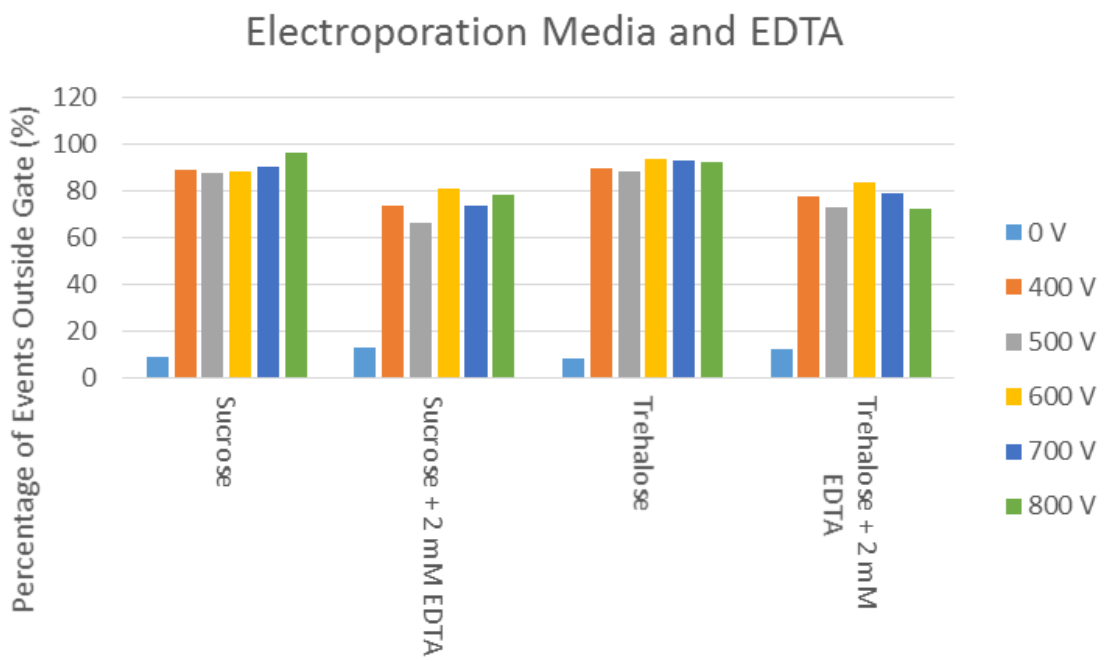

Figure 5-5: bar chart comparing the percentage of events outside of a control gated area for different electroporation media. Sucrose at 0 V was used to make the control gate. n=2.

Having settled on a media that is documented to reduce EV aggregates and appears to have a reduced amount of aggregates when it is electroporated, it was decided to test electroporation with the previously described reporter siRNA construct (Allstars siRNA non-coding siRNA labelled with Alexafluor 488). Samples of 0.05 µM Allstars siRNA were prepared in either 50 mM trehalose with 2 mM EDTA or 100 mM sucrose with 2 mM EDTA. Allstars siRNA was used alone initially to observe the flow cytometry events of the samples when they were electroporated (figure 5-6A). The presence of Allstars siRNA in the electroporation media does not appear to cause an increase in aggregates for most of the samples. An increase of 11 % was the largest increase seen between trehalose and EDTA when siRNA was added. Furthermore, on the fluorescent intensity histograms (figure 5-6B) the trehalose control sample initially shows an unmeasurable amount of fluorescent particles despite not containing Allstars siRNA. These histograms were not gated to a particular population. This same pattern was seen for the 2 previous samples of sucrose and EDTA with Allstars siRNA therefore this may be residue from a previous sample in the flow cytometer. Aggregation of the Allstars siRNA may cause the grouping of fluorescent particles to a level that may match that observed. If electroporation has caused aggregation of the Allstars siRNA it may have also caused its charge to change. This may make it difficult to wash out of the flow cytometer sampling capillary or off the stirrer in the flow cytometer.

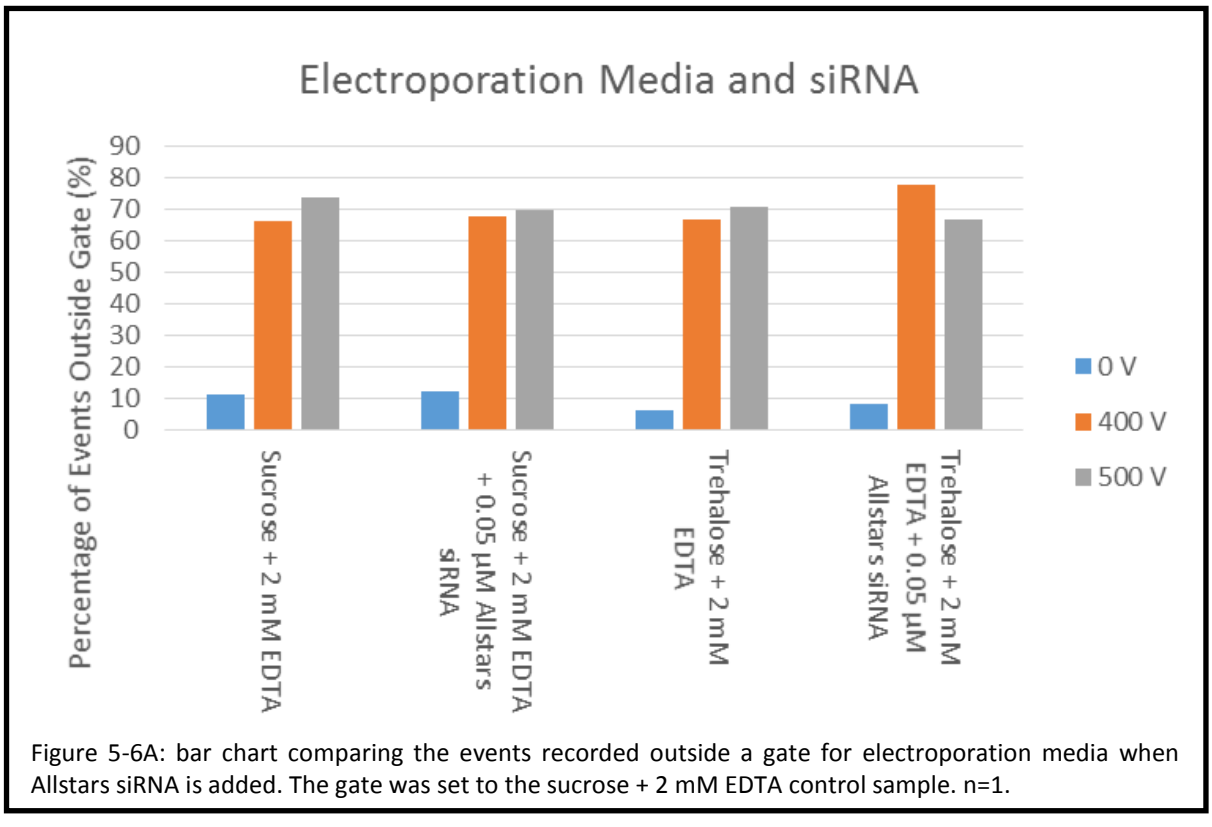

Figure 5-6A: bar chart comparing the events recorded outside a gate for electroporation media when Allstars siRNA is added. The gate was set to the sucrose + 2 mM EDTA control sample. n=1.

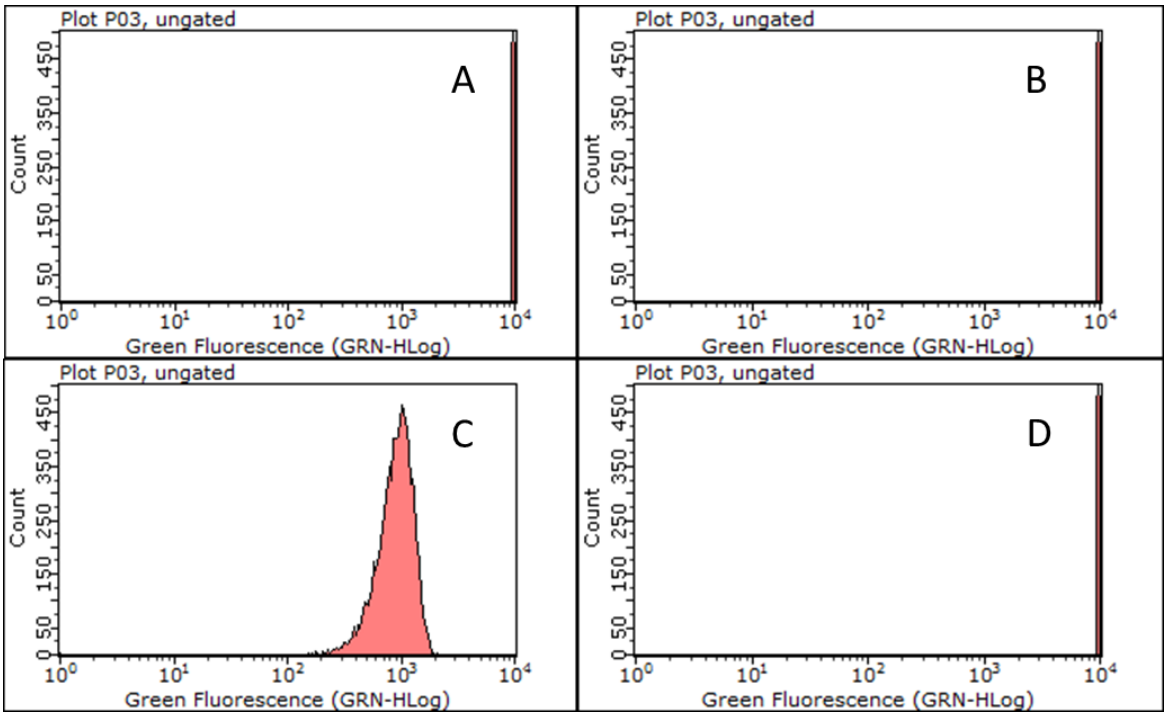

Figure 5-6B: fluorescent intensity histograms displaying the shift in fluorescent particle counts and intensity of fluorescence when Allstars siRNA is electroporated. Large amounts of fluorescence were recorded.
A: 50 mM Trehalose + 2 mM EDTA. B: 100 mM Sucrose + 2 mM EDTA + 0.05 µM Allstars siRNA at 400 V. C: 50 mM Trehalose + 2 mM EDTA + 0.05 µM Allstars siRNA. D: 50 mM Trehalose + 2 mM EDTA + 0.05 µM Allstars siRNA at 400 V.

Kooijmans *et al*. published a paper, during the ongoing experiments, describing the identification of siRNA aggregates in electroporated samples (Kooijmans *et al.,* 2013). Therefore, latex beads were used to wash away the unbound Allstars siRNA, as it should not interact with the latex beads. The extra bead capture step begins with the incubation of beads with sample at room temperature for 15 minutes. This is followed by an incubation on ice for 1 hour. Following this the samples are centrifuged and washed with PFN before analysis on the flow cytometer. As theoretically there would be no change in samples, presuming that the siRNA would not bind and be washed away, EVs were also added to this experiment. This may allow observation of interactions between EVs and Allstars siRNA. The flow cytometer settings were altered to detect the beads. The Allstars siRNA control sample shows low levels of fluorescence outside the gated area, comparable to the trehalose media and bead only control showing that the siRNA does not attach to the latex beads (figure 5-7A, bottom graph). The Allstars siRNA and EV in Trehalose control shows a small increase in fluorescence suggesting that all unbound Allstars siRNA was not washed away. However, the electroporated samples of this control show a further increase in fluorescence which continues to increase as the electroporation voltage increases. This suggests that the fluorescent events detected outside of the gated area are due to a combination of Allstars siRNA associated with EVs and Allstars siRNA aggregates. This is supported by the increase in events on the SSC and FSC dot plot outside of the gated area in figure 5-7A (top graph). When electroporation is applied to the media with EVs and siRNA the events outside the gate increase as the voltage increases. However the media and EVs control sample also shows a high number of events outside the gate. This experiment was therefore repeated with the addition of Allstars siRNA control samples electroporated alongside the EV and Allstars siRNA samples. This would indicate if the increase in SSC and FSC events was due to the presence of the EVs or Allstars siRNA. In figure 5-7B (top graph) a lower percentage of events outside the gated area is seen than figure 5-7A; all <10 %. Again the events outside the gate for the EV and Allstars siRNA samples increase as the electroporation voltage increases. There is also an increase in the events observed for the Allstars siRNA electroporated controls though these do not increase with the voltage and remain <6 %. In terms of fluorescent events (bottom graph) again there is an increase in fluorescence when a voltage is applied to the EV and Allstars siRNA samples. However the Allstars siRNA control samples also show an increase in fluorescence as the voltage increases, though smaller than the EV and siRNA samples. This suggests that the majority of the increase in fluorescence seen for EV and Allstars siRNA samples is due to the interaction of the siRNA with the EVs and only a small portion may be attributable to aggregation of siRNA and its inability to be totally washed away.

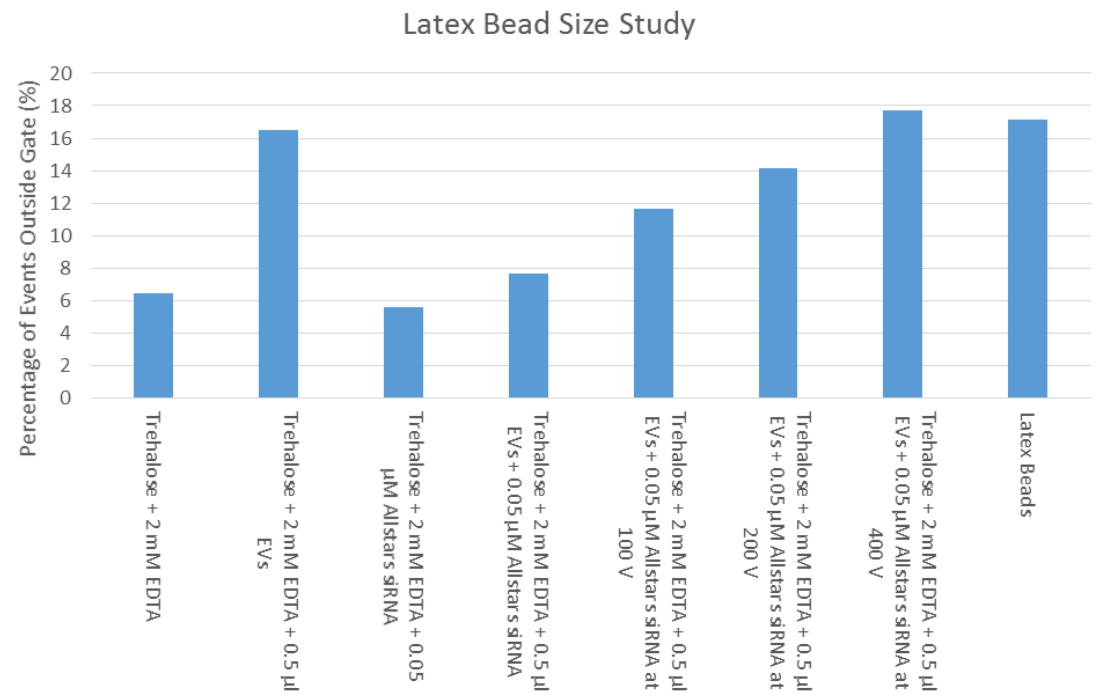

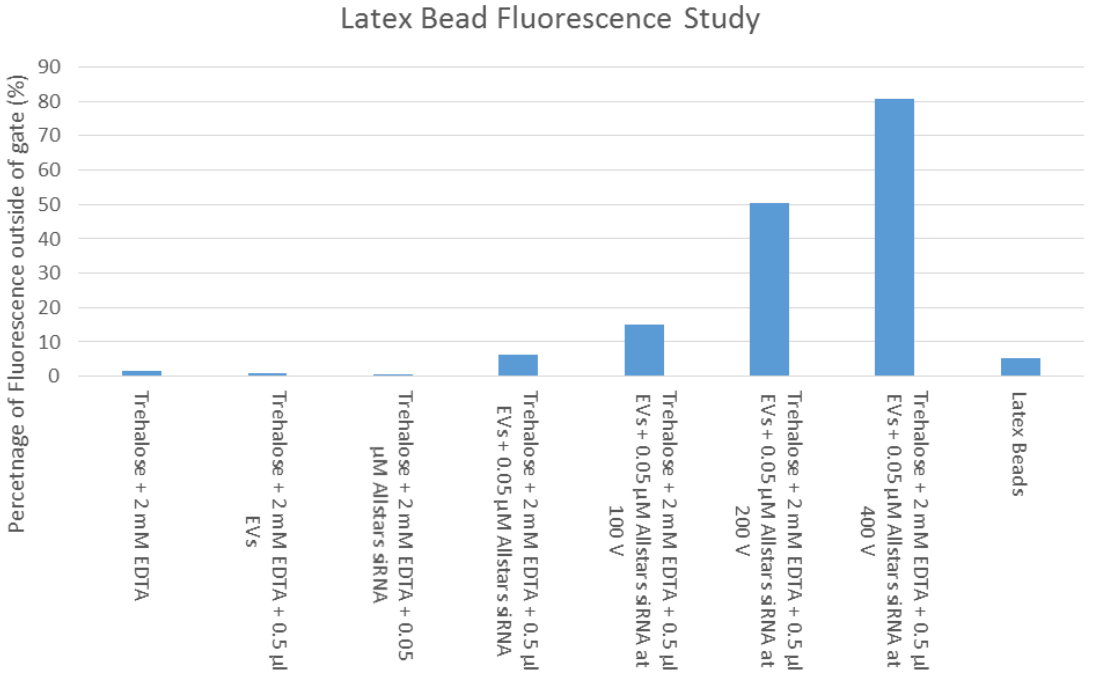

Figure 5-7A: bar charts showing the number of events and fluorescent events outside of a set gate. The gates for both were set to the trehalose + 2mM EDTA sample. n=1.

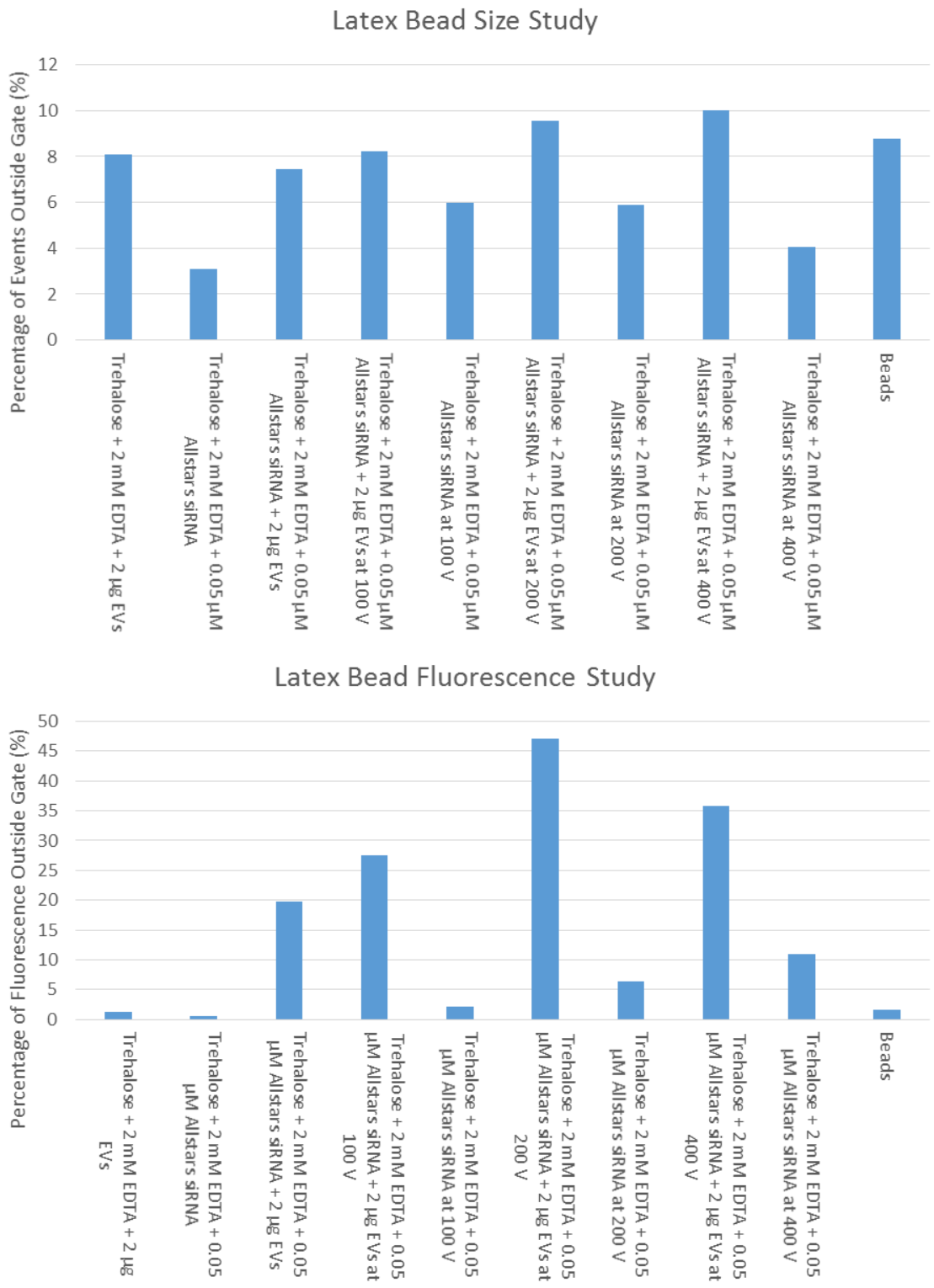

Figure 5-7B: bar charts showing the number of events and fluorescent events outside of a set gate. The gates for both were set to the trehalose + 2mM EDTA + 2 µg EV sample. This experiment was a repeat of figure 5-7A with extra controls and an increased concentration of EVs used. n=1.

To address the issue of removing unbound siRNA, and to discriminate between the Allstars siRNA encapsulated and the Allstars siRNA associated with the EV membrane, an RNase A wash step was introduced after the samples had been associated with the latex beads. The unelectroporated control samples (figure 5-8, bottom graph) show a low percentage of fluorescent events outside the set gate when exposed to RNase A. In particular the EV and Allstars siRNA control showed a 16 % decrease when RNase A was added therefore the RNase A removes almost all non-encapsulated Allstars siRNA. The EV and Allstars siRNA samples that had been electroporated at 100, 200 and 400 V without the RNase A incubation show an increase in fluorescence as the voltage increases (figure 5-8, bottom graph). However, the Allstars siRNA controls electroporated also increase in fluorescent events as the voltage increases suggesting that as the voltage increases the fluorescence due to Allstars siRNA aggregates may increase. When an RNase A wash is applied to these controls and samples, however, there is a major reduction to <5 % in the percentage of fluorescent events outside the gated area. These results demonstrate the critical importance of using RNase A to remove non-encapsulated siRNA, in this experimental system, which caused misleading fluorescence levels. In terms of aggregate formation (figure 5-8, top graph) there is a mixture of results. There does not appear to be a pattern between voltage and number of events detected outside the gate. However all Allstars siRNA controls (both with and without RNase A) show a lower percentage of events outside the gate compared to the EV and Allstars siRNA samples. This suggests that part of the EV population is detectable by conventional flow cytometry.

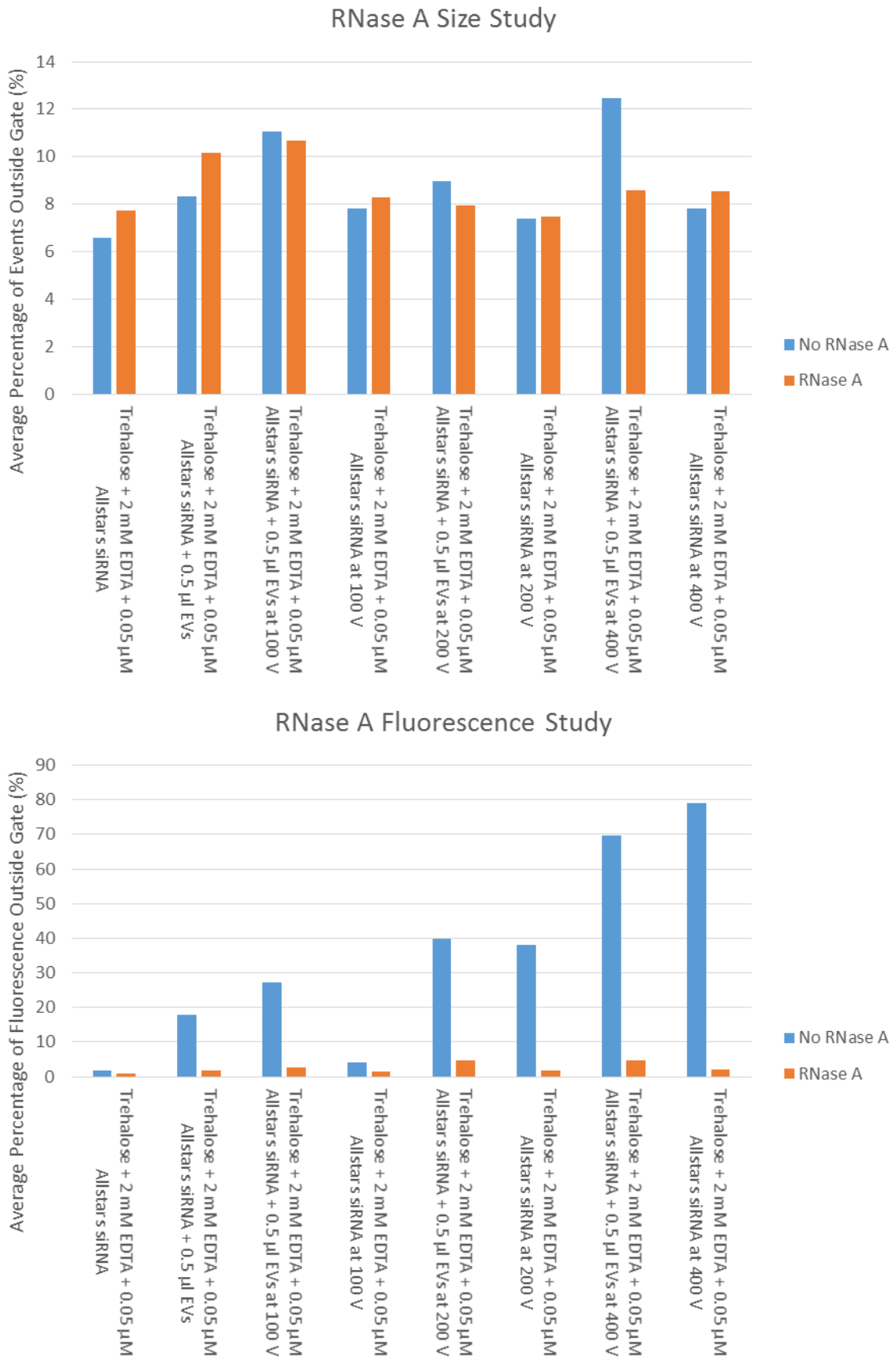

Figure 5-8: bar charts comparing the events and fluorescent events outside of a set gate for samples with an RNase A wash step. The gate was set to a trehalose + 2 mM EDTA control. n=2

As the current method of electroporation was not showing encapsulation of Allstars siRNA above 5 % a literature search was conducted for alternative electroporation methods. A multiple pulse method was described in a paper by Canatella and colleagues (Canatella *et al.,* 2001). The current method was adapted by adding multiple electroporation pulses. It was hypothesised that with multiple pulses there would be an increased chance of permeating the EVs. Initially 5 pulses were used and the RNase A incubation step was included. Whilst the RNase A step is able to remove the Allstars siRNA and EV control fluorescence (data not shown), there is no reduction in the percentage of fluorescence seen when electroporated samples are exposed to RNase A. In the previous section the RNase A removed the majority of the remaining Allstars siRNA. In figure 5-9 (bottom graph) there is a similar pattern present to figure 5-8, the RNase A appears to reduce the events detected outside the gated area where EVs and Allstars siRNA are concerned. Together this data suggests that the siRNA aggregates are destroyed by RNase A but that the siRNA is retained as the fluorescence seen outside the gate does not decrease.

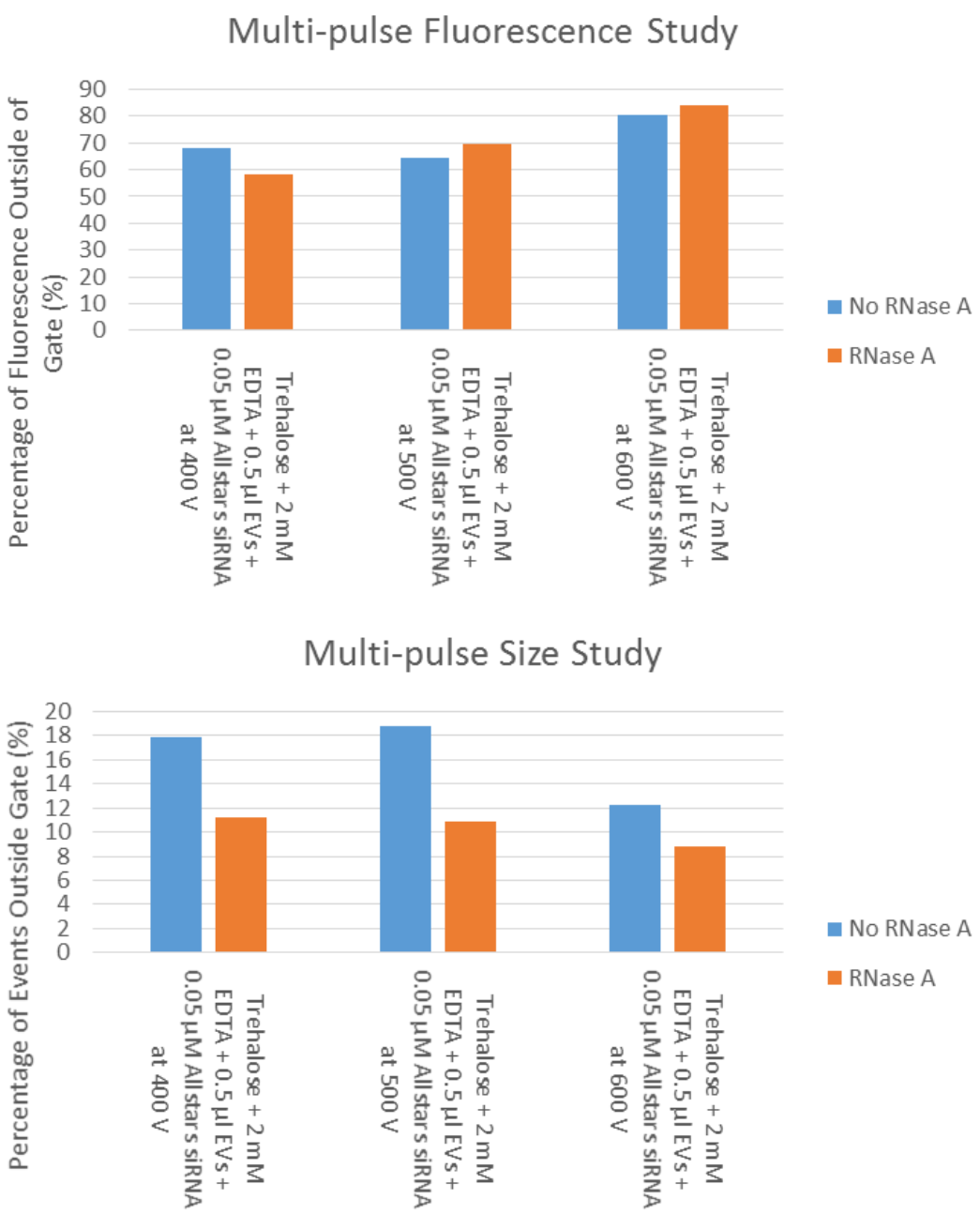

Figure 5-9: bar charts comparing samples with or without RNase A exposed to five pulses of electroporation. Percentages were calculated form a gate set to a control sample of trehalose + 2 mM EDTA. n=2.

A point of interest, yet to be explored, is the inhibition of ribonucleases (such as RNase A) by metal ions formed during electroporation (Breslow & Girotti, 1969). 2 mM EDTA was previously used to reduce aggregation caused by metal ions, however, to ensure that the increased number of pulses was not increasing the metal ions produced the concentration of EDTA was doubled to 4 mM. Reducing the metal ions may improve RNase A function. In figure 5-10 (top graph) the majority of samples show a decrease in fluorescence when electroporated in 4 mM EDTA compared to 2 mM EDTA. In the bottom graph there is no decrease in gated events for samples electroporated in 4 mM EDTA compared to 2 mM EDTA. Specifically there appear to be more events present outside the gate for the majority of 4 mM EDTA electroporated samples. However for the majority of samples there is a decrease in events observed outside the gate when RNase A is added. Together this suggests that increasing the concentration of EDTA does not prevent the aggregation of particles as seen earlier in this chapter. This also suggests that RNase A is reducing the number of aggregates observed. As the electroporation voltage increases there is also an increase in the fluorescent events observed outside of the gated area. For the samples exposed to RNase A there is a decrease in the fluorescence detected for both concentrations of EDTA, more so for 4 mM EDTA than 2 mM EDTA. Importantly, the addition of RNase A to the EV and Allstars siRNA control causes a decrease in the fluorescence observed. This suggests that increasing the EDTA concentration may improve RNase A function. Furthermore, the RNase A samples show that the fluorescence seen in the non-RNase A samples is due to Allstars siRNA associating with the outside of the EVs.

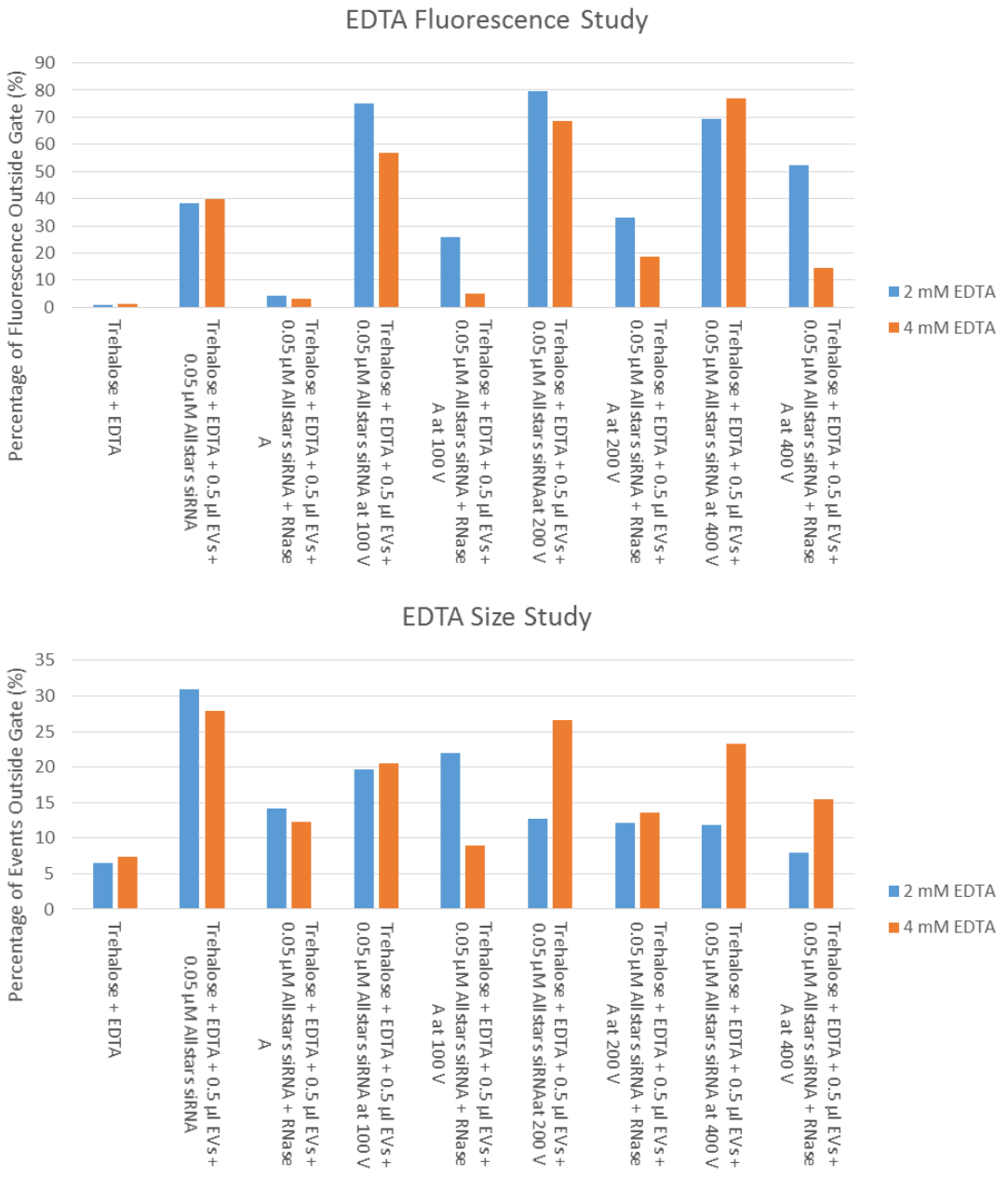

Figure 5-10: bar charts comparing the use of different concentrations of EDTA. The trehalose + EDTA control was used to set a gate and the events counted or fluorescent particles observed outside the gate calculated. n=2.

Next, samples were electroporated with 1, 2, 3, 4 and 5 pulses in 2 mM EDTA media to observe if there was a change in fluorescence as the pulses increased. For this experiment 400 V was used. In figure 5-11 (top graph) the fluorescence detected outside the gate increases with the number of electroporation pulses from 1 to 4 pulses and then decreases at 5 pulses. When exposed to RNase A the same samples show a reduced fluorescence in general but still follow the same pattern. Four pulses at 400 V shows the highest fluorescence with five pulses the second most fluorescent when RNase A is added. This suggests that four or five pulses may cause cargo encapsulation. On the bottom graph of figure 5-11 a mixture of results is seen again which do not indicate whether the number of pulses effects the formation of aggregates however all samples had a percentage of events outside the gate of <15 %.

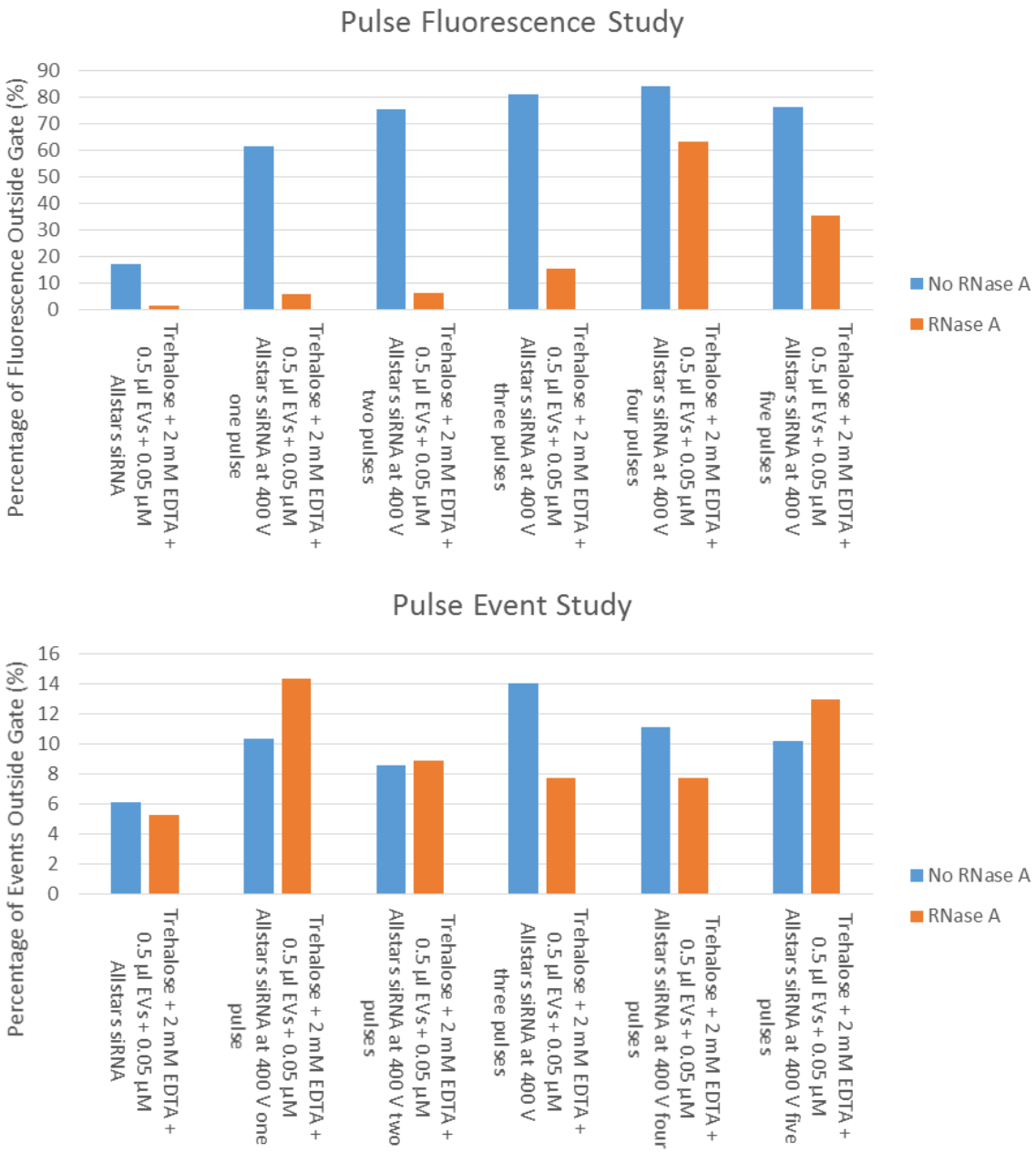

Figure 5-11: bar chart comparing changes in fluorescence or events observed when a series of electrical pulses are applied to samples. The fluorescence and events were measured outside of a gate set to a trehalose + 2 mM EDTA control. n=2.

The experiment was repeated with 4 mM EDTA in the electroporation media (figure 5-12). Similar to figure 5-11, there is an increase in fluorescence outside the gate with the number of electroporation pulses used for both concentrations of EDTA. However the 4 mM EDTA samples with RNase A do not retain fluorescence outside the gate above 5 %. This suggests that the fluorescence observed for 2 mM EDTA samples with RNase A may be a factor of the RNase A being bound by free ions. Together this suggests that the Allstars siRNA is associated with the outside of the EVs rather than encapsulated. The bottom graph of figure 5-12 shows that there are more events counted outside the gate for the samples with 4 mM EDTA than 2 mM EDTA. This suggests that more particles are aggregated.

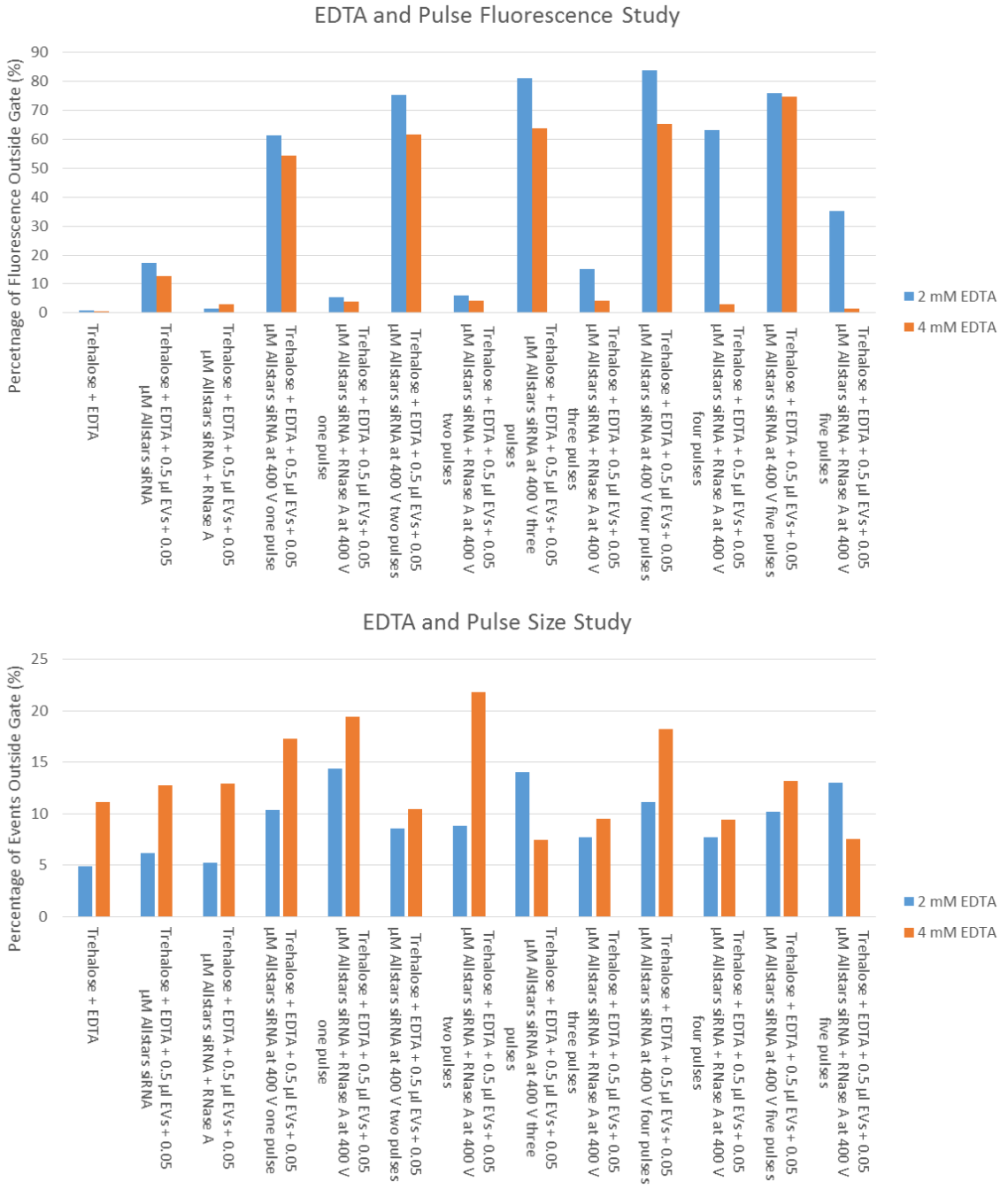

Figure 5-12: bar chart comparing changes in fluorescence or events observed when a series of electrical pulses are applied to samples containing different concentrations of EDTA. The fluorescence and events were measured outside of a gate set to a trehalose + EDTA control. n=2 for 2mM data, n=1 for 4 mM data.

A decisive indication of siRNA encapsulation by EVs would be a cell based assay. For this GAPDH siRNA was used. A downregulation of GAPDH expression would indicate that siRNA had been delivered, presumably by the EVs. HeLa cells were used as recipient targets. Samples containing EVs and Allstars siRNA were electroporated at 400 V with either 1 pulse or 4 pulses (the minimal and maximal number of pulses that an increase in fluorescence was observed for). The samples were then incubated with RNase A before addition to confluent HeLa Cells and left for 48 hours. Cells were then lysed and western blotted for GAPDH expression (GAPDH Ab) and HC dimer expression (HC10 Ab). GAPDH expression was normalised by HC dimer expression. Upon analysis (figure 5-13A and 5-13B) it was observed that there was a reduced expression of GAPDH in some of the samples compared to the HeLa cell control. For half the comparisons the 1 pulse sample showed the lowest expression and the other half the 4 pulses sample showed the lowest GAPDH expression. Whilst the 4 pulse sample of siRNA electroporated with EVs followed by an RNase A step showed 43 % expression, the siRNA and EV control both with and without the RNase A step also exhibited low GAPDH expression. This suggests that the downregulation cannot be credited to encapsulation of the siRNA in EVs.

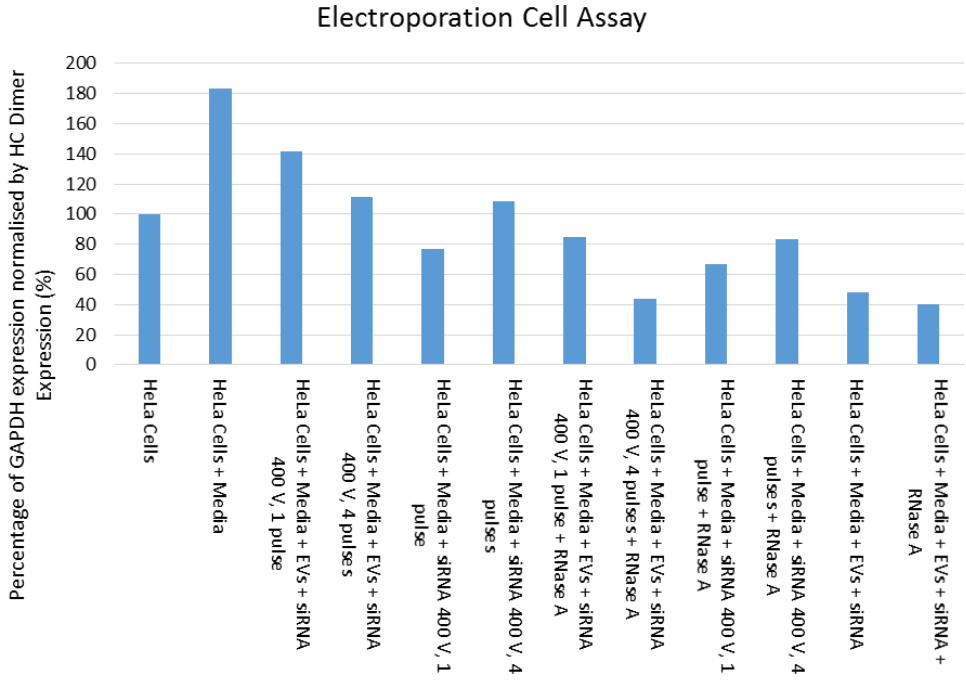

Figure 5-13A: bar chart showing the changes in GAPDH expression when EVs electroporated with GAPDH siRNA are incubated with HeLa cells. n=1.

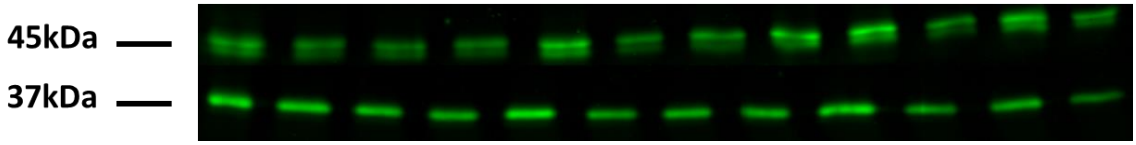

Figure 5-13B: western blot of GAPDH (37 kDa) and HC10 (45 kDa) expression of HeLa cells after incubation with electroporated EVs and GAPDH siRNA. Samples are ordered the same as figure 5-13A. HC10 was used to normalise GAPDH.

5.2 Discussion

It is worth starting by discussing the limitations of flow cytometry. The smallest vesicles detected by flow cytometry appear to be between 200 and 300 nm in diameter (Van der Pol *et al.,* 2014; Van Der Pol, Van Gemert, Sturk, Nieuwland, & Van Leeuwen, 2012). The diameter of exosomes is in the range of 50-200 nm. This suggests that flow cytometry is not a suitable platform for analysing exosomes. However it is possible to see changes in the percentage of events outside the gated areas of FSC and SSC dot plots throughout this chapter when EVs are added. This raises the question of what is actually being seen. An alternative theory is that the EVs are aggregating or swarming (Van Der Pol *et al.,* 2012). This means they are grouping together and being detected as a single larger particle, causing a false calculation of both size and concentration. Furthermore, if fluorescent tags were to be applied for specific vesicle population detection it is possible that exosomes would swarm with microvesicles. Therefore the flow cytometry data presented in this thesis should be analysed for the effects of conditions or components on EVs rather than looking at individual EVs. In hindsight, the use of a dedicated or high resolution flow cytometer might have yielded more informative single particle data (Pospichalova *et al.*, 2015; Van der Pol *et al.*, 2014; van der Vlist, Nolte-'t Hoen, Stoorvogel, Arkesteijn, & Wauben, 2012).

The first change that was made was the use of PBS to dilute sucrose. Whilst the electroporation of PBS on its own showed an increase in the background pattern observed, sucrose was also seen to slightly quench the increase (figure 5-3C). Together sucrose and PBS formed a media with less large particles. To further this investigation, the sugar in the electroporation media was changed to trehalose. Although the trehalose did not reduce the background more than sucrose media did, the trehalose was recorded to protect the particles more than sucrose. Trehalose has successfully been used as an electroporation media by many groups for electroporating both cells and bacteria (Johnsen *et al.*, 2016; Lu, Zhang, Lv, Bie, & Lu, 2012; Mohr *et al.*, 2006; Mussauer, Sukhorukov, & Zimmermann, 2001). Looking at the literature, trehalose has been used as an electroporation buffer for a while yet its use is not wide spread (Dad Abu-Bonsrah *et al.,* 2016; Fuhrmann *et al.,* 2014; Lamichhane, Raiker, & Jay, 2015). Evidence from this research supports the use of trehalose as an electroporation media.

EDTA was also added, initially as a free metal ion chelator to prevent the formation of aggregates. Later this was revisited with regards to ribonuclease inhibition and further metal ion production. There are few research papers that focus on the benefits of optimising EDTA levels (Lin, Lin, Chien, & Chern, 2011). Looking at the results of this chapter, it is obvious that increasing the concentration of EDTA prevents aggregation. However the use of a high concentration of EDTA can affect the calcium binding and re-adherence of adhesive cells. An avenue with regards to this that was

not able to be explored in this chapter is the use of RNase A and NAP-10 columns with electroporation. Additional enrichment by a NAP-10 sephadex column would allow transfer of the EVs into a media with a lower concentration of EDTA therefore increasing cell viability in cell assays. Using RNase A to remove un-encapsulated siRNA cargo is a key control. It is important to state that this is a step that is missing from a significant number of published studies where electroporation has been claimed to load cargo into exosomes. The use of siRNA conjugated to a fluorophore would aid in the identification of the percentage of siRNA that is encapsulated versus the siRNA that is associated with EVs. For an example of this please refer to the Sonication results presented later in this thesis.

In recent literature there has been use of multiple pulse methods (Canatella *et al.,* 2001; Lamichhane *et al.,* 2015; Mohr *et al.,* 2006; Salimzadeh, Jaberipour, Hosseini, & Ghaderi, 2013; Shtam *et al.,* 2013). Pulses range from 2 up to 10 pulses. An increase in pulses provides the opportunity to further permeate the membranes of EVs. In combination with the use of trehalose and EDTA the multi-pulse method may be a viable option, however this research has yet to see an improvement on using one pulse. To improve on the data obtained in this study, it would be productive to explore the effects of pulses above 5 times. This would allow insight into higher settings that may provide new data on encapsulation or particle formation.

It is obvious from the results encountered in this chapter that electroporation is complex. There are so many different parameters and settings involved that optimizing one setting may change the optimization of another. Changing the chemical composition has been briefly looked at and the effects of different voltages explored. Whilst chemical help, such as EDTA, countered problems that arose there are still adverse conditions that require optimisation. There were also quite a few questions still to be answered with regards to electroporation. An important question is whether the changes in event size and granularity are related to EV uptake. In a number of figures throughout this chapter there is a constant change in the number of events seen outside the gated area of the SSC and FSC control plots. This could suggest that a population of EVs is more susceptible to permeation. Alternatively, it could be aggregation of EVs, siRNA or both. As can be seen in figures 5-13A and 5-13B, the transfer of GAPDH siRNA into HeLa cells via EVs was unsuccessful. This may reflect on the stability of GAPDH siRNA compared to fluorophore conjugated siRNA. The most efficient type of cargo to transfer needs further optimisation.

Alvarez-Erviti and colleagues have published a paper claiming the ability to use electroporation to encapsulate siRNA in EVs and then deliver it to a target site (Alvarez-Erviti *et al.,* 2011). From the published methods replicated in this chapter, it is plain that their methods do not reproduce the same results. Achieving optimal electroporation conditions is time consuming and may

not produce reproducible results therefore making it unrecommendable as a method for loading usable EVs.

Chapter 6: PEI

Polyethylenimine (PEI) is a polycationic molecule available in linear and branched forms. PEI can transfect cells through complexing with cargo. Due to their large cationic charge they are able to form complexes with anionic siRNA in a non-covalent manner (Hobel & Aigner, 2010). In addition, it is thought that the cargo is released on the inside of the cell by the proton sponge method whereby the amines cause osmotic swelling (Behr, 1997). The increase in pressure causes the lysosome to burst open and the cargo is then free to disperse through the cytoplasm. PEI has successfully been used in previous studies as a transfection agent, and it was therefore assessed here for its ability to load cargo inside EVs (Günther *et al.,* 2011; Laroui *et al.,* 2014).

6.1 Results

To ensure that the PEI was able to transfect cells and was therefore functional it was complexed to 4 ERAP1 siRNAs from 4 different companies (Thermo fisher, Qiagen, R&D and Santa Cruz) then the complexes incubated with confluent Jesthom cells overnight. After western blot analysis it could be seen that the Thermo Fisher and Qiagen siRNAs were successful in some degree of ERAP1 knockdown (figure 6-1A and 6-1B) suggesting that the PEI is functional as a transfection agent.

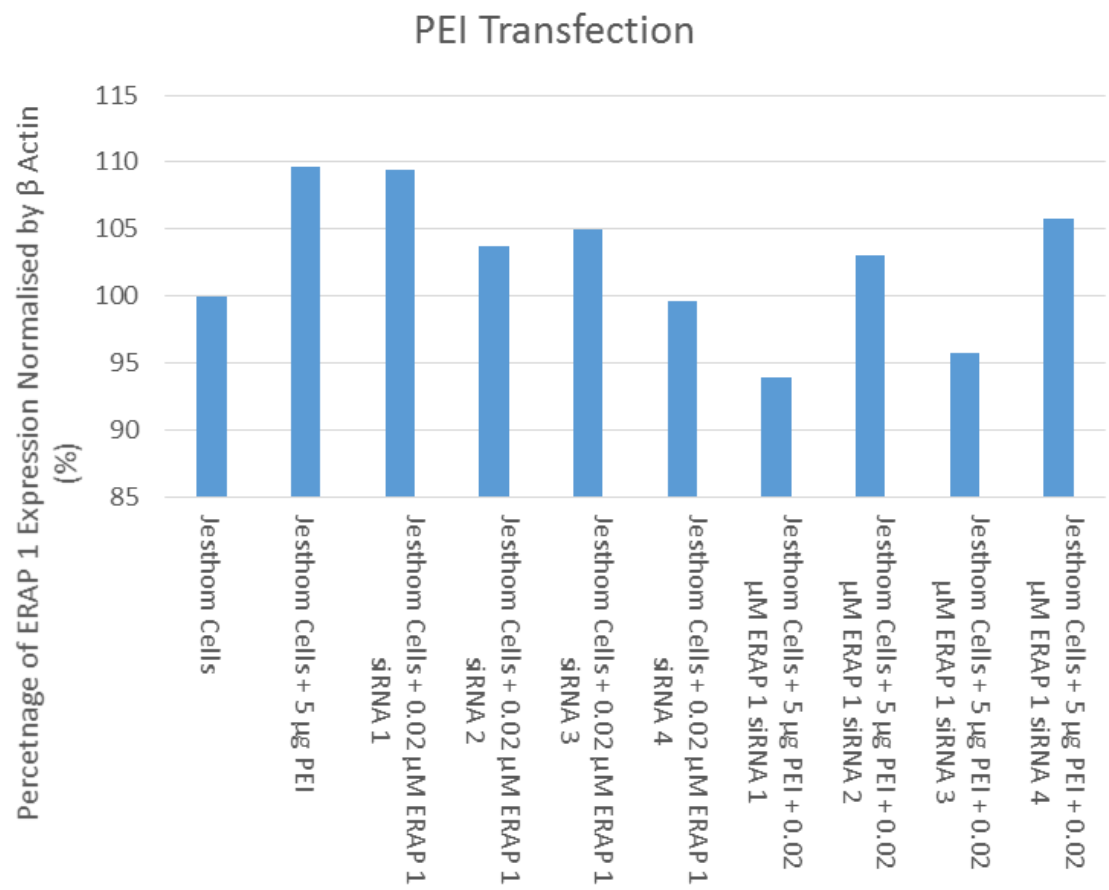

Figure 6-1A: bar chart showing the change in ERAP1 expression, as normalised by β Actin, compared to a Jesthom Cell control. siRNA 1 = Thermo Fisher, siRNA 2 = R&D, siRNA 3 = Qiagen and siRNA 4 = Santa Cruz. n=2.

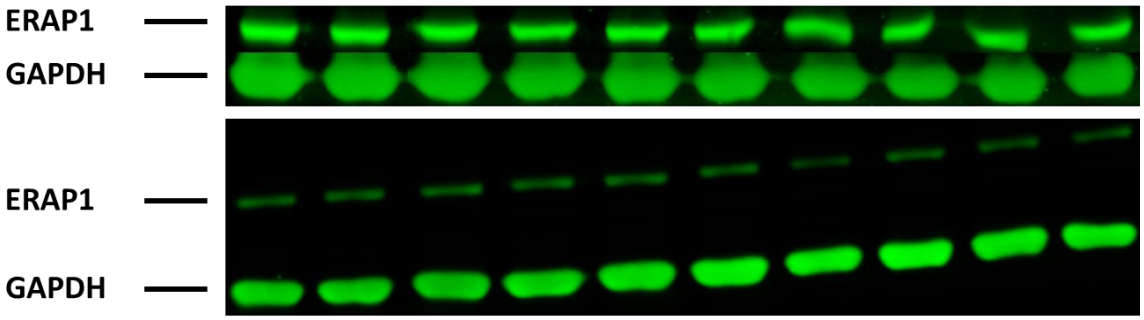

Figure 6-1B: western blot showing the expression of ERAP1 in Jesthom cells after incubation with PEI and ERAP1 siRNA. Samples are arranged in the same order as figure 6-1A.

Initial experiments were conducted with NTA analysis of HeLa cell supernatant with the addition of 0.5 or 1 µg PEI and 0.01 µM Allstars siRNA. If the EVs encapsulated the PEI-siRNA complexes the vesicles may change in size where PEI entry was repaired. This is because materials may be added or lost in the repair process. An increase in vesicle size in the presence of 0.5 µg PEI and 1 µg PEI with or without siRNA being present was observed (figure 6-2, top graph). However 0.5 µg PEI on its own showed the presence of aggregation on the concentration bar chart (figure 6-2, bottom graph). This may suggest a critical window for EV modification. The sample concentration for the EV samples also appeared to increase when PEI was added but not Allstars siRNA suggesting that PEI is able to form large molecules on its own. These same samples were also analysed on the flow cytometer where it was observed that the EV, PEI and siRNA samples showed a gradual increase in fluorescence with increase in PEI concentration (not shown). This suggests that PEI plays a direct role in delivering Allstars siRNA to the EVs.

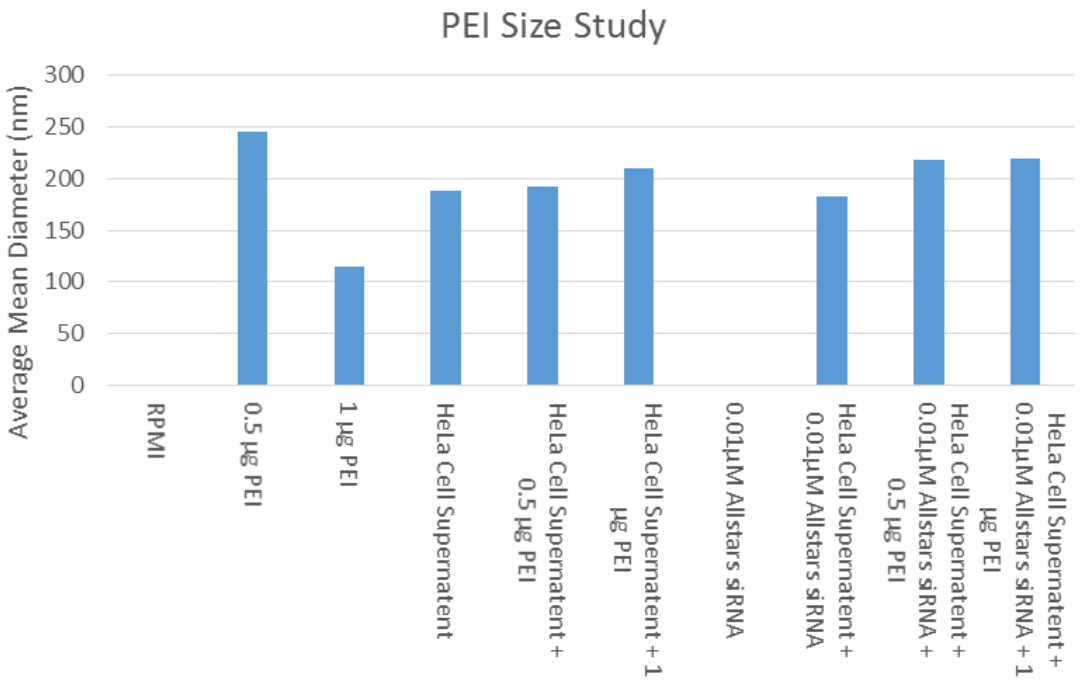

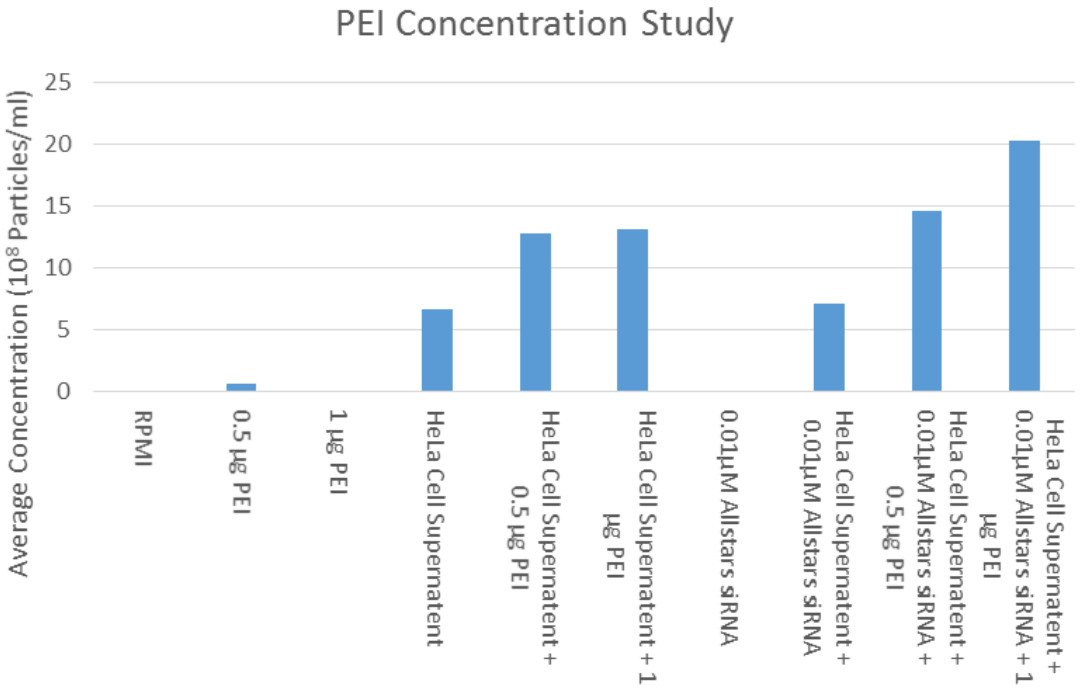

Figure 6-2: bar charts showing the change in Particle size and concentration for different concentrations of PEI with and without FITC siRNA on NTA. For all samples with Allstars siRNA an increase in particle size can be seen. n=2.

To determine if PEI was aggregating alone, and in different solvents, 4 concentrations of PEI were re-suspended in both ethanol and ddH_2O. PEI used previously in this chapter was dissolved in ethanol to prevent the formation of crystals during storage at -20 °C. After a literature search, it was discovered that recent studies involving PEI had used ddH_2O as the dissolving agent. The 4 concentrations of PEI were analysed by flow cytometry. A gate was set to an RPMI control FSC and SSC dot plot and the percentage of events outside of the gate measured. The percentage of events outside the gate refers to the number of events that increased in size or granularity. In figure 6-3, after 0.5 µg PEI there is a gradual increase in events detected outside the dot plot gate as the concentration increases. This suggests, with 0.5 µg PEI as the exception, aggregates increase with PEI concentration. For PEI dissolved in ethanol a similar pattern is not observed however for all samples except 1 µg PEI there is a lower event detection than PEI in ddH_2O. This data suggests that 0.5 µg is the optimal concentration for PEI dissolved in ethanol while 1 µg is the optimal concentration for PEI dissolved in ddH_2O. Importantly, it must be noted that all concentrations of PEI showed increases of <2.1 %. Altogether this data shows that both solutions are viable options.

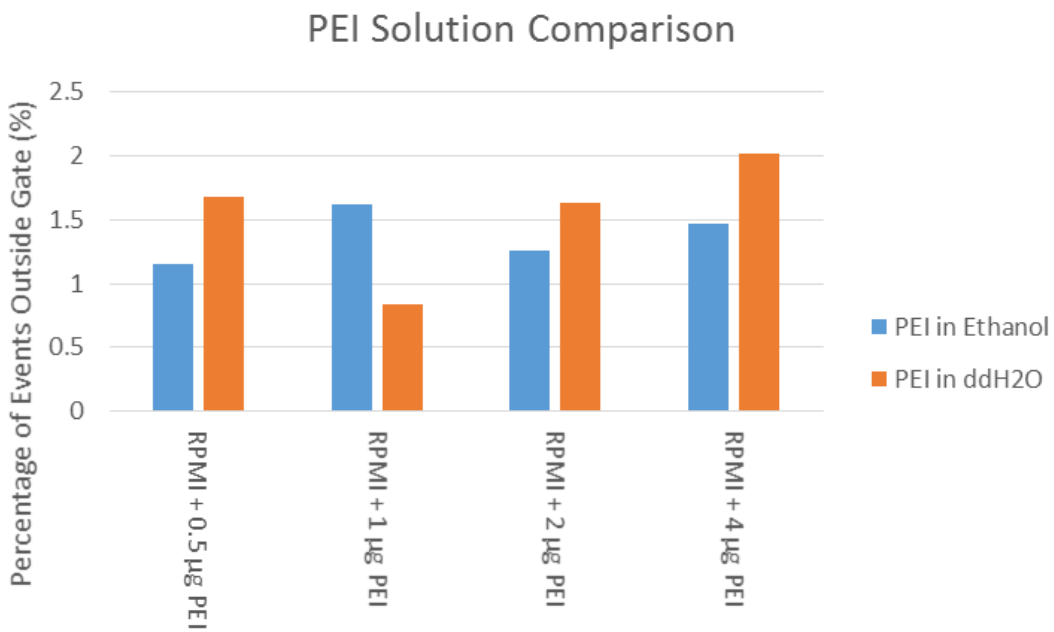

Figure 6-3: bar chart showing the background events detected for PEI in solution with either ethanol or ddH_2O. Percentage of events were calculated based on a gated RPMI control dot plot. n=1.

In the next section the behaviour and change in characteristics of EVs with the PEI in ethanol or PEI in ddH_2O were studied further (figure 6-4). Four concentrations of PEI (0.5, 1, 2 and 4 µg) were incubated with and without EVs in RPMI overnight. These samples were then analysed by flow cytometer as previously. In the ddH_2O suspended PEI samples there was little change in the percentage of events detected. However, the ethanol suspended PEI sample showed an increase in events detected when 4 µg of PEI was added and when 2 µg was added with EVs. An increase of this magnitude was not detected in the previous experiment. This suggests that PEI in ethanol at certain concentration thresholds can combine to form aggregates, potentially enhanced after overnight incubation. In this experiment it would appear that PEI suspended in ddH_2O does not form larger complexes as readily as PEI suspended in ethanol.

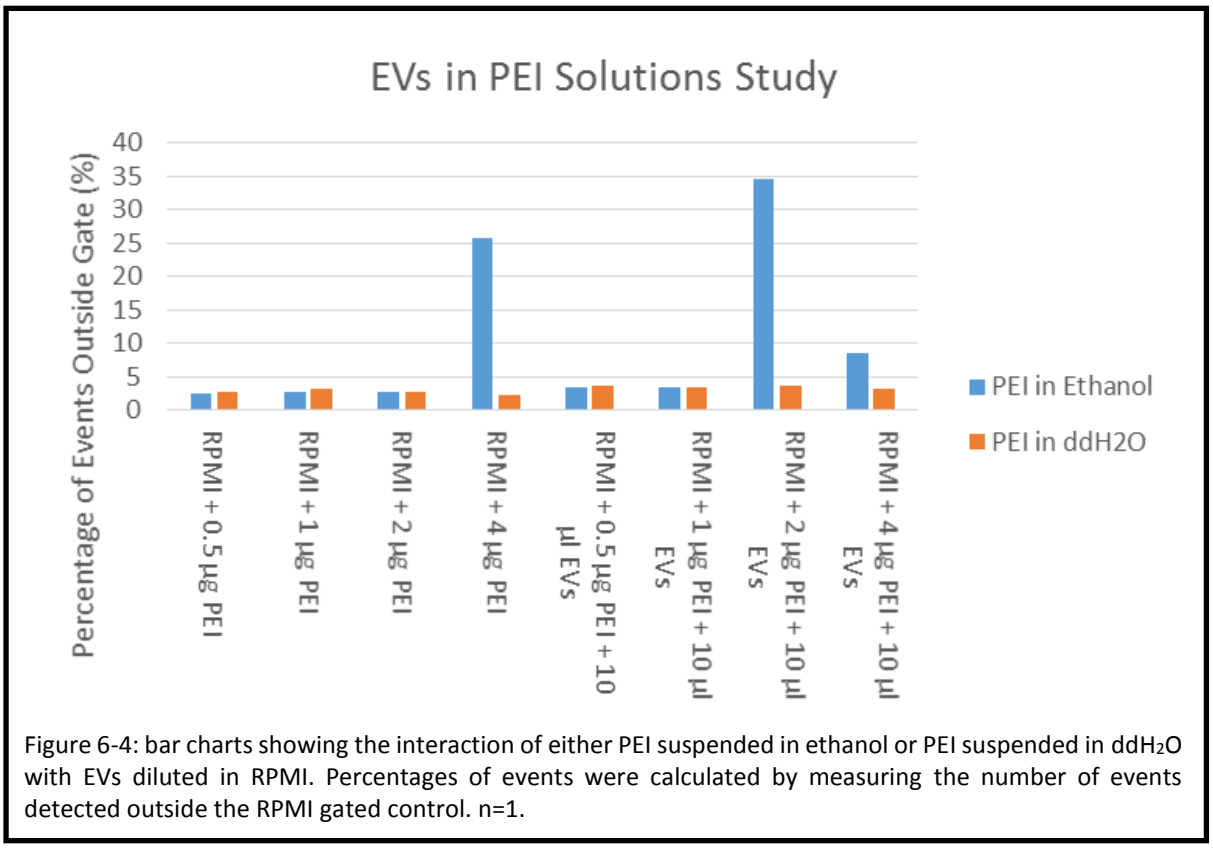

Figure 6-4: bar charts showing the interaction of either PEI suspended in ethanol or PEI suspended in ddH_2O with EVs diluted in RPMI. Percentages of events were calculated by measuring the number of events detected outside the RPMI gated control. n=1.

As the PEI suspended in ddH_2O showed the smallest increase in events outside the gate in the previous experiment its use was continued with this experiment. The previous method for PEI transfection of EVs that was used involved mixing all the components simultaneously. To encourage complex formation to occur before the PEI becomes associated with the EVs a new method was implemented. PEI and siRNA were incubated at 37 °C for 30 minutes before incubation with EVs at RT for 2 hours. This time 2 concentrations of EVs and Allstars siRNA were used with PEI and the samples left to incubate overnight. Samples were then analysed by flow cytometry and percentages of events or fluorescent events calculated. From the flow cytometry analysis, it can be seen that the samples containing Allstars siRNA all display an increase in fluorescence (figure 6-5, bottom graph) compared to the same samples without it, across all concentrations of PEI. Furthermore there is an increase in events detected as the concentration of EVs increases in the top graph of figure 6-5 when EVs are added indicating the possible presence of a population of EVs. Again there is a greater increase in events when 0.5 µg PEI is used compared to the other concentrations. However, for the fluorescence bar chart, none of the increases go above 10 %. Similarly, the increases in events outside the gate on the events bar chart does not go above 15 %. This may suggest that ddH_2O dissolved PEI only encourages small amounts of encapsulation.

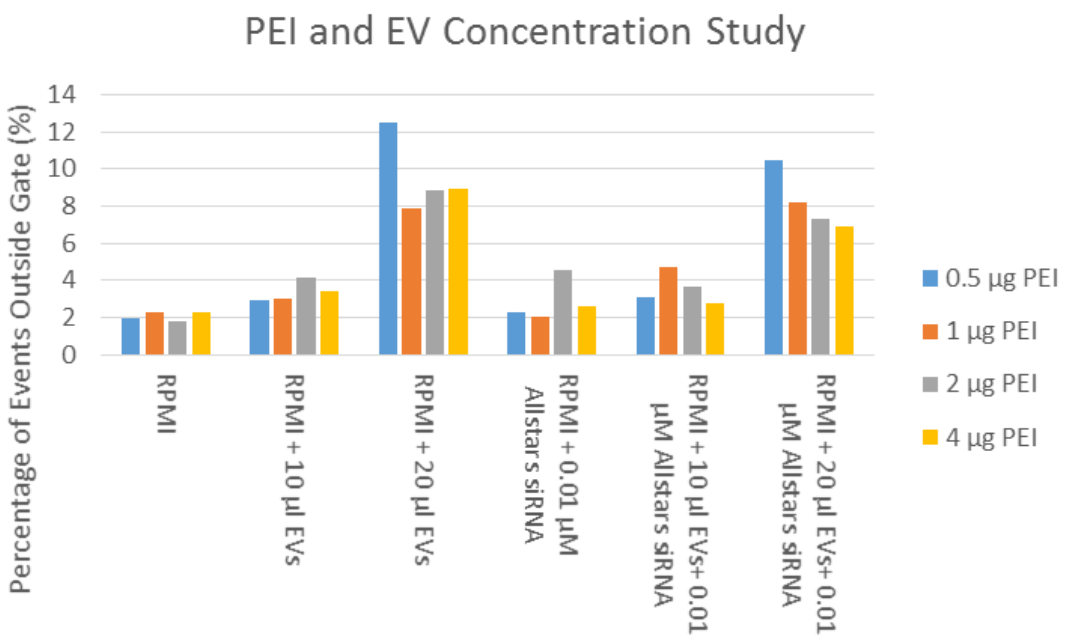

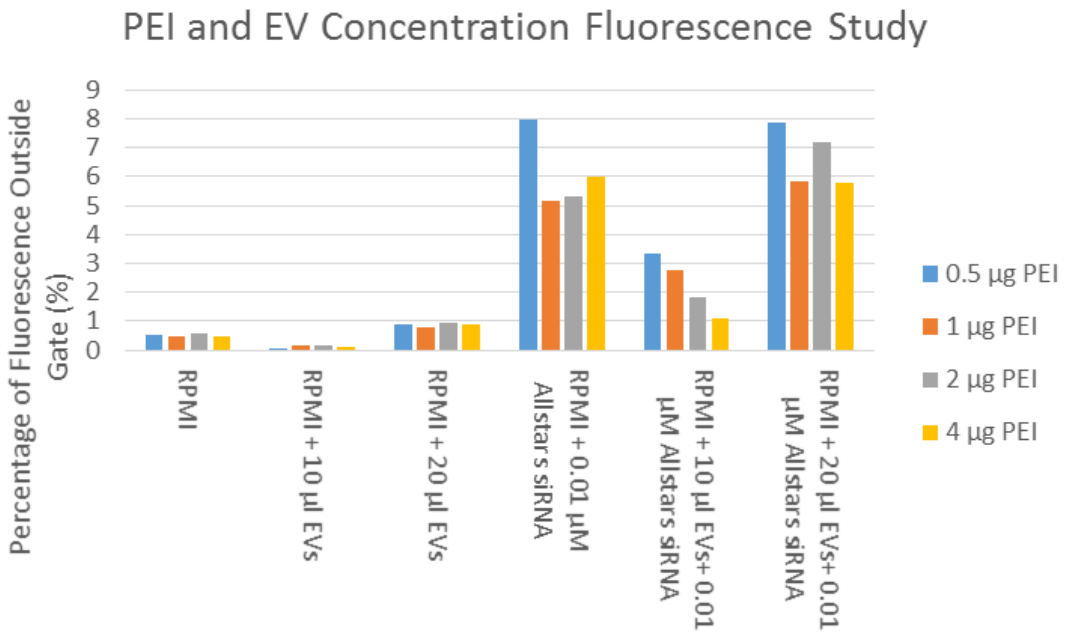

Figure 6-5: bar chart displaying the changes in events detected and fluorescent events detected on a flow cytometer when different concentrations of PEI and EVs are added to Allstars siRNA. Percentages are calculated by counting the percentage of events outside of a gated RPMI control (data not shown). n=1.

To assess the effect of the 4 ERAP1 siRNA associated EVs on cells, PEI-siRNA (0.02 µM siRNA) complexes were made according to procedure. Complexes were then incubated with 5.31 µg Jesthom EVs before finally incubating the mixture with Jesthom B cells. Western blot analysis of the cell lysates showed that the ERAP1 expression of the Jesthom cells incubated with PEI, EVs and ERAP1 siRNA (figure 6-6A and 6-6B) were downregulated when compared to untreated control cells. However, the control with Jesthom cells, EVs and PEI also showed ERAP1 downregulation, making it difficult to interpret the data (figure 6-6A). This data suggests that PEI or EVs may have undesired effects on the cells.

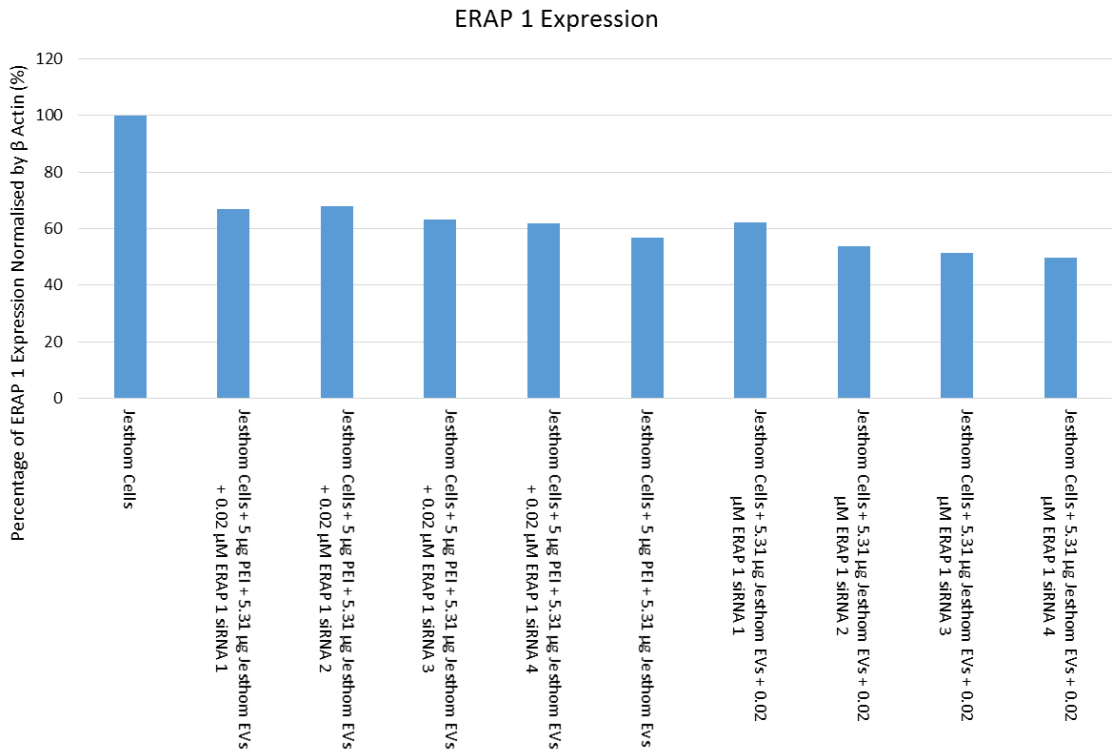

Figure 6-6A: bar chart displaying the changes in ERAP1 expression, as normalised by β Actin, compared to a Jesthom Cell control. n=1.

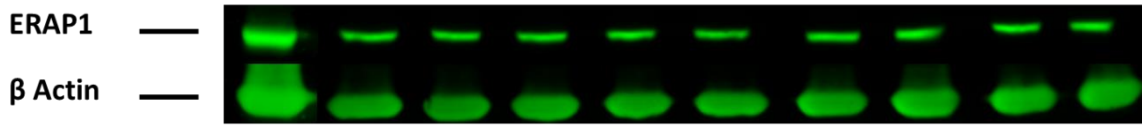

Figure 6-6B: western blot of ERAP1 and β Actin expression in Jesthom cells after incubation with EVs, PEI and ERAP1 siRNA. Samples are arranged in the same order as figure 6-6A.

In the absence of specific downregulation in the previous experiment this study took a step back. The flow cytometer was used to analyse samples of Jesthom cells incubated with Allstars siRNA and PEI with the addition of a trypsin wash. It was hypothesized that this would remove loosely attached siRNA/protein interactions associated at the surface of the cell. Therefore revealing how much siRNA was being encapsulated and how much was associating merely with the cell surface. As can be seen in figure 6-7, it was found that all the samples (except the PEI control), that had not been exposed to a trypsin wash (blue bar), had over 30% more fluorescence detected than the gated control. As expected, the trypsin wash (orange bars) resulted in greatly reduced levels of fluorescent intensity. This experiment demonstrates the importance of a step to remove un-encapsulated Allstars siRNA to prevent false positives.

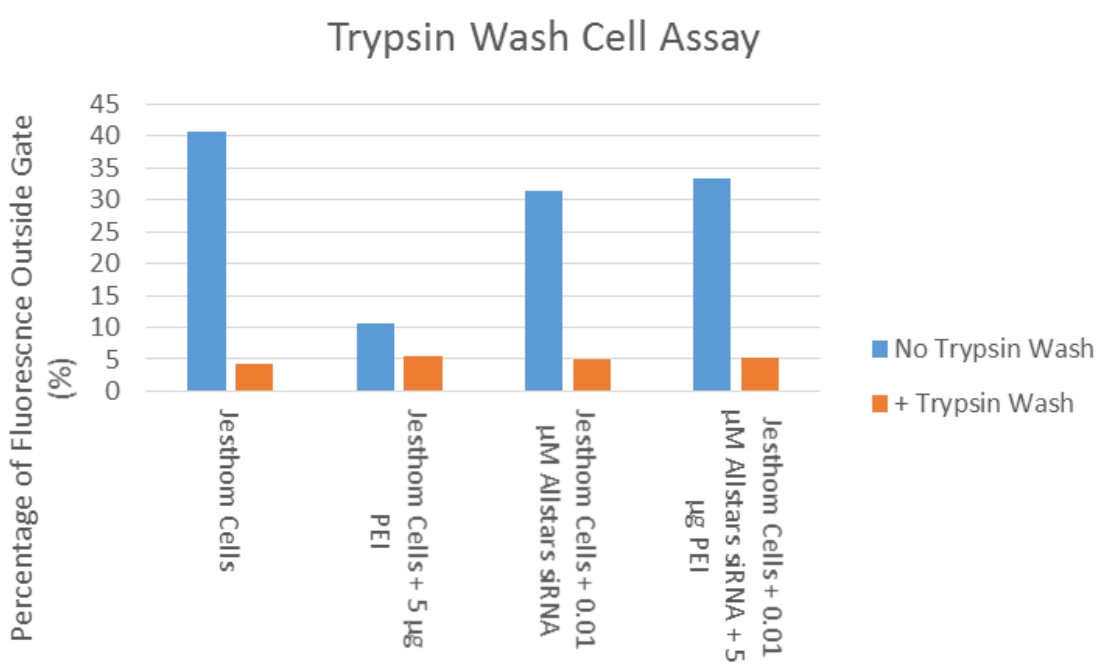

Figure 6-7: bar chart showing the decrease in fluorescent events detected by a flow cytometer when a trypsin wash is applied to samples. Percentage of fluorescent events were calculated from a gate set to the Jesthom cell with a trypsin wash control. n=1.

As some Allstars siRNA excess fluorescence was previously able to be removed, suggested by the results of the trypsin wash, it was next determined whether the fluorescence observed with the EVs was encapsulated rather than associated with the outside of the membrane. Amicon Ultra 15K spin filters were used for this. These filters would be able to enrich the sample by removing un-associated Allstar siRNA or siRNA aggregates that may be counted as a particle by the flow cytometer. For the unfiltered Allstars siRNA control there is a similar percentage of fluorescence to the previous experiment (figure 6-8, bottom graph). There is an even higher increase in fluorescence observed for the PEI, EVs and Allstars siRNA sample. However, when these samples are filtered there is a decrease in fluorescence to 3.5 % and 6.7 % respectively. This suggests there is a small amount of encapsulation. The top graph of figure 6-8 shows the change in size and granularity of events detected by the flow cytometer. When all 4 samples are filtered there is a decrease in the number of events outside the gate which could be a removal of aggregates. Alternatively, since there is no clear increase in the percentage of fluorescence (above 6.7 %) it could be suggested that material is being lost during the filtration process. This is supported by comparing the decrease in events detected from the EV control to the samples containing EVs; 60 % to 19 % and 21 % (EV control sample data not shown).

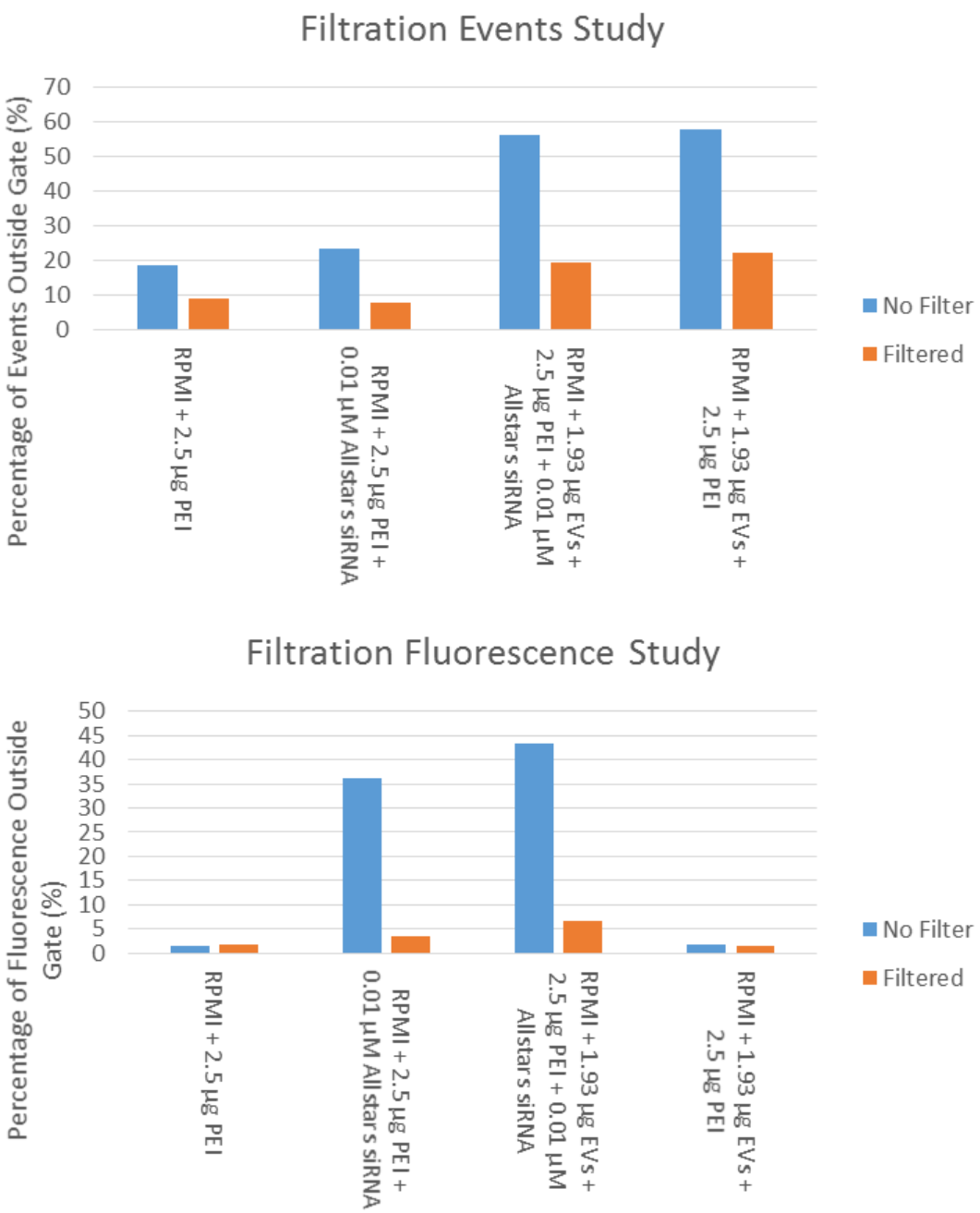

Figure 6-8: bar charts showing the changes in events detected and fluorescent events detected on a flow cytometer when samples are filtered. Percentages were calculated based on a gate set to an RPMI control. n=1.

As the Amicon filters appear to remove EVs as well as un-associated fluorescent particles an RNase A digestion step was applied in conjunction with Allstars siRNA. This would allow the removal of any siRNA that had not been encapsulated within the EVs as well as any siRNA that was associated with the outer membrane of the EVs. Two concentrations of Allstars siRNA were used; 0.025 µM and 0.05 µM. The Allstars siRNA was pre-incubated with 2 µg of PEI for 30 minutes in order to form complexes. These complexes were then incubated with 100 µg of U937 EVs for 90 minutes before half the mixture was enriched through a NAP-10 size exclusion column. The NAP-10 column removes free siRNA from the sample, leaving only EVs and PEI. The other half of the mixture was incubated with RNase A for 30 minutes before also being enriched. Subsequently, the fluorescence of the samples was analysed. Following this the samples were also analysed for their size characteristics by NTA. The samples enriched without the RNase A step (figure 6-9A) retained 51 % of 0.025 µM Allstars siRNA and 46 % of 0.05 µM Allstars siRNA. When these samples were exposed to RNase A before being enriched a large decrease in retention to 9 % and 13 %, respectively, of the input siRNA was observed. This would suggest that the majority of siRNA present is not encapsulated within the EVs. Figure 6-9B shows NTA diameter measurement results. The average size of the U937 EVs that were used for this experiment was 154 nm. It was observed that the size of EVs changed after enrichment to approximately 243 nm for the samples without an RNase A step. A smaller increase of approximately 233 nm was observed for the samples with an RNase A wash step. This suggests that the increase in size is due to the presence of PEI as it is still present after an RNase A treatment is applied. Overall this data shows that PEI has an encapsulation efficiency of 9 % when used with concentrations of 0.025 µM Allstars siRNA and encapsulation efficiency of 13 % when used with a concentration of 0.05 µM. This increase in encapsulation efficiency with Allstars siRNA concentration increase, whilst showing that PEI is not completely bound also demonstrates that the efficiency did not double. Thus suggesting that PEI is reaching saturation point. In order to assess the capacity of the concentration of PEI that was chosen the concentration of siRNA used must be increased in order to observe maximum saturation of cargo.

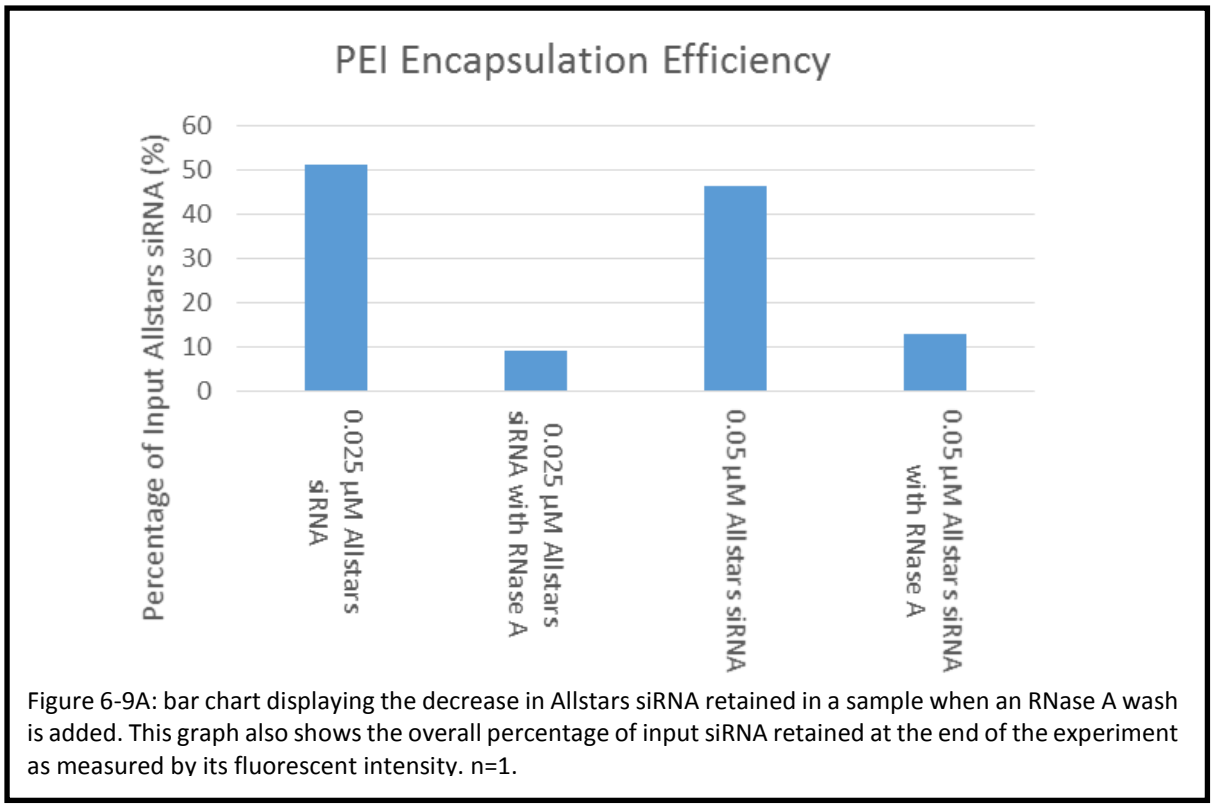

Figure 6-9A: bar chart displaying the decrease in Allstars siRNA retained in a sample when an RNase A wash is added. This graph also shows the overall percentage of input siRNA retained at the end of the experiment as measured by its fluorescent intensity. n=1.

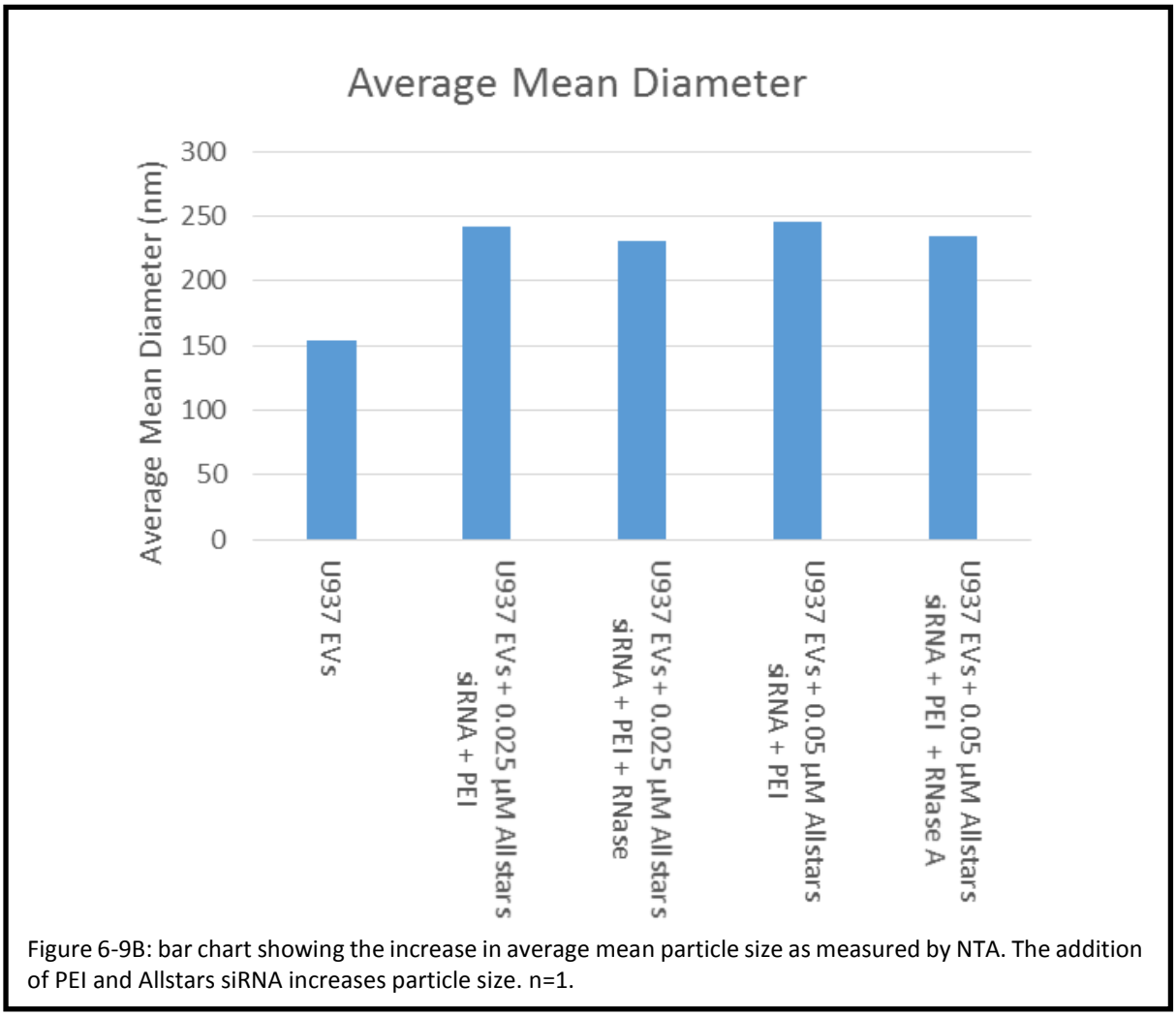

Figure 6-9B: bar chart showing the increase in average mean particle size as measured by NTA. The addition of PEI and Allstars siRNA increases particle size. n=1.

6.2 Discussion

Early in this study the most effective ERAP1 siRNA to use with PEI was characterised. This was an important result as it provided evidence for which ERAP1 siRNA should be used with other chapters' cell assays. ERAP1 siRNA from four different companies were evaluated to assess their effectiveness. It was found that Thermo Fisher ERAP1 siRNA provided the most downregulation of ERAP1. This result emphasizes the importance of testing products from multiple companies.

During this study a change in EV particle size was observed when EVs were associated with PEI. In the literature there is also an increase in EV size when PEI complexed particles are transfected (Su, Aldawsari, & Amiji, 2016). This is generally attributed to the encapsulation of cargo complexes. Later results in this chapter, when using RNase A to remove excess siRNA particles, show this increase in size also. However, when the contents of the EVs are assessed there is a significant decrease in the amount of input siRNA retained after an RNase A incubation. Yet there is still an increase observed in the size of the EVs. This data suggests that the increase in EV size may be associated with the presence of PEI rather than cargo complexes. As such it is pivotal that experiments dealing with encapsulating siRNA as a cargo must include a step to remove excess cargo. Without an RNase A wash it would have wrongly been presumed that EVs had encapsulated a larger concentration of cargo.

Traditionally PEI is dissolved in ddH_2O or sodium chloride. In this study it was observed that stock PEI in ethanol left a high background signal when associated with EVs. Therefore, PEI was dissolved in ddH_2O and characterised. There is evidence in the literature of studies performed where the PEI is dissolved in ddH_2O (Boussif *et al.,* 1995; Oral *et al.,* 2015; Rezvani Amin, Rahimizadeh, Eshghi, Dehshahri, & Ramezani, 2013). The use of sodium chloride is also featured in the literature (Fischer, Bieber, Li, Elsässer, & Kissel, 1999; Godbey, Wu, & Mikos, 1999; Höbel *et al.,* 2008; Kichler, Leborgne, Coeytaux, & Danos, 2001; Schäfer, Höbel, Bakowsky, & Aigner, 2010). The stock solution of PEI in the laboratory was dissolved in ethanol to prevent crystal formation when stored. However, in the literature there is no data relating to PEI dissolved in ethanol. It would have been interesting to compare the use of these 2 solutions in the later experiments.

The initial method used in this chapter for PEI delivery of cargo involved the mixing of all components simultaneously. This meant that components could interact in an order that decreased the chances of complex formation. Later in this chapter a complexation step prior to incubating with cells or EVs was employed. This encouraged the formation of PEI-cargo complexes as EVs would not be able to prematurely interact with the PEI. PEI functions primarily by being highly cationic. Therefore, it is able to interact with anionic siRNA or EVs. Perhaps more so with EVs given their size and therefore higher charge than siRNA. By incubating siRNA and PEI separately the PEI should become saturated. Then, when the complexes are mixed with cells or EVs, the percentage of PEI

travelling across the membrane carrying siRNA should be higher. In the majority of literature, the separate complexation of cargo and PEI is featured in the methods section (Boussif *et al.,* 1995; Fischer *et al.,* 1999; Godbey *et al.*, 1999; Höbel *et al.,* 2008; Kichler *et al.,* 2001; Klyachko *et al.,* 2012; Kurosaki *et al.,* 2013; Laroui *et al.,* 2014; Oral *et al.,* 2015; Schäfer *et al.,* 2010). An addition to the complexation method, that would improve the rate of cargo binding, is using the charge ratio of siRNA to PEI (Boussif *et al.,* 1995; Fischer *et al.,* 1999; Godbey *et al.,* 1999; Höbel *et al.,* 2008; Kurosaki *et al.,* 2013; Laroui *et al.,* 2014; Schäfer *et al.,* 2010). This would allow the calculation of exact concentrations required to saturate the binding of PEI.

Before the addition of column enrichment and RNase A incubation, a trypsin wash was used as a quick method of clearing excess siRNA/PEI complexes from the outside of cells. This method was only used with cells as at the time there was no quick method available for enriching EVs. The repeated 300 x*g* centrifugation steps would not have been long enough or fast enough to enrich the EVs. Furthermore, it is likely that the small amount of EVs added would have been lost during the process. The first attempt to enrich EVs in this study employed an Amicon Ultra spin filter. The decision to use these was based on the size of the filter as it would wash any un-associated siRNA through whilst retaining the EVs. Unfortunately, despite their specific filter size, the filters seemed to remove relevent material from the samples. The addition of an RNase A incubation was an improvement on using trypsin or Amicon filters. This was because it was specifically tailored to the destruction of the siRNA cargo rather than removing the PEI. Furthermore, with the aid of NAP-10 size exclusion columns, EVs could also be enriched without loss of material. This allowed us to analyse the interaction of cargo and PEI before adding it to a cell line.

Chapter 7: Cell Penetrating Peptides

7.1 CADY

CADY is a highly stable, amphipathic and hydrophobic CPP (Keller *et al.,* 2013). For these reasons it was chosen as the first CPP to be tested to encapsulate cargo into EVs. Furthermore, CADY is known to have a low cytotoxicity which should be of benefit in cellular assays. The helical conformation of CADY aids its amphipathicity and its amide group at the C terminus and acetylated N terminus further aid its interactions both with cargo and the plasma membrane (Laurence Crombez *et al.,* 2009).

To characterise the background signals produced by flow cytometry of CADY, three concentrations of CADY (1, 2 and 4 µg) were mixed with 0.5 ml of RPMI. The samples were then analysed by flow cytometer. Dot plots of the FSC and SSC were gated on the RPMI control and the percentage of events detected outside of this gate calculated. Therefore the data displayed shows the percentage of events detected outside the set gate. This allows detection of any increases in size or granularity of the events. As can be seen in the top graph of Figure 7.1-1, there is a gradual increase in events detected outside the gate as the concentration of CADY increases. This suggests that as more CADY is added it is able to aggregate with itself. In the bottom graph of figure 7.1-1 there is an initial 12 % increase when EVs are added to RPMI. This suggests that a larger population of EVs may be visible. However when CADY is added there is another increase to 62 % of events outside the gate. This continues to increase as the concentration of CADY increases similar to the top graph in the absence of EVs but with higher percentages. Together this data suggests that CADY is able to self-aggregate and most likely the addition of EVs causes further aggregation.

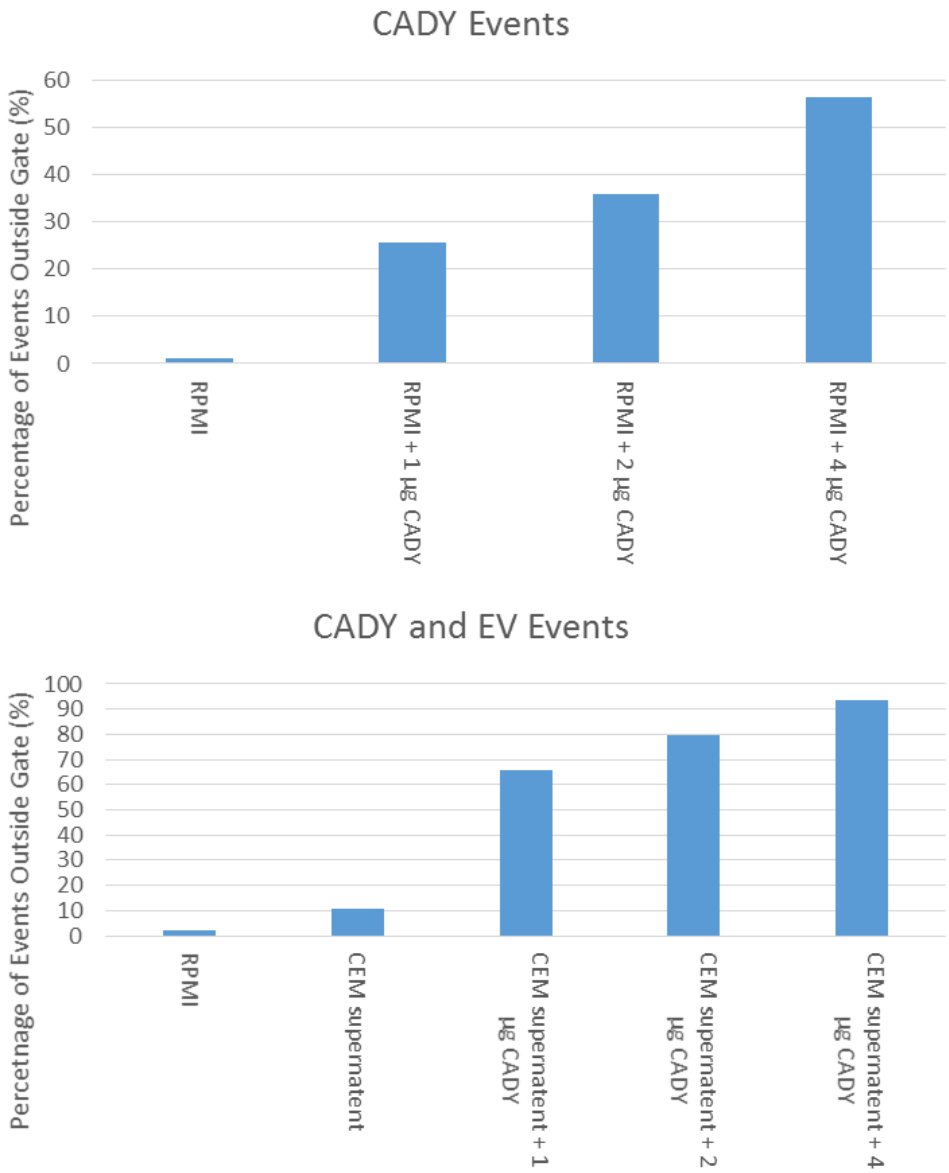

Figure 7.1-1: bar charts showing the changes in events observed on a flow cytometer. Percentage of events was calculated from a gate set to the RPMI control. n=2

Initial cargo loading experiments were carried out using FITC Ab. This is a useful protein control readily detectable through fluorescence (and can be regarded as a protein cargo model in the same vein as the previously described Allstars siRNA AF488 represents a nucleic acid cargo). 2 µl FITC Ab, RPMI or HeLa cell supernatant (containing EVs) and 2 µg CADY were incubated overnight and analysed by flow cytometer after 24 hours. Percentages were calculated as previously. The top graph in figure 7.1-2 shows that CADY on its own causes a large increase in the percentage of events detected outside the gate. It appears to do this also when mixed with EVs and siRNA. The bottom graph shows the fluorescent events detected outside the control gate. There is fluorescence above RPMI levels for the FITC Ab control as expected which increases when CADY and EVs are added. However there is fluorescence detectable outside the gate for the RPMI and EV control. Presuming that this is an unusual result, there is still a lot of aggregation occurring which could affect both non-fluorescent and fluorescent events detected.

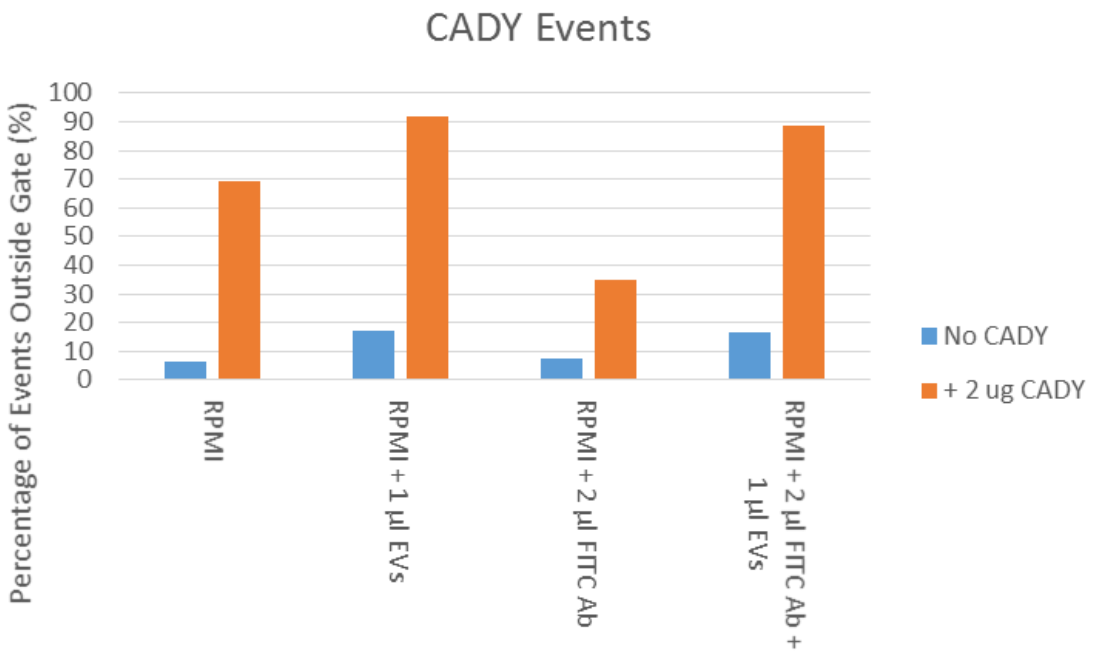

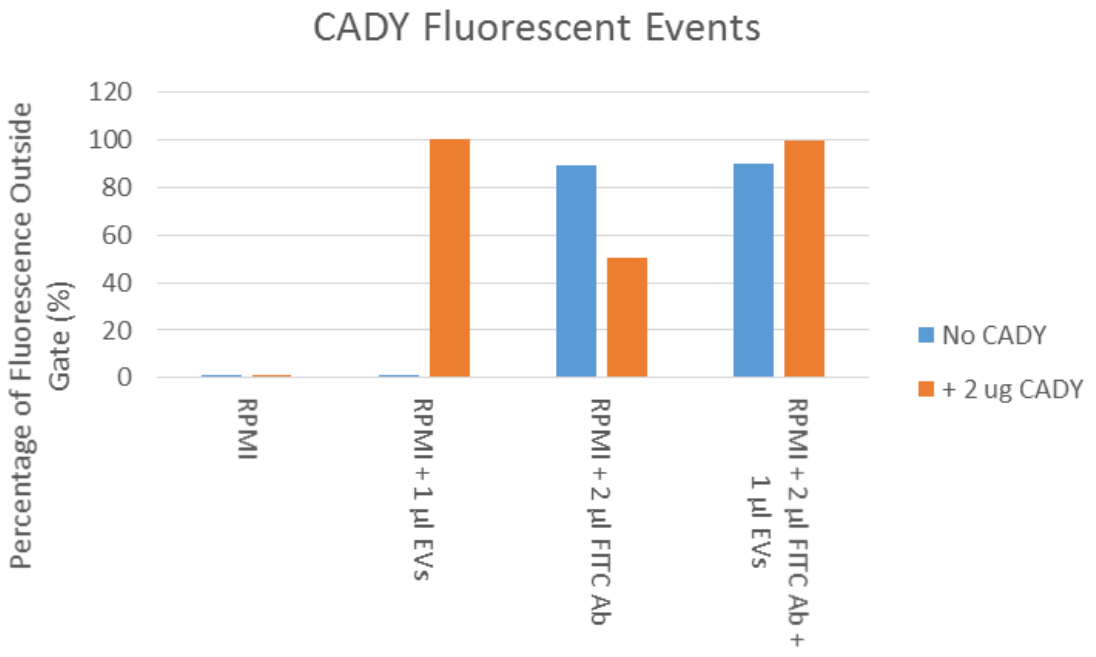

Figure 7.1-2: graphs showing the changes in events detected when samples are analysed by flow cytometer. Percentages were calculated from a gate set to the RPMI control. n=1

To check if aggregates were formed, CADY was first incubated O.N and then either sonicated in a water sonicator bath or spun at 20200 x*g* for 5 minutes, to remove aggregates. To clarify, a population of CADY particles where the size and granularity were very similar to the control was desired as they should be smaller than EVs. The area that the control occupies usually contains particles of around 100 nm or smaller (Figure 7.1-3A). Similarly, it was expected that the water sonication step would degrade any aggregates of CADY and reduce them to complexes smaller than EVs. Preliminary results showed that both the water sonicated samples (figure 7.1-3B, grey bars) and centrifuged samples (figure 7.1-3B, orange bars) had decreased in size and granularity. The 20200 x*g* centrifuged samples showed a greatly reduced background which was similar to the RPMI control. However, the water sonicated samples still showed an increase in events outside the gate that increased with the concentration of CADY used.

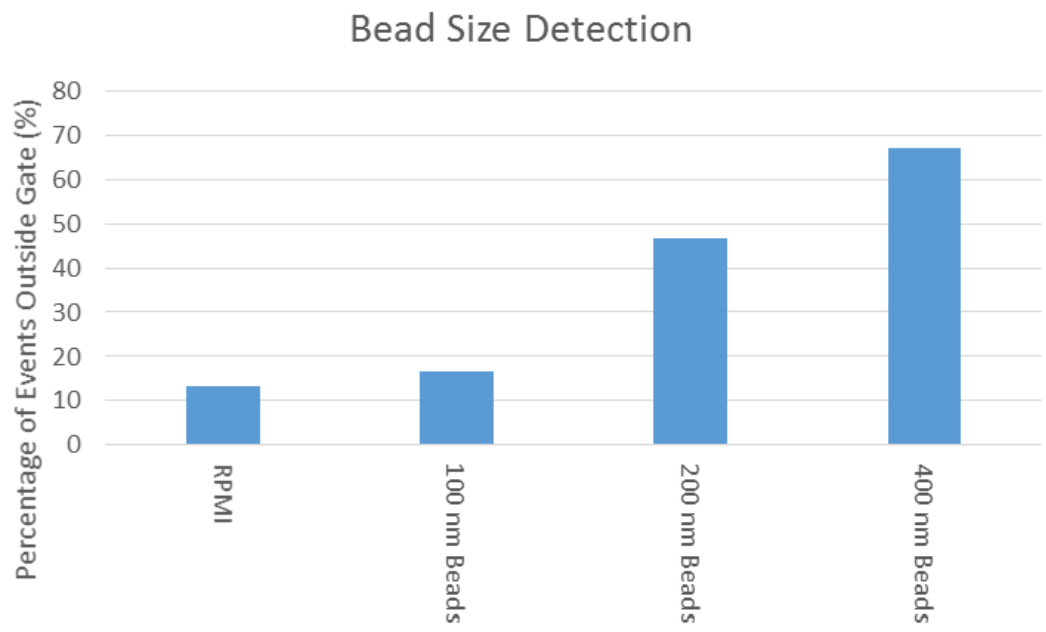

Figure 7.1-3A: bar chart showing the differences in events detected by a flow cytometer when 3 different sizes of beads are analysed. Percentages were calculated using a gate set to the RPMI control. n=1.

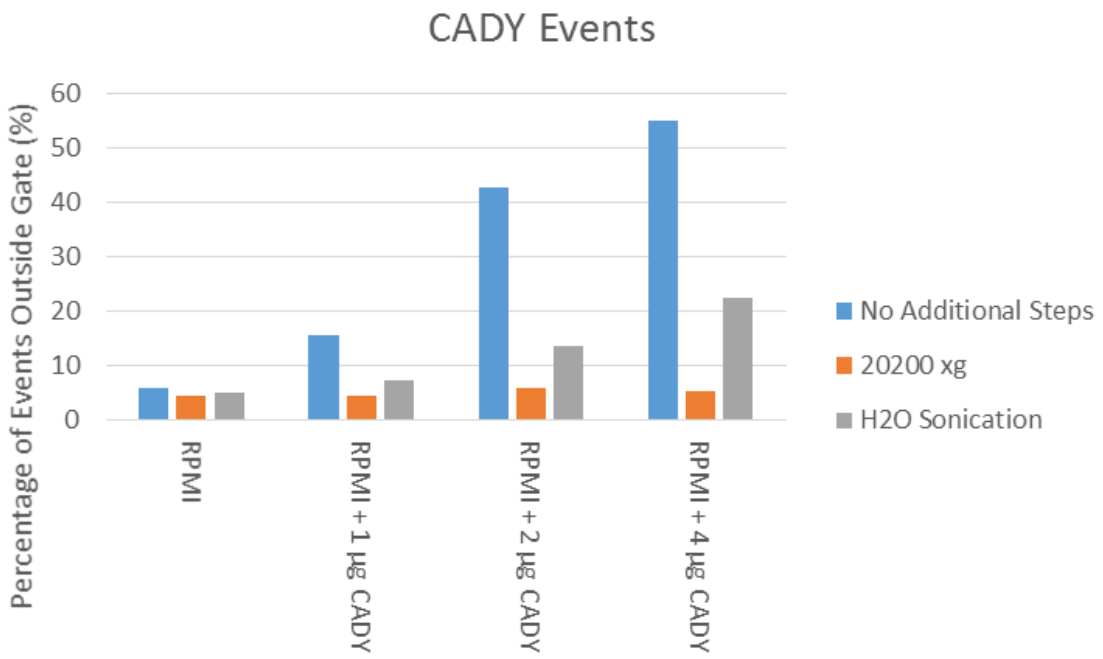

Figure 7.1-3B: bar chart displaying changes in events detected by a flow cytometer when CADY is exposed to different treatments. Percentage calculated from gate set to RPMI control. n=2

As the centrifugation step seemed to remove the most CADY aggregates a 20200 x*g* centrifuge step was added before the EV incubation step. This was to attempt to remove the CADY aggregates after a 1-hour incubation at 37 °C. Centrifugation after this incubation step would risk spinning out cargo as well as aggregates. Of note, HeLa cell supernatant was replaced with an ultracentrifuged (100000 x*g*, 2 hours) enriched HeLa EV stock. After the samples underwent flow cytometry it was hard to decide whether the extra 20200 x*g* centrifuge step had spun out the FITC Ab. This was because the FITC Ab control (figure 7.1-4, bottom graph) shows a smaller increase in fluorescent events outside the gate than the RPMI and 20200 x*g* control. In fact all centrifuged samples showed an increase in fluorescent events lower than their un-centrifuged counterpart. In figure 7.1-4, top graph, there is a notable decrease in events detected outside the gate for all bar one of the centrifuged samples to < 20 %. This suggests that the aggregates may have been spun out and that some of the FITC Ab may have spun out too. If FITC Ab had been encapsulated into EVs by CADY there would have been an increase in fluorescence above control levels.

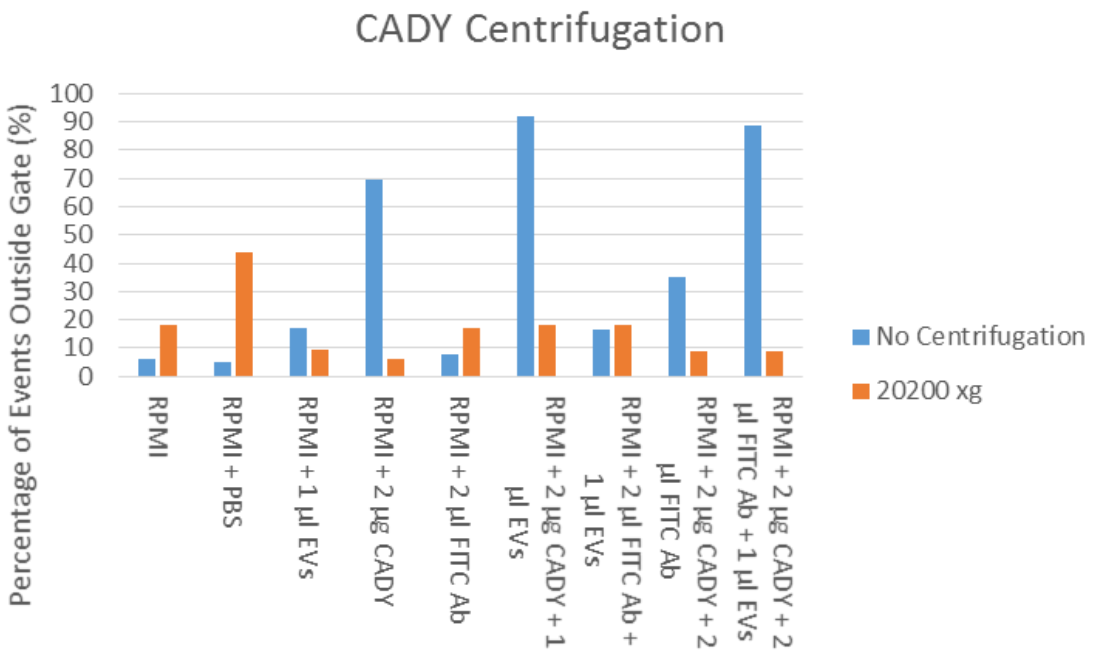

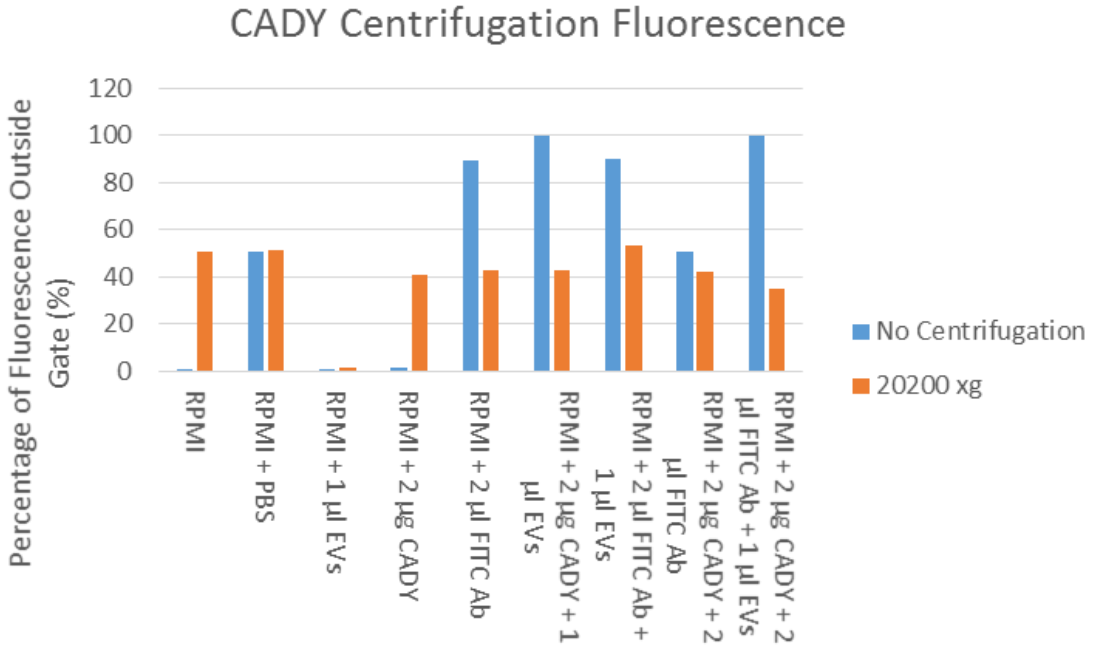

Figure 7.1-4: bar charts showing the changes in events detected on a flow cytometer after samples have been centrifuged at 20200 x*g*. Percentages were calculated from a gate set to the RPMI control. n=2.

To determine if the 20200 x*g* spin after CADY/FITC Ab complex formation removed active particles, centrifugation before complex formation was trialled. This would remove any preformed aggregates. To purely look at the complex formation, EVs were emitted from this experiment. In figure 7.1-5, top graph, the results are inconclusive as neither condition shows an advantage over the other in terms of events outside the gate. However in the bottom graph there is a higher increase in fluorescent events for the FITC Ab control centrifuged after complexation. This suggests that centrifugation before complexation may remove a portion of the FITC Ab therefore reducing the chances of encapsulating it. Despite trialling the 20200 x*g* spin at a different step in the procedure, attempts to spin down the aggregates in favour of retaining single molecules appears to have problems. Therefore changing other elements of the procedure should be explored next.

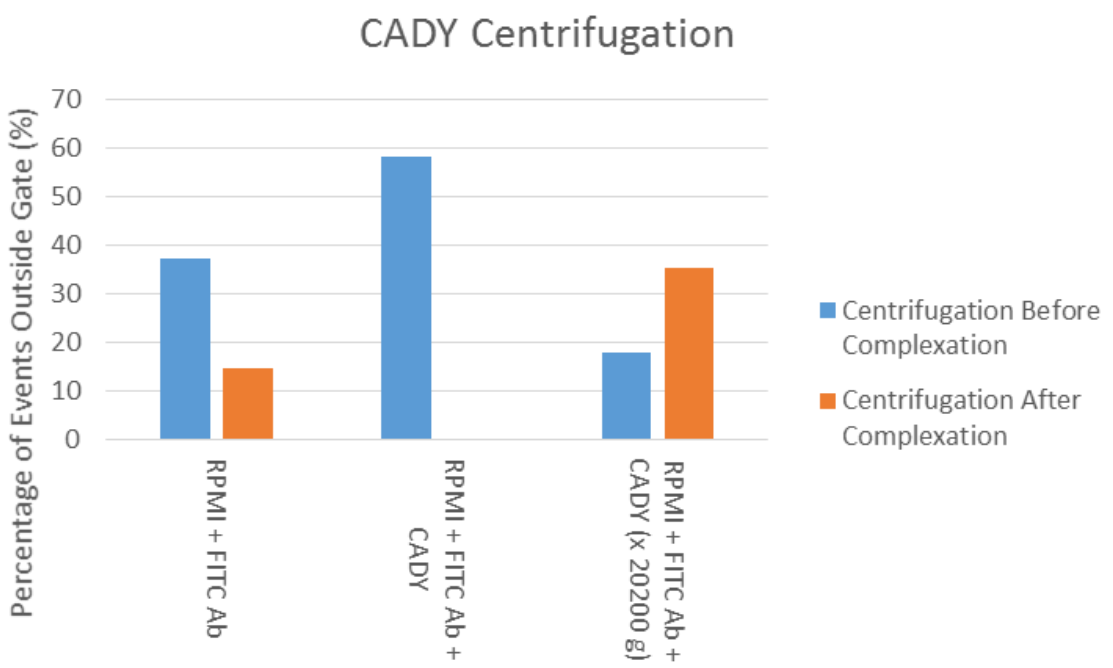

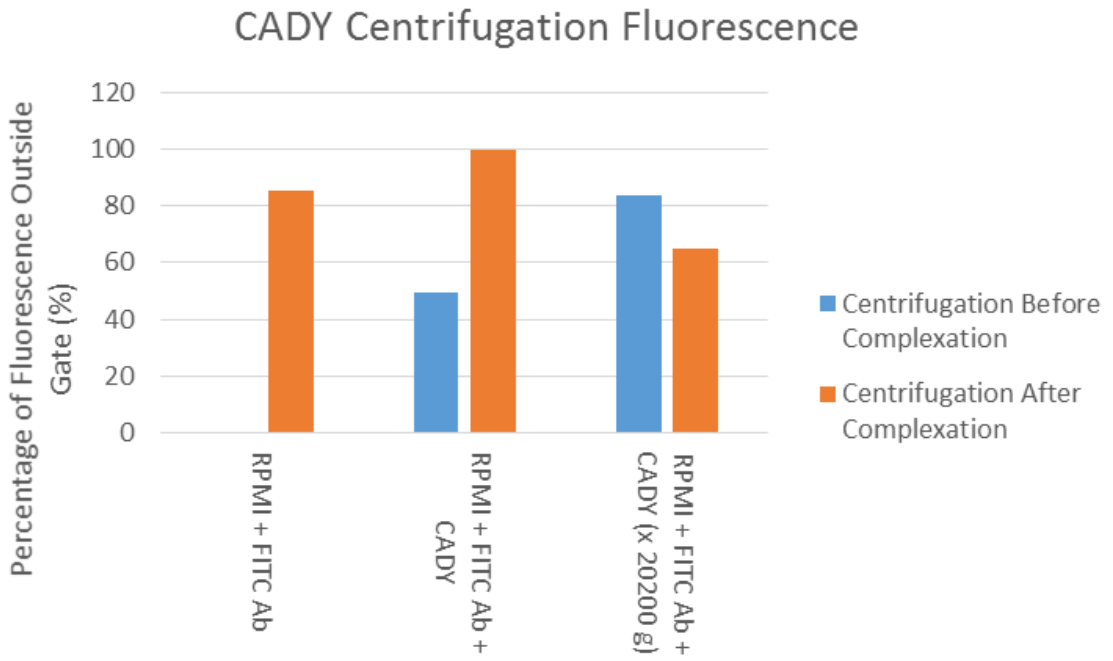

Figure 7.1-5: bar charts showing the changes in events detected by a flow cytometer when the centrifugation step is performed pre-complexation and post-complexation. Percentages were calculated based on a gate set to an RPMI control (data not shown). n=1.

The first element to be optimised in the next section of experiments is complex formation incubation time. It was expected that this could be a double edged sword as incubating the FITC Ab and CADY for too long may induce excessive aggregate formation. On the other hand, it may also encourage the CADY to bind with FITC Ab in a higher ratio than aggregate formation. Complex formation times of 30 minutes, 1 hour and 2 hours were chosen and procedure followed. The most striking result seen in figure 7.1-6, bottom graph, from this experiment was the huge amount of fluorescence observed from all samples except the RPMI control and RPMI and CADY control. This included fluorescence for samples that did not contain a fluorophore. This had not been observed previously. Whilst the fluorescent events detected appear irregular, the events detected (top graph) show similar results to previous studies. There is a small increase in events detected for the EV control suggesting that some of the EVs can still be detected and there are even higher increases in events detected for all samples containing CADY. This continues to support the supposition that CADY forms aggregates that increase further in size when more components such as FITC Ab or EVs are added.

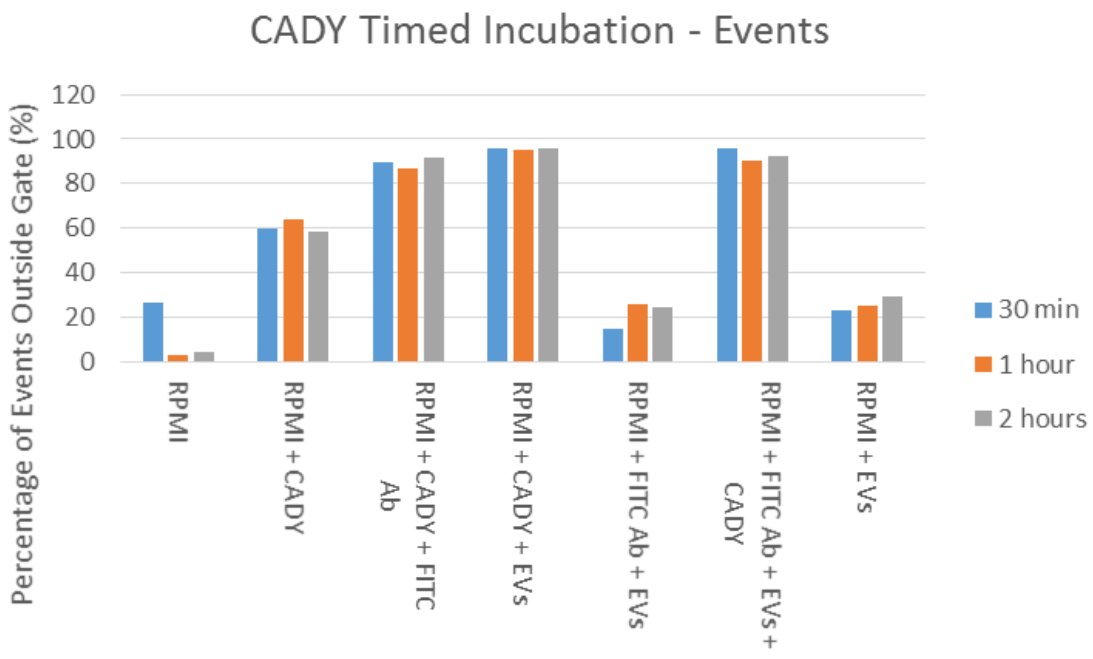

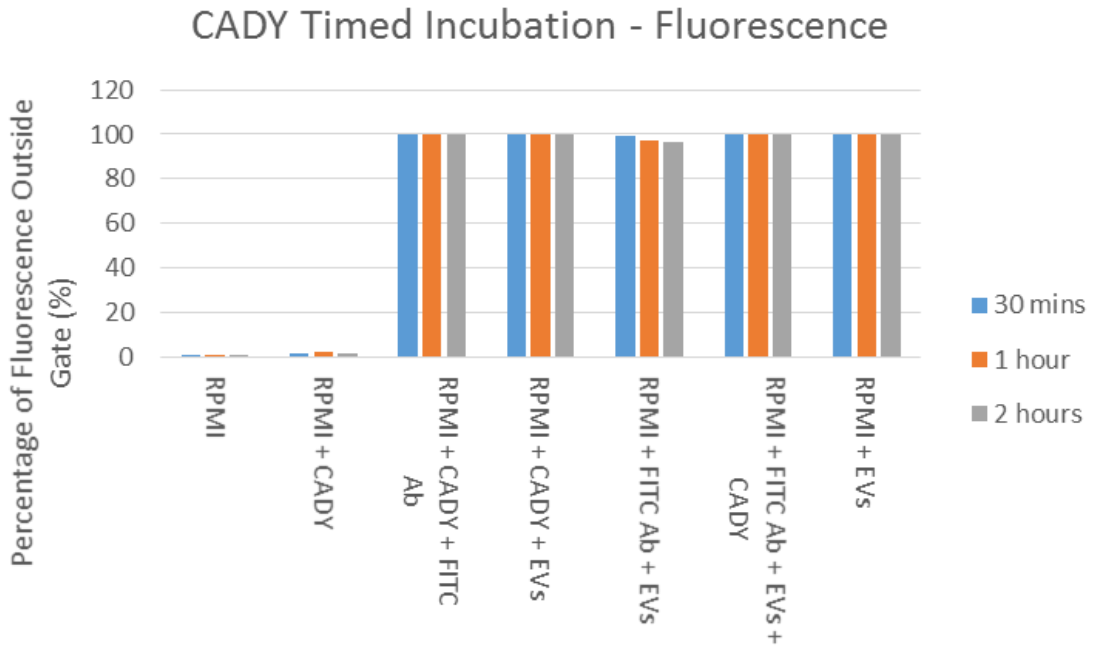

Figure 7.1-6: bar charts showing the changes in events and fluorescent events detected by a flow cytometer when CADY is incubated for 30 mins, 1 hour and 2 hours. Percentages were calculated from a gate set to the RPMI control. n=1.

Since the previous study showed a very high percentage of fluorescent events outside the gate after 30 mins, the 30-minute time course was broken down. Times of 1, 5, 10, 15, 20, 25 and 30 minutes were chosen. It was predicted that a gradual increase in events outside of the gate over time would be seen. This would allow the detection of when complex formation or aggregate formation was occurring. In figure 7.1-7 there is a small increase in the percentage of fluorescent events detected for the control without FITC Ab. For the samples containing FITC Ab there is an increase >80 % at all time points. For the first 3 time points there is a gradual increase in fluorescence as time increases however this drops at 15 minutes. The last 3 time points show a gradual decrease in fluorescent events detected as time increases. This high percentage of fluorescence suggests that the FITC Ab is aggregating rather than being encapsulated.

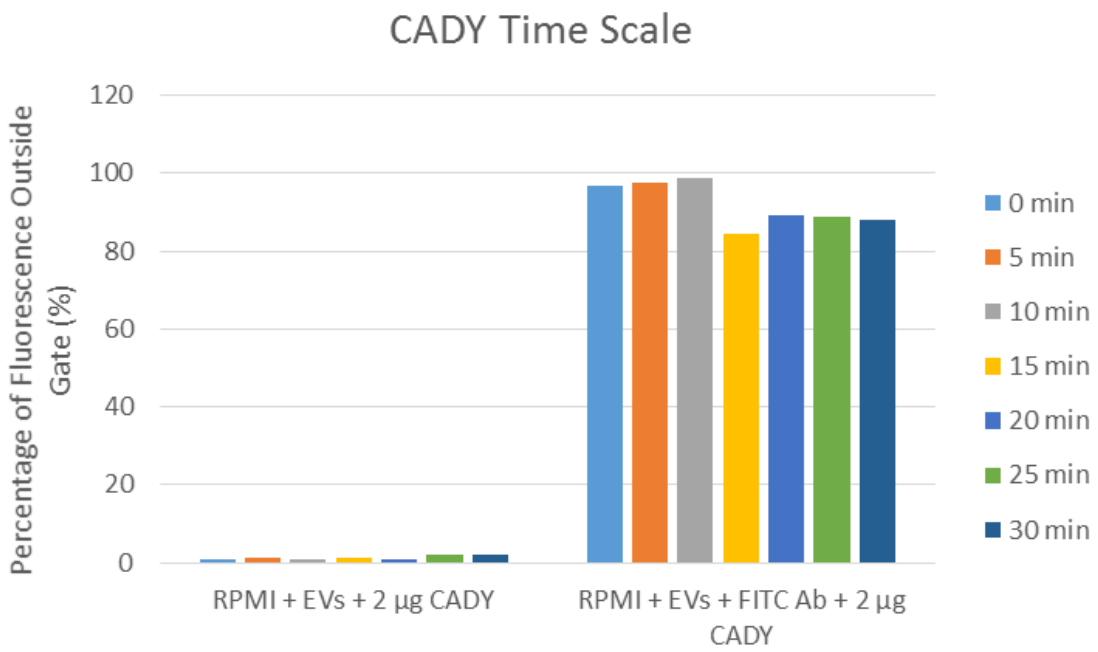

Figure 7.1-7: bar chart showing the changes in events detected by a flow cytometer over a 30 min time scale. Percentages were calculated from a gate set to the RPMI, EVs and 2 µg CADY control. n=1

Another important parameter to evaluate is the formation of complexes when left to incubate in a still environment or in an environment that is constantly mobile. The constant movement would be expected to increase the number of molecular collisions therefore encouraging complexes to form faster. This could have the potential to help form complexes before they become aggregates. In figure 7.1-8 there is again a consensus that all samples containing FITC Ab have a 100 % increase in the percentage of fluorescent events outside the gate. This is not seen for the majority of RPMI, EV and CADY controls therefore suggesting again that the FITC Ab is able to aggregate whether incubated still or shaking. Furthermore it is able to aggregate almost immediately as it comes into contact with the other sample components.

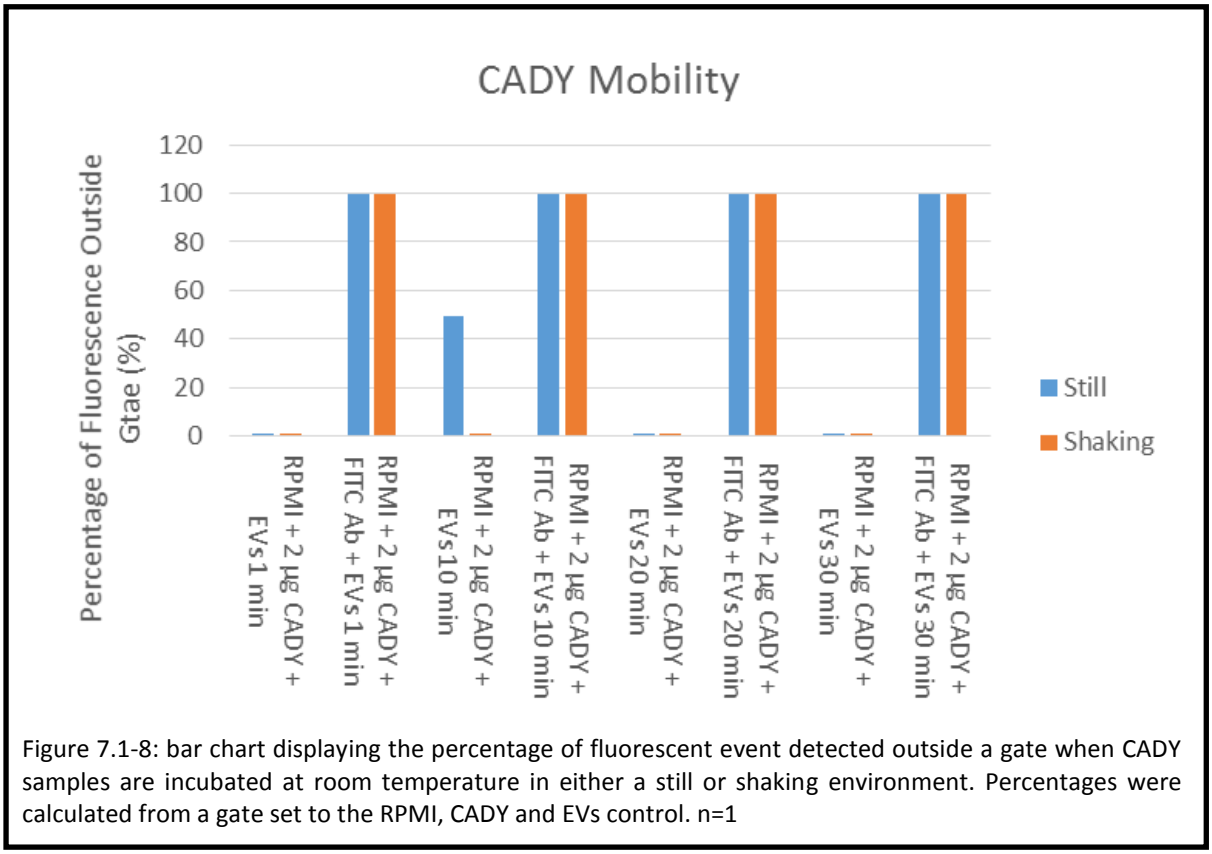

Figure 7.1-8: bar chart displaying the percentage of fluorescent event detected outside a gate when CADY samples are incubated at room temperature in either a still or shaking environment. Percentages were calculated from a gate set to the RPMI, CADY and EVs control. n=1

The third element to be explored was temperature. As with the last set of experiments a time course was combined along with a change in complex incubation temperature of 37 °C and 4 °C. A reduction in temperature to 4 °C was used as it was hypothesised that it would decrease the speed at which the particles were moving and therefore cause less collisions over time. Converse to the previous approach, if there are less particle collisions, then the chances of CADY aggregating should be decreased leaving the particles free to interact and bond to the FITC Ab cargo. The decrease in energy for collisions should also work in favour of capturing the time over which molecules complex or aggregate. In figure 7.1-9 there is a <1 % increase in the percentage of fluorescent events detected outside the gate for the controls without FITC Ab. Furthermore, there is an increase in fluorescence detected for the samples containing FITC Ab to >89 %. Unexpectedly, the increase in percentage of fluorescent events is smaller for the 37 °C incubated samples compared to the 4 °C incubated samples. These results suggest that 37 °C may result in less aggregation than 4 °C. Alternatively, though unlikely, it could be suggested that a 4 °C incubation allows more encapsulation.

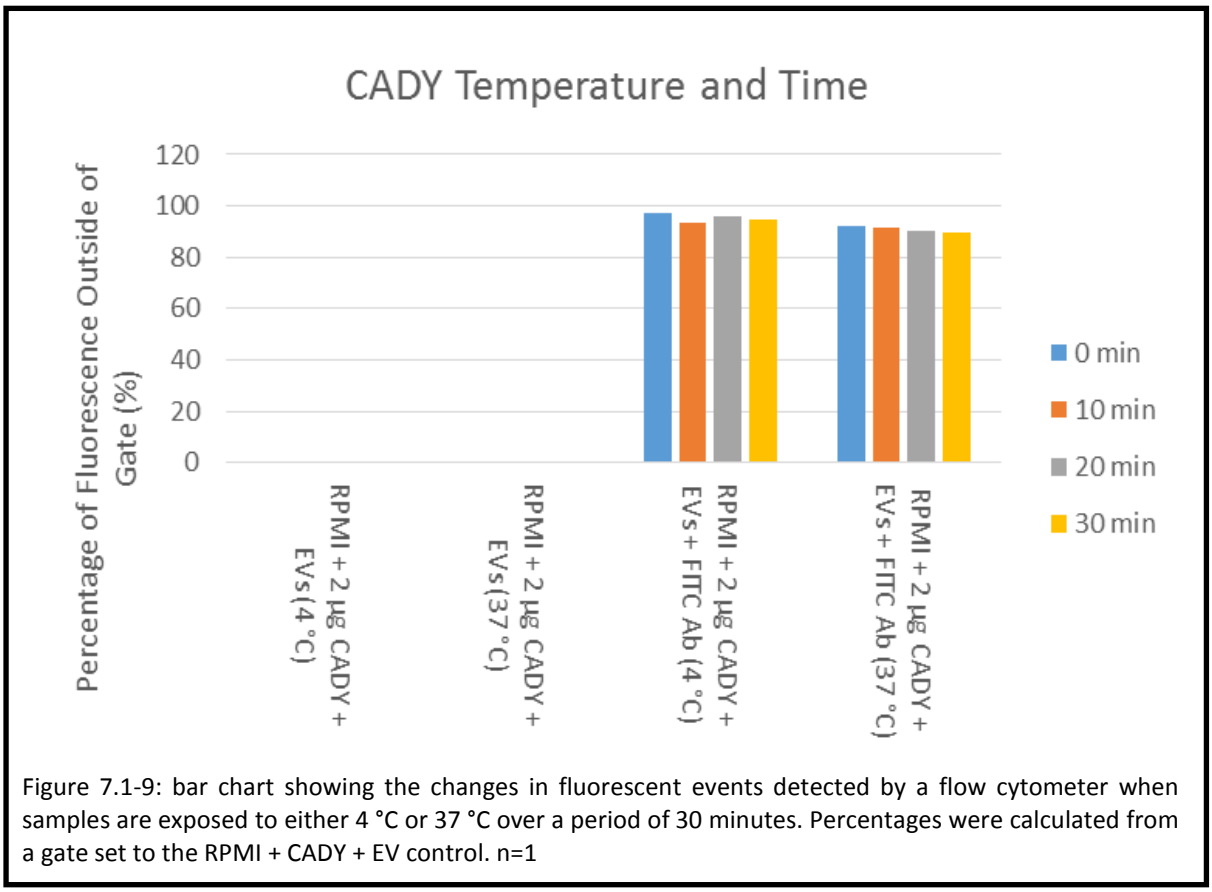

Figure 7.1-9: bar chart showing the changes in fluorescent events detected by a flow cytometer when samples are exposed to either 4 °C or 37 °C over a period of 30 minutes. Percentages were calculated from a gate set to the RPMI + CADY + EV control. n=1

To assess which concentration of CADY gave the lowest background at 30 minutes or an hour when on its own or with EVs three concentrations were chosen; 0.25 µg, 0.5 µg and 1 µg. In previous experiments CADY and EV samples have shown high aggregation. In figure 7.1-10 there is an increase in events detected outside the gate for samples containing CADY that increases as the concentration of CADY increases. This increase is more pronounced for the samples also containing EVs and as the incubation time increases. Together this data indicates that 1 µg of CADY is usable at a 30 minute incubation time however the obstacle of CADY aggregates remains.

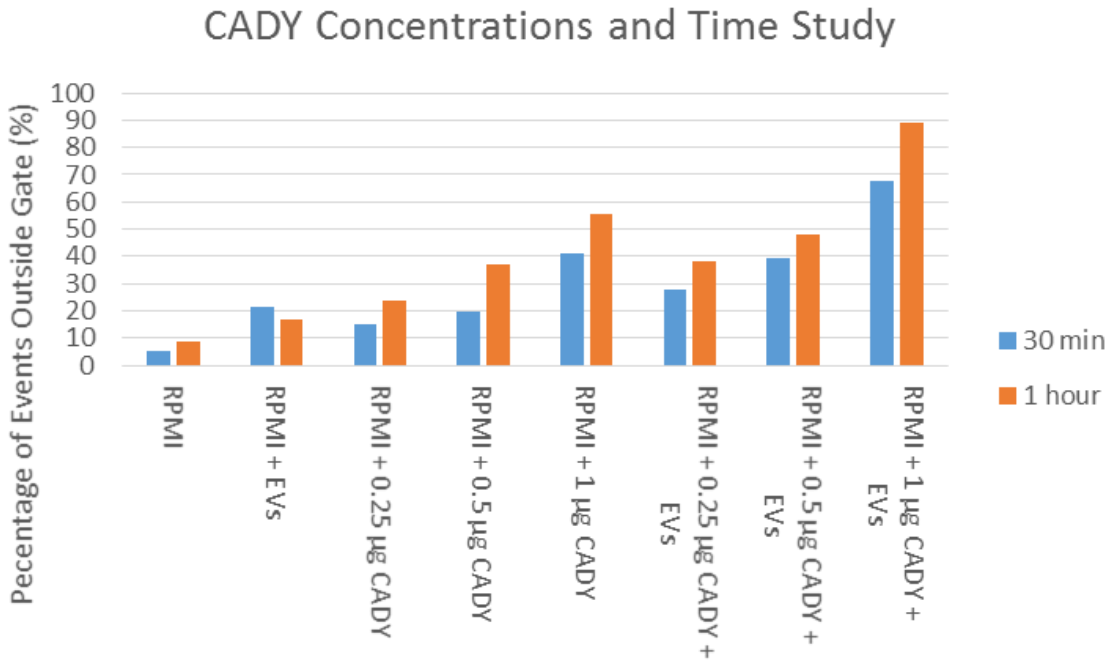

Figure 7.1-10: bar chart displaying the differences in fluorescent events detected by a flow cytometer when samples are incubated for 30 minutes or 1 hour. Percentages were calculated from a gate set to the RPMI control. n=2

Since conditions for encapsulation using CADY had been explored, the next step was to use CADY to perform a functional assay on a cell line using ERAP1 siRNA. The three cell lines that were chosen were CEM, Jesthom and Jurkat. In addition to ERAP1 siRNA, Allstars siRNA was used as a control. After complexation, cells were incubated O.N with complexes and then analysed to measure their expression of ERAP1 and β Actin. β Actin is present in most cells at high concentrations. Furthermore, its expression is not affected by either ERAP1 siRNA or Allstars siRNA therefore making it a good control for normalisation of data. In figure 7.1-11A and 7.1-11B it was observed that there was a decrease in the ERAP1 expression of CEM and Jurkat cell lines when CADY was used with ERAP1 siRNA 3. Furthermore, out of the three siRNAs used ERAP1 siRNA 3 showed the greatest decrease in ERAP1 expression for 2 out of 3 cell lines. This suggests that CADY can associate with siRNA to deliver it to cells. Therefore, the most consistently effective ERAP1 siRNA, for this chapter, is Qiagen.

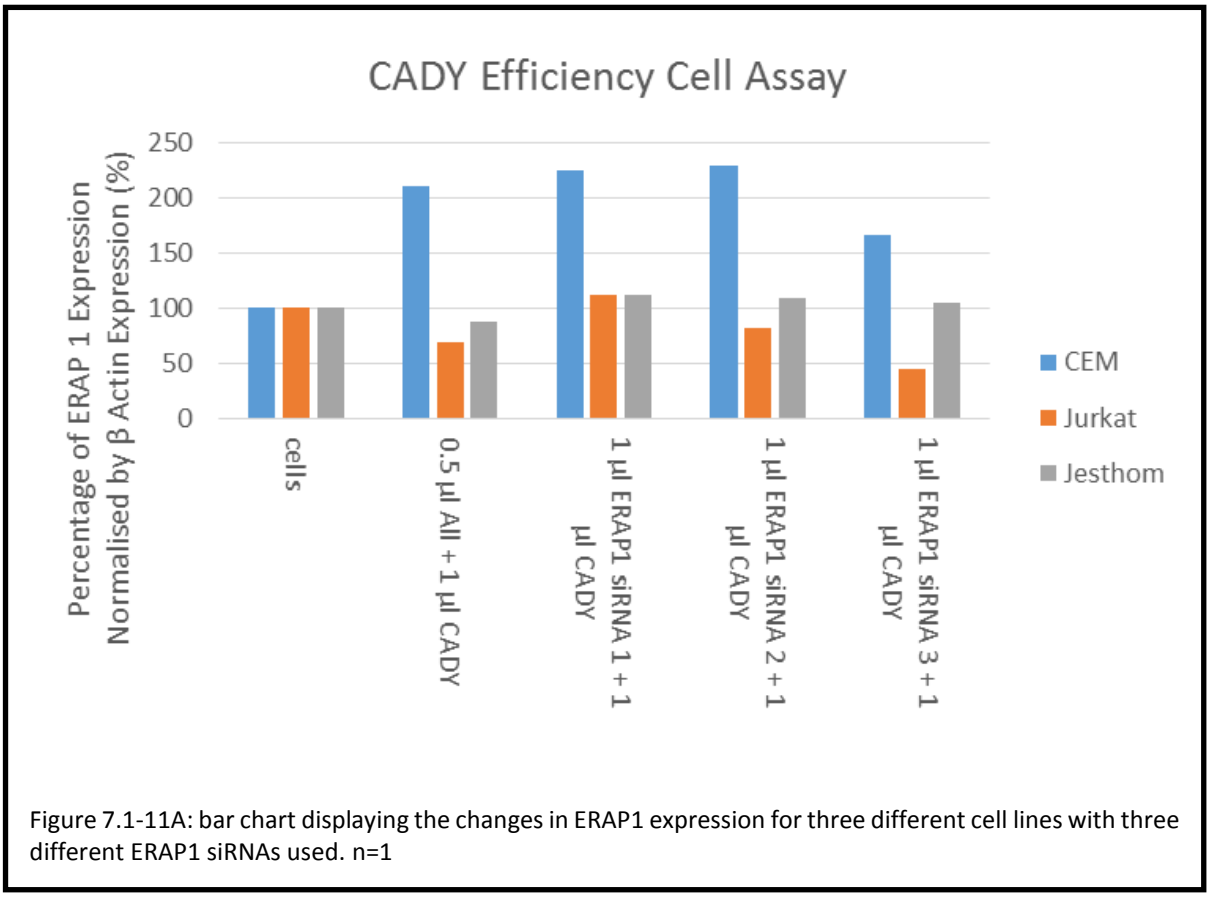

Figure 7.1-11A: bar chart displaying the changes in ERAP1 expression for three different cell lines with three different ERAP1 siRNAs used. n=1

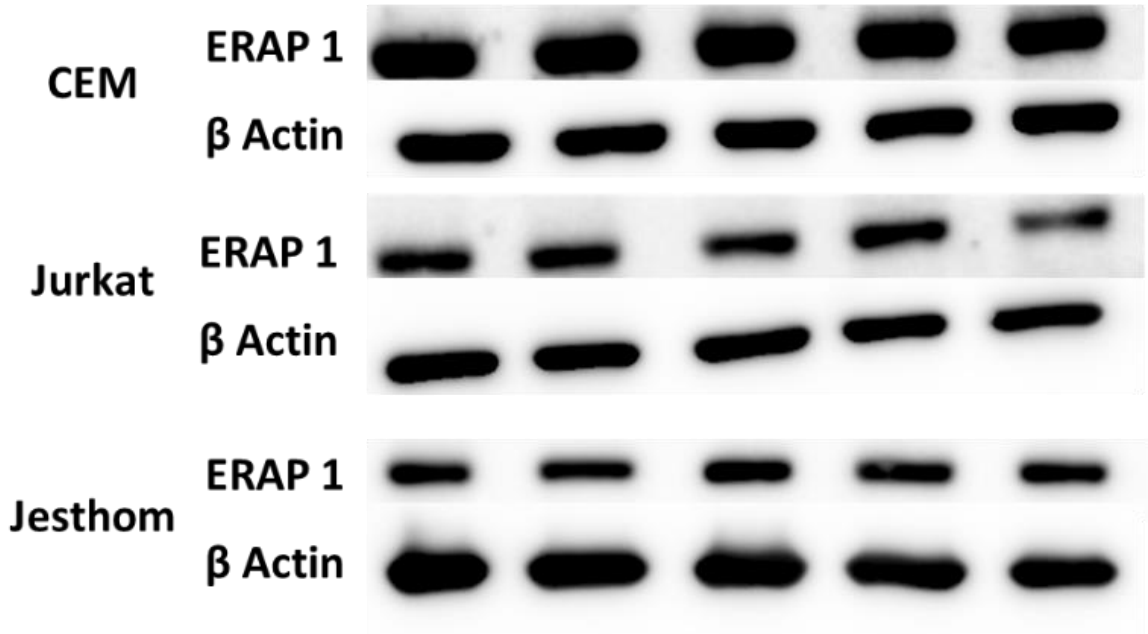

Figure 7.1-11B: western blots of ERAP1 and β Actin expression in CEM, Jurkat and Jesthom cells after incubation with CADY and ERAP1 siRNA. Samples are arranged in the same order as figure 7.1-11A.

In order to differentiate between encapsulated siRNA and free siRNA an extra step was needed which would degrade siRNA not encapsulated within the EVs. It is important that the siRNA cargo is encapsulated. This is because there is already evidence that EVs are cleared from the body before reaching their target if recognised by the immune system. Therefore, adding a drug to the outside would decrease the chance of EVs evading the immune system and reaching their target. Furthermore, displaying the therapeutic agent on the outside of the EVs may also raise an immune response against the therapeutic. This would render a multiple dose treatment ineffective. Originally this line of research was put on hiatus until the RNase A degradation method of checking encapsulation was adopted. This was developed in the sonication chapter later in this thesis. To determine if the siRNA was encapsulated within the EVs, EVs were loaded with Allstars siRNA. RNase A was then added and samples enriched using NAP-10 sephadex columns. This would remove unbound siRNA present in the sample. The fluorescence of the samples was then measured using a Fluorostar fluorimeter. The CADY, EV and Allstars siRNA control without RNase A treatment shows an association of 61% of the total siRNA added at the beginning of the experiment. After the addition of RNase A, fluorescence dropped by 55% suggesting that 6% of the original concentration of siRNA was encapsulated within EVs (figure 7.1-12).

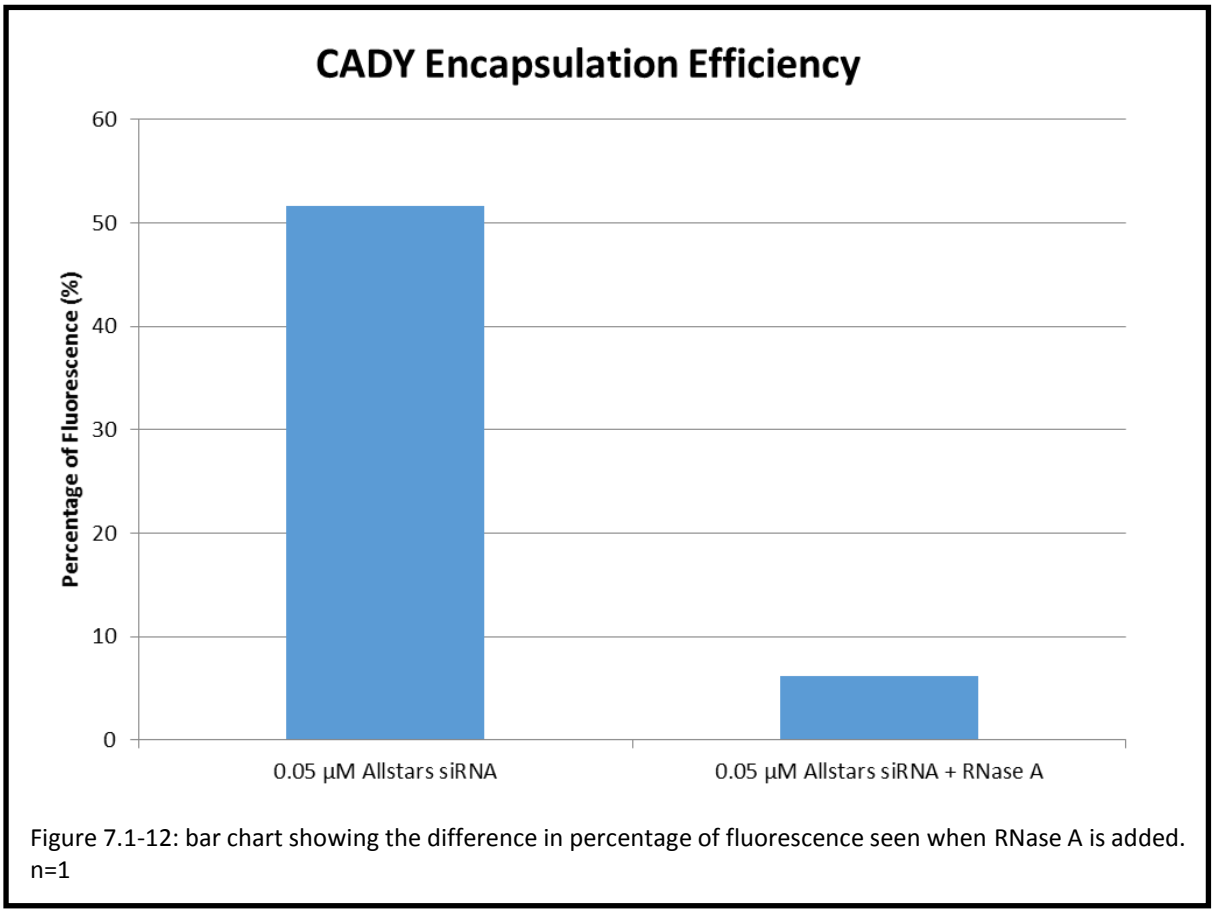

Figure 7.1-12: bar chart showing the difference in percentage of fluorescence seen when RNase A is added. n=1

7.2 MPGα

MPGα is an amphipathic CPP with the ability to deliver siRNA directly to the nucleus (Simeoni *et al.,* 2003). This is due to its Nuclear Localisation Sequence which also aids in electrostatic interactions with cargo. MPGα has been well characterised to deliver cargo as a CPP.

1, 2 and 4 μg MPGα were first incubated overnight with RPMI to analyse the characteristic background on flow cytometer FSC and SSC dot plots. A gate was set to an RPMI control and the events outside the gate measured to determine if changes in events had occurred upon addition of CPP. In figure 7.2-1 top graph, when MPGα is added to RPMI there is a 1.1-3 % increase in events outside of the gate. However when MPGα is added to a source of EVs there is an increase in events detected outside the gate that increases as the concentration of MPGα increases. The increase seen when MPGα is added to an EV source is between 34-74 % compared to the CEM supernatant control. Together this data suggests that MPGα may have minimal aggregation when incubated in RPMI, however the aggregation seen when EVs are included is much greater.

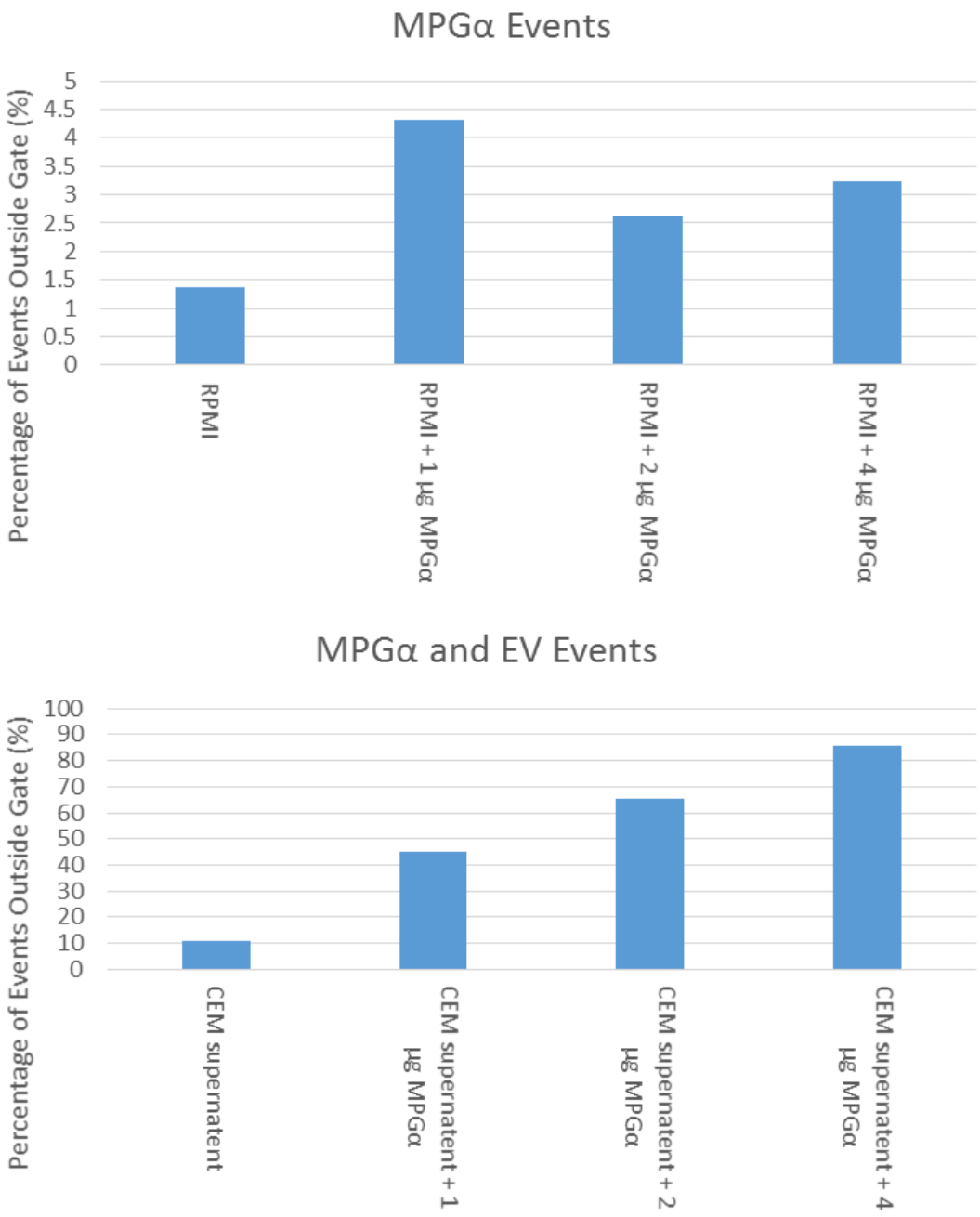

Figure 7.2-1: bar charts showing the changes in events detected by a flow cytometer as the concentration of MPGα increases. Percentages were calculated from a gate set to an RPMI control. n=2

The ability of MPGα to deliver cargo into EVs was next analysed. First 2 μg MPGα, HeLa cell supernatant containing EVs and 0.01 μM Allstars siRNA were left overnight at RT. Following this samples were analysed by flow cytometry (figure 7.2-2, top bar chart). There is an increase in events outside the gate when MPGα is added to the samples containing EVs and Allstars siRNA compared to the RPMI control. In the bottom graph 28-31 % of fluorescent events are outside the gate for the samples without Allstars siRNA. However this increases when Allstars siRNA is added. Furthermore this data shows that Allstars siRNA can associate with EVs without the presence of MPGα. Therefore a method to remove fluorescence that is not encapsulated should be sought.

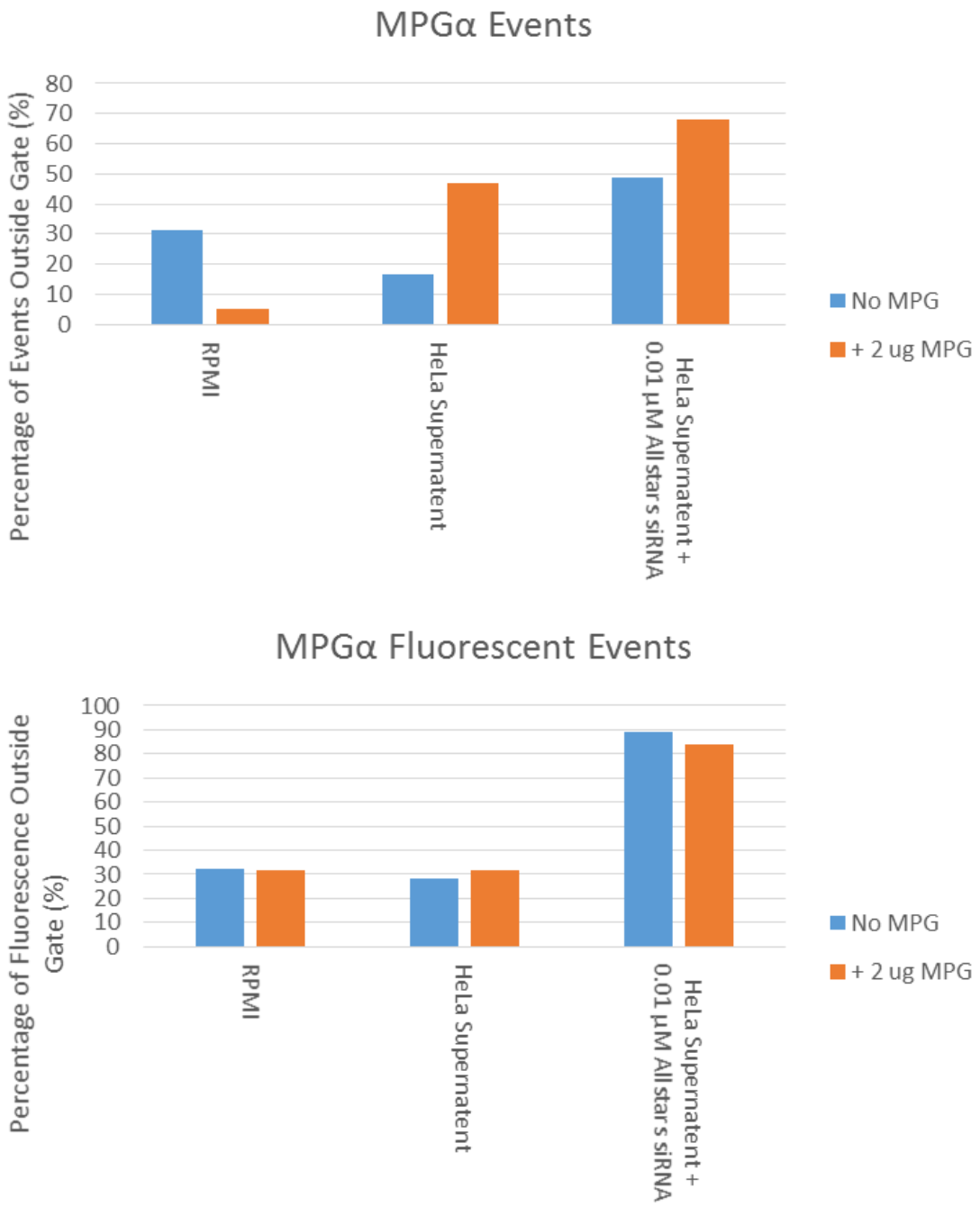

Figure 7.2-2: bar charts displaying the changes in events detected by a flow cytometer when MPGα is added to EVs or RPMI with Allstars siRNA. Percentages were calculated from a gate set to an RPMI control. n=1

To assess the efficiency of MPGα at encapsulating siRNA, 0.05 µM Allstars siRNA was first complexed with 2 µg MPGα. The complexes were then incubated with 100 µg U937 EVs. The mixture was then split in two; the first half was incubated with RNase A before enrichment of both. Samples were measured for their fluorescent intensity (figure 7.2-3, right) and particle size (figure 7.2-3, left). Encapsulation of the siRNA was measured by the fluorescent intensity retained after enrichment. The sample that was not exposed to RNase A showed a 54 % retention, however, after the RNase A incubation this figure dropped to 11 % (figure 7.2-3, right graph). Overall, this suggests that only 11 % of the fluorescence seen in the sample without the RNase A step can be attributed to encapsulated siRNA. The size of the EVs was measured by NTA. NTA analysis revealed that the size of the EVs increased from 154 nm (stock) to 234 nm and 226 nm for the samples without and with RNase A, respectively (figure 7.2-3, left graph). This increase in size observed in both samples suggests that internalisation of the complexes has either caused the EVs to increase in size, merge or aggregate.

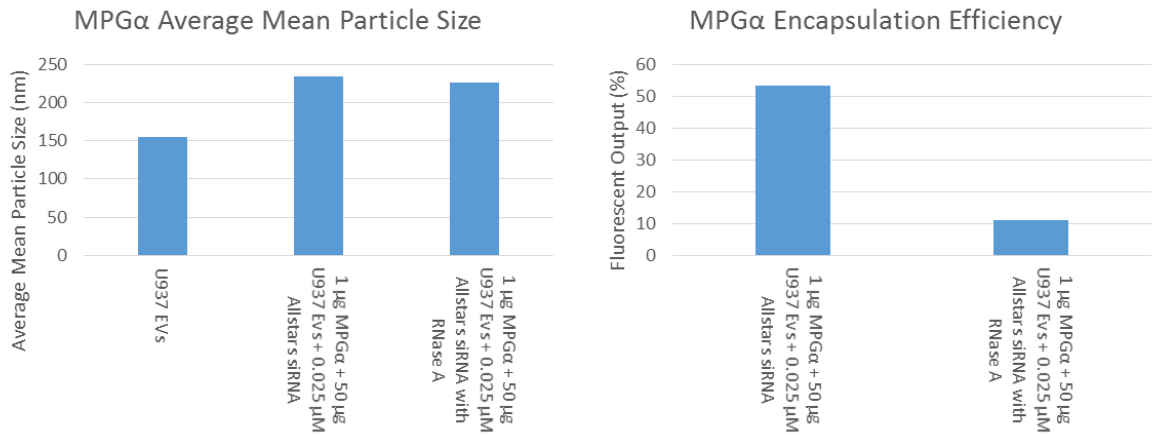

Figure 7.2-3: bar chart showing the decrease in fluorescence seen when RNase A is added before enrichment. The remaining fluorescence represents the siRNA that is protected by the encapsulation of the EVs compared to siRNA which is not inside the EVs and is degraded. n=1

A higher concentration (0.1 µM) of Allstars siRNA, EVs and MPGα was tested next. The same method was used as in the previous section. This time a 60 % retention of fluorescence for the sample enriched without RNase A was observed. For the sample enriched with RNase A a retention of 5 % was observed (figure 7.2-4). Thus the ability of 4 µg MPGα to encapsulate Allstars siRNA into EVs decreases after a certain concentration of input cargo between 0.05 and 0.1 µM. Due to this inefficiency, attempts were made to evaluate other methods.

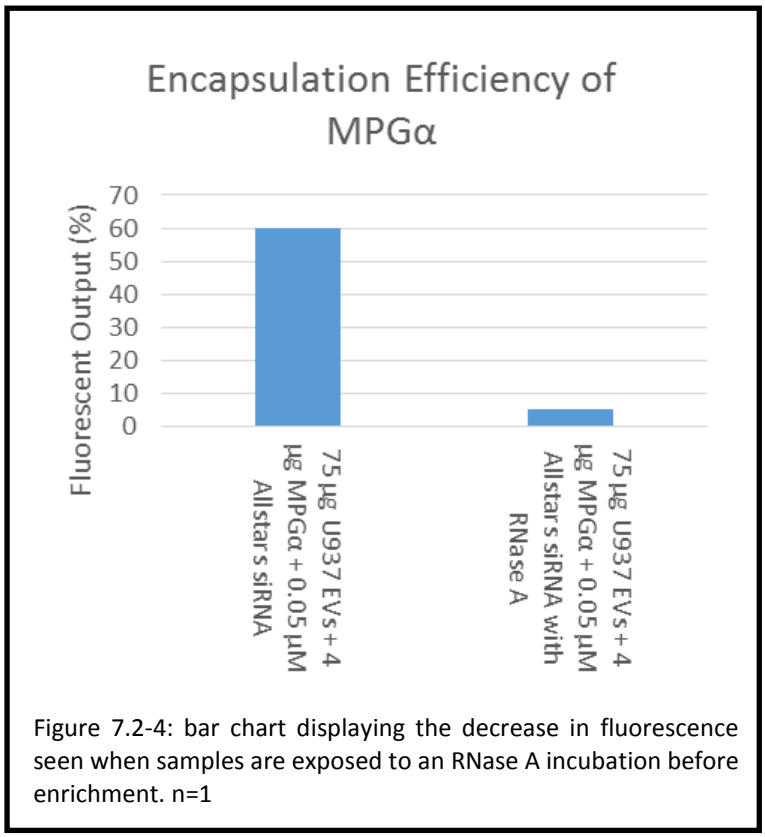

Figure 7.2-4: bar chart displaying the decrease in fluorescence seen when samples are exposed to an RNase A incubation before enrichment. n=1

7.3 JBS Nucleoducin

JBS Nucleoducin is a commercial mixture of different CPPs, therefore it is able to target a variety of different cargoes to multiple cell types. Given the variety of CPPs present it is more likely that any one will be able to deliver cargo to the inside of EVs. It was therefore used to transfer FITC Ab and Allstars siRNA into EVs.

Three concentrations of JBS Nucleoducin (0.09, 0.18 and 0.36 μg) were incubated first with the FITC Ab for 30 minutes at 37 °C before adding EVs and RPMI. The mixture was then incubated for a further hour at 37 °C, more RPMI added and the samples left to incubate overnight at 37 °C before analysis. In figure 7.3-1 the top graph shows the percentage of events detected outside a gate for the samples. It was observed that upon addition of JBS to any sample the percentage of events increases with the concentration of JBS Nucleoducin. Compared to the RPMI and JBS controls the controls with EVs all showed an increase in events suggesting that, similar to the previous chapters, a population of EVs are visible by flow cytometry. Interestingly, when FITC Ab was added to the mixture there was less of an increase in events than the majority of the EV and JBS Nucleoducin controls. In the bottom graph of figure 7.3-1 there is an increase in the fluorescence outside the set gate when FITC Ab is added. This increase with the concentration of JBS Nucleoducin is seen for three out of four of the JBS concentrations. This suggests that FITC Ab association with the EVs may increase with JBS concentration. However the increase in events outside of the gate together with this data may suggest the formation of fluorescent aggregates. The fluorescence seen for the RPMI and 0.09 μg JBS Nucleoducin control is presumed to be a contaminant as it was not present in the repeat experiment.

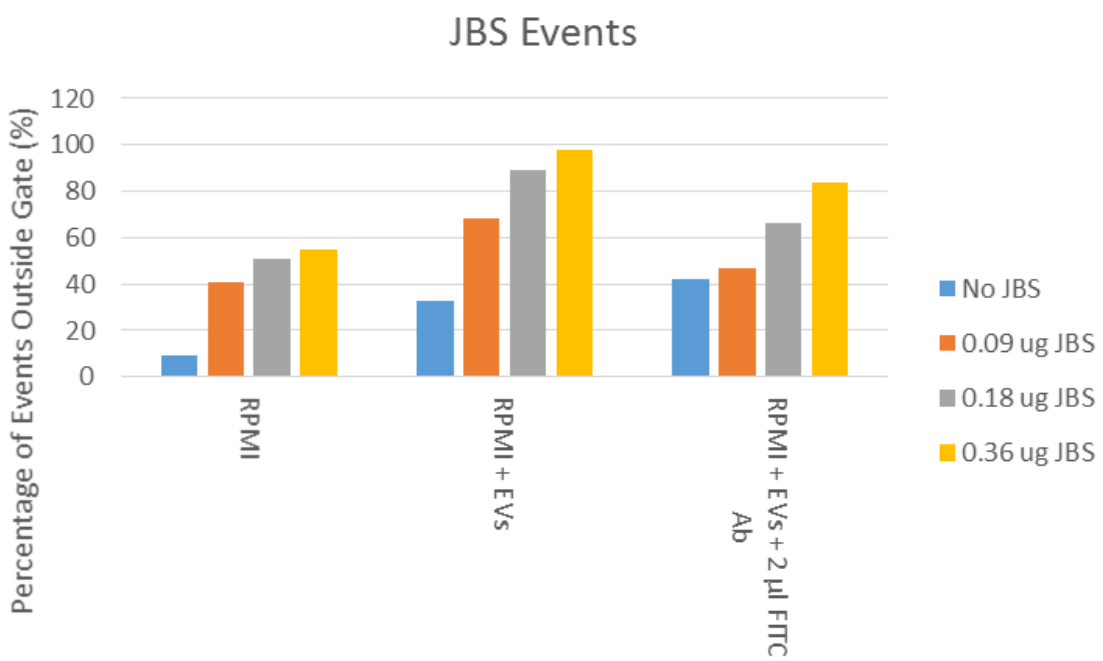

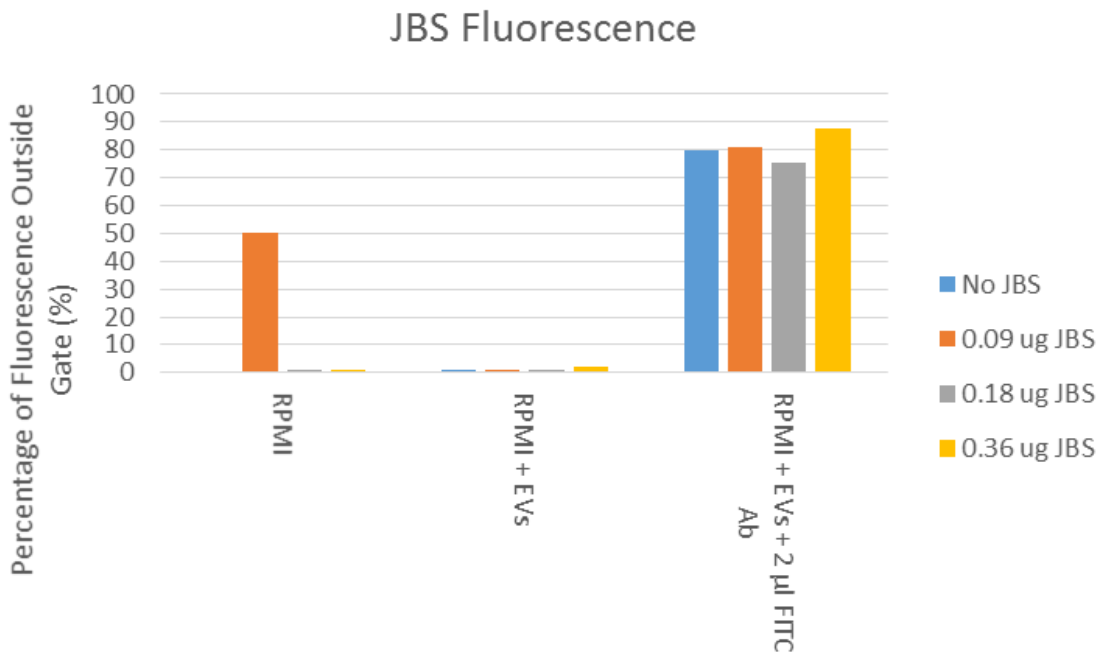

Figure 7.3-1: bar charts displaying the changes in events and fluorescent events detected by a flow cytometer. Events were calculated from a gate set to an RPMI control. n=2

To determine if aggregates were present in JBS Nucleoducin samples were prepared and incubated for 1 hour. Samples were then analysed using NTA to estimate size and concentration of particles. Aggregates, over 100 nm in diameter, were observed in the JBS Nucleoducin control samples (figure 7.3-2, top graph). Furthermore, this pattern did not correlate with an increase in JBS Nucleoducin concentration or particle concentration (figure 7.3-2, bottom graph). This suggests that the 0.18 µg concentration is more likely to form aggregates in the EV size range.

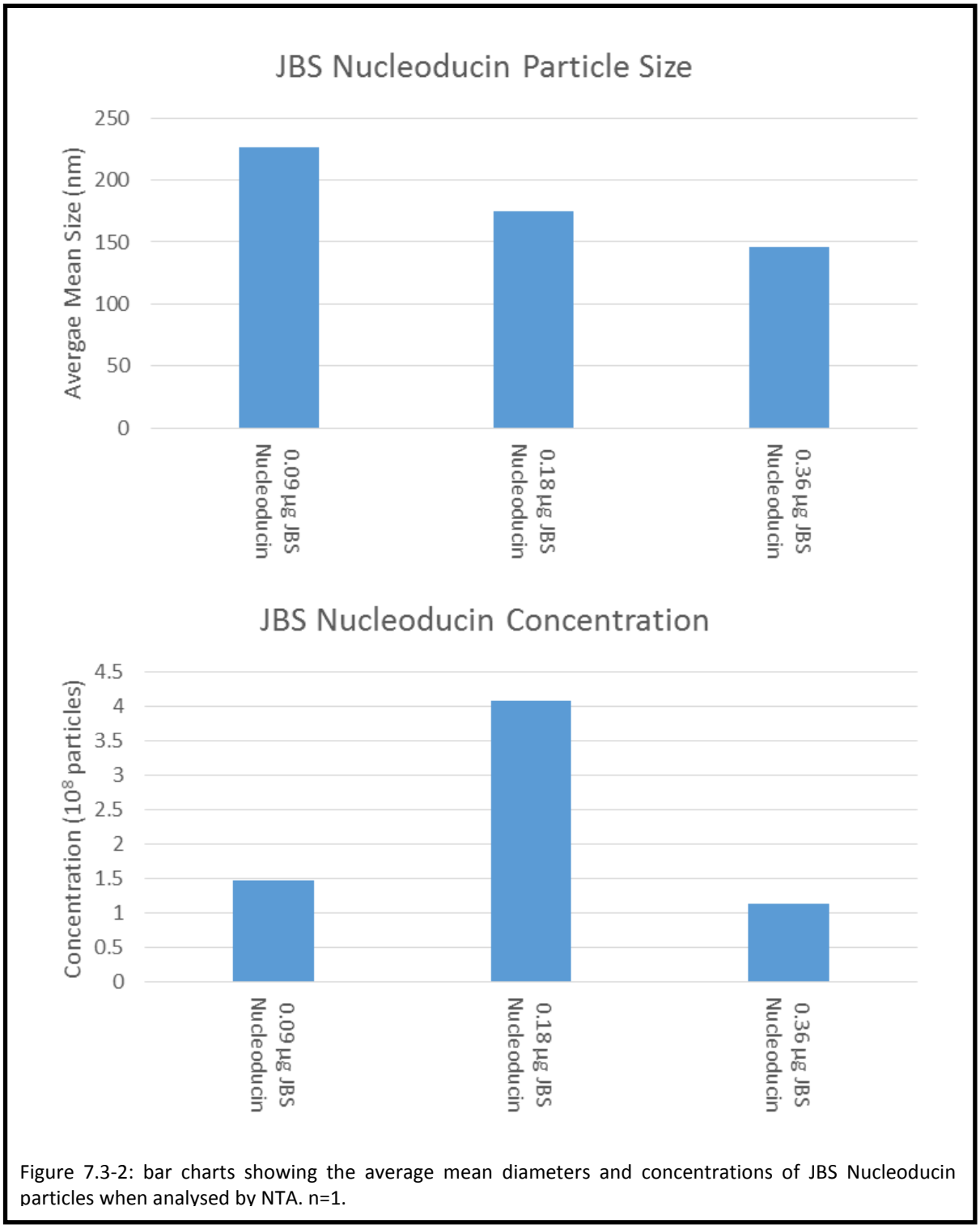

Figure 7.3-2: bar charts showing the average mean diameters and concentrations of JBS Nucleoducin particles when analysed by NTA. n=1.

The effects of JBS Nucleoducin with Allstars siRNA, a closer substrate to the intended cargo than FITC Ab, were next analysed. In figure 7.3-3, top graph, there is an increase in events outside the gate when EVs are added confirming their presence. However, this time there is no pattern of event increase seen with the RPMI controls when increasing concentrations of JBS Nucleoducin are added. When Allstars siRNA is added to the RPMI controls there is an increase in events detected outside the gate compared to the RPMI controls. Furthermore this increase is exaggerated when EVs are added however not to the same levels as the EV and RPMI controls. For all samples where JBS was added to another component there is an increase in events detected outside the gate that increases as the concentration of JBS increases. In the bottom graph there is only fluorescence where samples contain Allstars siRNA as expected, however the increase in fluorescence for the siRNA and EV sample without JBS Nucleoducin compared to the samples containing JBS Nucleoducin has a very similar pattern. 0.09 μg JBS has the highest number of fluorescent events outside the gate followed by 0.36 μg. Together this data suggests that Allstars siRNA and EVs may form aggregates on their own however when they are incubated together they appear to bind and reduce the number of events detected outside the gate. Despite seeing an increase in events for the EV and siRNA samples, as the control without JBS Nucleoducin also shows similar fluorescence this again suggests that the fluorescence of encapsulated cargo may be masked by background fluorescence.

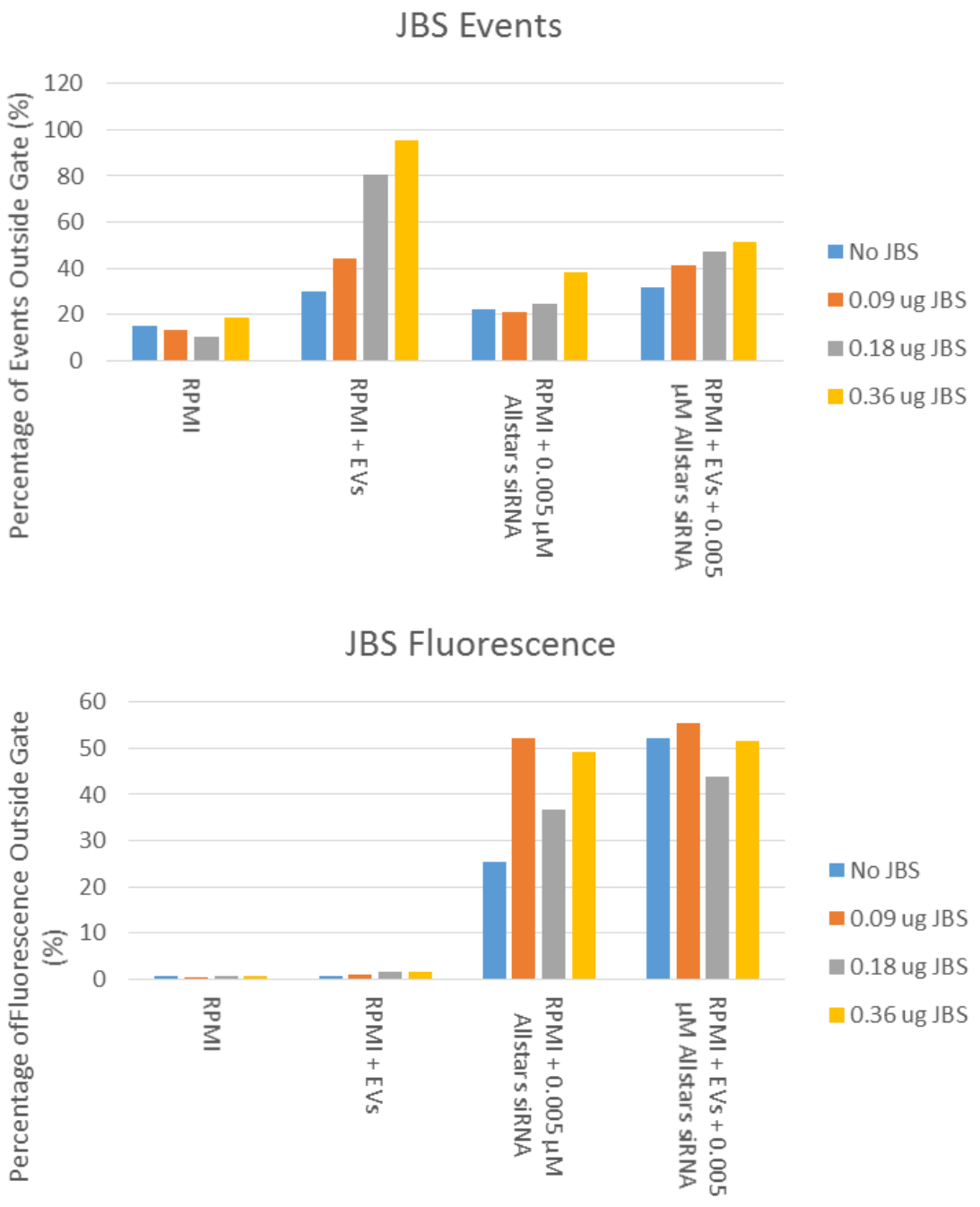

Figure 7.3-3: bar charts displaying the changes in events detected by a flow cytometer when various concentrations of JBS Nucleoducin are added. Percentage were calculated using a gate set to an RPMI control. n=2

To evaluate the percentage of siRNA retained by EVs exposed to cargo/JBS Nucleoducin complexes, 0.05 µM and 0.1 µM Allstars siRNA were complexed with 0.36 µg JBS Nucleoducin. Complexes were then incubated with 100 µg U937 EVs for 90 minutes before splitting in two and adding 10 µg RNase A to one half and incubating at 37 °C for 30 minutes. Both halves were then enriched by filtering them through a NAP-10 size exclusion column. Enriched samples were then diluted and analysed in terms of fluorescent intensity, particle size and particle concentration. Similar to other CPPs, an increase in size of the particles present (presumed to be EVs) in the samples was observed. This was from 123 nm diluted stock EVs (data not shown) to 221 nm and 223 nm for the 0.025 µM Allstars siRNA samples enriched without and with an RNase A incubation, respectively (figure 7.3-4) and 242 nm and 237 nm for the 0.05 µM Allstars siRNA samples enriched without and with an RNase A incubation, respectively. Of note, there is a slight increase in particle size observed when the higher concentration of Allstars siRNA is used. This is presumed to be siRNA aggregates. The percentage of siRNA retention for the sample without an RNase A incubation was calculated to be 47 %, decreasing to 9 % for the sample with RNase A incubation (figure 7.3-4). This pattern is also repeated for the higher concentration of Allstars siRNA. The 41 % retention seen for the sample without RNase A decreases to almost 10 % when RNase A is added. Considering that only 9-10 % of the siRNA was encapsulated, a different average mean diameter for the particles may also be expected. Furthermore, the decrease in siRNA encapsulation after RNase A incubation demonstrates that approximately 31-38 % of the siRNA input associates with EVs in a manner which is not protected from RNase A degradation.

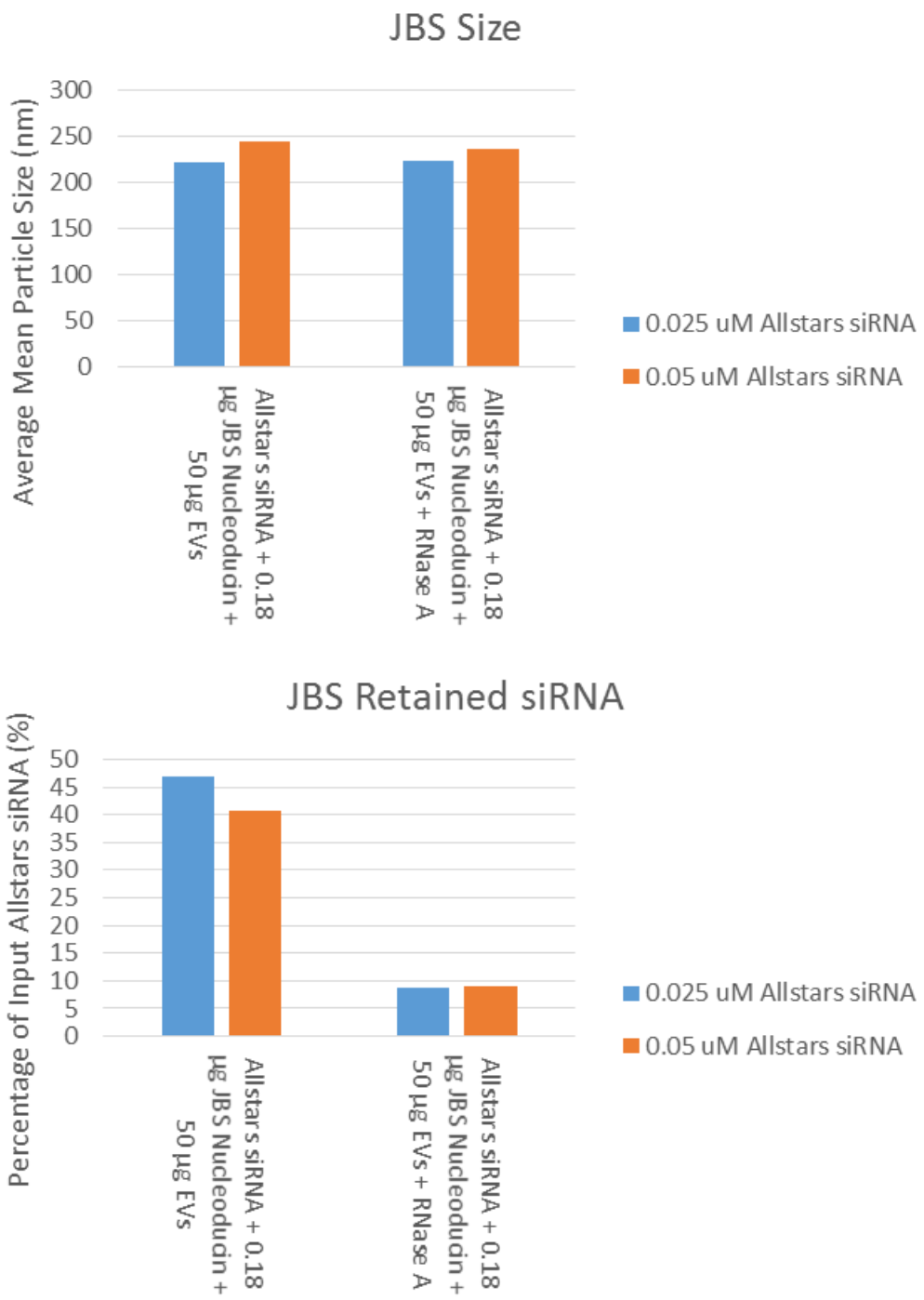

Figure 7.3-4: bar charts showing the differences in size and Allstars siRNA retained when samples are incubated with two different concentrations of JBS Nucleoducin. n=1.

To determine if the saturation of JBS Nucleoducin was related to binding of cargo rather than aggregation the previous experiment was repeated. This time double the concentration of JBS Nucleoducin was used. The percentage of fluorescent particles associated with the samples both with and without RNase A incubation was first analysed. It was observed that with the higher concentration of JBS Nucleoducin there was a lower percentage of fluorescence retained (figure 7.3-5, bottom graph). This suggests less binding of CPP and cargo to the EVs. For the sample with an RNase A wash a similar amount of fluorescence retained was observed as the previous experiment. One again an increase in mean particle diameter was observed upon the addition of JBS Nucleoducin/siRNA complexes (figure 7.3-5, top graph). There is still also no relationship between particle size and siRNA encapsulated suggesting that perhaps the JBS Nucleoducin is able to bind to the outside of the EVs or form aggregates. Together these results suggest that an increase in JBS Nucleoducin concentration causes less general binding of siRNA to EVs. However it does not change the percentage of siRNA encapsulated by EVs.

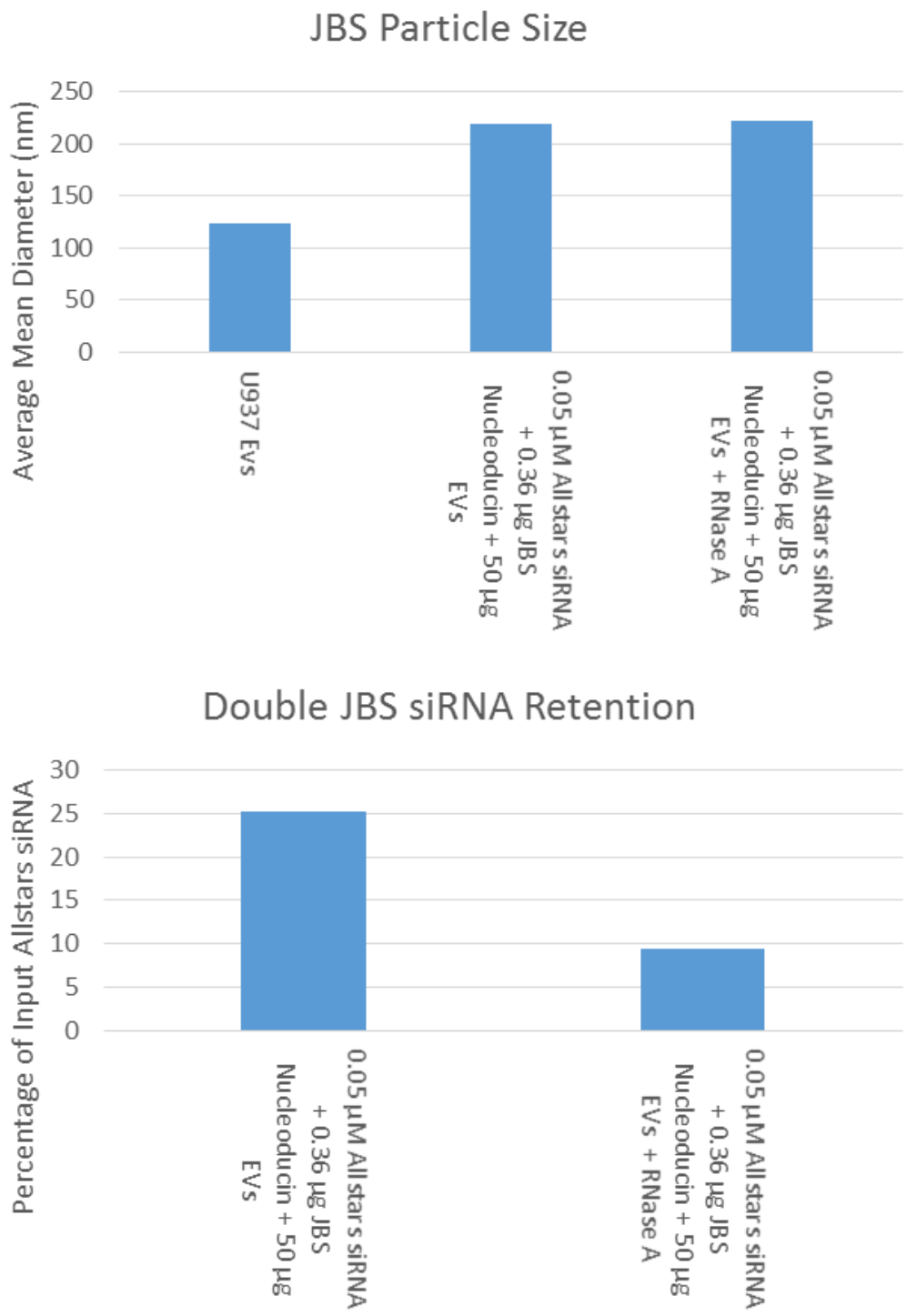

Figure 7.3-5: bar charts showing the percentage of Allstars siRNA retained after an RNase A incubation when the concentration of JBS Nucleoducin is doubled. n=1.

7.4 Discussion

CADY is a well-researched molecule and has been documented to successfully breach the PM of cells (Laurence Crombez *et al.,* 2009; Keller *et al.,* 2013; Konate *et al.,* 2010; Mussbach *et al.*, 2011). The majority of literature relating to MPGα within the last 4 years is in the form of reviews (L Crombez, Morris, Deshayes, Heitz, & Divita, 2008; May C Morris, Deshayes, Heitz, & Divita, 2008; Müller, Triebus, Kretzschmar, Volkmer, & Boisguerin, 2012). There are 2 recent pieces of literature that are not reviews. These characterise the structure and cellular uptake of cargo, and study enhancing the cellular uptake of nanoparticles (Deshayes *et al.,* 2010; Steinbach, Seo, & Saltzman, 2016). The literature associated with JBS Nucleoducin is sparse. Considering that the earliest publication is from 2011, it would be expected to see more than two (Keller *et al.,* 2013; Mussbach *et al.,* 2011). There are other papers that cite the use of JBS Proteoducin, the cytosol targeting version of JBS Nucleoducin. Little is currently know about this mixture of CPPs, however if the composition of the cocktail was known previous data of the CPP components would be comparable.

It was found that whether due to the cargo or CPPs themselves, high levels of EV associated delivery were not observed. It is important to note that evidence of CADY delivering to cells was seen. CPPs rely heavily on their ionic charges to complex with cargo (Mussbach *et al.,* 2011). The hydrophobicity of CADY and MPGα induces interactions with the PM of the cell to allow entry. The population of EVs concerned with this study are released from the endosome of the parent cell so they should have a very similar membrane composition. Exosomes are enriched in cholesterol, ceramide, sphingomyelin, phosphatidylserine, phosphatidylethanolamine, lyso-phosphatidylcholine, phosphatidylcholine and phosphatidylinositol. The ionic charge and hydrophobicity that these membrane components induce must be taken into account (Vlassov, Magdaleno, Setterquist, & Conrad, 2012).

Normally lipids attract cations to the membrane giving it an overall positive charge. By increasing the proportion of cholesterol in the membrane this charge shifts. CPPs like CADY and MPGα are highly hydrophobic and cationic in charge, therefore they displace cations present at the PM and interact with the hydrophilic head groups of the lipids. An increase in membrane cholesterol results in a decrease in cations associated with the head groups therefore making the membrane charge overall more neutral. Ceramide on the other hand is involved in endosomal budding in the MVB. It also segregates itself with lipid rafts present on the EV membrane where it is formed from sphingomyelins by sphingomyelinases (Gulbins & Kolesnick, 2003). These ceramide containing lipid rafts have a role in the gathering and dimerising of certain receptors, an example of one is CD95 (Grassme *et al.,* 2001). As mentioned in Section 1.12.3, these lipid raft areas on the PM of cells enable

uptake of molecules and cargoes by cells as well as being the hubs for cell communication. Considering this, the CPPs may require a cell capable of active endocytosis in order to deliver cargo.

The activity of CADY at 4 °C and at room temperature was observed in this chapter. This helped to discern whether CADY associated cargo delivery was energy dependent. At 4 °C the increase in EV size, with time, was still observed. This means that the formation of complexes and uptake of complexes by EVs may be an energy independent process. Furthermore, the incubation of samples on a rocker did not accelerate the formation of complexes or the association of CADY with EVs. Suggesting that CADY does not require an active target to deliver its cargo to. These experiments were not repeated for MPGα and JBS as they had not yielded solutions to the aggregation problems experienced with CADY. However, as they are different CPPs it would be interesting to compare them with CADY.

Throughout this chapter an increase in events detected outside the gate with CPP alone and also with EVs has been observed. This is both with and without cargo. The logic behind this is that the cargo/CPP complexes may cause the EVs to increase in size, similar to PEI. The events detected outside the gates are increases in side scatter (SSC) and forward scatter (FSC) on a dot plot. However, FSC and SSC can have multiple interpretations as an increase in SSC can refer to granularity also. This means it could be an increase in density of the EVs if they have taken up complexes. There has also been no mention of changes in EV size in the relevant literature.

Looking at the literature, there are no studies concerning the formation of aggregates associated with CPPs. Potentially, the aggregation of CPPs could prevent binding with the cargo due to the masking of interaction sites. Possible aggregates were identified over the duration of this study however there was no way to positively identify them. Furthermore, the size of aggregates was undiscernible. This makes it difficult to assess whether EVs or aggregates are observed on NTA. Whilst the RNase A incubation, incorporated later, removes any exposed siRNA aggregates, CPP aggregates would remain intact. Enrichment of the sample by a NAP-10 size exclusion column would also not be able to remove any large CADY aggregates. This would result in a false NTA concentration and particle size reading. Furthermore using a size exclusion column the correct size for removing aggregates may also remove EVs.

The change that first occurred over the course of this chapter was the use of siRNA. Previously a FITC Ab had been used however the size and properties of the Ab appeared to make it a poor substitute for a siRNA. This was first used because it was the only fluorophore readily available at the time. Whilst it is likely that the majority of aggregation was due to CADY and JBS, there was also a lot of fluorescent events detected in some of the experiments performed in this chapter. This suggested that the FITC Ab also aggregated meaning that the EVs might have FC receptors (FcR) on their surface. The parent cell lines of the EVs used with the FITC Ab in this chapter were HeLa cells and Jesthom cells.

Whilst epithelial cells such as HeLa cells should not have FcR, B cell lines like Jesthoms may. This suggests that using FITC Ab as a cargo may not be suitable with specific EVs or for cell assays with their parent cells. JBS Nucleoducin is a nuclear targeting CPP and as such the optimal cargo for it is a nucleoside. The final cargo was ERAP1 siRNA. Allstars siRNA, a FITC conjugated siRNA, made for a similar cargo that could be visualised without using cell expression assays. As cell assays have a time constraint, it is important to carry out simpler experiments first. This allowed determination of the characteristics and abilities of the CPP with EVs in a focussed system.

Since the introduction of MPGα in 1997 there has been a push to produce more CPPs (M. C. Morris *et al.,* 1997). This has provided the scientific community with a large amount of choice in terms of CPP and encouraged the use of newer CPPs. More recent CPPs are usually chimeras of old CPPs and therefore need characterising anew. Considering that knowledge of the earlier CPPs produced is incomplete, users of new CPPs should be wary of toxicity and secondary binding.

RNase A was introduced in the latter half of this study to remove any un-associated siRNA cargo. As CPPs are highly cationic, they can ionically bind it as cargo. Furthermore, the cationic charge on CPPs allows interaction with the EV or cell membrane. The ability of CPPs to bind both types of membrane emphasises the importance of removing siRNA that is not encapsulated in EVs. If it is able to bind directly to cells in cell assays, this could result in misleading downregulation of protein expression that is not related to EV cargo delivery. As with other chapters it was important to ensure the data accurately reflected the fluorescent cargo encapsulated in the EVs. As you can see in figures 7.1-12, 7.2-4 and 7.3-4 it would be easy to falsely claim that CPPs retain over 40% of the input siRNA. Having controls that remove excess siRNA are extremely important, especially in the case of loading EVs.

On a similar subject, there is an intriguing observation surrounding the increase in size of the EVs post enrichment. When it is considered that <10 % of siRNA is encapsulated inside of the EVs and that even when the siRNA that is associated with the EV membranes is removed, the EVs retain their increase in size. This is suggestive of the EVs retaining or encapsulating another molecule in their membrane. The only other molecule present is the CPP. This suggests there may be a large population of CPP that does not complex with siRNA but still manages to cross or incorporate itself into the EV membrane. This would also suggest that the CPPs present do not bind strongly to the siRNA. To evaluate the strength of the bond between the complexes binding assays should be performed. This would allow measurement of the ability of the siRNA to bind to the CPPs versus a competitive molecule such as an antibody or protein cargo.

As seen in this chapter the addition of EVs to RPMI occasionally causes a noticeable increase in the percentage of events detected outside of the set gate. However, as discussed previously, due

to the density and size of exosomes, they should not be visible. This data supports the idea that EVs are a population of vesicles with different properties. This suggests that the EVs able to cause events outside the gates may be from a population that is larger and denser than exosomes. These vesicles are most likely microsomes or aggregates of EVs. In the case of microsomes, there should be further research into using more specific enrichment methods such as sucrose gradient density ultracentrifugation. This would be to enrich the population in exosomes as opposed to microsomes. In the case of exosome aggregation there is no need for further action, particularly if it is a natural occurrence. It would be interesting to analyse this population of vesicles further by using a sorting flow cytometer to collect vesicles that are detected outside of the set gate. These vesicles could then be characterised and a definitive answer reached.

An interesting approach used by Alves and colleagues is Differential Scanning Calorimetry (DSC). In their paper they used DSC to look at the interactions of CPPs with a bacterial membrane substitute (Alves *et al.,* 2008). It may be possible to use EVs or a substitute with this method and observe the activity of CPPs. Alternatively, as the CPPs must disrupt the membrane to deliver cargo, perhaps a similar method to patch clamp could be used to perform ion influx studies.

Chapter 8: Internal Loading

The previous chapters have focussed on attempts to externally load EVs by several different methods. However, an alternative approach would be to allow the host cells to produce the cargo of interest and to load this into secreted EVs. The draw of this approach is that, in theory, loading efficiency could reach 100% in that all the EVs could contain an amount of the cargo. Three options studied to load EVs in this manner are discussed in this chapter.

8.1 miR-US4-1

Human Cytomegalovirus (HCMV) miR-US4-1 specifically targets ERAP1 enzyme expression thereby altering the production of peptides by ERAP1 for binding by MHC class I (Kim *et al.,* 2011). Cells expressing miR-US4-1 endogenously loaded EVs were tested as a mechanism to alter ERAP1 expression in distant cells. First pSuperRetro miR-US4-1 plasmids were obtained from the laboratory of Kwaesong Ahn (South Korea) in dried format and rehydrated. Plasmid Maxi preps were then performed to generate transfectable quantities of material (figure 8.1-1A). Plasmids were transfected into the HeLa cell line, selected and then western blotted to check the expression of ERAP1. Compared to HeLa cells and HeLa cells transfected with a gfp plasmid, it can be seen that the miR-US4-1 transfected cells have an unexpected increase in ERAP1 expression (figure 8.1-1B and 8.1-1C). The reason for this is unclear. This system was not analysed further, but remains an option for future studies if miR-US4-1 expression could be confirmed.

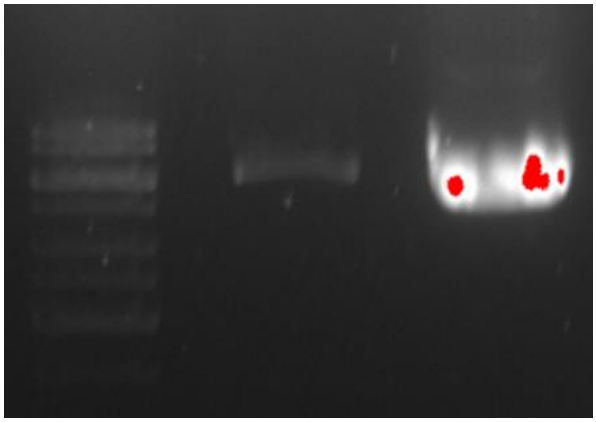

Figure 8.1-1A: agarose gel of plasmids extracted by Maxi prep. The first lane (left to right) is the 1 kbp DNA ladder, the second lane contains pSuperRetro gfp plasmid (control) and the third lane contains pSuperRetro US4-1 plasmid.

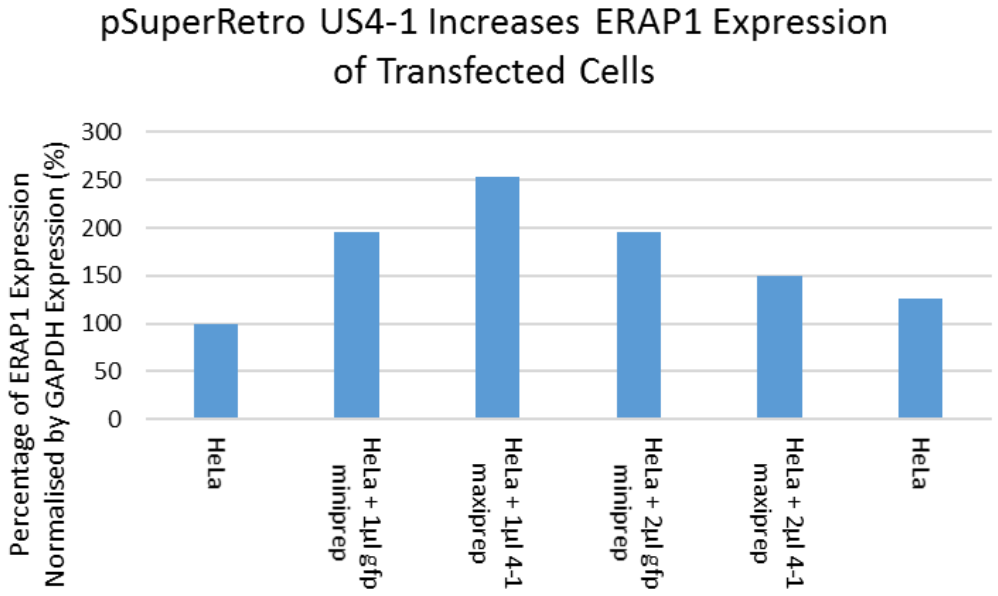

Figure 8.1-1B: bar chart showing the increase in ERAP1 expression when either a control pSuperRetrogfp plasmid or pSuperRetro US4-1 plasmid is transfected into the CEM cell line. n=1.

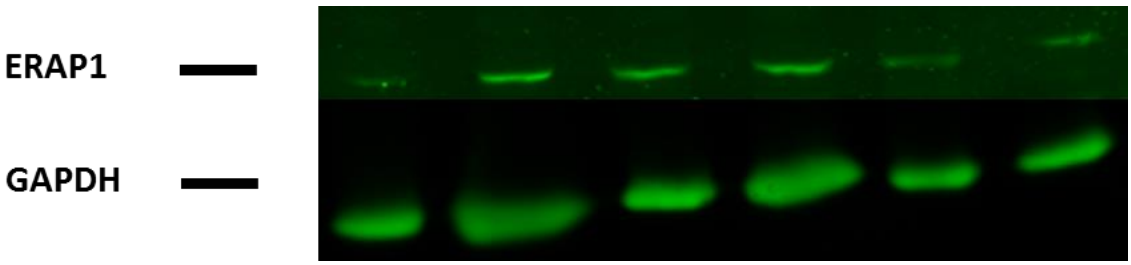

Figure 8.1-1C: western blot of ERAP1 expression in HeLa cells after transfection with pSuperRetro plasmids. Samples arranged in the same order as figure 8.1-1B.

8.2 ERAP1 shRNA Lentivector

Viral vectors pose risks for *in vivo* gene therapy. However, they can potentially be used *in vitro* initially and then the products of those cells delivered to patients. Due to the nature of Lentivectors, immediate transfection with a cell line is possible. This is because, unlike the plasmids in the previous section, lentiviruses are able to enter the host and be delivered to the nucleus of the cell. Once there they can permanently incorporate part of their genetic data into the host genome. An ERAP1 shRNA XMIRXpress lentivector (XMIR) with a Puromycin resistance gene and ERAP1 shRNA incorporated into its genome was chosen.

First the ERAP1 shRNA XMIR was transfected into HeLa cells. This was done as described in the manufacturer's instructions. Puromycin was then administered to select for those HeLa cells expressing the resistance gene. A cell line with a scrambled version of ERAP1 shRNA XMIR (XMIR SCRAM) was also produced as a control. Cultures were grown further and analysed by flow cytometry for their ME1 and HC10 expression (figure 8.2-1A). The clones showed a lower level of HC10 than controls. In particular clone 1.1 showed the greatest decrease (figure 8.2-1A, part D). These clones were also lysed and western blotted for ERAP1, HC10 and GAPDH protein expression (figure 8.2-1B and 8.2-1C). It can be seen that, compared to the positive control, the XMIR clones all show a decrease in ERAP1 expression. Due to time constraints further exploration of the XMIR clone lines was not possible, however, these cells will form a good basis for future research.

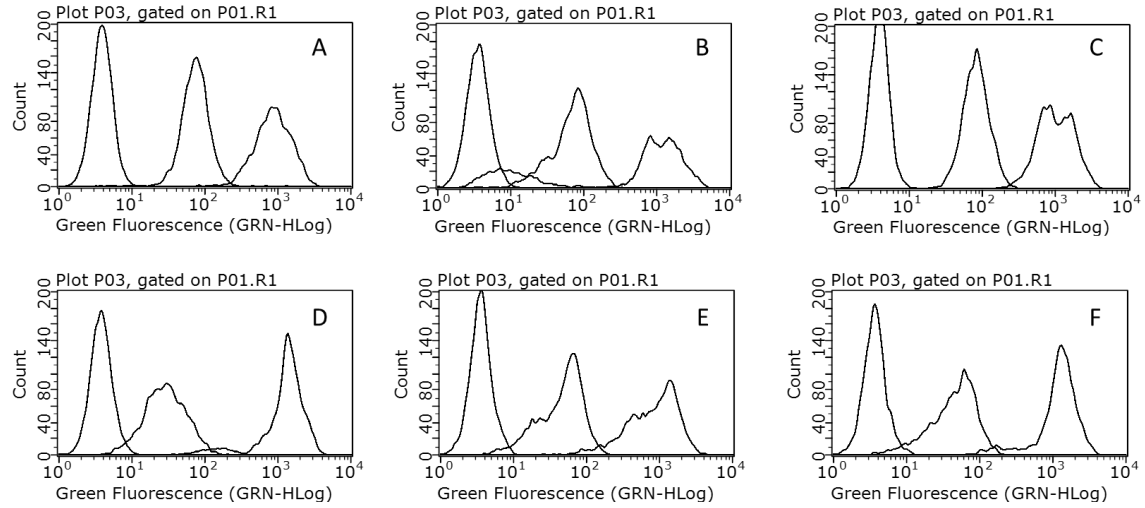

Figure 8.2-1A: fluorescent intensity histograms of XMIR cell clones. The left peak shows base line background fluorescence, the middle peak shows HC10 expression and the right peak shows ME1 expression.
A: XMIR SCRAM stock. B: XMIRshRNA 2 stock. C: XMIR SCRAM clone 1.1 D: XMIR clone 1.1. E: XMIR clone 2.1. F: XMIR clone 2.2.

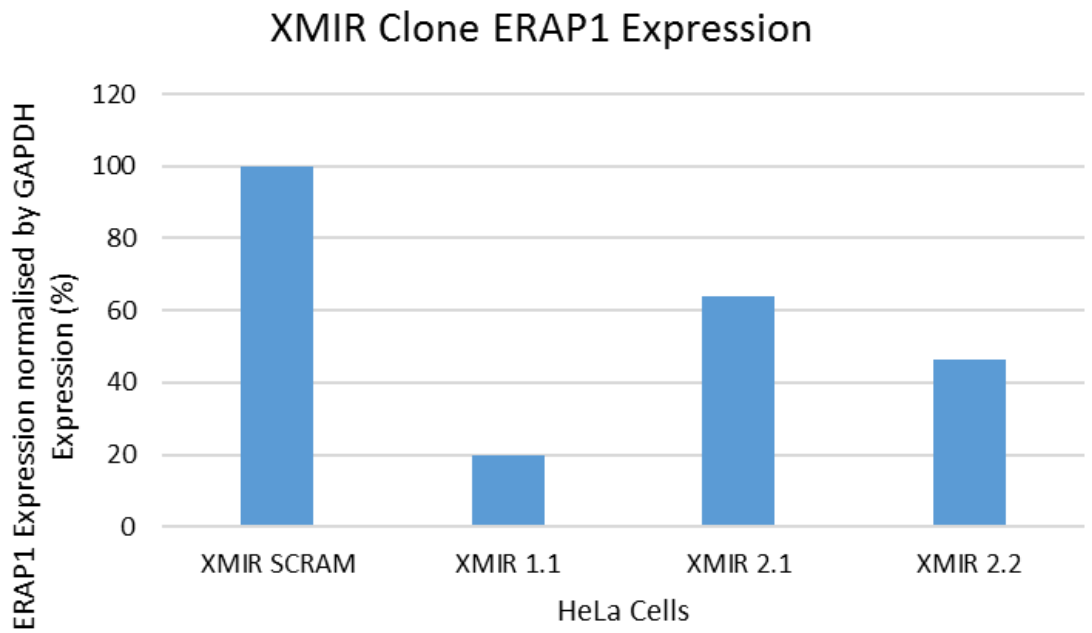

Figure 8.2-1B: bar chart of the changes in ERAP1 expression in HeLa cells transfected with ERAP1 shRNA. n=1.

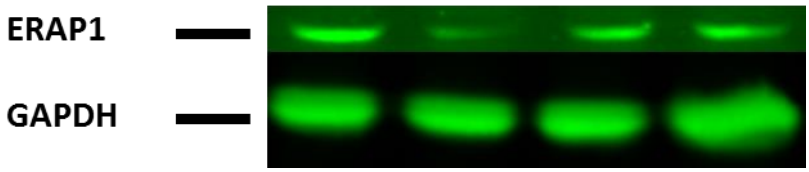

Figure 8.2-1C: western blot of ERAP1 and GAPDH expression in HeLa cells transfected with ERAP1 shRNA. Samples arranged in the same order as figure 8.2-1B.

8.3 ShRNA2 Inhibition of ERAP1

As part of a previous study in the Powis Laboratory, a CEM line expressing an ERAP1 shRNA had been generated. This cell line was generated by transfecting a CEM cell line with a shRNA insert plasmid. The sequence of the shRNA insert was: TGGGTACAACAAATCAATTCT. To assess the ERAP1 expression in these cells a western blot was performed. Compared to control CEM cells, the CEM shRNA2 cells had an almost undetectable amount of ERAP1 (figure 8.3-1A). It was hypothesised that the shRNA may be produced in excess in these cells, and thus be packaged in to exosomes. Jesthom cells were chosen to co-culture overnight with CEM and CEM sh2 cells as the exosomes would travel between cell lines. Jesthom and CEM or CEM sh2 cell co-cultures were then lysed and western blotted for ERAP1 and GAPDH expression. Upon analysis it was found that the percentage of ERAP1 expression, normalised by GAPDH expression, for the mixed culture was 5 % of the Jesthom alone culture (figure 8.3-1B). However, there was also a decrease with the control cells and CEM or C58.B27 (to 18% and 19 %, respectively). The GAPDH western blot (figure 8.3-1C) rules out the possibility of cytotoxicity being the cause for this. Despite this there is a 13 % reduction in ERAP1 expression compared to the positive controls. It is more likely that cell-cell contact is causing the downregulation of ERAP1 in the positive controls or the cell populations are producing cytokines to cause reduction of ERAP1 expression.

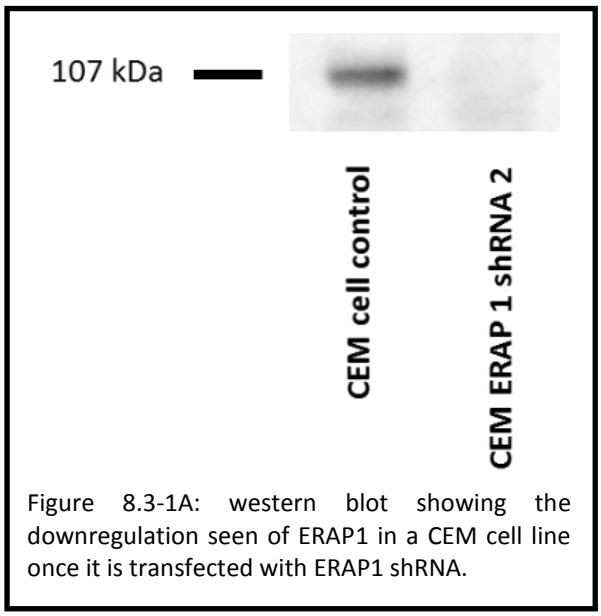

Figure 8.3-1A: western blot showing the downregulation seen of ERAP1 in a CEM cell line once it is transfected with ERAP1 shRNA.

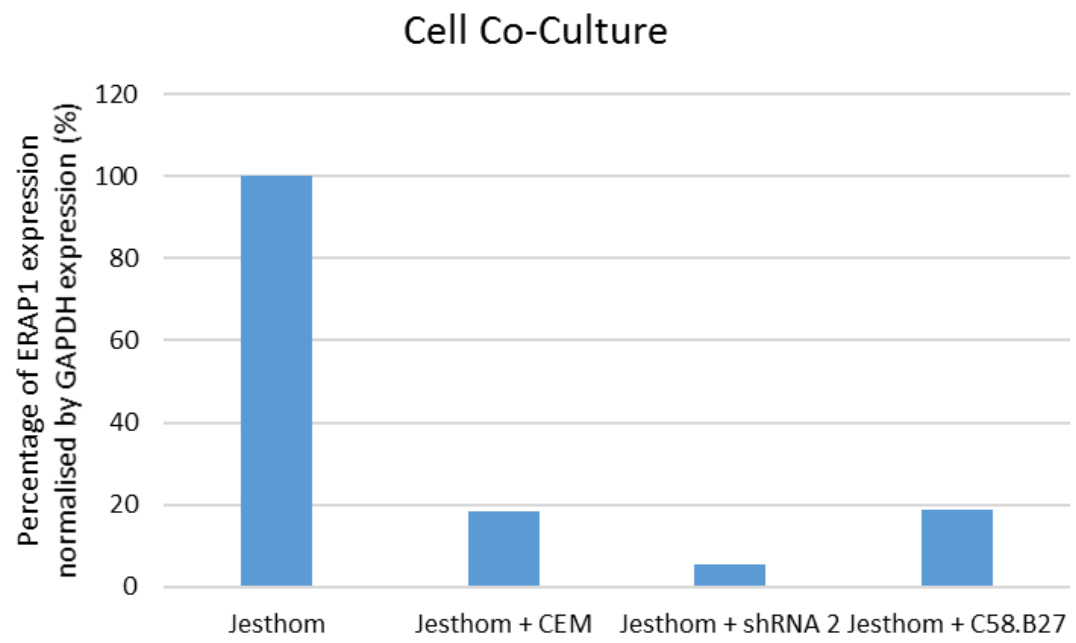

Figure 8.3-1B: bar chart showing the downregulation of ERAP1 seen when Jesthom cells are co-cultured with ERAP1 shRNA transfected CEM cells. n=1.

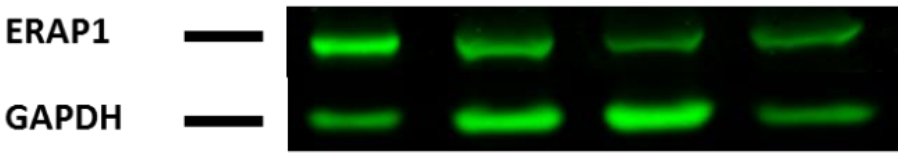

Figure 8.3-1C: western blot showing ERAP1 expression of Jesthom cells after co-culturing with CEM, CEM sh2 and C58.B27 cell lines. Samples are arranged in the same order as figure 8.3-1B.

To assess whether the small reduction in ERAP1 expression was due to EVs containing ERAP1 shRNA, a different cell layering experiment was performed. This involved using a layer of adherent HeLa.B27 cells and then layering non-adherent CEM or CEM shRNA2 cell line on top. In theory, the non-adherent cells could be washed off separately before analysing the adherent HeLa.B27 cells alone. HeLa.B27 cells are appropriate to use for these experiments as they are HeLa cells that express HLA-B27. Therefore these cells are a model for AS. Under these conditions it was observed that the HeLa.B27 cell control incubated with CEM cells gave 108 % ERAP1 expression (figure 8.3-2A and 8.3-2B). The ERAP1 expression of HeLa cells incubated with CEM shRNA2 averaged 98 % compared to the HeLa.B27 control. The high ERAP1 expression of the HeLa and CEM cell positive control suggests activation of the HeLa cells. It is possible that cell activation may cause an increase in ERAP1 expression therefore masking the decrease due to the ERAP1 shRNA. Despite showing a decrease in expression, a 2-10 % decrease is not great enough to suggest that the ERAP1 shRNA was transferred to the HeLa.B27 cells.

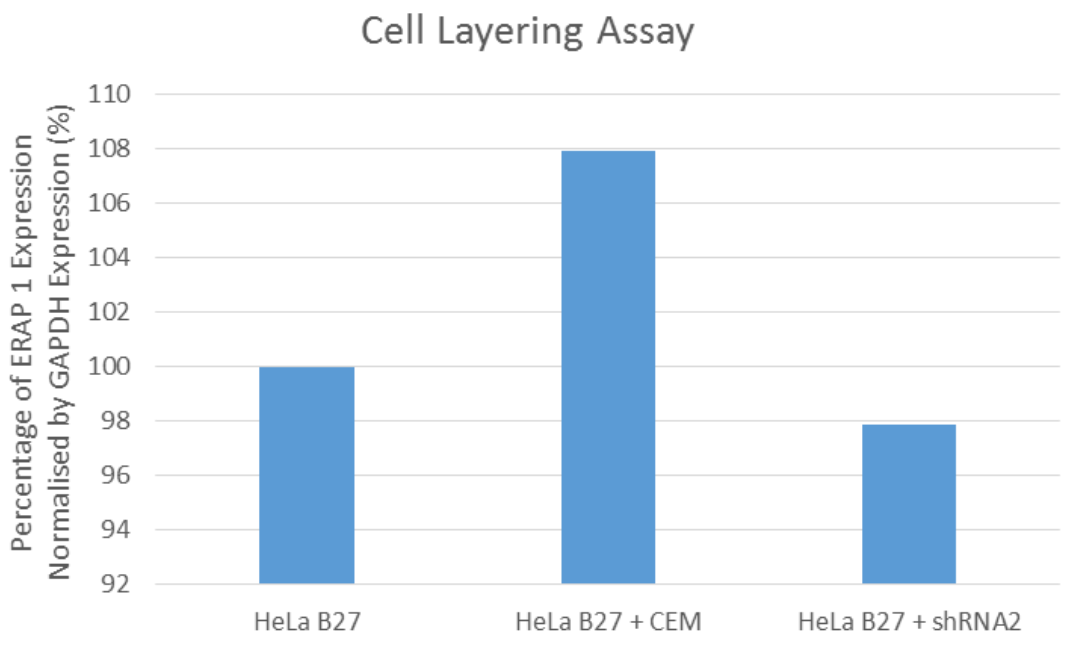

Figure 8.3-2A: bar chart showing the changes in ERAP1 expression when HeLa.B27 cells are layered with either CEM or CEM shRNA2 cells overnight. n=3.

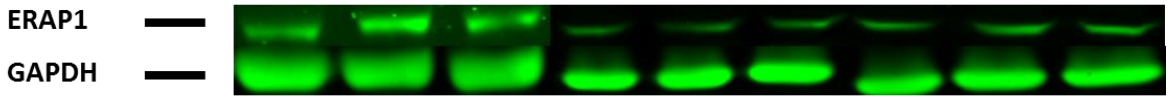

Figure 8.3-2B: western blot of ERAP1 expression of HeLa.B27 cells after cell layering study. HeLa cells were layered with either CEM or CEM sh2 cells. Samples are arranged in 3 sections of 3, each section in the same order as figure 8.3-2A.

To determine if ERAP1 levels were masked by cell activation, HeLa cells and HeLa.B27 cells were incubated with 10 ng/ml of IFNγ alongside the CEM and shRNA2 cells. The samples not incubated with IFNγ were compared to the cell alone control and a percentage calculated. The samples with an INFγ incubation had their percentage calculated based on the cell incubated with IFNγ negative control. The positive controls for both cell lines with and without IFNγ showed an increase in ERAP1 expression (figure 8.3-3A and 8.3-3B). The CEM shRNA2 and IFNγ incubated HeLa cell sample showed a decrease to 78% expression suggesting that associating the HeLa cells with the CEM sh2 cells did downregulate ERAP1 expression. To evaluate the difference between those cells incubated with IFNγ and those without, the data was re-plotted using the difference between the two values (figure 8.3-3C). When these values are compared it can be seen that the HeLa positive control shows ERAP1 expression above the IFNγ activated negative control. However the HeLa.B27 positive control shows levels of ERAP1 expression similar to the relative negative control cells. Unfortunately the HeLa.B27 ERAP1 shRNA sample did not show reduction in ERAP1 expression compared to either control however the HeLa sample did. Together this data suggests that that the shRNA did not reduce or effect the HeLa.B27 cells however it did decrease ERAP1 expression in the HeLa cells. Possibly more than seen here due to the cell activation observed above the IFNγ activation in the positive control.

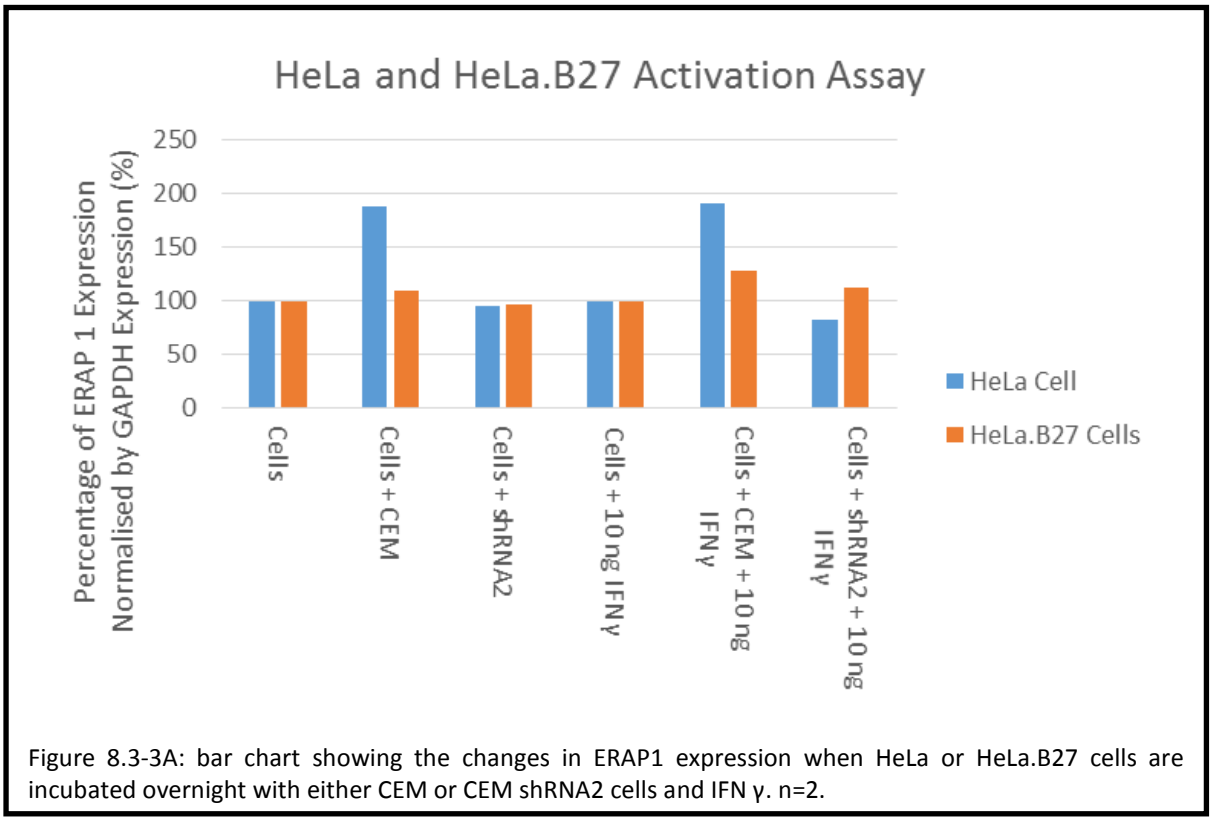

Figure 8.3-3A: bar chart showing the changes in ERAP1 expression when HeLa or HeLa.B27 cells are incubated overnight with either CEM or CEM shRNA2 cells and IFN γ. n=2.

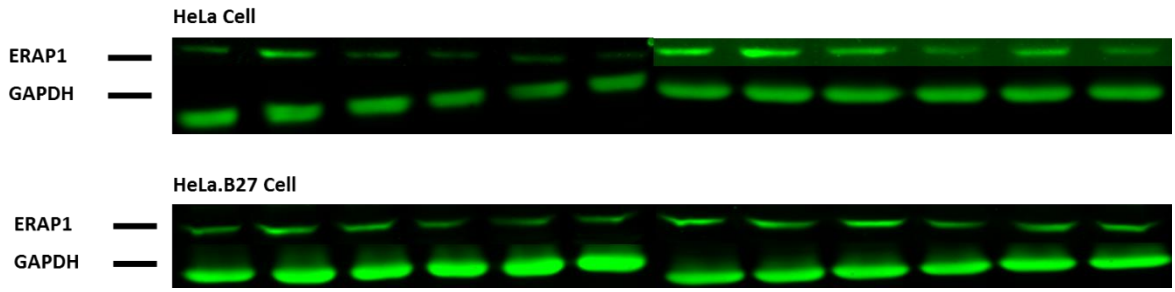

Figure 8.3-3B: western blot showing the ERAP1 expression of HeLa and HeLa.B27 cells after incubation with either a cell line or IFNγ. There are 2 western blots of 6 samples. The repeat blot follows on from the first blot. Each group of 6 samples are arranged in the same order as figure 8.3-3A.

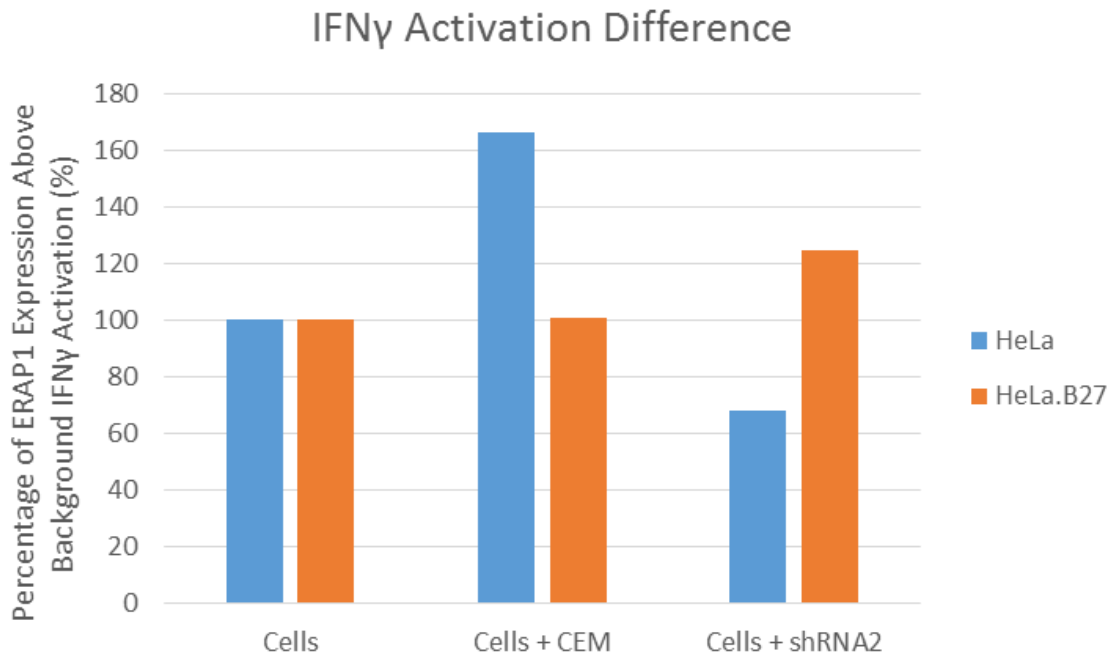

Figure 8.3-3C: bar chart showing the difference in ERAP1 expression between samples incubated with and without IFNγ. n=2.

To pursue this line of investigation further a trans-well system was used. Trans-wells separate two culture chambers by a porous membrane. 200 nm sized pores were used in the hope that exosomes would be able to pass through. In addition a control cell line was developed, CEM SCRAM. This is a CEM line transfected with a scrambled shRNA that when transcribed does not produce an active RNA silencing inducer. Therefore, CEM SCRAM should act as an ideal positive control to CEM shRNA2 as it will show any cell activation whilst not triggering ERAP1 downregulation. Culture plates were set up with trans-wells and HeLa cells were co-cultured with either CEM shRNA2 cells, CEM cells or CEM SCRAM cells. Trans-wells were harvested and the HeLa cells analysed. At first, the culture of HeLa and CEM shRNA2 cells together appears to enhance ERAP1 expression (figure 8.3-4A and 8.3-4B). However, compared to the HeLa and SCRAM cell co-cultures it has a lower ERAP1 expression. This suggests that the CEM SCRAM control is a suitable comparison to determine expression levels of ERAP1.

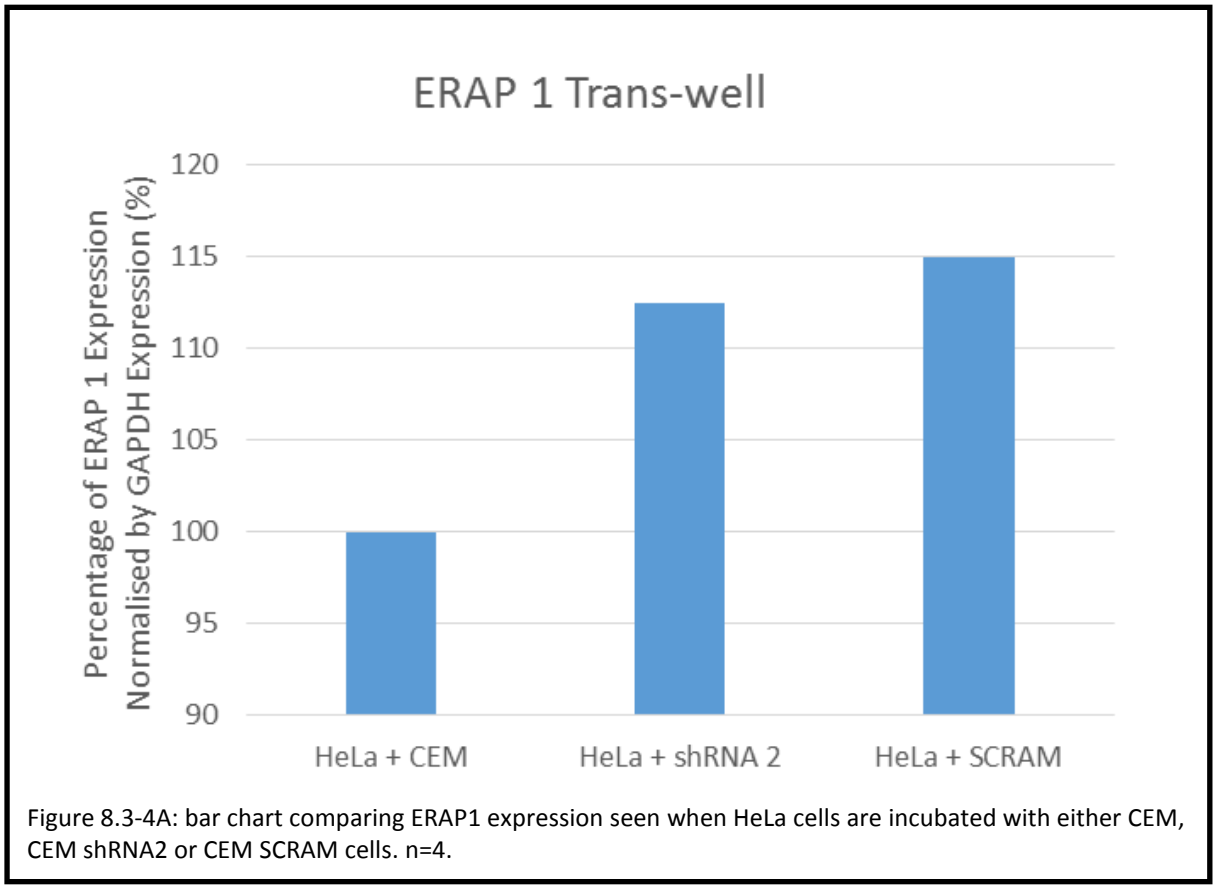

Figure 8.3-4A: bar chart comparing ERAP1 expression seen when HeLa cells are incubated with either CEM, CEM shRNA2 or CEM SCRAM cells. n=4.

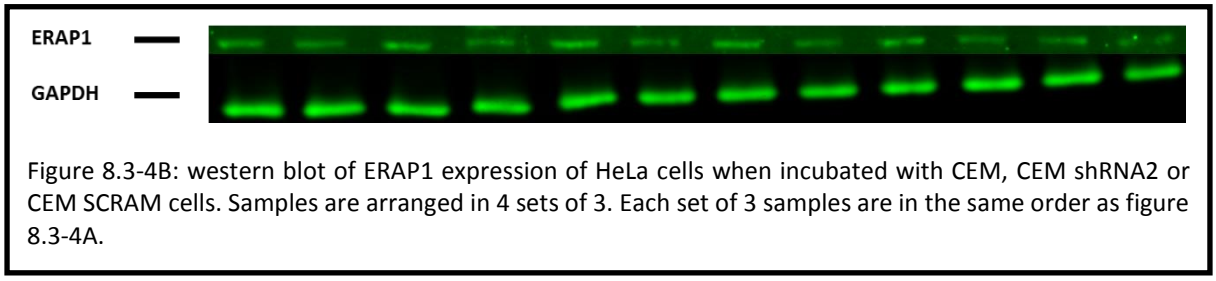

Figure 8.3-4B: western blot of ERAP1 expression of HeLa cells when incubated with CEM, CEM shRNA2 or CEM SCRAM cells. Samples are arranged in 4 sets of 3. Each set of 3 samples are in the same order as figure 8.3-4A.

Next the effect of incubating the CEM sh2 and control cell lines on other non-adherent cell lines was assessed. Wells were seeded with either CEM, Jurkat or U937 cell lines. Once the cells reached confluency, a trans-well was placed in the plate well and either CEM, CEM NEG or CEM shRNA2 (sh2) cells added to the trans-well. CEM NEG cells are the negative control cells generated as a control to another experiment. However, they were transfected to produce a scrambled form of miR-US4-1 and therefore can serve as a control in this experiment too. After overnight incubation trans-wells were removed and the remaining cells in the plate analysed for ERAP1 expression (figure 8.3-5A and 8.3-5B). Compared to the cell and CEM control the CEM cell line was the only cell line that showed downregulation in ERAP1 expression when incubated with CEM sh2 cells. However when comparing samples to the positive CEM NEG control only Jurkat and U937 cell lines show a reduction in ERAP1 expression. As CEM cells are being incubated with CEM cells it is likely that the cells may not cause as much activation as previously seen however the CEM NEG incubated control should still show ERAP1 expression above CEM sh2 incubated sample levels. Together this data suggests that CEM sh2 downregulated ERAP1 expression in the Jurkat and U937 cell lines.

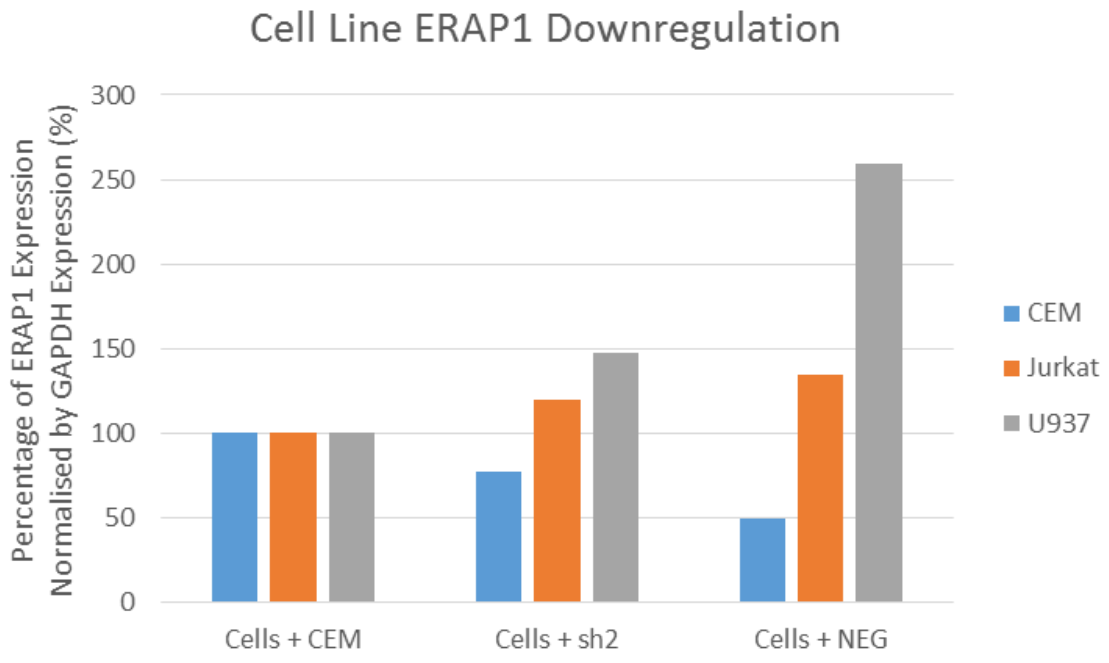

Figure 8.3-5A: bar charts showing the changes in ERAP1 expression when either CEM, Jesthom, Jurkat or U937 cells are incubated with either CEM, CEM sh2 or CEM NEG cells. The blue bars represent the first western blot whilst the orange bars represent the repeat blot. n=2.

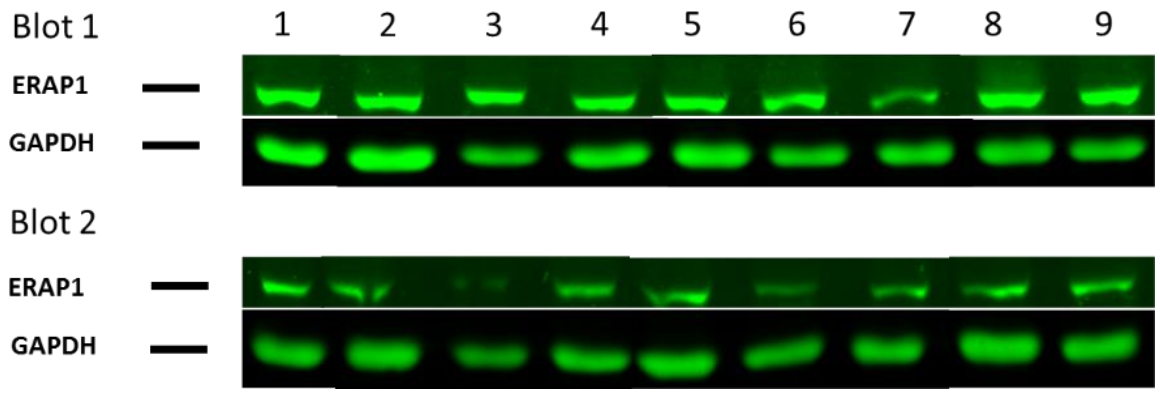

Figure 8.3-5B: western blot of ERAP1 expression of CEM, Jesthom, Jurkat or U937 cells when incubated with either CEM, CEM sh2 or CEM NEG cells.
1: CEM + CEM. 2: Jurkat + CEM. 3: U937 + CEM. 4: CEM + sh2. 5: Jurkat + sh2. 6: U937 + sh2. 7: CEM + NEG. 8: Jurkat + NEG. 9: U937 + NEG.

The adherent HUVEC hTERT cell line was analysed next. ERAP1 displays a slight alteration in PAGE migration in some cell lines. After screening a number, this difference was noticed in HUVECS (figure 8.3-6A). The size difference would allow the tracking of ERAP1 expression in target HUVEC cells in co-culture studies. Confluent HUVEC hTERT cells were co-cultured with either CEM, CEM sh2 or CEM NEG cells. After 24 hours non-adherent cells were washed off and adherent HUVEC hTERT cells were analysed for their ERAP1 expression. Decrease in the HUVEC ERAP1 signal was detected by western blot (figure 8.3-6B and 8.3-6C) for HUVECs incubated with CEM sh2 when compared to the HUVECs incubated with either CEM or CEM NEG cells (7 and 12 % respectively). This suggests that a maximum of 12 % ERAP1 downregulation is observed after cells are activated.

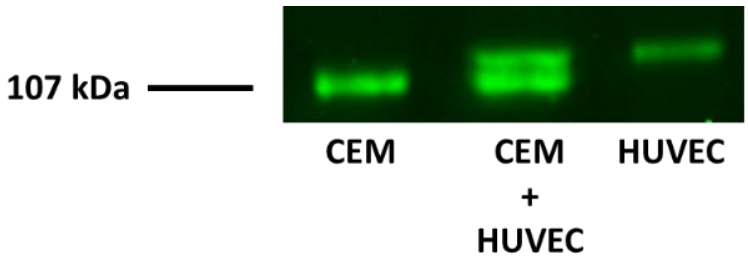

Figure 8.3-6A: western blot showing the subtle differences between CEM and HUVEC ERAP1 protein sizes.

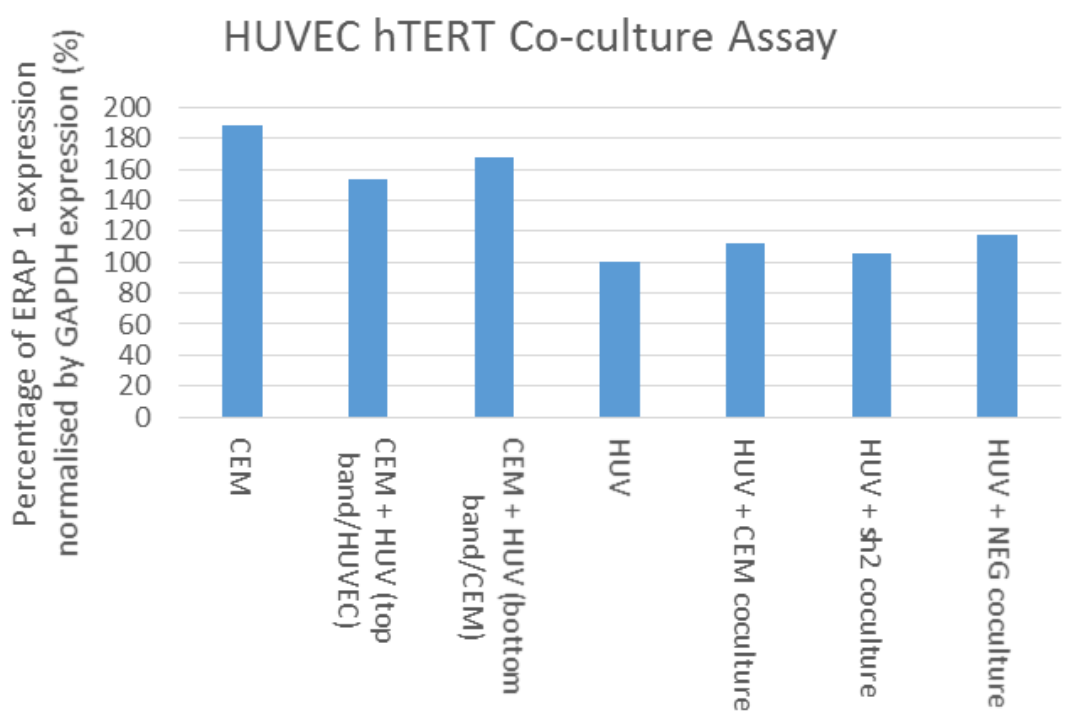

Figure 8.3-6B: bar chart showing the changes in ERAP1 expression when HUVEC hTERT cells (HUV) are co-cultured with either CEM, CEM sh2 or CEM NEG cells. n=2.

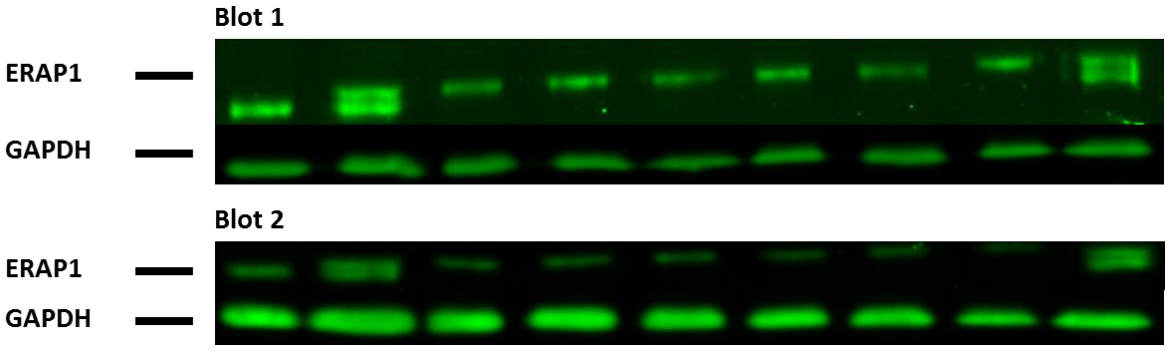

Figure 8.3-6C: western blot showing the ERAP1 expression of HUVEC hTERT cells when they are co-cultured with either CEM, CEM sh2 or CEM NEG cells. Samples are arranged in the following order: CEM, CEM + HUVEC, HUVEC, HUVEC + CEM, HUVEC + CEM, HUVEC + sh2, HUVEC + sh2, HUVEC + NEG and HUVEC + CEM. Both blots are arranged in the same order.

8.4 Discussion

This chapter began with the transfection of miR-US4-1. There are three studies based on miR-US4-1 in the literature. The first was published in 2012 and is the paper that the transfection earlier in this chapter was based on (Kim *et al.,* 2012). One of the other two papers focuses on how US4-1 promotes cell apoptosis and the other studies the presence of it to predict Hepatitis B treatment outcome (Pan *et al.,* 2016; Shao *et al.,* 2016). Whilst the second study looking at the promotion of apoptosis was able to identify the effected enzyme target in their study, the Hepatitis B study reported that the mechanistic basis of their findings was still unclear. miR-US4-1 research is still in its infancy. So far two targets have been identified in human cells; ERAP1 and Glutaminyl-tRNA Synthetase (QARS). Considering that the aim was to downregulate ERAP1 in this study, perhaps a cell viability assay should also have been employed to monitor the expression of QARS. If it is true that miR-US4-1 can downregulate both these proteins, users should be warier of any secondary effects.

The cell layering studies that were engaged in this chapter, took advantage of the characteristics of adherent and non-adherent cells. This set-up would provide an environment similar to two tissues communicating *in vivo*. However, it is likely that cell-cell communication between the two populations was causing an observable increase in ERAP1. The increase in ERAP1, as seen in figure 8.3-2A, caused an increase in dual cell control wells that was not seen in single cell population control wells. This suggested that the cells were activating each other. The obvious test to ensure this was the case, was to manually active the cells with IFNγ. There is evidence in the literature that IFNγ induces ERAP1 expression (Fenimore & Young, 2016; Saric *et al.,* 2002). IFNγ activated cells showed a higher profile compared to dual incubated cells. However, the concentration administered may have been higher or lower than the IFNγ produced during cell contact. To check if the adherent cells were being activated, an assay for activation factors such as NFκB could have been performed. A follow-on experiment for this section would have been to use different concentrations of IFNγ. This would have allowed the true ERAP1 downregulation in figure 8.3-3C to be calculated.

A device to remove the activation presumed to be caused by cell-cell contact is the trans-well. It was observed that, once again, there were samples showing an increase in ERAP1 expression that would not be expected. This ruled out the possibility that cell-cell contact alone was the problem of the previous experiment. As mentioned in the previous paragraph, there is evidence in the literature that IFNγ induces ERAP1 expression. However, IFNγ is induced by cell surface receptors (Fenimore & Young, 2016). Therefore, it is unlikely that IFNγ induction in the cells is the sole cause of ERAP1 expression increase. The levels of ERAP1 downregulation seen when CEM cells were incubated with CEM NEG cells in figure 8.3-5A demonstrates the subtle differences in cell communication. It appears that incubating the same cell line together causes downregulation of ERAP1 expression or at least

prevents an increase in expression. Whereas incubating the CEM cell lines with another cell line such as Jurkat or U937 appears to cause an upregulation in ERAP1. This will be due to the receptors on the outside of the cells.

The SCRAM transfected CEM cells (CEM SCRAM) and dysfunctional miR-US4-1 transfected cells (CEM NEG) were used as controls during this study. As the data had suggested that IFNγ activation was not the cause of ERAP1 upregulation, the next step was to use cells that produced EVs containing non-transcribing cargo. Incubation with either CEM SCRAM or CEM NEG saw ERAP1 expression levels upregulate to levels of controls that had been incubated with another cell type. This suggested that sample ERAP1 levels should be compared to SCRAM or NEG controls as opposed to the cell line control alone. Upon this comparison it is possible to see up to 113 % ERAP1 downregulation (figure 8.3-5A, U937 cell line) (percentages compared to the dual cell control).

The introduction of HUVEC hTERT cell line resulted in a step back to co-culturing and cell layering experiments. It has been ascertained through this study that a compound smaller than 200 nm was travelling through the trans-wells to activate the cells. Therefore, there was no advantage in the continued use of trans-wells. Employing HUVECS as the receiving cells however did create an advantage. This is because their ERAP1 has a heavier molecular weight than the ERAP1 of other cell lines used in this chapter. This allowed us to differentiate between samples that contained ERAP1 from a cell line other than HUVEC. For example, HUVECs were incubated with CEM shRNA2 cells. If a decrease was seen in the ERAP1 expression of the HUVEC cells, it could be suggested that it was caused by delivery of an ERAP1 down regulator from the CEM shRNA2 cells. Provided of course that all the controls did not also show the decrease. In order to continue down this path PCR should be used to analyse the content of the vesicles emitted by the CEM shRNA2 cells.

Endogenous loading of a stably expressed shRNA directed to a target miRNA of interest remains an attractive proposition. Whilst downregulation of ERAP1 expression has been seen in this study numerous times it remains to be determined if the EVs contain any shRNA in an active form capable of acting on ERAP1 mRNA. As there is a lot of cell communication occurring during these experiments it is important that the contents of the EVs be explored to ensure that cytokines do not play a part in the ERAP1 downregulation observed. Specific targeting of EVs would be the next area to target in this research.

Chapter 9: Sonication

Sonication as a method of external loading of EVs was first reported by Haney *et al*., Sonication was used as one of 4 methods to load EVs using catalase as a cargo substrate (Haney *et al.*, 2015). It is essentially the process of forming and collapsing microbubbles to cause a change in pressure known as cavitation. Cavitation pressures of hundreds of atmospheres and temperatures of thousands of Kelvins can be focussed during the collapse of these microbubbles to tear molecules apart (Gong, 1998).

9.1 Results

The first cargo chosen for the sonication study was FITC Ab. This cargo was sonicated at 20% amplitude 6 times over a 36 second period according to the methods of Haney *et al.* The samples were then placed on ice for 2 minutes before repetition. Latex beads were then added to adsorb the EVs present in the sample. Samples were analysed for fluorescent events on a flow cytometer. As shown in figure 9-1, >80 % of fluorescent events observed are outside the gate for both the FITC Ab and EV samples. This suggests that FITC Ab is binding to the beads in the absence of sonication potentially masking any cargo loading. Furthermore there is a high percentage of fluorescence seen outside the gate for both the FITC Ab controls. This suggests that FITC Ab that has not been encapsulated or associated with EVs may further contribute to the fluorescence seen.

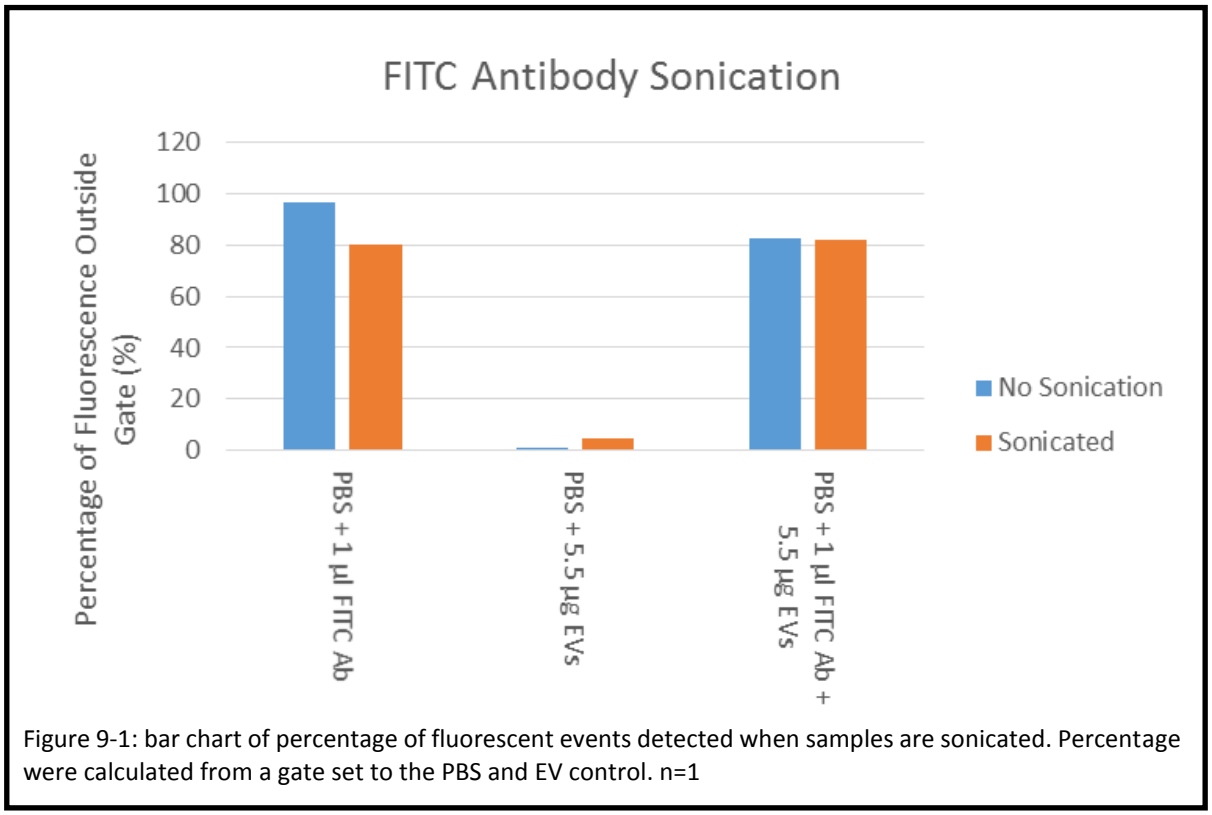

Figure 9-1: bar chart of percentage of fluorescent events detected when samples are sonicated. Percentage were calculated from a gate set to the PBS and EV control. n=1

Continuing with FITC Ab, a trypsin wash step was incorporated to digest any FITC Ab that had not been encapsulated by the EVs. It was observed that the FITC Ab and EV sample increased in fluorescence when sonicated (figure 9-2) compared to the EV control. However the FITC Ab control showed a similar level of fluorescence which maintained a higher percentage of fluorescence outside the gate throughout all conditions compared to the EV and FITC Ab sample. Whilst the trypsin wash does reduce the percentage of fluorescence seen outside the gate, the addition of sonication appears to further reduce it. It was also queried whether trypsin may disrupt the EV structure on latex beads, thus alternative washing procedures were sought. Beum and colleagues used an acid wash to remove unbound Ab from the outside of B Cells (Beum *et al.,* 2011). Therefore, an acid wash step was tested to replace the previous trypsin wash step. Samples were prepared and analysed on flow cytometer as previously. In figure 9-3 the samples and controls that contained FITC Ab all showed an increase in fluorescence outside the gate that remained after either a 100 mM or 200 mM Glycine acid wash. This suggests that an acid wash shows no advantage for this cargo over a trypsin wash.

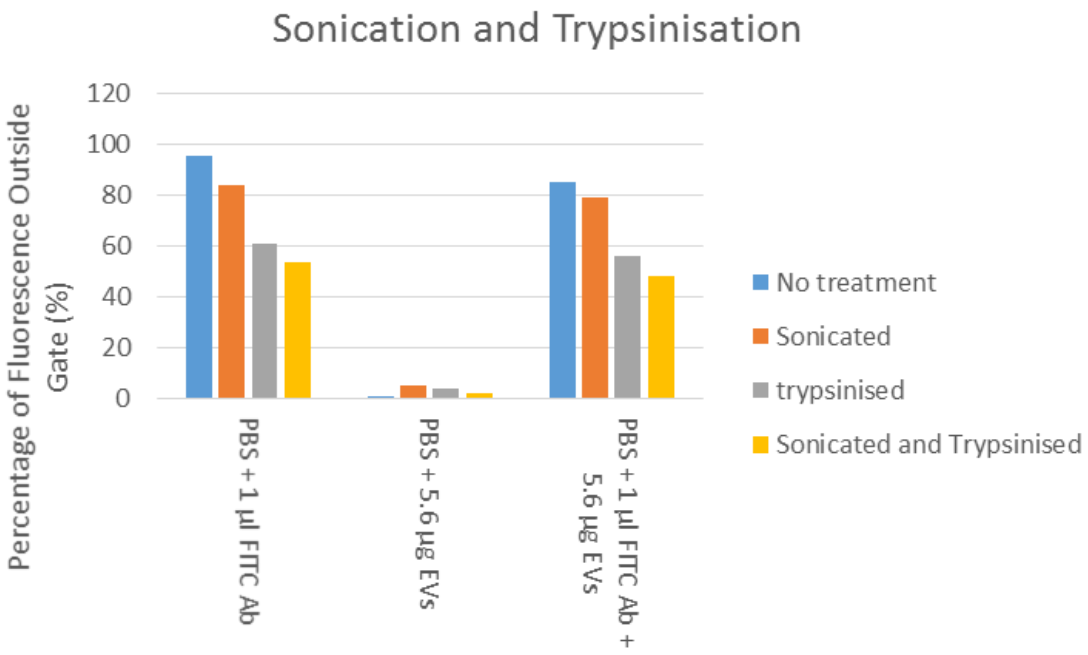

Figure 9-2: bar chart showing the differences in fluorescent events detected on flow cytometer when samples are sonicated and trypsinised. Percentages were calculated from a gate set to the PBS and EV untreated control. n=2.

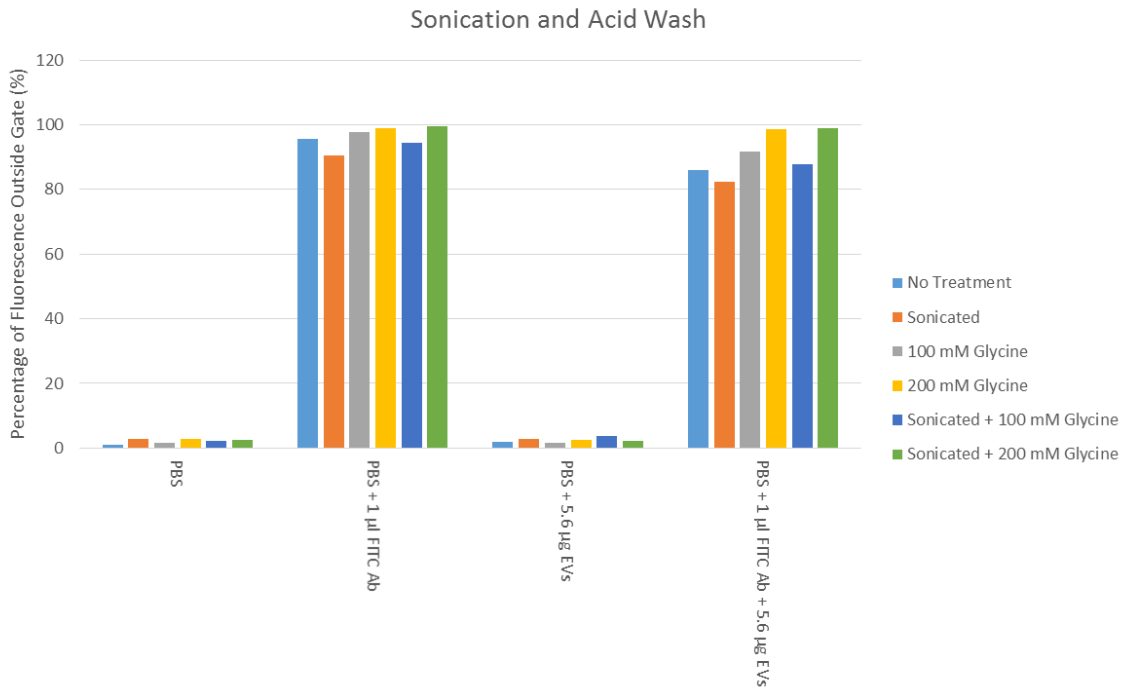

Figure 9-3: bar chart displaying the differences in fluorescent events detected by a flow cytometer when samples are sonicated and acid washed. The samples were acid washed in either 100 mM glycine or 200 mM glycine. Percentages were calculated from a gate set to the PBS control. n=2.

As FITC Ab may be an unfavourable cargo the next cargo used was Allstars siRNA as it is closer to ERAP1 siRNA. 0.5 ml of PBS with components was sonicated as previously. EVs were adsorbed again so that they could be incubated with RNase A. This would remove non-encapsulated fluorescent signal. In figure 9-4, unexpectedly, the highest increase in fluorescence is seen for the sample incubated with RNase A and the EV control incubated with RNase A. However it must be taken into account that all increases in fluorescence observed were below 8 %. These changes are so small that it is hard to interpret if they show importance. This data suggests the use of RNase A is inconclusive.

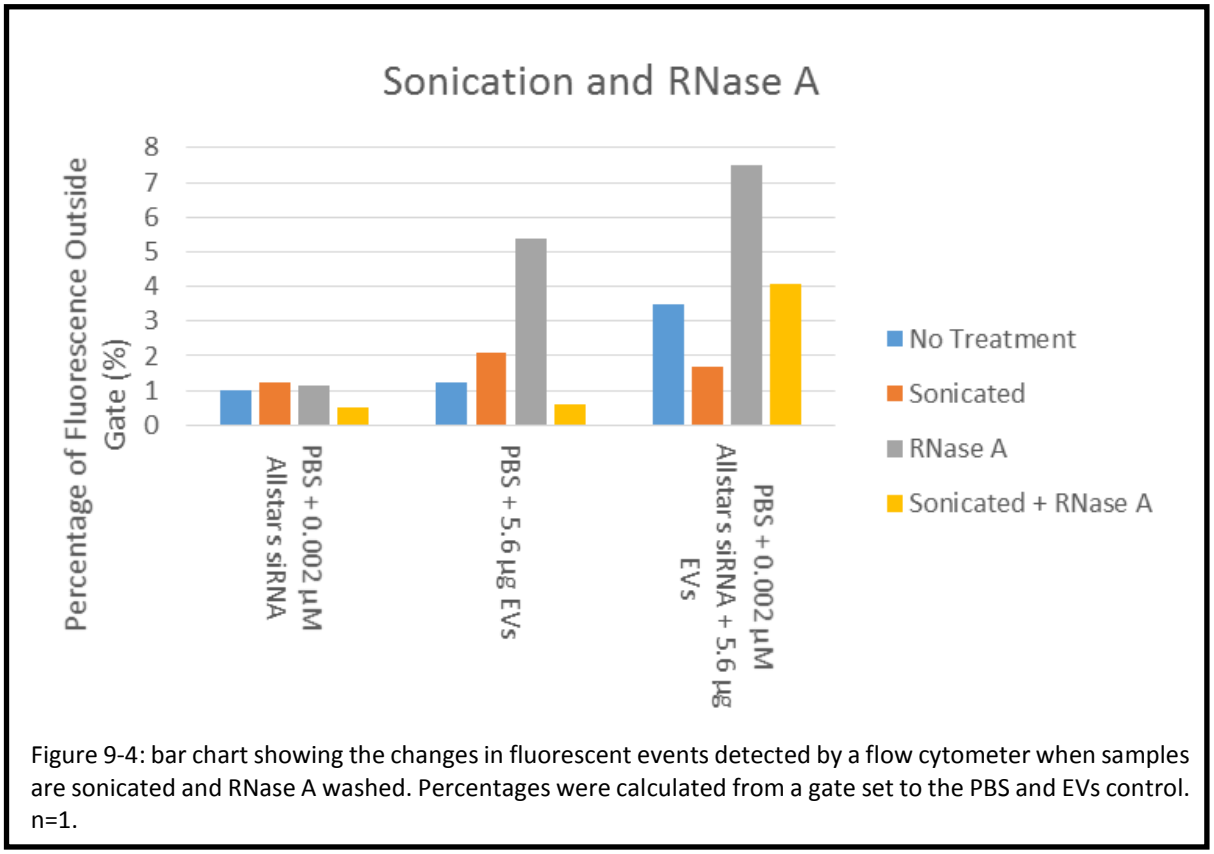

Figure 9-4: bar chart showing the changes in fluorescent events detected by a flow cytometer when samples are sonicated and RNase A washed. Percentages were calculated from a gate set to the PBS and EVs control. n=1.

As efforts to remove fluorescent background had been so far unsuccessful, the problem was approached from an alternative angle. The possibility to enrich EVs therefore leaving excess fluorescence behind was analysed. Magnetic beads coupled to Ab have been used to extract MHC class II positive EVs (Clayton *et al.,* 2001). Therefore magnetic beads were used to isolate EVs for analysis by flow cytometry. Anti-CD63 magnetic beads were tested as CD63 is a 'typical' exosome marker. Sample was sonicated and bound to anti-CD63 beads to enrich them before measuring their fluorescence on the flow cytometer. As shown in figure 9-5, all samples showed an increase in fluorescence outside the gate of <8 %. Whilst this suggests that there is little unbound Allstars siRNA left in the samples this also suggests that there is little encapsulated siRNA.

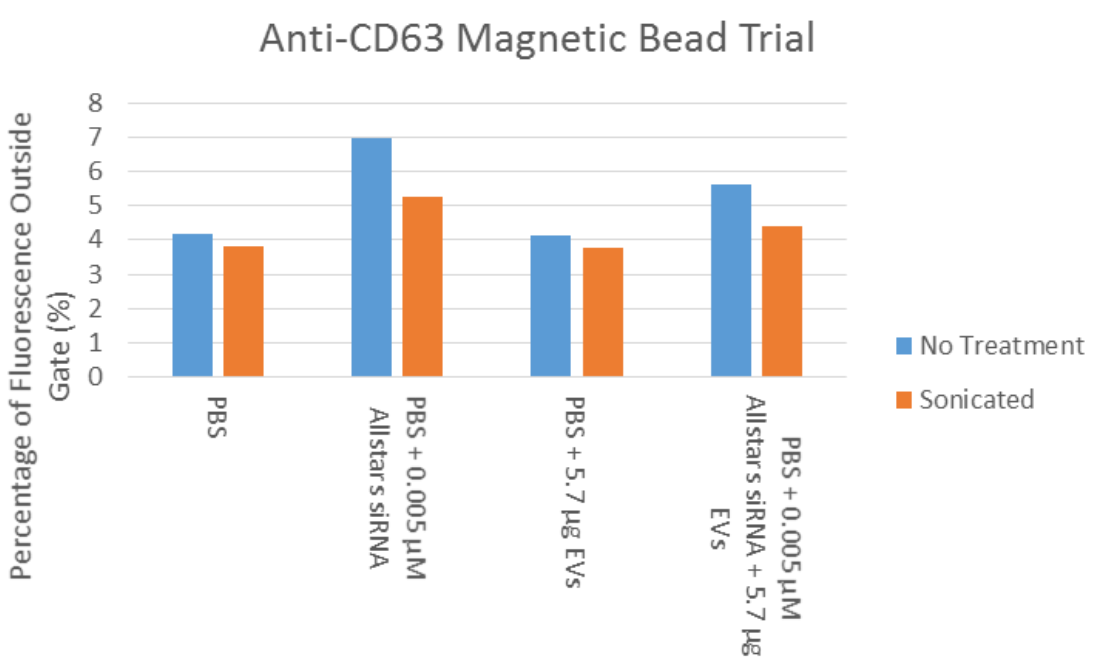

Figure 9-5: bar charts showing the changes in fluorescent events detected when anti-CD63 magnetic beads are used instead of latex beads. Percentage were calculated from a gate set to the PBS control. n=2

The efficiency of the sonication settings were also optimised. The 20 % amplitude was increased to 40 %, which was the maximum recommended setting for the size of probe used. The concentration of siRNA was also doubled. EVs were sonicated with Allstars siRNA and then associated with anti-CD63 labelled, magnetic beads. The beads were then analysed by flow cytometry. However, this time, the percentage of fluorescence outside the gate for all samples was <3 % (figure 9-6). Whilst some fluorescence was seen for the sonicated EV and Allstars siRNA sample, a slightly higher percentage was seen for the sonicated EV control. Due to the low percentages observed deductions from this data would be unreliable. To determine the surface expression levels of CD63 on the U937 EVs, the EV Characterisation chapter data was reflected upon. From the data it was confirmed that U937 EVs clearly expressed CD63. From these results it was decided that future CD63 magnetic bead experiments should be delayed.

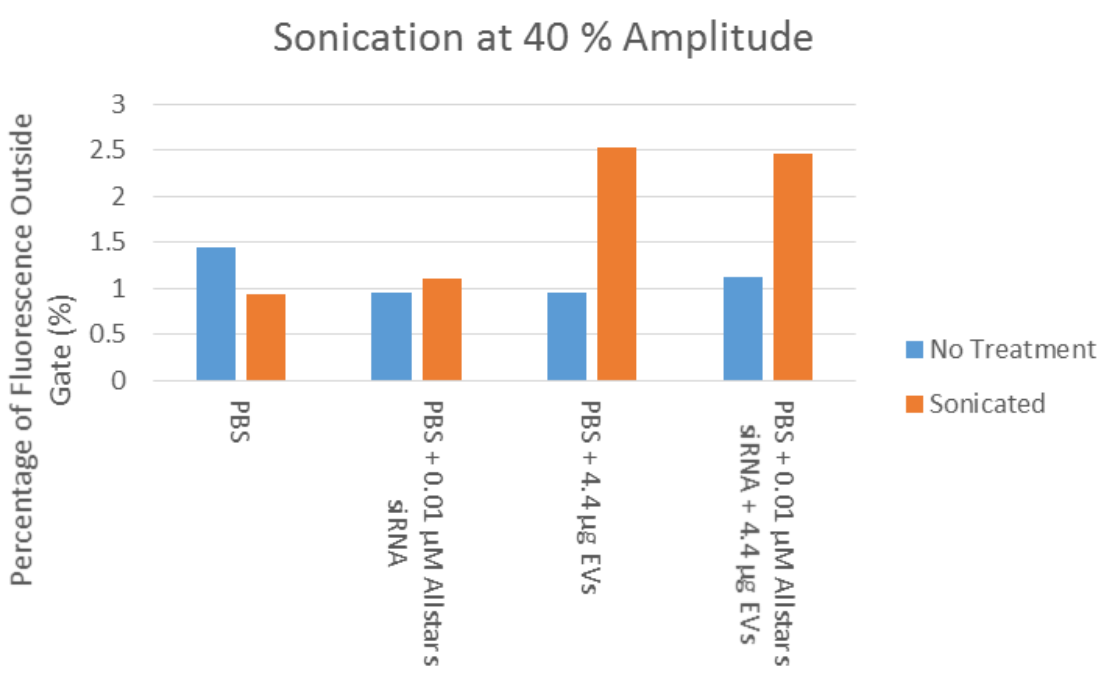

Figure 9-6: bar chart displaying the changes in fluorescent events detected when samples are sonicated at an increased amplitude and then the EVs extracted by anti-CD63 magnetic beads. Percentages were calculated from a gate set to the PBS control. n=1

In order to understand the exact technique and process used to sonicate in Haney *et al.* a trip was planned to the Batrakova laboratory at the University of North Carolina (UNC), US. This involved a visit to the laboratory to sonicate samples of Allstars siRNA with RAW264.7 EVs, following their exact method. The samples were diluted into Triton-X100 and enriched in a NAP-10 sephadex G-25 size exclusion column. The encapsulation results were quantified by measuring the fluorescence of the sample on a fluorimeter. Triton X-100 is a detergent, used in this case to gently lyse the EVs. This, in theory, allows the fluorescent contents to be measured more accurately. A BCA assay was also performed to attain the concentration of protein in the EV sample. Applying their methods, it was observed that as the concentration of Allstars siRNA sonicated increased, the concentration of fluorescence measured after enrichment for EVs also increased (figure 9-7A). Using this method, fractionation assays with PD-10 columns (existing laboratory stock) were performed to ensure EVs were enriched (figure 9-7B). Samples of U937 EVs were passed through a column and the eluate collected in 3 fractions of approximately 0.5 ml. The fractions were then visualised on the NTA and particle size and concentration measured. An average mean diameter of 206 nm was observed. Eluate 1 contained 30 %, eluate 2 contained 64 % and eluate 3 contained 3 % of the total concentration of EVs pipetted into the column giving a total of 97 % recovery of the original input concentration. This data indicates that the whole eluate should be used and that the columns enrich the majority of my sample.

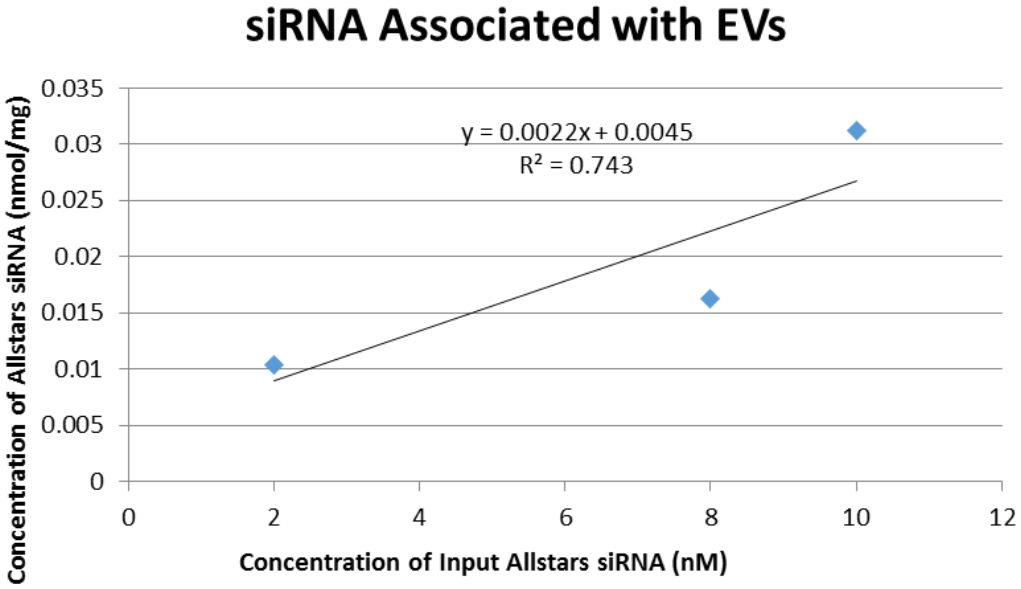

Figure 9-7A: dot plot showing the concentration of Allstars siRNA associated with EVs after sonication as the concentration of input Allstars siRNA sonicated increases. n=1

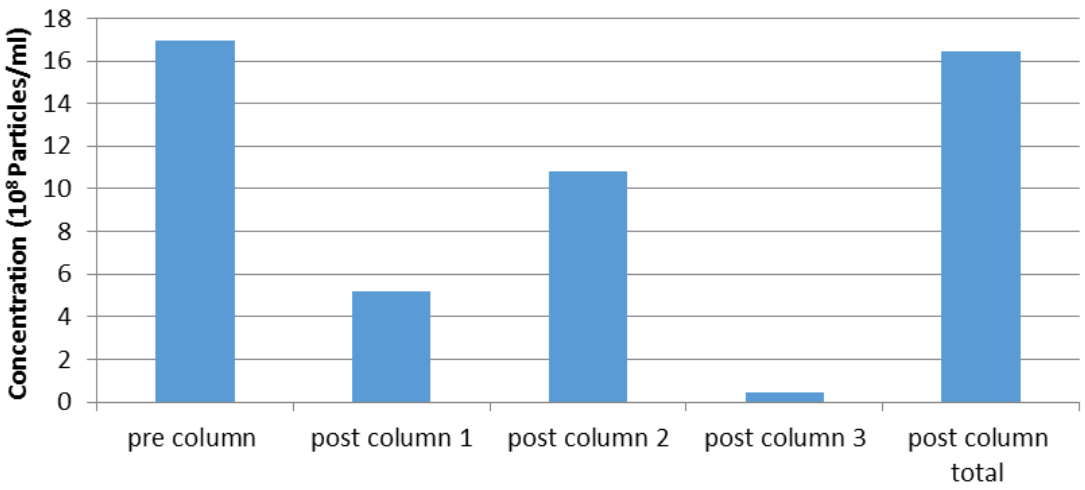

Figure 9-7B: bar chart showing the number of particles present for fractions of EVs before and after enrichment through a PD-10 sephadex size exclusion column. Note the post column total is very close to the pre column total. n=1

Having established the effectiveness of the enrichment columns, the next step was to sonicate samples of EVs and Allstars siRNA, enrich them and measure the fluorescence based on UNC methods, but with Powis laboratory equipment. To begin, five concentrations of Allstars siRNA; 0.01, 0.02, 0.03, 0.04 and 0.05 µM with two conditions; with or without Triton X-100 were analysed. The samples used with Triton X-100 saw a return of approximately 45 % of the original input fluorescence whereas the samples processed without Triton X-100 had a fluorescent return of approximately 58-90 % (figure 9-8A). This suggests that the Triton X-100 partially quenches the fluorescence of the Allstars siRNA rather than its presumed function of releasing the Allstars siRNA from the EVs. Furthermore, when the fluorescence per 10^8 particles was calculated for both conditions, the majority of the samples without Triton X-100 showed a higher concentration per 10^8 particles compared to the Triton X-100 treated samples (figure 9-8B). It appears that more fluorescence can be observed without Triton X-100 and this study will move forward without using this in the experiments. In addition to having a higher fluorescence per 10^8 particles than the Triton X-100 treated samples, the samples without Triton X-100 also suggested that as concentration of sonicated Allstars siRNA increases the concentration of Allstars siRNA associated with the EVs also increases (figure 9-8B).

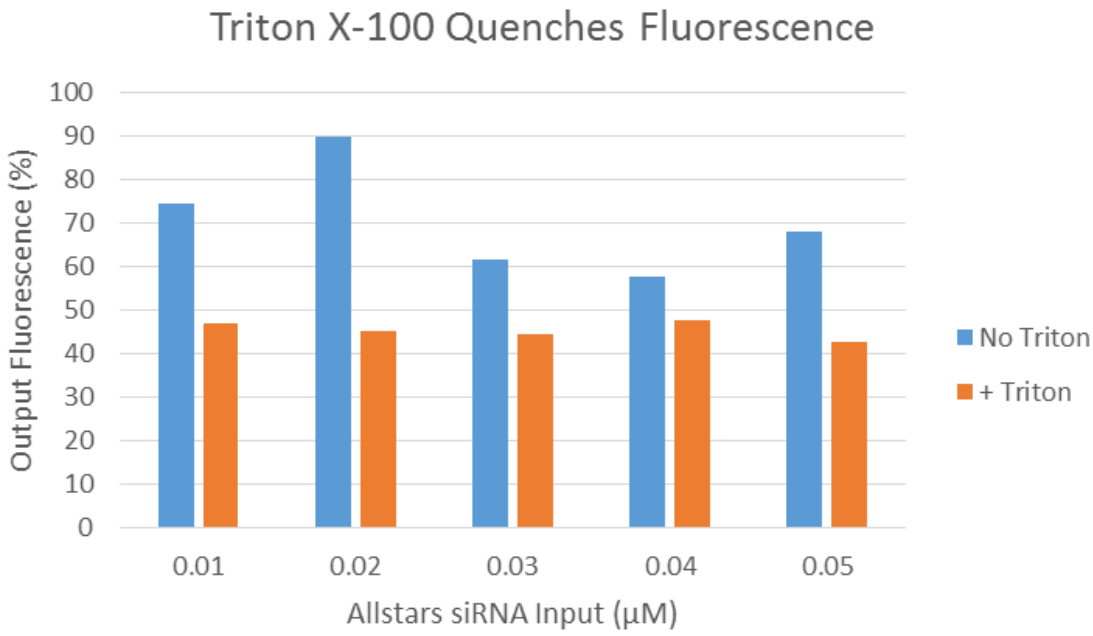

Figure 9-8A: bar chart showing the decrease in output fluorescence as a percentage of the input fluorescence when Triton X-100 is used. n=1 per siRNA concentration.

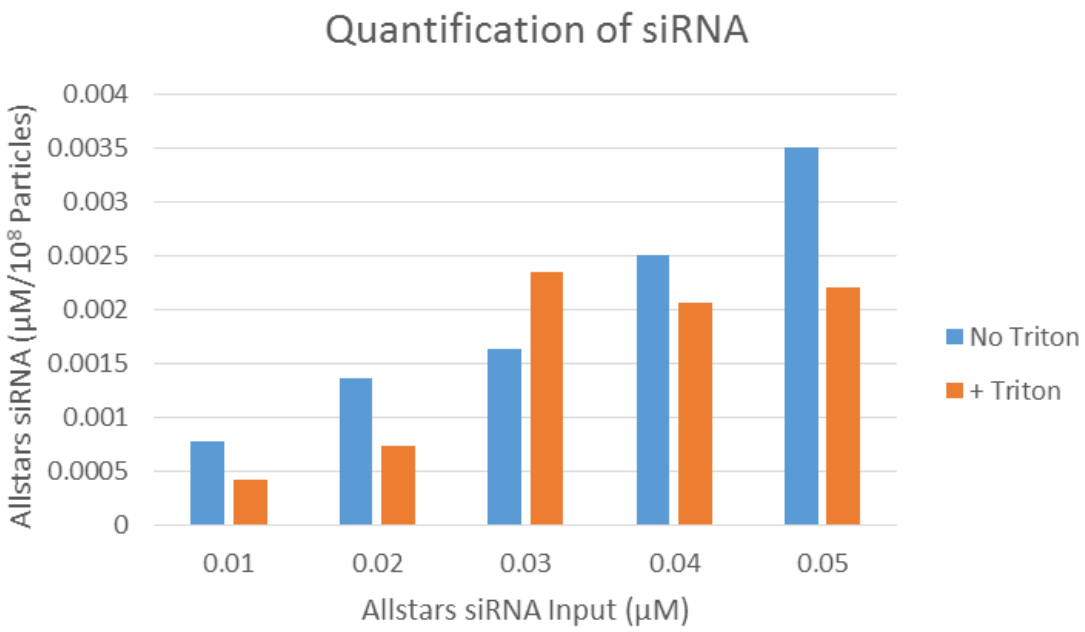

Figure 9-8B: bar chart showing the fluorescence associated per 10^8 particles when Triton X-100 is used or not used in the experiment. n=1 per siRNA concentration.

Having established a method to ascertain the fluorescence associated with EVs, it was time to add in the RNase A wash. Adding this before enrichment would help work out the concentration of Allstars siRNA encapsulated by EVs. As the highest concentration of Allstars siRNA that could be associated with EVs had not been reached yet, three higher concentrations (0.1, 0.2 and 0.3 µM) were used to test the RNase A method. As expected, the samples incubated with RNase A showed a 75 % decrease in fluorescence per 10^8 particles (figure 9-9A). However, the RNase A did not remove the fluorescence totally, suggesting the remaining 25 % fluorescent particles are likely to have been encapsulated by EVs during sonication. At these larger concentrations of Allstars siRNA, the samples without RNase A showed a gradual decrease in the percentage of input siRNA encapsulated as the concentration of input siRNA increases. The samples with the RNase A step however, show a much shallower decrease suggesting that the encapsulation efficiency is approximately 30 % of the original Allstars siRNA input (figure 9-9B).

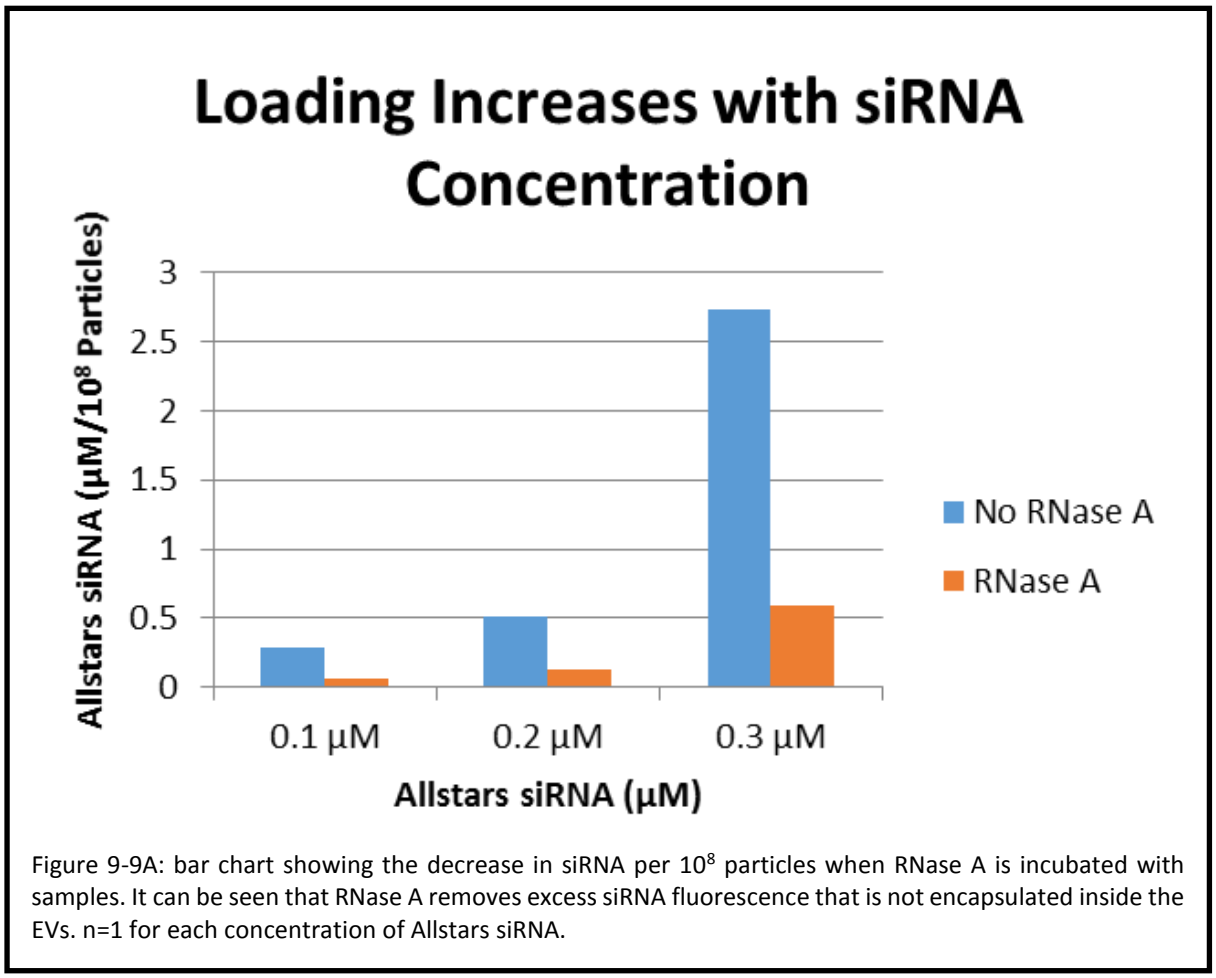

Figure 9-9A: bar chart showing the decrease in siRNA per 10^8 particles when RNase A is incubated with samples. It can be seen that RNase A removes excess siRNA fluorescence that is not encapsulated inside the EVs. n=1 for each concentration of Allstars siRNA.

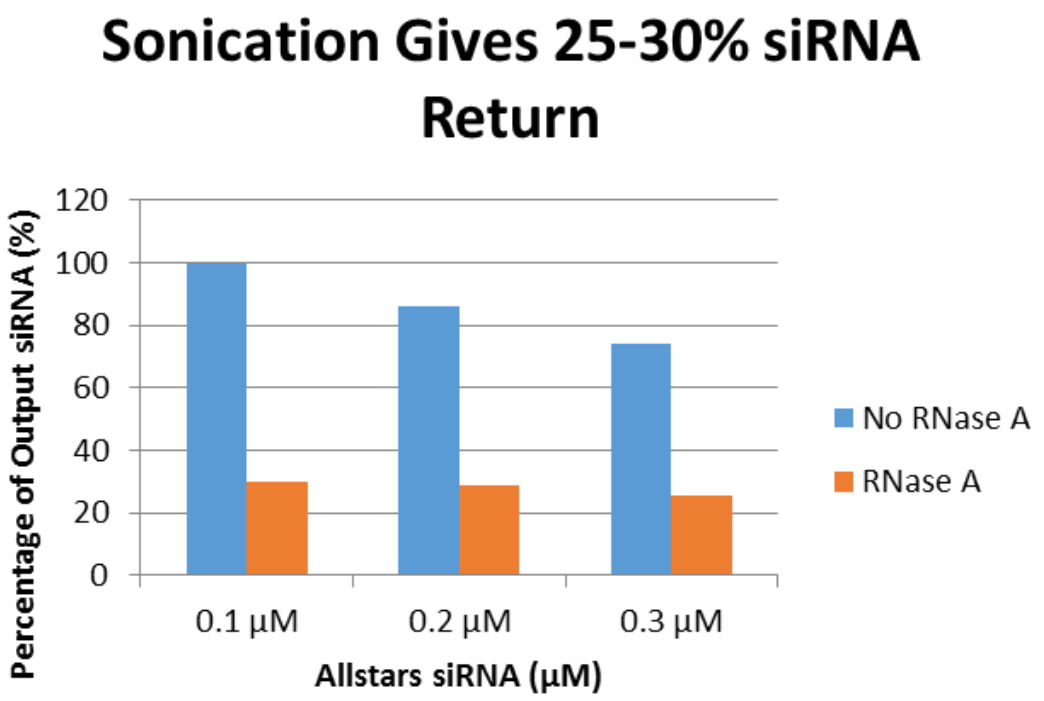

Figure 9-9B: bar chart showing the decrease in output fluorescence seen when an RNase A step is added to remove siRNA that is not encapsulated within EVs. It can be seen that for 75 µg of EVs the maximum encapsulation appears to be 25-30 % for input concentration of Allstars siRNA greater than 0.1 µM. n=1 for each Allstars siRNA concentration.

Having established that current encapsulation is at 30 % of the Allstars siRNA input at concentrations >0.1 µM Allstars siRNA, the sonication technique was applied to cells in preparation for using ERAP1 siRNA. First the use of RPMI was trialled instead of PBS as it would allow the cells longer to incubate with the EVs before needing to change the media in order to prevent cell death. Furthermore, the experiment would need to be carried out in sterile conditions if the samples were to be added to cell culture. The data for Allstars siRNA and EVs sonicated in RPMI showed an improved loading capacity compared to the PBS sonicated sample (figure 9-10). Both samples included the RNase A step. This suggests that RPMI may increase the efficiency of encapsulation. The samples were also visualised on NTA to ensure that the columns still enriched the EVs in the samples. The columns were found to be still capable of the same levels of enrichment (data not shown).

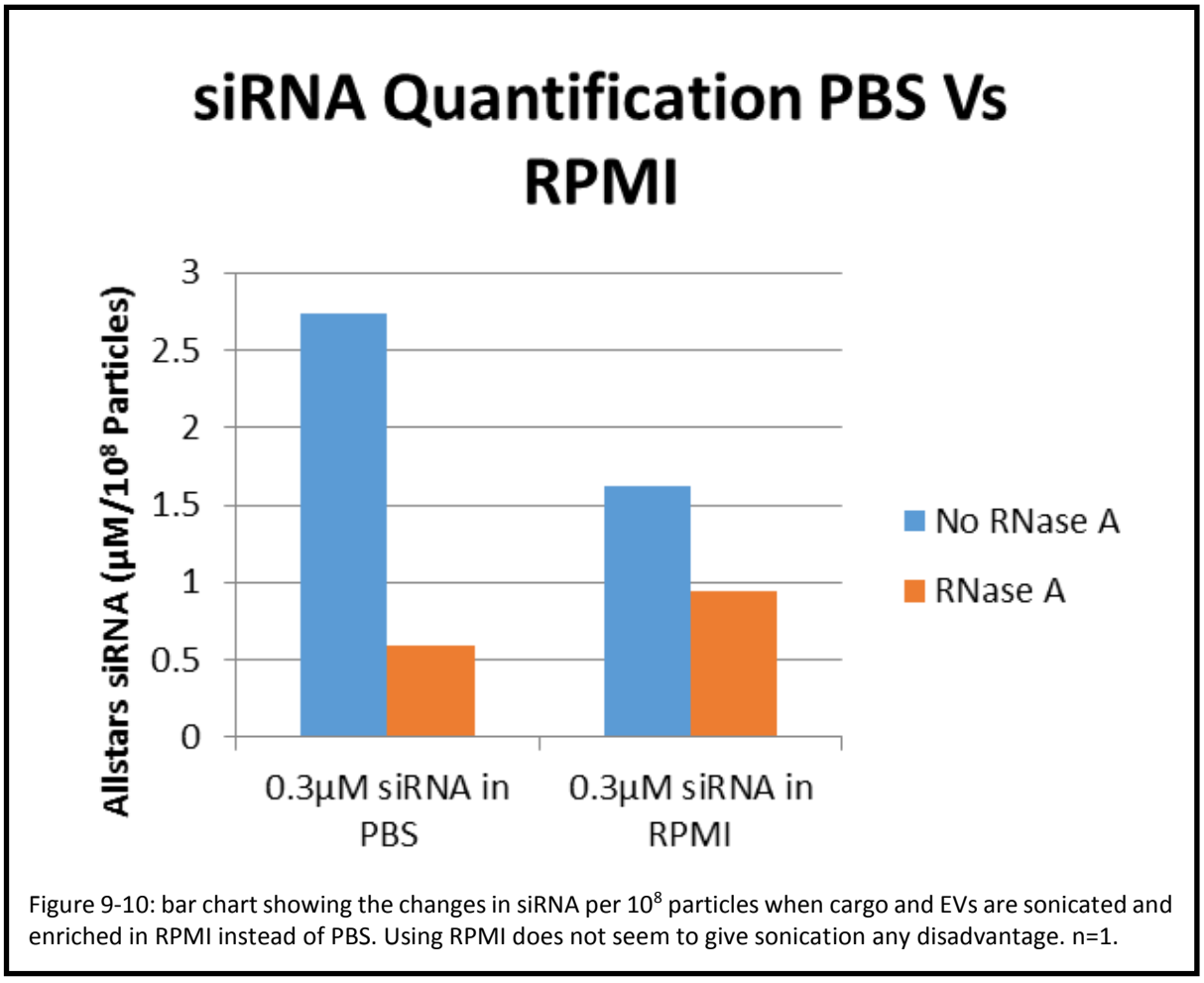

Figure 9-10: bar chart showing the changes in siRNA per 10^8 particles when cargo and EVs are sonicated and enriched in RPMI instead of PBS. Using RPMI does not seem to give sonication any disadvantage. n=1.

As RPMI could be used both for sonication and in the columns with minimal loss of particles, samples of 0.2 µM ERAP1 siRNA and 75 µg EVs were sonicated, enriched through the NAP-10 columns and incubated with confluent HeLa.B27 cells overnight. Cells were then analysed. Upon analysis the EV control with no treatment caused a large increase in ERAP1 expression (figure 9-11A and 9-11B). Furthermore, the ERAP1 siRNA control also shows an increase in ERAP1 expression above control cell levels. When sonicated ERAP1 siRNA and EVs were added to HeLa.B27 cells there was almost a 300% increase in ERAP1 expression. Whilst this was a 600 % reduction compared to the untreated EV and siRNA control, the other sonicated controls show a lower ERAP1 expression. This suggests that the HeLa.B27 cells may have responded to the EVs or siRNA by increasing cell ERAP1 expression. Of note the ERAP1 expression for the HeLa.B27 control on both blots was very low. As the ERAP1 expression of other samples is calculated with this sample based as 100 % this could cause the other samples to appear to express more ERAP1. However as the sonicated ERAP1 siRNA samples show a lower increase in ERAP1 expression it is likely that this alone is not the cause.

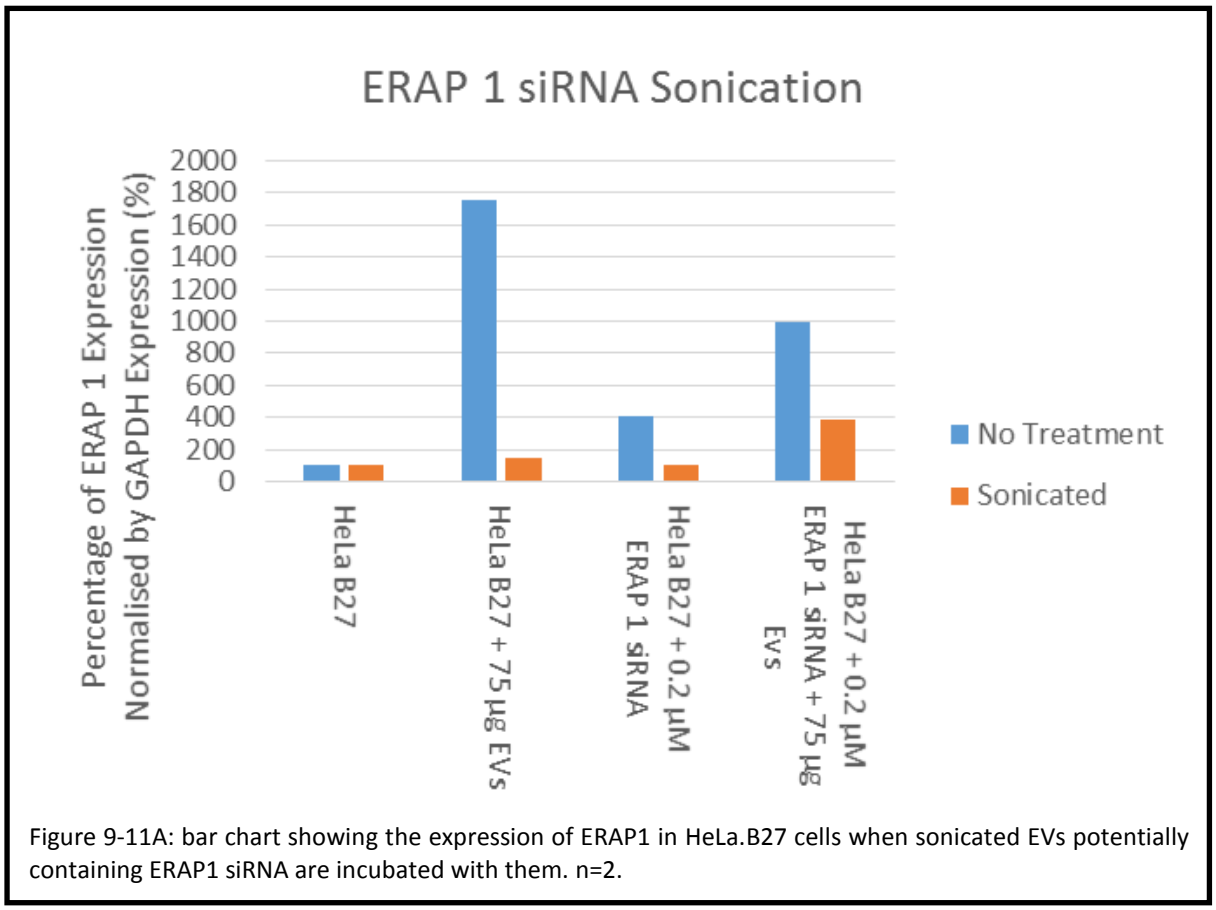

Figure 9-11A: bar chart showing the expression of ERAP1 in HeLa.B27 cells when sonicated EVs potentially containing ERAP1 siRNA are incubated with them. n=2.

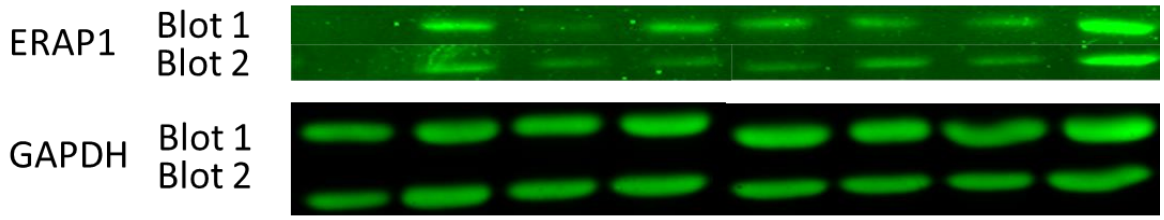

Figure 9-11B: western blot showing ERAP1 expression of HeLa.B27 cells when incubated with sonicated EVs and ERAP1 siRNA. Samples are arranged in the same order as figure 9-11A with the no treatment samples first followed by the sonicated samples.

9.2 Discussion

Sonication is a potentially powerful method. Thus it has been used in the literature for lysis and degradation (McLaughlin *et al.,* 2010; Reich *et al.,* 2007; Sartorello *et al.,* 2010; Sharma *et al.,* 2014; Steinbach *et al.,* 2016; Zhao *et al.,* 2014). However, in this study, disruption of membranes was sought rather than destruction. This meant using a reduced power method to retain the EVs' general structure. A method that seemed to produce results was reported by Haney and colleagues (Haney *et al.,* 2015). Replicating this method in the laboratory proved unsuccessful therefore a visit was arranged with the Batrakova laboratory. This enabled the determination of the exact method and equipment that the laboratory employed to attain its results. Furthermore, during the visit, results suggesting that Allstars siRNA had been encapsulated in EVs were achieved. Upon the use of these exact methods in the Powis laboratory similar results were observed.

One difference noticed when comparing samples exposed to this method, was with the samples diluted in Triton-X100. Triton-X100 was employed as a detergent to analyse the contents of the EVs after sonication. However, it was observed that Triton-X100 caused quenching of the fluorophore conjugated to the siRNA reporter. There does not appear to be any examples of this mentioned in the relevant literature. As such it was decided to avoid using Triton-X100. However, an interesting follow-up experiment that could be carried out is the incubation of siRNA tagged with a fluorophore in Triton-X100. Following this the structure of the siRNA could be analysed. This would determine whether the fluorophore had been changed or degraded by the Triton-X100.

Another query left at the end of this study is the fate of the ERAP1 siRNA. The results achieved at the end of this chapter showed no definitive sign of ERAP1 expression decrease. One explanation is the destruction of the siRNA during the sonication process. Whilst polymer degradation during sonication has been reported there have been no reports of degradation of siRNA (Freifelder & Davison, 1962). Cavitation produces free radicals that are used in chemical reactions therefore they could chemically alter the siRNA and invalidate its ability to downregulate ERAP1. Once again there is no literature on this topic. A third option is to presume that the ERAP1 siRNA was not able to be encapsulated due to repulsive interactions with EVs that prevent their entry into the vesicles. In order to assess these theories, the ERAP1 siRNA should be characterised and compared to the Allstars siRNA (cargo that was encapsulated). Analysis may reveal the presence of charges that repel the siRNA from EV entry or damage from sonication.

It is important to know where the cargo binds to in relation to the EV. This is so that later in the drug production process, any drug not encapsulated does not cause an immune response. Most treatments use drugs in multiple doses over a time period. Therefore, drug design involved with EVs should include steps to assure that the drug is not presented on the outside of the vesicle. On the

outside of the vesicle it can readily be detected by immune cells and cleared by the spleen. Two methods adopted to ensure cargo was not on the outside of EVs were a trypsin wash and an acid wash. Both were used to remove Ab. However, the trypsin wash may degrade the EVs. Alternatively, the acid wash was not strong enough to remove all particles associated with the outside of the EVs. RNase A was used to remove non-encapsulated siRNA from the EVs. Analysis of these EVs, versus EVs that had not been exposed to RNase A, revealed that the majority of the cargo was associated with the outside of the EVs. However, success with the use of Allstars siRNA as a cargo was observed.

Before the introduction of NAP-10 columns, magnetic anti-CD63 beads were studied. Despite the presence of CD63 on EV stocks, significant enrichment was not observed. It was unknown why the beads had not enriched the EV population. Another approach to this would have been to use a different Ab conjugated bead. CD9 is another 'typical' EV marker however it was not present on all EV stocks. Alternatively this could imply that a large percentage of the EV population is not characteristically exosomal. However, EV characterisation was determined in Chapter 3 showing EV isolations for all cell lines to contain vesicles characteristically in the size range and presenting the correct proteins to suggest they are exosomal in origin.

Sonication is therefore a promising method of encapsulating siRNA or drugs inside of EVs. It may be possible to develop this method further with time and larger quantities of reagents towards both experimental *in vivo* and clinical use.

Chapter 10: Celecoxib

Celecoxib (CXB) is a selective COX-2 inhibitor used in pain relief therapy for arthritic and similar conditions, including AS. It has higher levels of side effects and complications than other NSAIDs and is therefore not used as a first line treatment, but is introduced when other NSAIDs prove ineffective. In recent years it has been shown that CXB also impacts on other pathways in cells, and at higher concentrations induces ER stress and the removal of some proteins from the ER. As such, this side effect has the potential to remove misfolded HLA-B27 from the ER during CXB treatment. 2, 5 – dimethyl Celecoxib (DMC) is a derivative of CXB that does not inhibit COX-2 but retains its ER stress induction capacity. The impact of these two drugs on the misfolding of HLA-B27 molecules and their ability to load into EVs was therefore studied.

10.1 Results

The ER stress induction capacity of CXB relies on higher doses than that used for pain relief. The FDA suggested dose is 1 μM, whereas papers published on ER stress induction regularly use up to 100 μM (Pyrko *et al.,* 2008). Induction of apoptosis occurs at these higher doses. Research with CXB began with a viability titration to establish the toxicity of CXB in this system. HeLa.B27 cells were cultured to confluency and then CXB ranging from 1 μM to 50 μM added for a 24-hour incubation at 37 °C. A cell viability assay was performed by adding 1 in 20 of Alamar Blue to each well of the cell culture plate and then incubating the plate for 30 minutes. An aliquot of cell culture medium was then taken and diluted for analysis. The protocol for using Alamar Blue allowed for the use of either a fluorimeter or spectrophotometer to measure the change in colour or fluorescence therefore both were trialled in order to see which gave the clearest result. In the samples measured by the spectrophotometer (figure 10-1A) there is a steady decrease in viability as the concentration of CXB increases. For the samples measured by fluorimeter (figure 10-1B) the same trend was observed however the decrease in viability was emphasised. Also, using a light microscope, it was observed that the HeLa.B27 cell well that had been incubated with 50 μM CXB showed significant and obvious cell death. It was concluded from this that measuring the fluorescent intensity of the Alamar Blue gave the cleanest and most sensitive data with regards to interpretation of results.

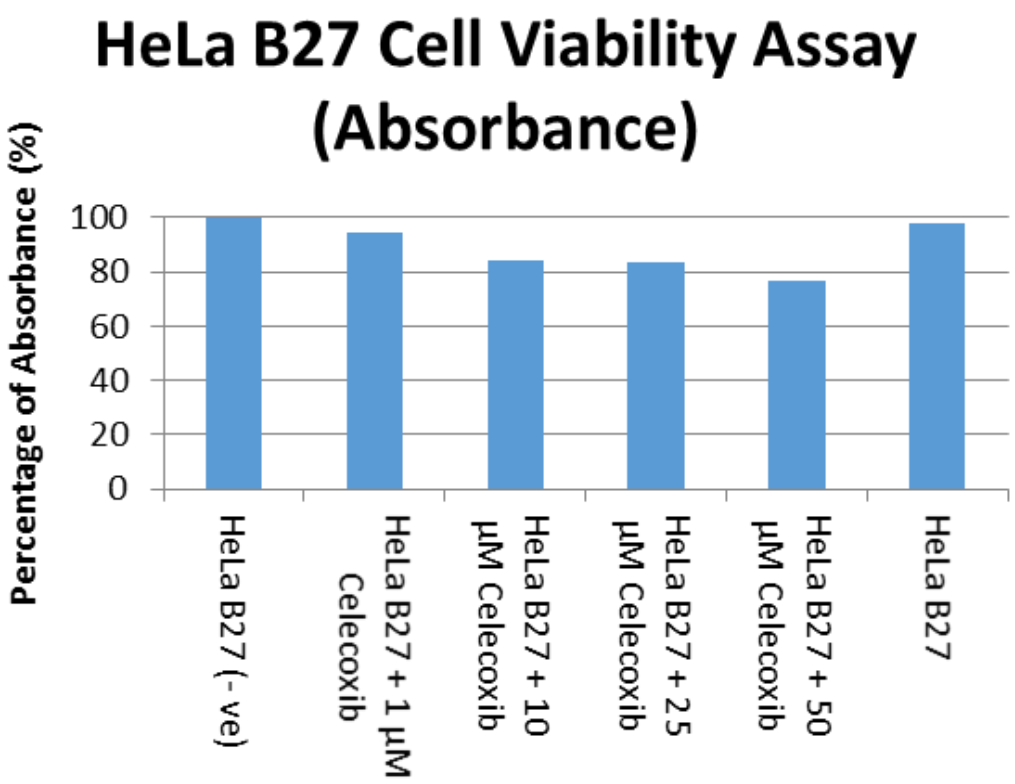

Figure 10-1A: bar chart showing the decrease in absorbance observed when an Alamar Blue test is applied to samples of cell incubated with increasing concentrations of Celecoxib. n=1

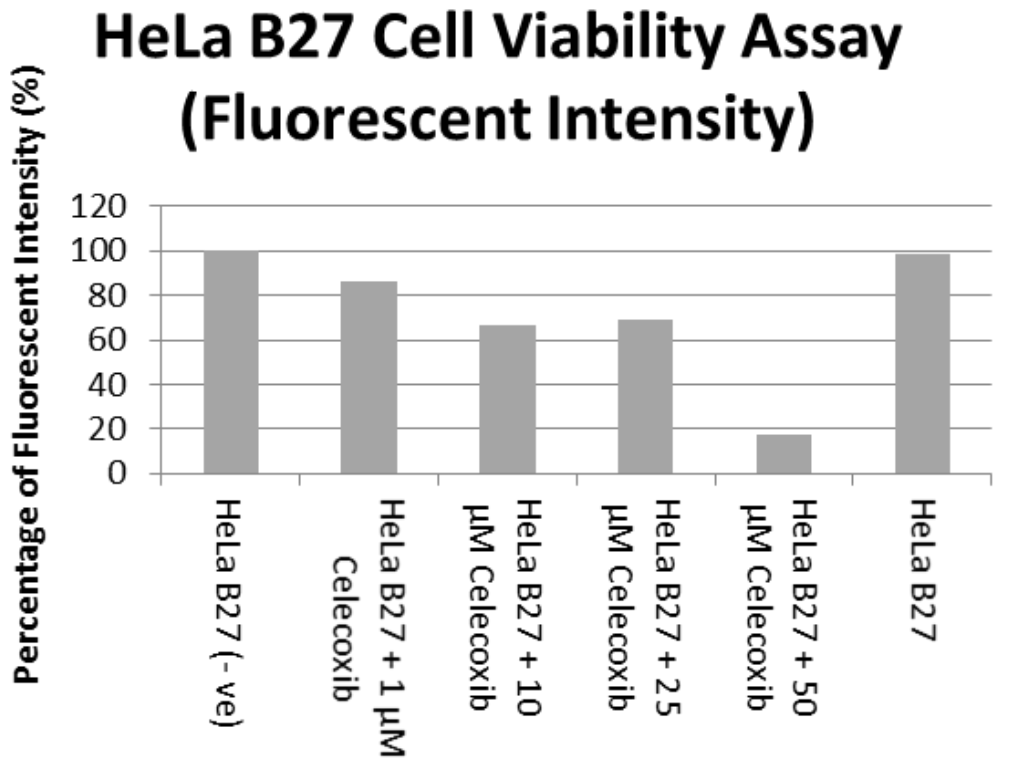

Figure 10-1B: bar chart showing the second method of measuring a change in Alamar Blue. As can be seen the samples show the same trend as the graph above except the trend is more emphasized. n=1

Since 50 µM CXB was over 80 % cytotoxic, the next experiment was set up with a drug titration of either CXB or DMC within the range of 0 to 25 µM. A plate of confluent HeLa.B27 cells were incubated with either 0, 1, 10 or 25 µM of either of the drugs overnight at 37 °C then a cell viability assay was performed. Duplicates were also analysed for proteins of interest. The Alamar Blue assay showed that the HeLa.B27 cells were more sensitive to DMC as at 25 µM a drop to 25 % viability was observed (figure 10-2A, orange bars). This suggests that the highest concentration of DMC that can be used is around 10 µM. For HeLa.B27 cells incubated with either drug it was observed that as the concentration of the drug increases there was a decrease in heavy chain (HC) dimer expression (figure 10-2B and 10-2C). However, dimer expression is normalised by monomer expression. Therefore, the dimer expression seen for the 25 µM DMC sample is higher than it should be as this well had a viability of 25 %. Otherwise, this suggests that both CXB and DMC encourage clearing of misfolded protein from the ER. Calnexin, on the other hand, sees an increase for CXB incubated cells as drug concentration increases (figure 10-2D, blue bars and figure 10-2E) suggesting that more chaperones are produced in response to the UPR. This could aid repair and restore order to the ER. Calnexin expression for DMC incubated cells seems to remain constant (figure 10-2D, orange bars), dropping for the 25 µM concentration. This suggests that the DMCs effect on the cells ER activity may be dependent on a different pathway than CXB as it would seem that CXB acts in a pro-survival fashion at the concentrations used in this study.

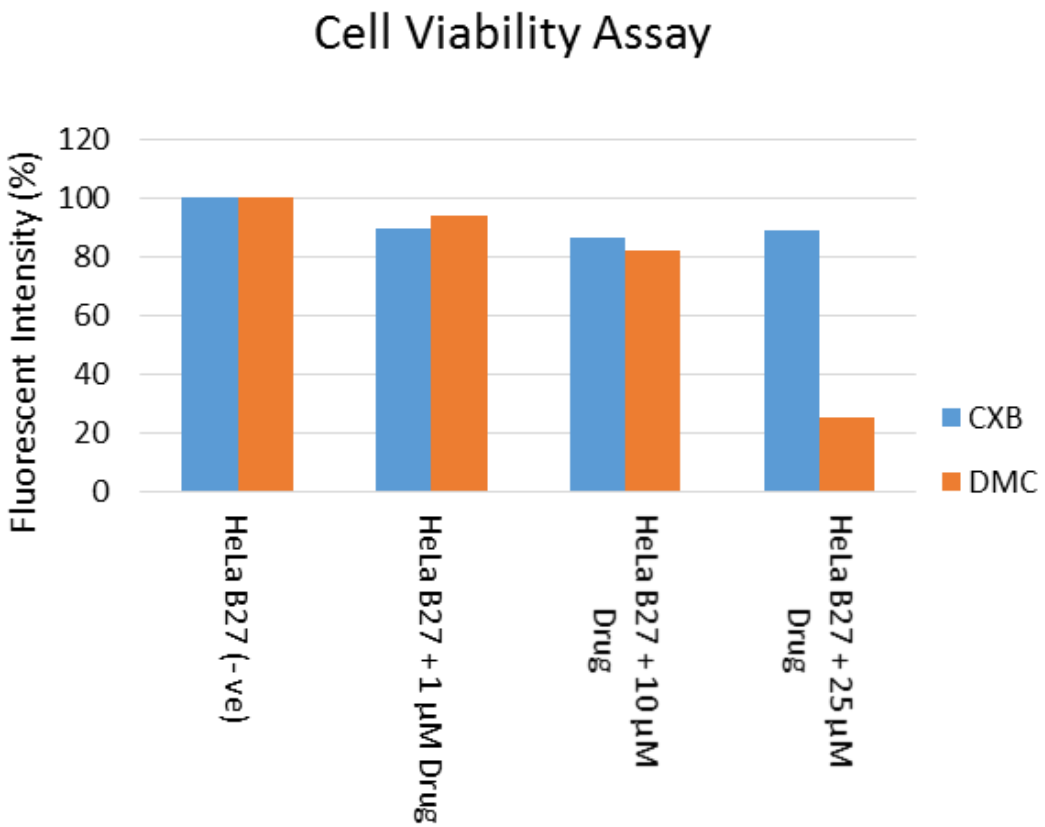

Figure 10-2A: bar chart comparing the changes in cell viability with increases in drug concentration. It can be seen that the viability of the CXB incubated samples remains high whilst the viability of the DMC incubated samples drops. In particular, 25 µM DMC is cytotoxic. n=1

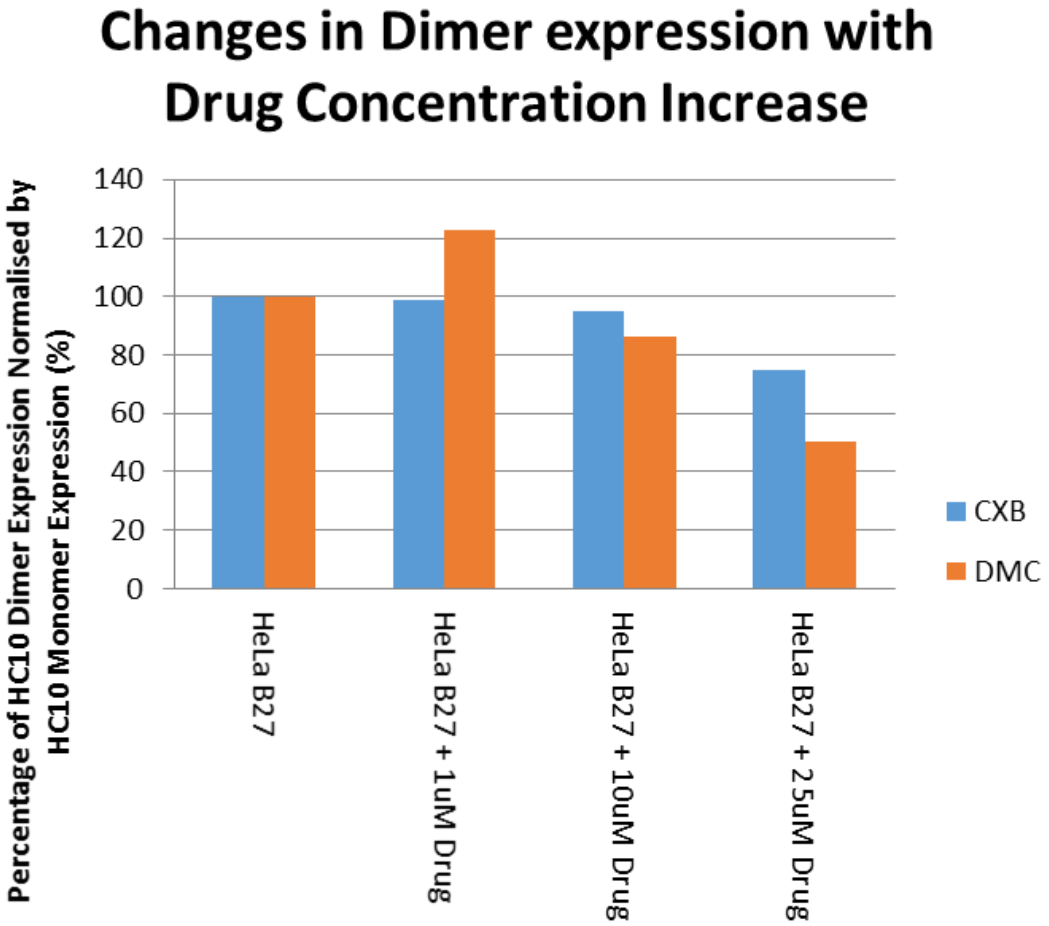

Figure 10-2B: bar chart showing the changes in HC10 dimer expression as Drug concentration increases. n=1

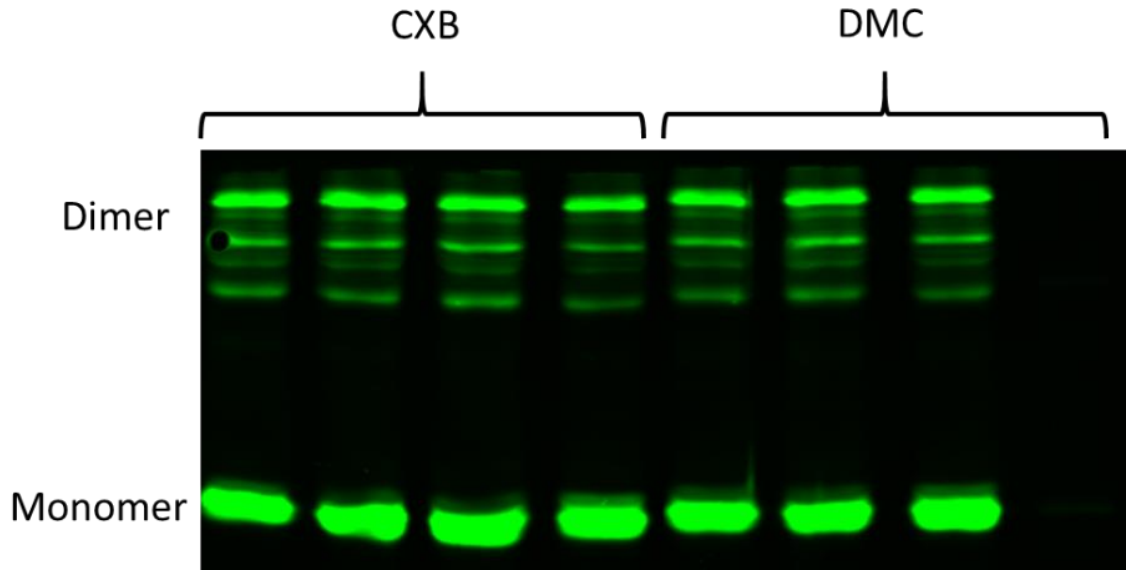

Figure 10-2C: western blot showing expression of (upper band) HLA-B27 dimers and (lower band) HLA-B27 monomers of HeLa.B27 cells when incubated with either CXB or DMC. Samples arranged in the same order as figure 10-2B, except CXB samples are displayed first and DMC samples are displayed second. n=1

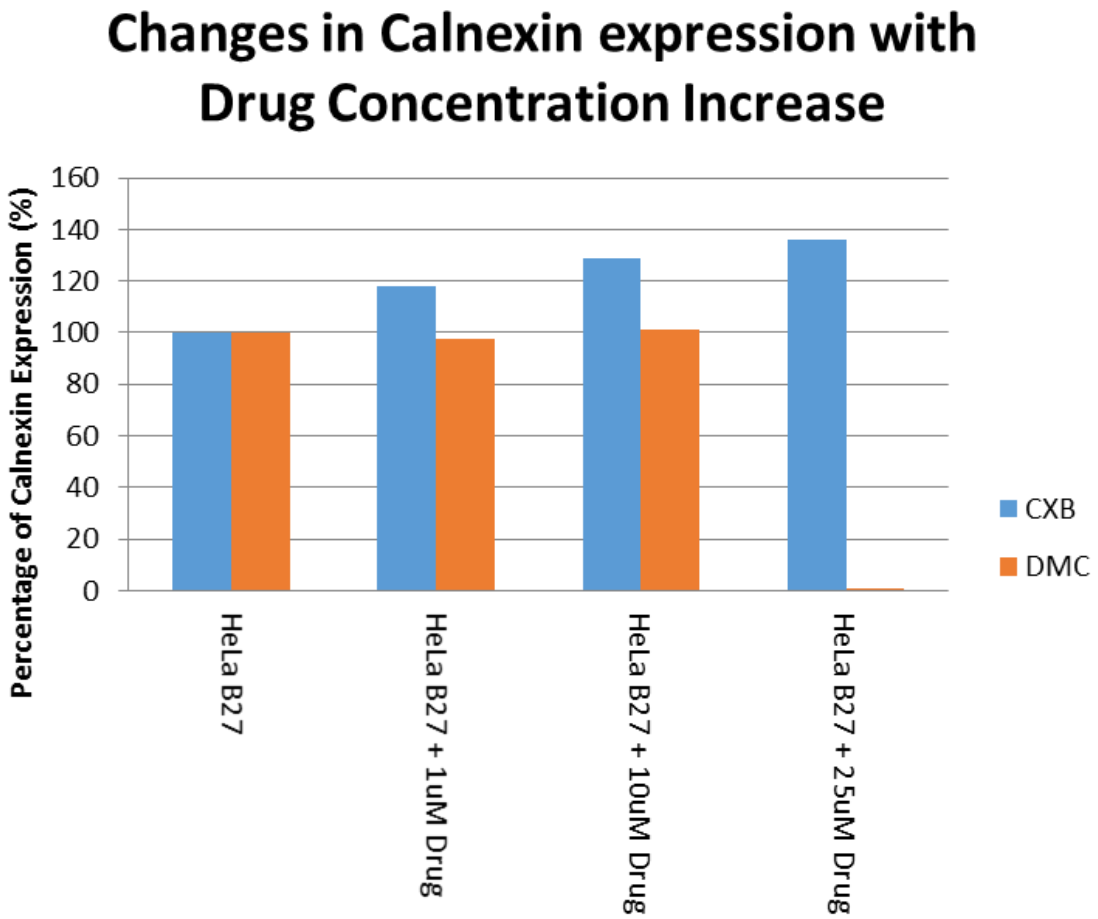

Figure 10-2D: bar chart showing the changes in calnexin concentration with increased drug concentration. The HeLa.B27 control was used as 100%. n=1

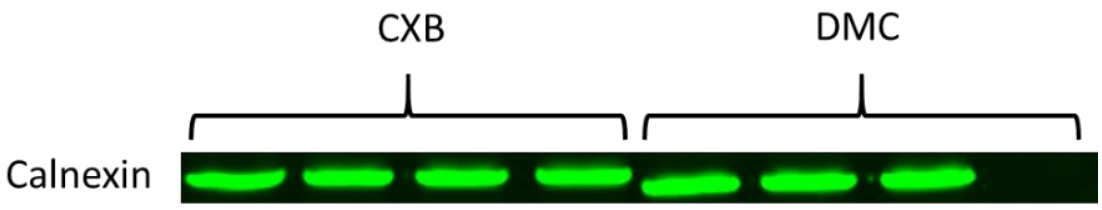

Figure 10-2E: western blot of calnexin expression seen in HeLa.B27 cells when either CXB or DMC are added. Samples are arranged as in figure 10-2D except CXB are presented first and then DMC second. n=1

Simultaneously a time course experiment was performed to observe the cytotoxicity and effects of both drugs on Calnexin expression and HC dimer expression over a 12-hour period. Confluent HeLa.B27 cells were incubated with 25 µM of either CXB or DMC over the course of 12 hours. After 12 hours a cell viability assay was performed and protein expression analysed. It was observed that the addition of CXB to HeLa.B27 cells causes a decrease in cell viability to 75 %, generally at almost every time point (figure 3A, blue bars). However, DMC has a more pronounced effect, decreasing viability to 54 % in the first 2 hours, 53 % after 4 hours, 47 % after 8 hours and 22 % at 12 hours (figure 10-3A, orange bars), similar to the value seen with the same concentration of DMC overnight. Homodimer expression tends to decrease for both drugs as the time scale increases though DMC shows an increase between the 8 and 12-hour time points (figure 10-3B and 10-3C). Calnexin expression also generally follows this trend with DMC averaging at 87 % expression for the first 4 hours and then averaging at 48 % for the next 8 hours following this (figure 10-3D and 10-3E). The CXB calnexin expression is slightly different in that a small increase is observed initially for the first 4 hours followed by a decrease in calnexin expression, compared to control levels. This suggests that DMC is more cytotoxic that CXB however it also has a greater effect upon calnexin and dimer expression.

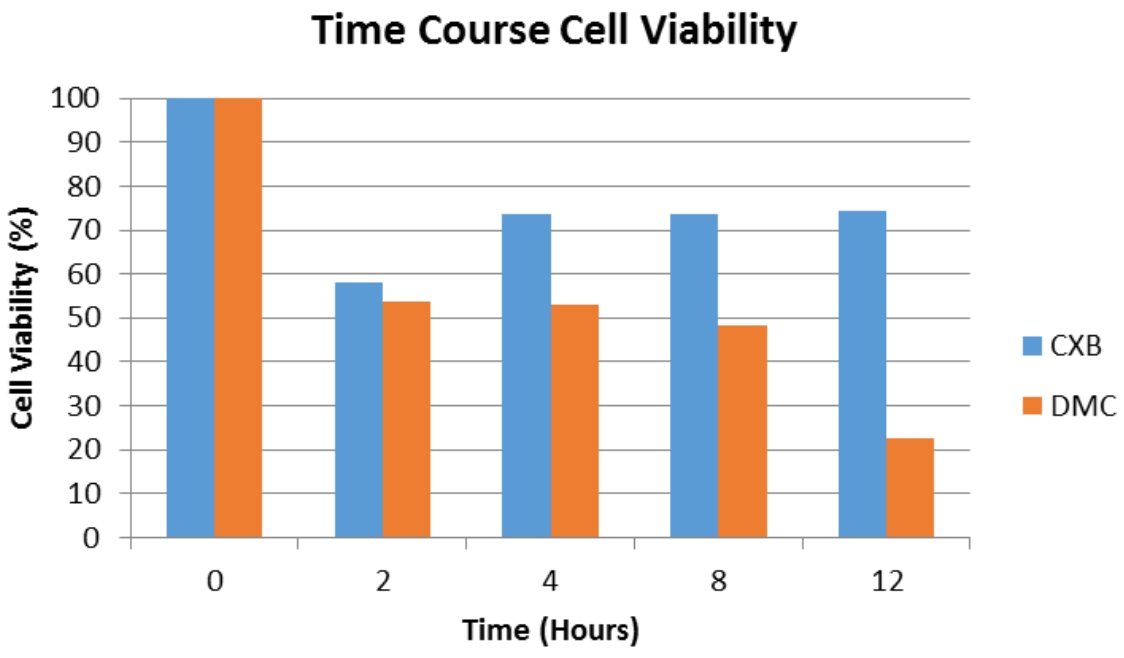

Figure 10-3A: bar chart showing the changes in cell viability over time for HeLa.B27 cells when 25 µM of either drug is added. Time 0 hours was used as 100 %. n=1

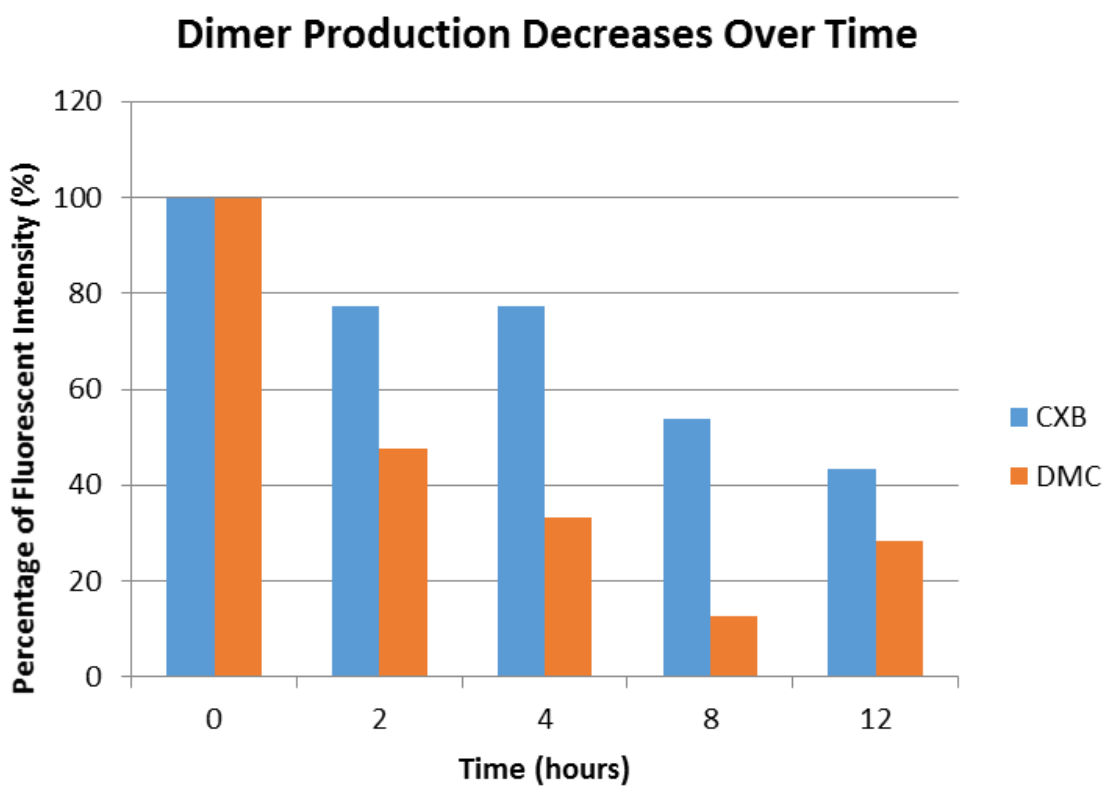

Figure 10-3B: bar chart displaying the general decrease in homodimer expression seen over time. 0 hours was used as 100 %. n=1

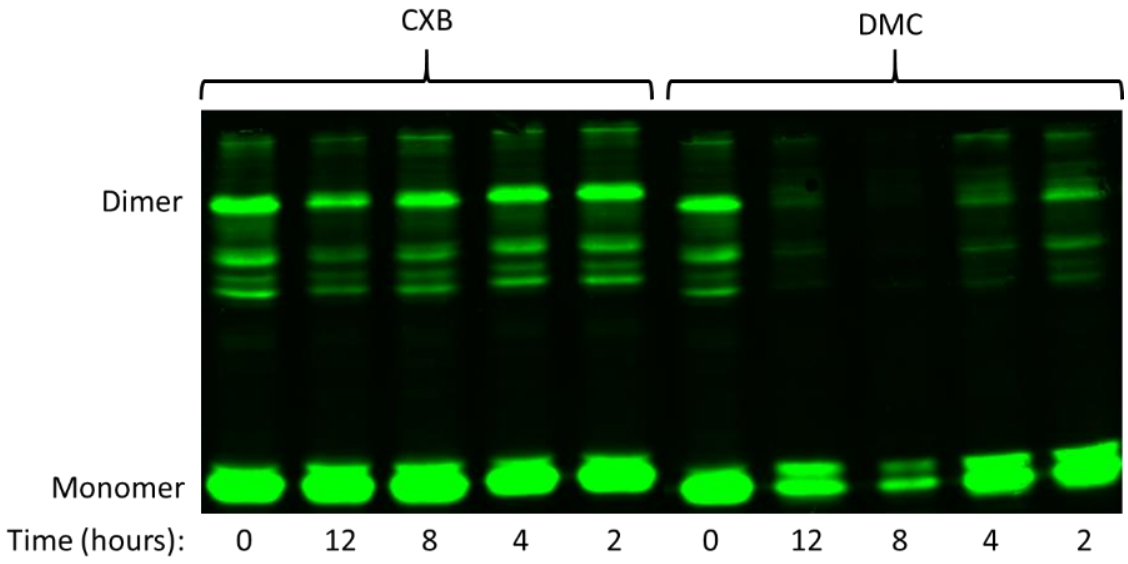

Figure 10-3C: western blot of HLA-B27 dimer (upper band) and monomer (lower band) expression in HeLa.B27 cells when 25 µM CXB or DMC is added over a time course. Samples are arranged in the same order as figure 10-3B except CXB is first and DMC second. n=1

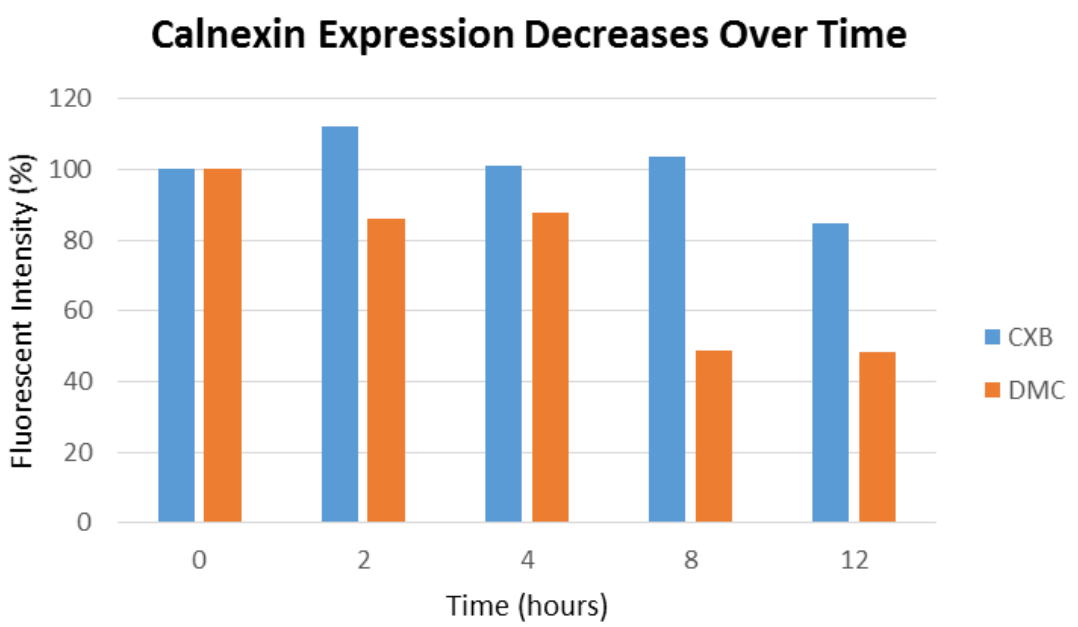

Figure 10-3D: bar chart displaying the changes in calnexin expression seen over time when HeLa.B27 cells are incubated with 25 µM of either drug. 0 hours was used as 100%. n=1

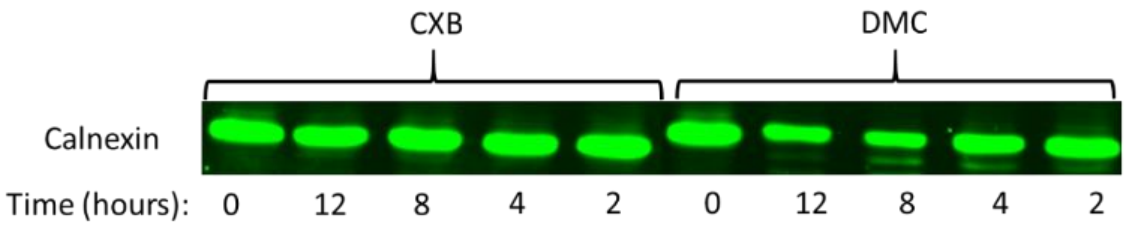

Figure 10-3E: western blot of calnexin expression in HeLa.B27 cells after incubation with either 25 µM CXB or DMC over a time course. Samples are arranged in the same order as figure 10-3D. n=1

As 12 hours was detrimental to cells incubated with 25 µM DMC the time course was repeated with different conditions. This time a range of 8 hours and a drug concentration of 10 µM DMC or 25 µM CXB was used as even at 4 hours almost 50 % cell viability in the DMC samples was observed in the previous experiment. This time the cell viability was assessed followed by analysis for the expression of HC homodimers, calnexin, HRD1 and calreticulin. These four proteins were chosen as they are all either ER chaperones or associated with UPR. For CXB, the cell viability assay revealed that for 1, 2, 4 and 8-hour incubation periods the cell viability was 90, 97, 101 and 95 %, respectively (blue bar, figure 10-4A). For DMC the cell viability assay showed for 1, 2, 4 and 8 hours the cell viability was 98, 96, 110 and 100 %, respectively (figure 10-4A, orange bars). This means that both drugs at a range of 8 hours allow good cell preservation and are essentially not cytotoxic. The HC dimer expression for both CXB and DMC showed no relationship between repeat experiments (not shown), whereas the expression of calnexin is observed to increase over the control value for 2, 4 and 8 hours when DMC is applied (figure 10-4B, orange bars). Both drugs are known to cause ERAD and UPR. This should cause a decrease in dimer expression as the UPR should work to decrease the number of misfolded proteins retained in the ER and therefore are unable to be expressed on the outside of the cell. This data supports a theory that the HC dimers are also formed upon recycling of the HLA-B27 molecules. Furthermore, the majority of the population detected here may be from expression on the outside of the cell suggesting that recycling of HLA-B27 molecules may be upregulated. There is an increase in calnexin expression above control levels observed at 4 hours followed by a decrease at 8 hours (figure 10-4B, blue bars). During the UPR chaperones such as calnexin become sequestered to incorrectly folded proteins therefore sending feedback to the cell to increase the expression of calnexin. Therefore, an increase in calnexin would help to keep the cell functioning. The decrease in calnexin expression seen at the 8 hour DMC (figure 10-4B, orange bars and figure 10-4C) may be a sign that CHOP has been expressed. This indicates that the cell is heading down the apoptosis pathway. HRD1 expression levels saw an initial drop to 60 %, for CXB incubated cells, and then expression recovers with time to 76 % (figure 10-4D, blue bars). Expression of HRD1 for DMC incubated cells, in contrast, shows a decrease over incubation time (figure 10-4D, orange bars and figure 10-4E). HRD1 is an Ubiquitin Ligase which tags proteins in the ER for breakdown. Therefore, the initial drop in expression may be a reaction to the introduction of the drug. The increase in expression observed could be explained by the increased need for ubiquitination in order to transport misfolded proteins out of the ER. This aids the prevention of overcrowding and relieves some of the stress. This could be encouraged by the induction of GRP78 expression that has been documented with these drugs. There is an initial decrease in calreticulin expression after the first 2 hours of incubation with CXB, then a recovery of expression after 4 hours and a slight increase above control levels at 8 hours (figure 10-4F, blue bars).

Whereas, for cells incubated with DMC, there is an initial decrease in expression to 80 % for 1 and 2-hour time points. However, at 4 hours there is a drastic drop in expression to 8 % and then a slight recovery of expression at the 8-hour time point to 34 % (figure 10-4F, orange bars and figure 10-4G). Calreticulin, like calnexin, is also a chaperone for protein folding in the ER. Thus an increase in expression might be expected as was seen for the CXB incubated cells. However, looking at the data for DMC incubated cells it can be seen that the decrease in calreticulin is more extreme which may take longer to recover from. In this case the time scale may need extending. Alternatively the downregulation of calreticulin observed may signal, along with the HRD1 expression, that the cell is entering a phase of CHOP production. Cell viability, however, is more than equal to control cell viability. This suggests that if cells are preparing to undergo apoptosis they have not lost their reduced environment in the cytosol yet as this would have been indicated by the cell viability assay.

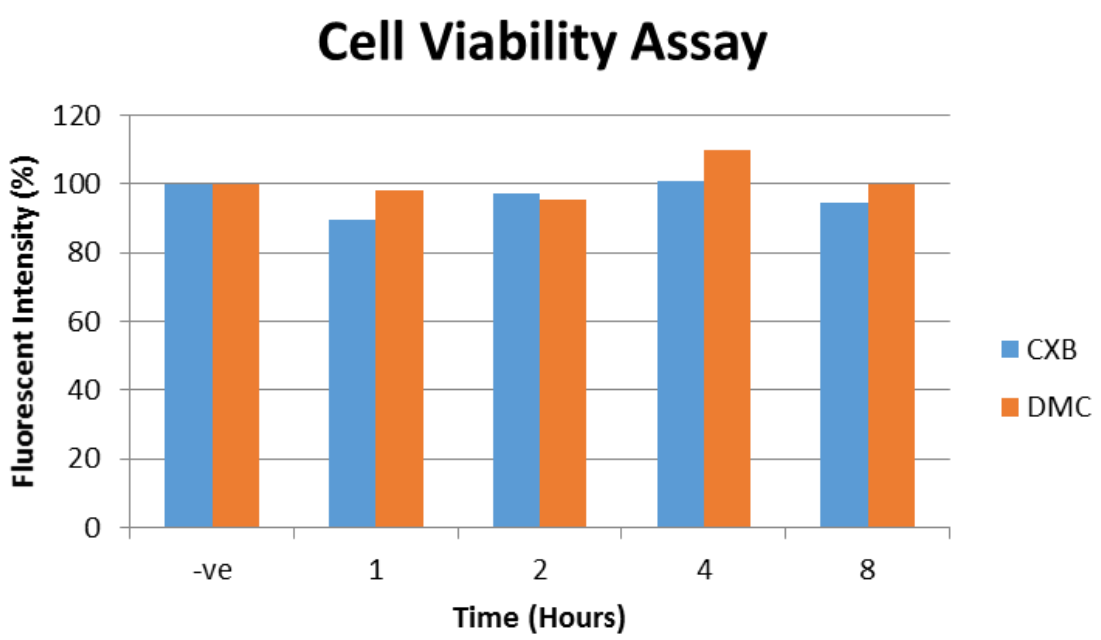

Figure 10-4A: bar chart showing the cell viability of HeLa.B27 cells when either 25 µM CXB or 10 µM DMC are added over a period of 8 hours. The negative control was used as 100 %. n=1

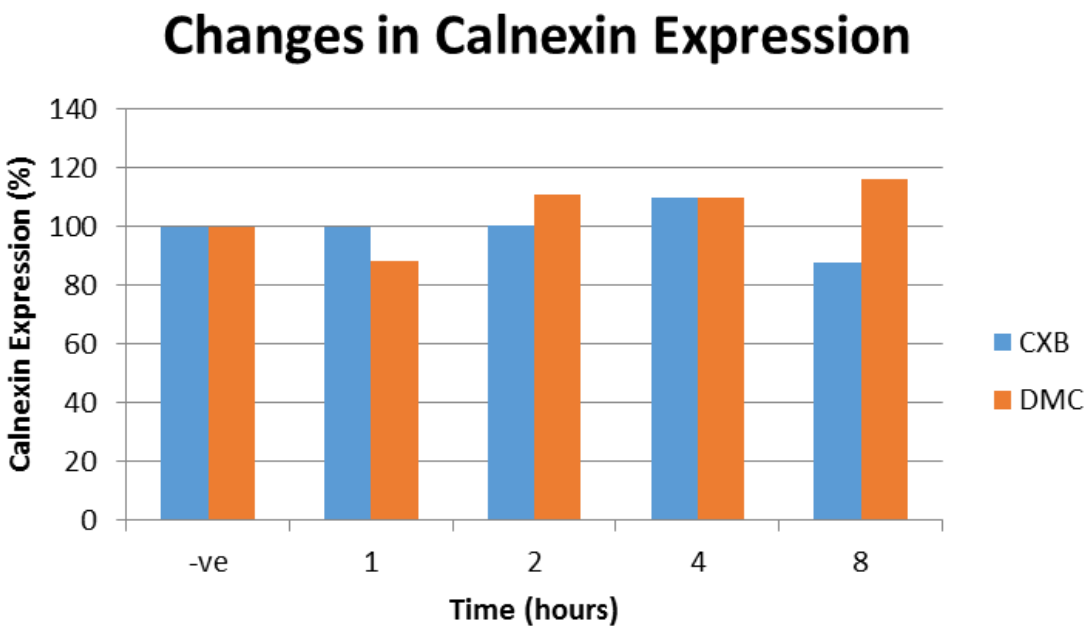

Figure 10-4B: bar chart displaying the changes in calnexin expression of HeLa.B27 cells over an 8-hour time course with either 25 µM CXB or 10 µM DMC. Negative control was used as 100 %. n=1

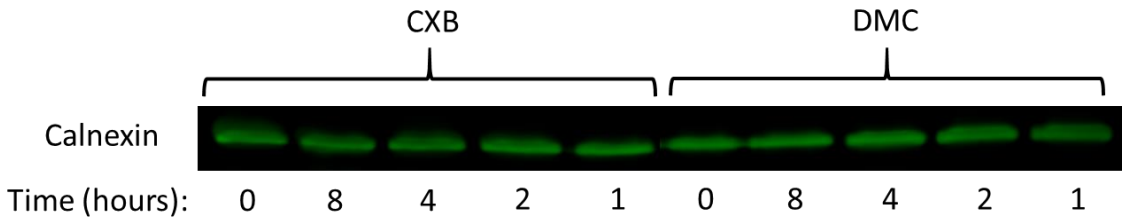

Figure 10-4C: western blot displaying calnexin expression of HeLa.B27 cell after incubation with either 25 µM CXB or 10 µM DMC over a time course. Samples are arranged in the same order as figure 10-4B with CXB first. n=1

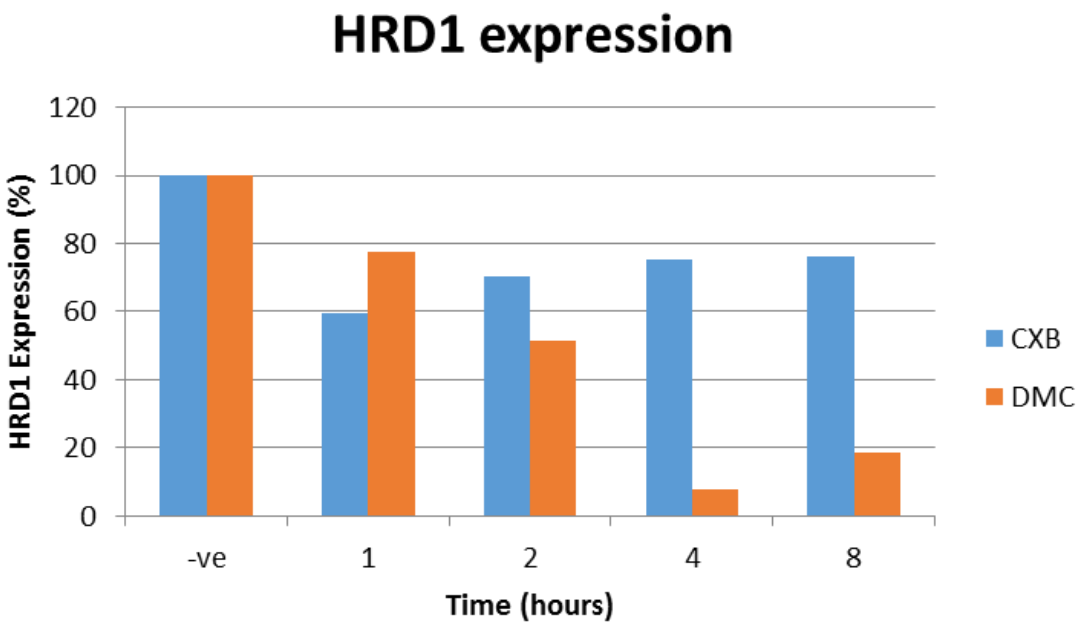

Figure 10-4D: bar chart showing the changes in HRD1 expression over an 8-hour period when cells are either incubated with 25 µM CXB or 10 µM DMC. The negative control was used as 100 %. n=1

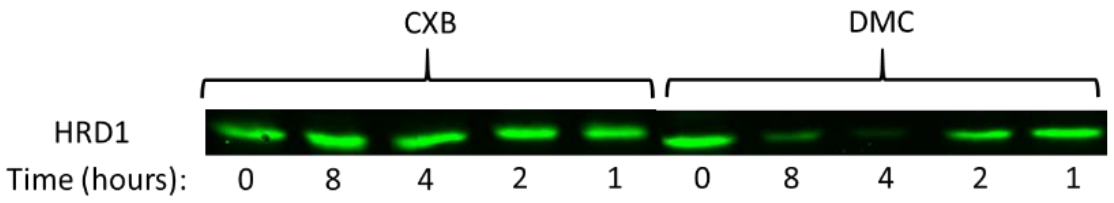

Figure 10-4E: western blot displaying the HRD1 expression of HeLa.B27 cells when incubated with either 25 µM CXB or 10 µM DMC over a time course. Samples are arranged in the same order as figure 10-4D. n=1

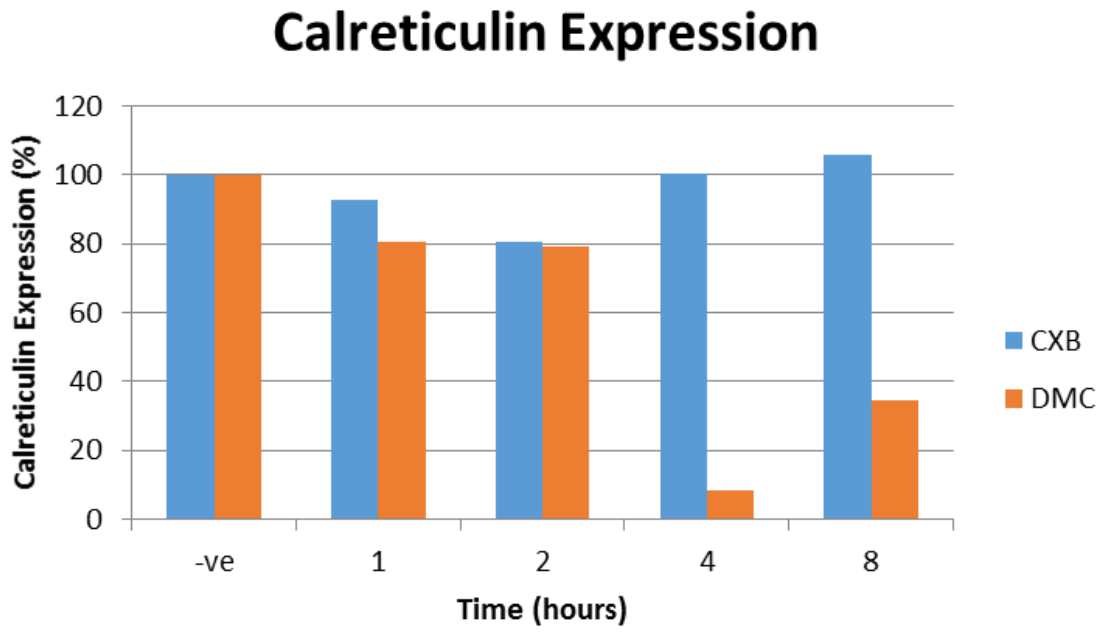

Figure 10-4F: bar chart displaying the changes in calreticulin expression over an 8-hour period when either 25 µM CXB or 10 µM DMC are added to confluent HeLa.B27 cells. The negative control was used as 100 %. n=1

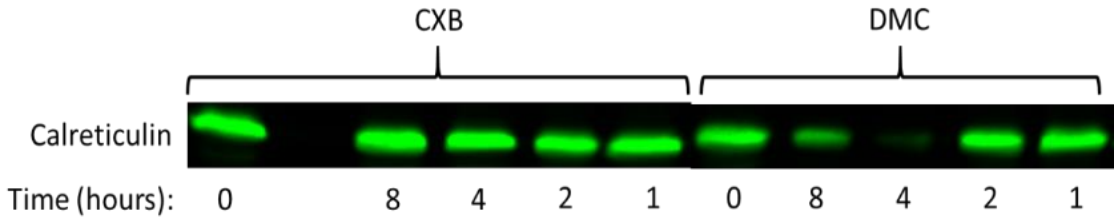

Figure 10-4G: western blot displaying the calreticulin expression of HeLa.B27 cells when incubated with either 25 µM CXB or 10 µM DMC over a time course. Samples are arranged in the same order as figure 10-4F. n=1

CXB in patient serum has been reported to be bound by serum albumin, with as much as 95 % sequestered in this manner. Most publications studying CXB for stress induction use 5 or 10 % FCS. As a side control experiment, drug was added to cells incubated in different concentrations of Foetal Calf Serum (FCS) enhanced RPMI. Standard media is RPMI with 5 % FCS and 100 µg/ml Kanamycin. The concentrations of FCS used were 0, 2.5, 5 and 10 %. C58.B27 cells were grown to confluency in growth media. C58.B27 is a non-adherent, rat T cell line stably transfected with HLA-B*27:05. Media was then removed before adding an FCS enhanced RPMI media and adding either 0, 1, 10, 25 or 50 µM of CXB. Cells were then left to incubate for 5 hours at 37 °C before a cell viability assay was performed. Upon analysis of the assay (figure 10-5), it was clear that the presence of FCS inhibited the toxicity of CXB. Thus, in order to observe the real dose of CXB that is effective in this system, future experiments were performed in a serum free setting.

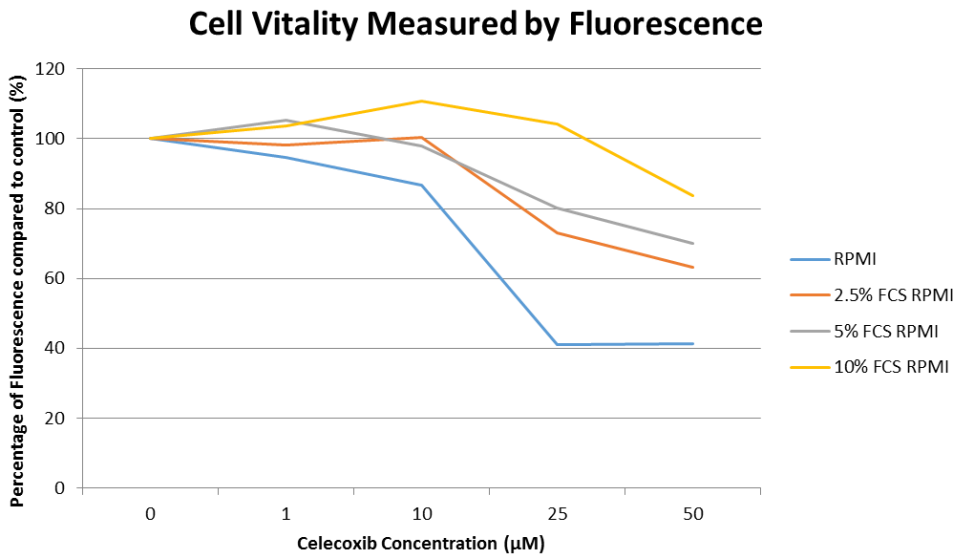

Figure 10-5: line chart displaying the change in viability of HeLa.B27 cells incubated with increasing concentrations of CXB in media containing different concentrations of Foetal Calf Serum. Increasing the concentration of FCS appears to increase the viability of the cells even in the higher concentrations of CXB. n=1

The prime aim of this research is to assess the suitability of EVs as drug delivery vesicles therefore the next experiment used the sonication method of loading EVs to attempt delivery to HeLa.B27 cells. The sonication method trialled earlier, in the sonication chapter, exhibited a 30 % encapsulation rate for Allstars siRNA however it turned out not to be suitable for ERAP1 siRNA. Therefore, the possibility to encapsulate CXB or DMC was tested. This may allow targeting of CXB to specific cells in future work. Drug encapsulated EVs were prepared by sonicating 1 mM of either CXB or DMC with 150 µg EVs. EVs were then enriched in NAP-10 size exclusion columns to remove unbound drug. Confluent HeLa.B27 cells were incubated overnight with the enriched EVs. A cell viability assay was then performed and the cells analysed. A high dose of CXB and DMC was used as sonication can encapsulate up to 30 % of cargo. Furthermore, if the higher dose was delivered there would be a greater visibility of effects than a lower dose which might have marginal effects. The proteins checked for regulation this time were HERP, PDI, GAPDH, HC10, calnexin and calreticulin. The cell viability assay showed that all samples remained at a viability of 100% or more compared to the control, except the sample with sonicated DMC and EVs which dropped to 20 % (figure 10-6A). This is a strong indication that a high dose of DMC has been delivered. The first protein to be analysed was HERP. It was observed that the sonicated CXB and EV sample retained approximately (96 %) the same level of expression (figure 10-6B and 10-6G). However, the sonicated EV control decreased to 90 % and the sonicated RPMI control expression levels dropped further to 78 %. The expression levels seen in the sonicated DMC and EV sample however showed the lowest expression levels of HERP by far with less than 1 %. The decrease in HERP expression seen for the two controls suggests that sonication and the presence of EVs themselves can cause a decrease in expression though not a decrease in viability. The decrease seen for the sonicated EV and DMC sample furthermore correlates with the decrease in viability therefore it is most likely due to a lack of cell presence. As HERP is associated with cell stress induction, it would be expected to see an increase in its expression if drug had been delivered and induced UPR. Therefore, it is unlikely that CXB was encapsulated. However, as there was a large amount of cell death in the sonicated DMC and EV sample it is not possible to say whether an increase in HERP expression occurred. Furthermore, HERP expression is induced alongside GRP78 expression at the start of the UPR and then decreases along with the expression of other chaperones. This occurs after the expression of CHOP suggesting that it would not be present as the cell is heading towards apoptosis.

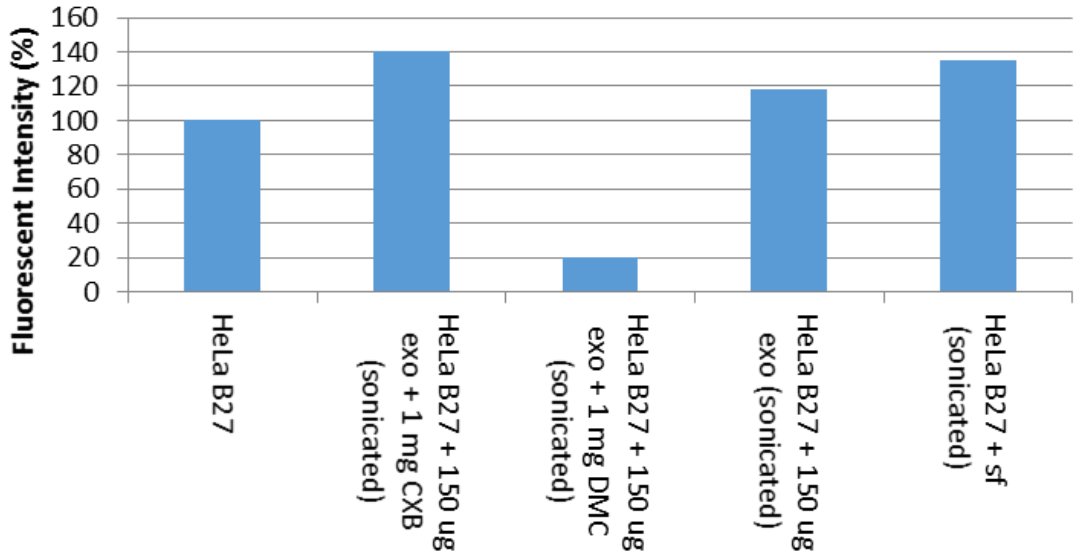

Figure 10-6A: bar chart showing HeLa.B27 cell viability when incubated with 150 µg EVs associated with 1 mg of either CXB or DMC. The HeLa.B27 control was used as 100 %. n=1

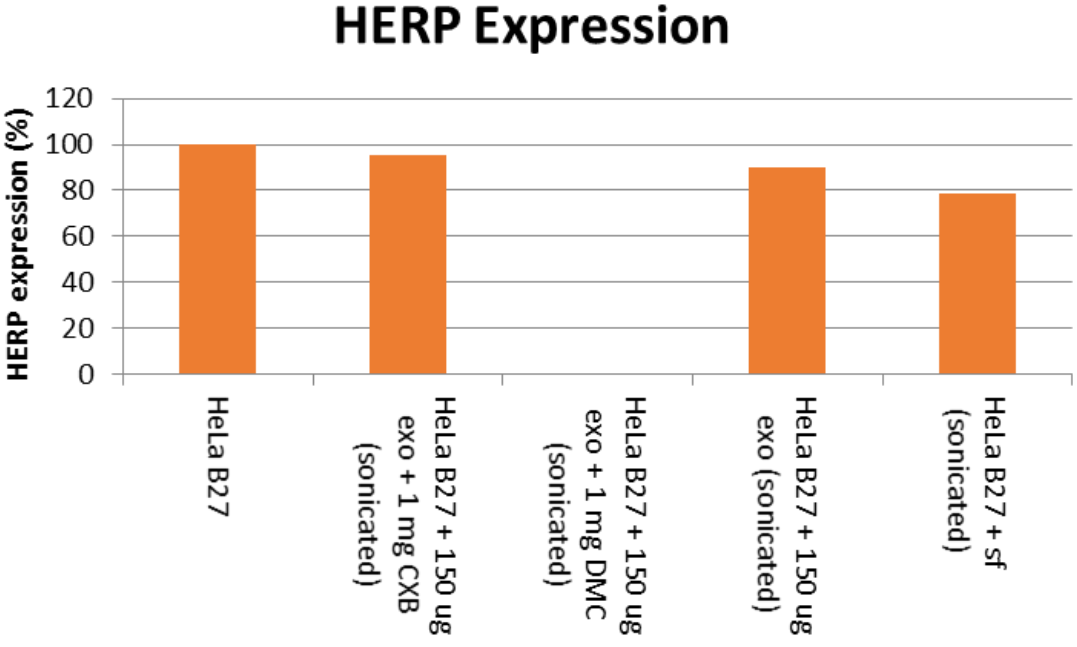

Figure 10-6B: bar chart showing the expression of HERP protein after cell incubation with EV encapsulated CXB or DMC. The HeLa.B27 control was used as 100 %. n=1

The second ER protein to be analysed was Protein Disulphide Isomerase (PDI). For PDI it was observed that the controls both retained a similar expression (98 %) compared to the HeLa.B27 cell control well (figure 10-6C and 10-6G). However, for the sonicated CXB and EV sample a minor decrease in PDI expression to 91 % was observed. Once again the lowest expression was seen in the sonicated DMC and EV sample with an expression of less than 1 %. Again, this can be attributed to the lack of cell viability. PDI as a chaperone aiding in the formation and correction of disulphide bonds may also be downregulated after CHOP induction as it is no longer required.

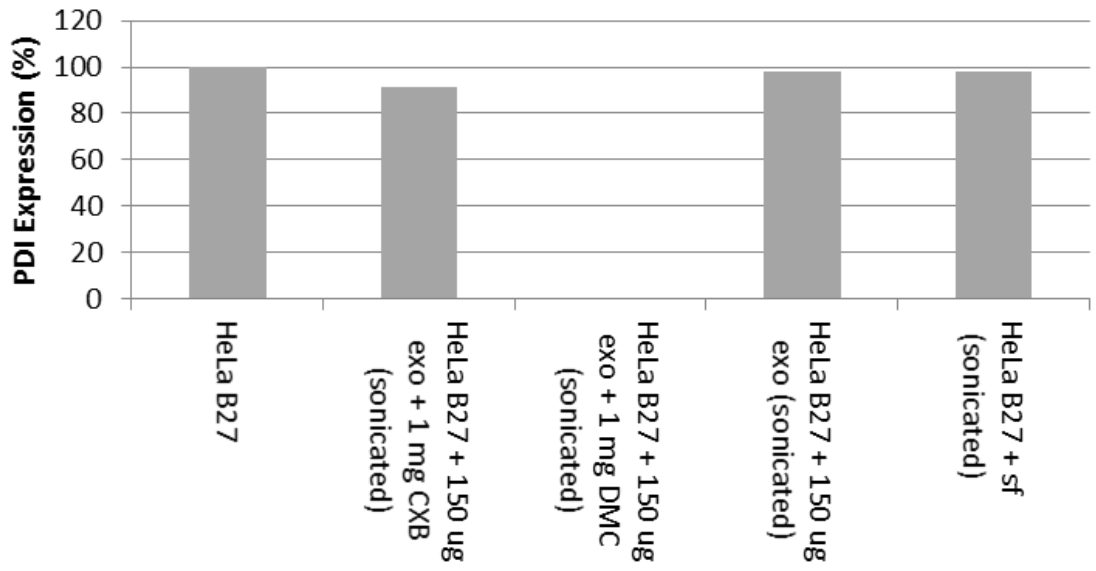

Figure 10-6C: bar chart showing the changes in PDI expression with either CXB or DMC loaded EVs are added. The HeLa.B27 control was used as 100 %. n=1

HLA class 1 expression of the samples was assessed next. Anti-HC10 showed 2 bands on a western blot; one for HC monomeric HLA class I and the second for HC homodimeric HLA class I. As the western blot was ran non-reduced it was possible to maintain the homodimeric structures present on the outside of the HeLa.B27 cells. It would be expected to find a mixture of monomers and dimers inside of the cell however dimers would be expected to be present on the outside of the cell. In this experiment there may be a decrease in dimers as they are degraded by the UPR. The results showed that the sonicated CXB and EV sample decreased in dimer expression however not to levels lower than controls (figure 10-6D and 10-6G).

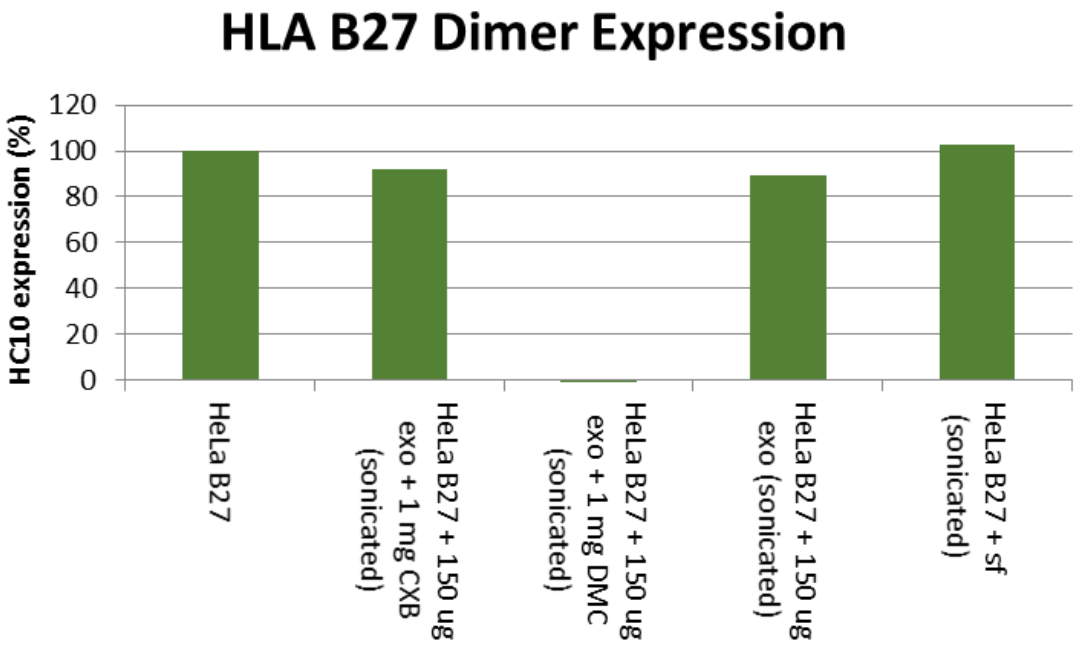

Figure 10-6D: bar chart displaying change in HLA-B27 Dimer expression when drug loaded EVs are incubated with HeLa.B27 cells. The HeLa.B27 control was used as 100 %. n=1

As calnexin is an important component of the ER chaperone system, it was also analysed. Upon analysis it was found that the expression of calnexin had decreased to 95 % compared to the HeLa.B27 cell control for the sonicated CXB and EV sample. However, a decrease in the sonicated EV control and sonicated RPMI control to 92 and 89 %, respectively, was also observed (figure 10-6E and 10-6G). The calnexin expression for the sonicated DMC and EV sample, similar to results seen already, showed a huge decrease to less than 1 %. This may mostly be accredited to the large amount of apoptosis seen in this sample.

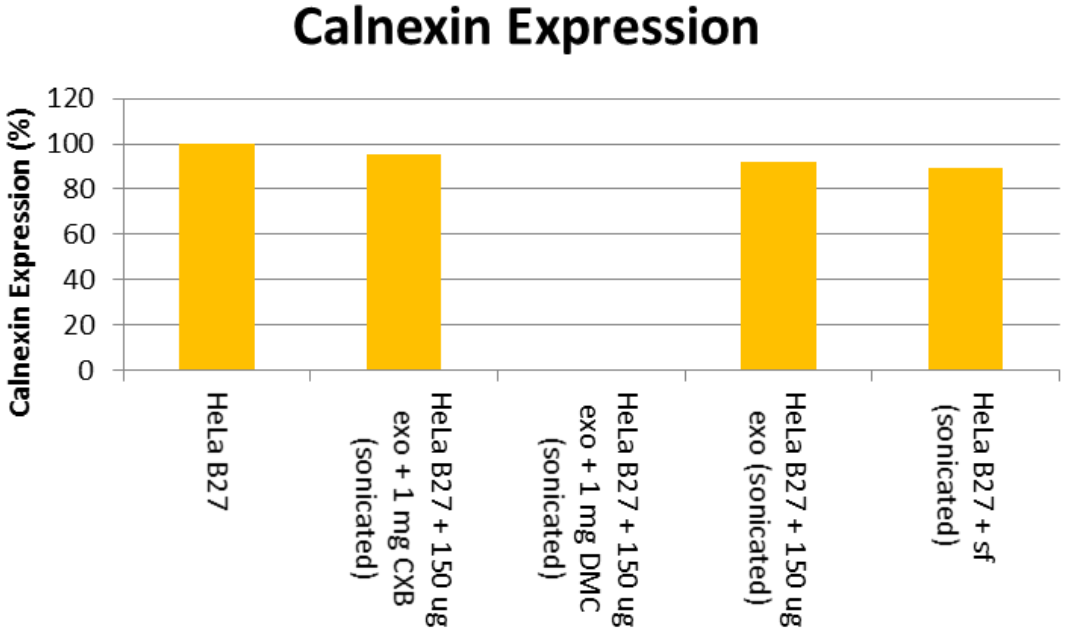

Figure 10-6E: bar chart showing the change in expression of calnexin when cells are exposed to either CXB or DMC containing EVs. The HeLa.B27 control was used as 100 %. n=1

The calreticulin expression observed is slightly different in that the sonicated CXB and EV sample shows a slight increase of 2 % over the HeLa.B27 control however the sonicated EV control and sonicated RPMI control decrease in calreticulin expression to 99 and 88 %, respectively (figure 10-6F and 10-6G). Normally an increase in calreticulin would suggest an upregulation in proteins associated with protein folding. This would be to form a UPR however the observed increase is too small to make any assumptions. Once again the large decrease in calreticulin expression seen for the sonicated DMC and EV sample should be attributed primarily to the loss of cell viability.

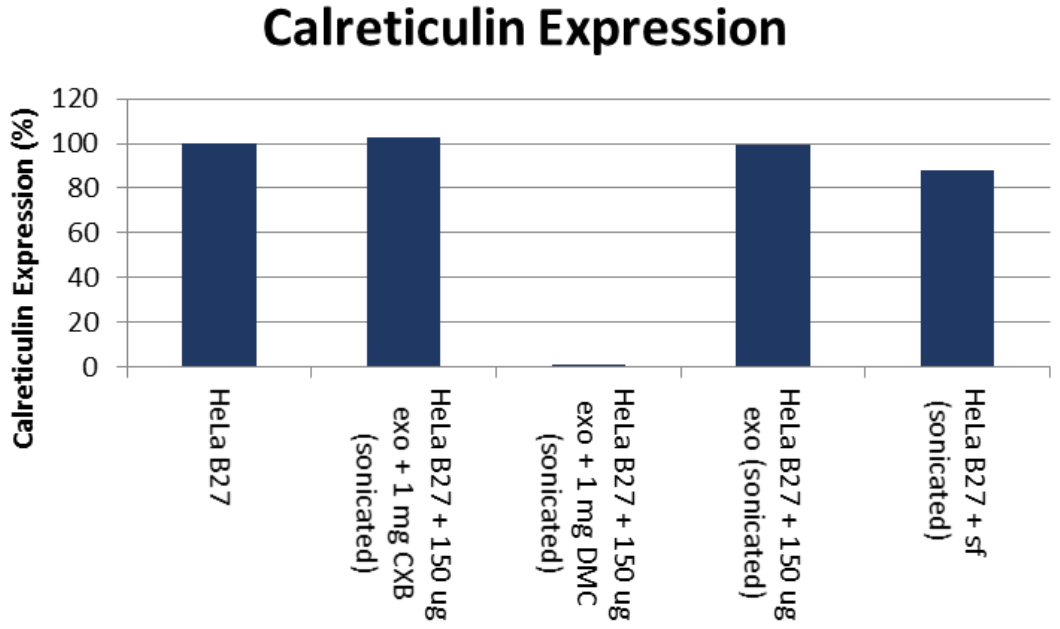

Figure 10-6F: bar chart displaying the changes in calreticulin expression when HeLa.B27 cells are incubated with EVs containing either CXB or DMC. The HeLa.B27 control was used as 100 %. n=1

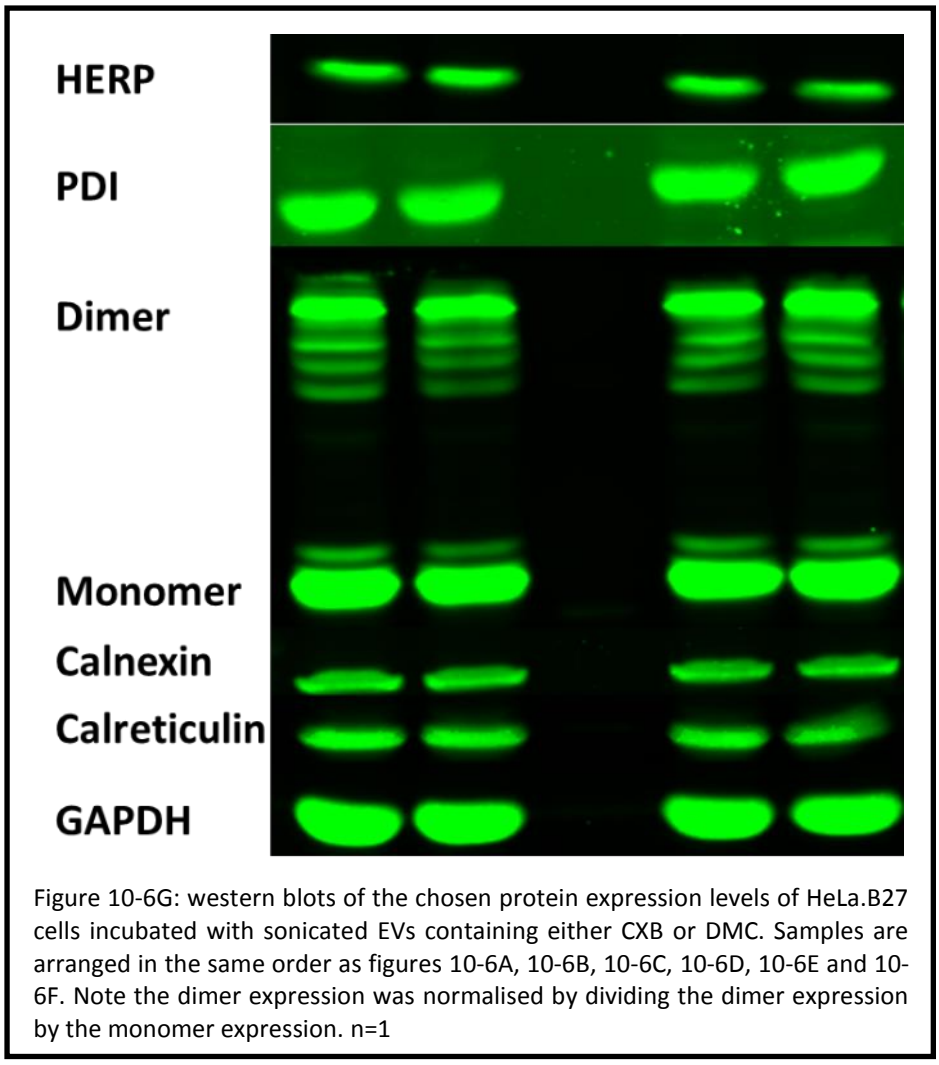

Figure 10-6G: western blots of the chosen protein expression levels of HeLa.B27 cells incubated with sonicated EVs containing either CXB or DMC. Samples are arranged in the same order as figures 10-6A, 10-6B, 10-6C, 10-6D, 10-6E and 10-6F. Note the dimer expression was normalised by dividing the dimer expression by the monomer expression. n=1

10.2 Discussion

Celecoxib and its derivative DMC have effects on cells that at high concentrations push them towards cell death involving an autophagic process. However at the appropriate lower concentrations it is clear from this current data that the autophagic process can lead to the removal of misfolded heavy chain HLA-B27 molecules. This could be of significant benefit to limiting the inflammatory process in AS. Targeted delivery to immune cells could therefore be of clinical use. Exosomes might be a useful delivery agent, if loaded successfully with drug.

Toxicity, however, as previously mentioned remains a key issue. From this chapter it can be seen that both CXB and DMC have limits for their use with regards to cytotoxicity. Studies, with regards to both existing and new CXB related drugs, tend to feature assessments of toxicity (Bento, Daumal, Sampol, & Gutierrez, 2016; Davies, McLachlan, Day, & Williams, 2000; Huang et al., 2012; Puratchikody, Sriram, Umamaheswari, & Irfan, 2016; Pyrko et al., 2007, 2008; Schönthal, 2006; Sobolewski et al., 2015; Thompson et al., 2016; Wanders et al., 2005; Ward & Kuzis, 2002). Of particular note are the studies where CXB or its derivative are used primarily for their cytotoxic properties (Pyrko *et al.,* 2007; Schönthal, 2006; Sobolewski *et al.,* 2015). The demonstration that there is a thin line between productive cell death and cytotoxicity is also observed in this chapter. When incubated with HeLa.B27 cells, CXB shows significant cytotoxicity at concentrations over 25 µM. HeLa.B27 cells display HLA-B27 homodimers on their surface. Therefore, it could be suggested that they are more susceptible to CXB or DMC. This is because the drugs increase the stress occurring in the ER by downregulating GRP78 expression and inducing CHOP expression (Huang *et al.,* 2012; Pyrko *et al.,* 2007). Contrasting with the aims of other studies, this study aimed to prevent cell death. Thus, assessing the cytotoxicity of the drugs was a pivotal step in the use of HeLa.B27 cells. The use of these cells is unique to this study.

The binding of CXB to albumin has been documented in the literature (Seedher & Bhatia, 2006). Therefore, it is not surprising that an increase in cell viability was observed when samples were prepared in media containing albumin. This was most likely because CXB or DMC when bound by albumin, are in their non-active state. This means that if they were endocytosed by cells in this state, they may not revert back to their active form. There are many studies carried out without assessing the drug binding interactions with albumin. This will result in a concentration that is too low for noticeable biological changes. The albumin content in vivo is much higher than that used in cell medium. Therefore, CXB is more likely to become bound and inactive. A potential solution to this was the encapsulation of drug with EVs. This method would theoretically protect the drug from interactions with albumin and therefore prevent its inactivation. In this study it was observed that the CXB sonicated EVs did not have any significant effect on the cells. However, a cytotoxic reaction with

DMC sonicated EVs was observed. The experiment performed contained a step to exclude unbound drug from the EVs. This suggests that the effects observed were caused by drug associated with EVs rather than a large concentration of free drug. Furthermore, the CXB sonicated EVs not having any major effect proves that excess drug was removed by the size exclusion columns.

In this chapter a variety of antibodies was used to detect the expression changes of proteins associated with ER stress. Whilst some were related to UPR, some were also related to ERAD. Together, it was predicted, they would identify which stage of stress cells were in. It could be seen, with CXB, a pathway related to cell survival was occurring in the cells. This was seen in the increase in calnexin (figure 10-2D), decrease in dimer production with increase in viability (figures 10-3A and 10-3B), increase in HRD1 expression (figure 10-4D) and the recovery of calreticulin expression (figure 10-4F). Unfortunately, encapsulating CXB inside of EVs does not appear straight forward and no meaningful results were observed. In contrast, it is evident that DMC is more cytotoxic than CXB as shown in the cell viability assays (figures 10-2A, 10-3A and 10-6A). Furthermore, the decrease observed in HRD1 and CRT expression without a drop in cell viability suggests that DMC may tend toward cell death. On the other hand, DMC appeared to be associated with EVs (Figure 10-6A) as evidenced by the cytotoxicity seen. It may be possible to use DMC at a concentration where it shows similar effects to CXB. To assess this possibility a drug concentration study should be performed which increases drug concentration in fine increments. According to this study so far, this encapsulated concentration should be below 10 μM.

The outlook for the use of EVs to deliver CXB or DMC is potentially promising. The current rate limiting step is the ability to load the EVs. Future directions to continue the study in this chapter would involve assessment of DMC loading and determining the minimal concentration needed to load EVs with DMC in order to observe an effect. An EV loading assessment would need to consider how to recognise whether drug is associated to the outside of the EVs or encapsulated. Trypsin may remove any unloaded drug. Though the EVs would subsequently need enriching before incubation with cells. The incorporation of a fluorophore to DMC would be interesting to load. This would allow testing using a fluorimeter similar to the tests carried out in the sonication chapter with Allstars siRNA. Once loading efficiency had been assessed a loading titration experiment could be devised to assess the optimum concentration for specific use with the HeLa.B27 cell line.

Conclusion

The aim of this thesis was to assess the use of EVs as drug delivery vesicles. To do this loading was studied via multiple methods. At first many of the methods proved problematic and looking to optimise them exposed hidden problems. For a simple technique like extrusion the question of optimal pore size and force applied emerged. These are 2 variables which were unable to be explored. However it was observed that 16 % of the input Allstars siRNA could be encapsulated (conclusion figure). Unfortunately when ERAP1 was used as cargo such a clear answer was not observed. Most downregulation in ERAP1 expression was masked by cellular upregulation in reaction to one of the components.

For chemical methods involving complexing, PEI and CPPs were studied. These are molecules which associate with the cargo to aid EV loading. Once again optimisation resulted in uncovering more problems. The primary issue with these types of method appears to be aggregation of the molecules. In this research it was observed that the molecules both aggregate with themselves and EVs. This was observed to the extent where the aggregates were causing a noticeable increase in concentration of samples and were visible on NTA. Despite these problems EV loading was seen with all these methods though to various extents. For PEI 13 % encapsulation was observed and for CADY, MPGα and JBS Nucleoducin 6, 8 and 9 % was observed, respectively (conclusion figure). Whilst all these encapsulations were carried out with 0.05 μM Allstars siRNA, they varied in both their EV concentration and PEI or CPP concentration therefore it is hard to compare them. For a true comparison experiments should be carried out under the same conditions. Unfortunately, unlike later Sonication and Celecoxib chapters, loading capabilities were not able to be studied on a cell line assay.

The most complex and time consuming methods used in this research were internal loading. The rate limiting step for most of the studies was the transfection of plasmids or other DNA variants into a cell line. Whilst an ERAP1 expression downregulated cell line was produced with Lentivector constructs it was a struggle to achieve the same with a miR-US4-1 plasmid transfection. Studies in chapter 8 using the shRNA2 CEM cell line that had been previously made in the laboratory outlined the difficulties that may have occurred with the Lentivector cell line, had research continued. The CEM shRNA2 cell line was already documented to downregulate its own cellular ERAP1. Furthermore, when this cell line or EVs produced from it were incubated with other cell lines a decrease in ERAP1 expression was observed when samples were compared to the positive controls. However more work should be done to clarify what is inside the EVs produced by the CEM shRNA2 line and to clarify the role played by cytokines in ERAP1 downregulation. Unfortunately, due to the nature of the internal loading chapter, the data is not comparable to Allstars siRNA loading experiments in other chapters.

Chapters 5 and 9 studied methods that were more disruptive. Electroporation uses the electrical potential between 2 metal plates to form openings in EVs. Sonication uses the formation and collapse of bubbles to achieve a similar goal. As these methods physically alter the EVs using equipment, there were many conditions to optimise. Similar to the other methods discussed in this research the formation of aggregates was observed therefore attempts were made to resolve this. Ultimately the presence of aggregates in these methods seems unavoidable. However different electroporation media compositions and altering the sonication settings can reduce the amount of aggregates formed. Both chapters ended with a cell assay which did not give conclusive results however sonication was used to encapsulate 30 % of input Allstars siRNA (conclusion figure). Unfortunately Allstars siRNA encapsulation with RNase A and NAP-10 columns in conjunction with electroporation was unable to be studied.

The final chapter in this thesis looks at the use of drugs specifically relating back to AS. Celecoxib and its analogue DMC have been shown here and in ongoing studies in the Powis lab to aid in the removal of misfolded HLA-B27 heavy chains from cells, most likely by the induction of acute ER stress and autophagic processes. Therefore targeted delivery of CXB or DMC could be of future clinical benefit. As sonication had proven the most efficient method of encapsulating cargo in EVs it was used to encapsulate CXB and DMC. CXB appeared to have no conclusive effect in a cell assay, leading to the conclusion that it was probably not associated with EVs. DMC however had a cytotoxic effect in a cell assay. This led to the assumption that DMC had remained associated with the EVs post size exclusion column enrichment. However DMC concentration studies are required to ensure that drug can be delivered at non-cytotoxic concentrations. Furthermore, there needs to be a step to ensure that DMC or CXB are not associated with the outside of the EVs. Having fully encapsulated drug will help to prevent off target effects and immunological responses to multiple drug doses.

All the successful Allstars siRNA loading methods have been included in the conclusion figure. However, the definition of successful loading must be considered. Technically a loading efficiency as low as 1 % can be classed as successful as long as a biological effect is seen in the target. Encapsulation is described here by the fluorescence observed from the cargo however using a non-fluorescent cargo such as ERAP1 would require qPCR to determine the concentration of loaded cargo. Therefore more methods of determining loading success should be assessed and applied.

The co-enrichment of RNases must be taken into account when enriching EVs from cell media (Stremersch, Brans, Braeckmans, De Smedt, & Raemdonck, 2017). The RNases co-enriched may be destroying encapsulated siRNA. This demonstrates the importance of EV isolate purity as these RNases can also effect RNase A. This suggests that the concentration of encapsulated cargo may be smaller. This would lead to higher concentrations of cargo needed to load EVs in order to see a biological effect.

EVs for use in clinical trials would have to be enriched further to dismiss co-enriched RNases. In addition to how EVs are isolated, the origin of the EV is also important. As seen in Chapter 3, when EVs and cell lines are characterised, it is revealed that some cell lines and therefore their EVs do not express 'typical' EV markers. This limits the manipulation of EVs as it is not possible to use certain antibodies to enrich the population or attach the EVs to beads for group analysis. Therefore careful consideration should go into the source of EVs and how they are isolated.

Whilst this research is far from clinical trials the barriers that it would have to pass should be considered. As mentioned, EV isolates should be very clean and not be tainted with contaminants like RNases. Furthermore it must be considered whether the method of loading can be scaled-up for production. In this thesis cell assays were performed with $1 \times 10^5 – 2 \times 10^6$ cells per well. In a clinical setting it would be ideal to adjust the dose of EV loaded cargo administered. Post-administration the bio-distribution of the EVs would need to be specific for AS. However, as discussed in the introduction, there is no definitive answer as to which cell type causes AS. The closest answer to an AS target is downregulation of inflammation in the sacroiliac joint and therefore targeting macrophages. The problem with targeting macrophages is that there are more than one type of macrophage and as such EVs would need to target pro-inflammatory macrophages.

Some of the methods in this study have been published by other groups as successful. However a key note of caution must be included in all studies that claim loading in the absence of proper controls that can remove RNA or protein cargo from the surface of exosomes. Whilst on one hand it might actually not matter – cargo embedded in the surface of exosomes might actually be biologically and clinically active - claims of internal loading need to be treated with caution. The success to loading EVs seems to revolve around the cargo. Smaller cargoes, such as siRNA, load more easily than larger cargoes, such as antibodies. This is supported by the research of Inoh *et al.* (Inoh, Nagai, Matsushita, Nakanishi, & Furuno, 2017). Studies in literature, however document the loading of siRNA by various methods. This may be due to the lack of an RNase A wash step in their methods. As observed in this thesis, it is possible to see false positive results when an enzyme is not employed to degrade excess siRNA either attached to the EVs or aggregating in the sample volume. All studies should describe whether their cargo is associated with EVs or encapsulated within EVs. From the results in this thesis, in conjunction with the literature, it can be concluded that EVs can be used to encapsulate cargo and most likely drugs. However further research is required before they may be of use in a clinical setting or for AS treatment.

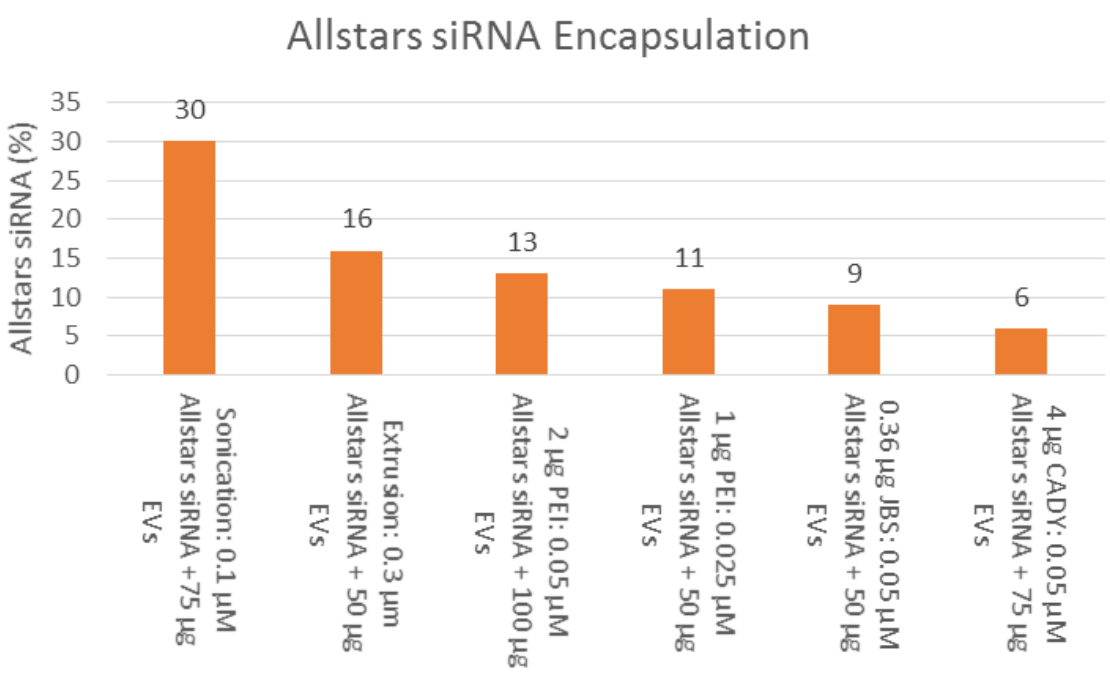

Conclusion Figure: bar chart showing the percentage of Allstars siRNA encapsulated by various methods. All samples were treated with RNase A and enriched through a size exclusion column.

Publications

Guiliano, D., North, H., Panayoitou, E., Campbell, E. C., McHugh, K., Cooke, F., … Antoniou, A. N. (2016). Polymorphisms in the F Pocket of HLA-B27 Subtypes Strongly Impact on Assembly, Chaperone Interactions and Heavy Chain Misfolding. Arthritis Rheumatol. 2017 Mar;69(3):610-621. doi: 10.1002/art.39948.

McReynolds, N., Cooke, F., Chen, Mingzhou., Powis, SJ., Dholakia, Kishan. (2016). Multimodal Discrimination of Immune Cells Using a Combination of Raman Spectroscopy and Digital Holographic Microscopy. Sci Rep. 2017 Mar 3;7:43631. doi: 10.1038/srep43631.

Synowsky SA, Shirran SL, Cooke FGM, Antoniou AN, Botting CH, Powis SJ. (2017). The major histocompatibility complex class I immunopeptidome of extracellular vesicles. J Biol Chem. 2017 Oct 13;292(41):17084-17092. doi: 10.1074/jbc.M117.805895.

Ramirez MI, Amorim MG, Gadelha C, Milic I, Welsh JA, Freitas VM, Nawaz M, Akbar N, Couch Y, Makin L, Cooke F, Vettore AL, Batista PX, Freezor R, Pezuk JA, Rosa-Fernandes L, Carreira ACO, Devitt A, Jacobs L, Silva IT, Coakley G, Nunes DN, Carter D, Palmisano G, Dias-Neto E. (2017). Technical Challenges of Working with Extracellular Vesicles. Nanoscale. 2017 Dec 21. doi: 10.1039/c7nr08360b. [Epub ahead of print] Review. PMID:29265147.

Bibliography

Aggarwal, S., Ghilardi, N., Xie, M. H., De Sauvage, F. J., & Gurney, A. L. (2003). Interleukin-23 promotes a distinct CD4 T cell activation state characterized by the production of interleukin-17. *Journal of Biological Chemistry*, *278*(3), 1910–1914. https://doi.org/10.1074/jbc.M207577200

Agrawal, D., Rukkannagari, S., & Kethu, S. (2007). Pathogenesis and clinical approach to extraintestinal manifestations of inflammatory bowel disease. *Minerva Gastroenterologica E Dietologica*, *53*(3), 233–248.

Agromayor, M., & Martin-Serrano, J. (2006). Interaction of AMSH with ESCRT-III and deubiquitination of endosomal cargo. *Journal of Biological Chemistry*, *281*(32), 23083–23091. https://doi.org/10.1074/jbc.M513803200

Allen, R. L., O'Callaghan, C. a, McMichael, a J., & Bowness, P. (1999). Cutting edge: HLA-B27 can form a novel beta 2-microglobulin-free heavy chain homodimer structure. *Journal of Immunology (Baltimore, Md. : 1950)*, *162*(9), 5045–8. Retrieved from http://www.ncbi.nlm.nih.gov/pubmed/10227970

Alvarez-Erviti, L., Seow, Y., Yin, H., Betts, C., Lakhal, S., & Wood, M. J. a. (2011). Delivery of siRNA to the mouse brain by systemic injection of targeted exosomes. *Nature Biotechnology*, *29*(4), 341–5. https://doi.org/10.1038/nbt.1807

Alvarez-Navarro, C., & López de Castro, J. a. (2014). ERAP1 structure, function and pathogenetic role in ankylosing spondylitis and other MHC-associated diseases. *Molecular Immunology*, *57*(1), 12–21. https://doi.org/10.1016/j.molimm.2013.06.012

Alves, I. D., Goasdoué, N., Correia, I., Aubry, S., Galanth, C., Sagan, S., … Chassaing, G. (2008). Membrane interaction and perturbation mechanisms induced by two cationic cell penetrating peptides with distinct charge distribution. *Biochimica et Biophysica Acta - General Subjects*, *1780*(7–8), 948–959. https://doi.org/10.1016/j.bbagen.2008.04.004

Babst, M., Katzmann, D. J., Snyder, W. B., Wendland, B., & Emr, S. D. (2002). Endosome associated complex ESCRT-2 recruits transport machinery for protein sorting at the Multi vesicular body. *Developmental Cell*, *3*, 283–289.

Bache, K. G., Brech, A., Mehlum, A., & Stenmark, H. (2003). Hrs regulates multivesicular body formation via ESCRT recruitment to endosomes. *Journal of Cell Biology*, *162*(3), 435–442. https://doi.org/10.1083/jcb.200302131

Baietti, M. F., Zhang, Z., Mortier, E., Melchior, A., Degeest, G., Geeraerts, A., … David, G. (2012). Syndecan–syntenin–ALIX regulates the biogenesis of exosomes. *Nature Cell Biology*, *14*(7), 677–685. https://doi.org/10.1038/ncb2502

Behr, J. (1997). The proton sponge: a trick to enter cells the viruses did not exploit. *International Journal for Chemistry*, *2*(1), 34–36. https://doi.org/0009-4293

Bento, L., Daumal, J., Sampol, A., & Gutierrez, A. (2016). Lenalidomide , celecoxib , and azacitidine therapy for blastic plasmocytoid dendritic cell neoplasm : a case report, 5507–5511.

Beum, P. V, Peek, E. M., Lindorfer, M. a, Beurskens, F. J., Engelberts, P. J., Parren, P. W. H. I., … Taylor, R. P. (2011). Loss of CD20 and bound CD20 antibody from opsonized B cells occurs more rapidly because of trogocytosis mediated by Fc receptor-expressing effector cells than direct internalization by the B cells. *Journal of Immunology (Baltimore, Md. : 1950)*, *187*(6), 3438–47. https://doi.org/10.4049/jimmunol.1101189

Bird, L. A., Peh, C. A., Kollnbeger, S., Elliott, T., McMichael A.J., A. J., & Bowness, P. (2003). Lymphoblastoid cells express HLA-B27 homodimers both intracellularly and at the cell surface following endosomal recycling. *European Journal of Immunology*, *33*(3), 748–759. https://doi.org/10.1002/eji.200323678

Blaese, R. M., Culver, K. W., Miller, a D., Carter, C. S., Fleisher, T., Clerici, M., … Anderson, W. F. (1995). T lymphocyte-directed gene therapy for ADA- SCID: initial trial results after 4 years. *Science (New York, N.Y.)*, *270*(5235), 475–480. https://doi.org/10.1126/science.270.5235.475

Bohnsack, M. T., Czaplinski, K., & Gorlich, D. (2004). Exportin 5 is a RanGTP-dependent dsRNA-binding protein that mediates nuclear export of pre-miRNAs. *RNA (New York, N.Y.)*, *10*(2), 185–91. https://doi.org/10.1261/rna.5167604

Bondi, J. F., Oyler, K. D., Ke, X., Schiffer, P., & Schaak, R. E. (2009). Chemical synthesis of air-stable manganese nanoparticles. *Journal of the American Chemical Society*, *131*(26), 9144–9145. https://doi.org/10.1021/ja901372q

Boucheix, C., Benoits, P., Frachetli, P., Billards, M., Worthingtons, R. E., Gagnonil, J., & Uzanll, G. (1991). Molecular Cloning of the CD9 Antigen. *The Journal of Biological Chemistry*, *266*(1), 117–122.

Boussif, O., Lezoualc'h, F., Zanta, M. a, Mergny, M. D., Scherman, D., Demeneix, B., & Behr, J. P. (1995). A versatile vector for gene and oligonucleotide transfer into cells in culture and in vivo: polyethylenimine. *Proceedings of the National Academy of Sciences of the United States of America*, *92*(16), 7297–301. Retrieved from http://www.pubmedcentral.nih.gov/articlerender.fcgi?artid=41326&tool=pmcentrez&rendertype=abstract

Bowness, P., Ridley, A., Shaw, J., Chan, A., Wong-Baeza, I., Fleming, M., … Kollnberger, S. (2011). Th17 cells expressing KIR3DL2 + and responsive to HLA-B27 homodimers are increased in ankylosing spondylitis. *Journal of Immunology*, *186*, 2672–2680. https://doi.org/10.4049/jimmunol.1002653

Breban, M., Fernandez-Sueiro, J. L., Richardson, J. A., Hadavand, R. ., Maika, S. D., Hammer, R. E., & Taurog, J. D. (1996). T cells, but not thymic exposure to HLA-B27, are required for the inflammatory disease of HLA-B27 transgenic rats. *The Journal of Immunology*, *156*, 794–803. Retrieved from http://www.jimmunol.org/content/156/2/794.short

Breslow, E., & Girotti, A. (1969). The Interactin of Ribonuclease with Metal Ions. *The Journal of Biological Chemistry*, *245*(7), 1527–1536.

Brewerton, D. A., Hart, F. D., Nicholls, A., Caffrey, M., James, D. C., & Sturrock, R. D. (1973). Ankylosing spondylitis and HL-A 27. *Lancet*, *1*(7809), 904–907. Retrieved from http://www.scopus.com/inward/record.url?eid=2-s2.0-0015938046&partnerID=tZOtx3y1

Brophy, S., Pavy, S., Lewis, P., Taylor, G., Bradbury, L., Robertson, D., … Calin, A. (2001). Inflammatory eye, skin,

and bowel disease in spondyloarthritis: genetic, phenotypic, and environmental factors. *The Journal of Rheumatology*, *28*(12), 2667–2673.

Burr, M. L., Cano, F., Svobodova, S., Boyle, L. H., Boname, J. M., & Lehner, P. J. (2011). HRD1 and UBE2J1 target misfolded MHC class I heavy chains for endoplasmic reticulum-associated degradation. *Proceedings of the National Academy of Sciences of the United States of America*, *108*(5), 2034–2039. https://doi.org/10.1073/pnas.1016229108

Buzas, E. I., Manc, M., Llorente, A., Lo, J., Revento, J., Portillo, H. A., & Schallmoser, K. (2015). Biological properties of extracellular vesicles and their physiological functions, *1*, 1–60.

Canatella, P. J., Karr, J. F., Petros, J. A., & Prausnitz, M. R. (2001). Quantitative study of electroporation-mediated molecular uptake and cell viability. *Biophysical Journal*, *80*(2), 755–64. https://doi.org/10.1016/S0006-3495(01)76055-9

Capkin, E., Karkucak, M., & Cosar, A. (2014). Treatment of ankylosing spondylitis with TNF inhibitors does not have adverse effect on results of liver function tests: a longitudinal study. *International Journal of Rheumatic Diseases*, 1–5. https://doi.org/10.1111/1756-185X.12311

Cartier, R., & Reszka, R. (2002). Utilization of synthetic peptides containing nuclear localization signals for nonviral gene transfer systems. *Gene Therapy*, *9*, 157–167. https://doi.org/10.1038/sj/gt/3301635

Chabaud, M., & Miossec, P. (2001). The combination of tumor necrosis factor alpha blockade with interleukin-1 and interleukin-17 blockade is more effective for controlling synovial inflammation and bone resorption in an ex vivo model. *Arthritis and Rheumatism*, *44*(6), 1293–303. https://doi.org/10.1002/1529-0131(200106)44:6<1293::AID-ART221>3.0.CO;2-T

Charrin, S., Le Naour, F., Oualid, M., Billard, M., Faure, G., Hanash, S. M., … Rubinstein, E. (2001). The major CD9 and CD81 molecular partner. Identification and characterization of the complexes. *Journal of Biological Chemistry*, *276*(17), 14329–14337. https://doi.org/10.1074/jbc.M011297200

Charrin, S., Manie, S., Oualid, M., Billard, M., Boucheix, C., & Rubinstein, E. (2002). Differential stability of tetraspanin / tetraspanin interactions : role of palmitoylation. *FEBS Letters*, *516*, 139–144.

Chen, G., Yue, A., Ruan, Z., Yin, Y., Wang, R., Ren, Y., & Zhu, L. (2016). Comparison of the effects of different cryoprotectants on stem cells from umbilical cord blood. *Stem Cells International*, *2016*. https://doi.org/10.1155/2016/1396783

Chen, J., Lin, S., & Liu, C. (2014). Sulfasalazine for ankylosing spondylitis (Review), (11). https://doi.org/10.1002/14651858.CD004800.pub3.www.cochranelibrary.com

Chen, J., Liu, C., & Lin, J. (2006). Methotrexate for ankylosing spondylitis. *Cochrane Database Syst Rev*, (2). Retrieved from http://onlinelibrary.wiley.com/doi/10.1002/14651858.CD004524.pub3/pdf/standard

Chen, L., Ridley, A., Hammitzsch, A., Al-mossawi, M. H., Bunting, H., Georgiadis, D., … Bowness, P. (2015). Silencing or inhibition of endoplasmic reticulum aminopeptidase 1 (ERAP1) suppresses free heavy chain expression and Th17 responses in ankylosing spondylitis, 1–8. https://doi.org/10.1136/annrheumdis-2014-206996

Christianson, H. C., Svensson, K. J., van Kuppevelt, T. H., Li, J.-P., & Belting, M. (2013). Cancer cell exosomes depend on cell-surface heparan sulfate proteoglycans for their internalization and functional activity.

Proceedings of the National Academy of Sciences of the United States of America, *110*(43), 17380–5. https://doi.org/10.1073/pnas.1304266110

Clague, M. J. (2002). Membrane Transport : A Coat for Ubiquitin Lysosomally directed receptors are concentrated at, *12*(2), 529–531.

Clayton, A., Court, J., Navabi, H., Adams, M., Mason, M. D., Hobot, J. A., … Jasani, B. (2001). Analysis of antigen presenting cell derived exosomes, based on immuno-magnetic isolation and flow cytometry. *Journal of Immunological Methods*, *247*(1–2), 163–174. https://doi.org/10.1016/S0022-1759(00)00321-5

Cocucci, E., Racchetti, G., Podini, P., & Meldolesi, J. (2007). Enlargeosome traffic: Exocytosis triggered by various signals is followed by endocytosis, membrane shedding or both. *Traffic*, *8*(6), 742–757. https://doi.org/10.1111/j.1600-0854.2007.00566.x

Colbert, R. A. (2000). HLA-B27 misfolding: A solution to the spondyloarthropathy conundrum? *Molecular Medicine Today*, *6*(6), 224–230. https://doi.org/10.1016/S1357-4310(00)01699-3

Colbert, R. A., Tran, T. M., & Layh-Schmitt, G. (2014). HLA-B27 misfolding and ankylosing spondylitis. *Molecular Immunology*, *57*(1), 44–51. https://doi.org/10.1016/j.molimm.2013.07.013

Corthay, A. (2009). How do regulatory t cells work? *Scandinavian Journal of Immunology*, *70*(4), 326–336. https://doi.org/10.1111/j.1365-3083.2009.02308.x

Crombez, L., Aldrian-Herrada, G., Konate, K., Nguyen, Q. N., McMaster, G. K., Brasseur, R., … Divita, G. (2009). A new potent secondary amphipathic cell-penetrating peptide for siRNA delivery into mammalian cells. *Molecular Therapy : The Journal of the American Society of Gene Therapy*, *17*(1), 95–103. https://doi.org/10.1038/mt.2008.215

Crombez, L., Morris, M. C., Deshayes, S., Heitz, F., & Divita, G. (2008). Peptide-based nanoparticle for ex vivo and in vivo drug delivery. *Curr Pharm Des*, *14*(34), 3656–3665. Retrieved from http://www.ncbi.nlm.nih.gov/pubmed/19075741

Dad Abu-Bonsrah, K., Zhang, D., & Newgreen, D. F. (2016). CRISPR/Cas9 Targets Chicken Embryonic Somatic Cells In Vitro and In Vivo and generates Phenotypic Abnormalities. *Nature Publishing Group*, (February), 1–10. https://doi.org/10.1038/srep34524

Dagfinrud, H., Hagen, K., & Kvien, T. (2009). Physiotherapy interventions for ankylosing spondylitis (Review) Physiotherapy interventions for ankylosing spondylitis. *Rehabilitation*, (2). https://doi.org/10.1002/14651858.CD002822.pub3.Copyright

Dakwar, E., Reddy, J., Vale, F. L., & Uribe, J. S. (2008). A review of the pathogenesis of ankylosing spondylitis. *Neurosurgical Focus*, *24*(1), E2. https://doi.org/10.3171/FOC/2008/24/1/E2

Dangoria, N. S., Delay, M. L., Kingsbury, D. J., Mear, J. P., Uchanska-Ziegler, B., Ziegler, A., & Colbert, R. A. (2002). HLA-B27 misfolding is associated with aberrant intermolecular disulfide bond formation (dimerization) in the endoplasmic reticulum. *Journal of Biological Chemistry*, *277*(26), 23459–23468. https://doi.org/10.1074/jbc.M110336200

Davies, N. M., McLachlan, A. J., Day, R. O., & Williams, K. M. (2000). Clinical Pharmacokinetics and Pharmacodynamics of Celecoxib. *Clinical Pharmacokinetics*, *38*(3), 225–242. https://doi.org/10.2165/00003088-200038030-00003

Dean, L. E., Jones, G. T., Macdonald, A. G., Downham, C., Sturrock, R. D., & Macfarlane, G. J. (2013). Global prevalence of ankylosing spondylitis. *Rheumatology (Oxford, England)*, 1–8. https://doi.org/10.1093/rheumatology/ket387

DeLay, M. L., Turner, M. J., Klenk, E. I., Smith, J. A., Sowders, D. P., & Colbert, R. A. (2009). HLA-B27 misfolding and the unfolded protein response augment interleukin-23 production and are associated with Th17 activation in transgenic rats. *Arthritis and Rheumatism*, *60*(9), 2633–2643. https://doi.org/10.1002/art.24763

Deng, J., Yeung, V. P., Tsitoura, D., DeKruyff, R. H., Umetsu, D. T., & Levy, S. (2000). Allergen-induced airway hyperreactivity is diminished in CD81-deficient mice. *Journal of Immunology (Baltimore, Md. : 1950)*, *165*(9), 5054–5061. https://doi.org/10.4049/jimmunol.165.9.5054

Denic, V., Quan, E. M., & Weissman, J. S. (2006). A Luminal Surveillance Complex that Selects Misfolded Glycoproteins for ER-Associated Degradation. *Cell*, *126*(2), 349–359. https://doi.org/10.1016/j.cell.2006.05.045

Deshayes, S., Konate, K., Aldrian, G., Crombez, L., Heitz, F., & Divita, G. (2010). Structural polymorphism of non-covalent peptide-based delivery systems: Highway to cellular uptake. *Biochimica et Biophysica Acta - Biomembranes*, *1798*(12), 2304–2314. https://doi.org/10.1016/j.bbamem.2010.06.005

Dougados, M., Dijkmans, B., Khan, M., Maksymowych, W., van der Linden, S., & Brandt, J. (2002). Conventional treatments for ankylosing spondylitis. *Annals of the Rheumatic Diseases*, *61 Suppl 3*, iii40-50. https://doi.org/10.1136/ard.61.suppl_3.iii40

Dougados, M., Gueguen, A., Nakache, J. P., Velicitat, P., Veys, E. M., Zeidler, H., & Calin, A. (1999). Ankylosing spondylitis: What is the optimum duration of a clinical study? A one year versus a 6 weeks non-steroidal anti-inflammatory drug trial. *Rheumatology*, *38*(3), 235–244. https://doi.org/10.1093/rheumatology/38.3.235

Draz, M. S., Fang, B. A., Zhang, P., Hu, Z., Gu, S., Weng, K. C., … Chen, F. F. (2014). Nanoparticle-mediated systemic delivery of siRNA for treatment of cancers and viral infections. *Theranostics*, *4*(9), 872–892. https://doi.org/10.7150/thno.9404

Dubey, S. G., Leeder, J., & Gaffney, K. (2008). Physical therapy in anti-TNF treated patients with ankylosing spondylitis. *Rheumatology (Oxford, England)*, *47*(7), 1100–1. https://doi.org/10.1093/rheumatology/ken191

Dudley Hart, F., & Robinson, K. C. (1959). Ankylosing spondylitis in women. *Ann. Rheum. Dis.*, *18*(15), 15–23.

Eiríksdóttir, E., Konate, K., Langel, U., Divita, G., & Deshayes, S. (2010). Secondary structure of cell-penetrating peptides controls membrane interaction and insertion. *Biochimica et Biophysica Acta*, *1798*(6), 1119–28. https://doi.org/10.1016/j.bbamem.2010.03.005

Escola, J.-M. J. M., Kleijmeer, M. J., Stoorvogel, W., Griffith, J. M., Yoshie, O., & Geuze, H. J. (1998). Selective enrichment of tetraspan proteins on the internal vesicles of multivesicular endosomes and on exosomes secreted by human B-lymphocytes. *Journal of Biological Chemistry*, *273*(32), 20121–20127. https://doi.org/10.1074/jbc.273.32.20121

Feng, D., Zhao, W.-L., Ye, Y.-Y., Bai, X.-C., Liu, R.-Q., Chang, L.-F., … Sui, S.-F. (2010). Cellular internalization of

exosomes occurs through phagocytosis. *Traffic (Copenhagen, Denmark)*, *11*(5), 675–87. https://doi.org/10.1111/j.1600-0854.2010.01041.x

Fenimore, J., & Young, H. A. (2016). Regulation of Cytokine Gene Expression in Immunity and Diseases, *941*, 1–19. https://doi.org/10.1007/978-94-024-0921-5

Fernández-Messina, L., Gutiérrez-Vázquez, C., Rivas-García, E., Sánchez-Madrid, F., & de la Fuente, H. (2015). Immunomodulatory role of microRNAs transferred by extracellular vesicles. *Biology of the Cell / under the Auspices of the European Cell Biology Organization*, 1–36. https://doi.org/10.1111/boc.201400081

Fert, I., Cagnard, N., Glatigny, S., Letourneur, F., Jacques, S., Smith, J. A., … Breban, M. (2014). Reverse interferon signature is characteristic of antigen-presenting cells in human and rat spondyloarthritis. *Arthritis and Rheumatology*, *66*(4), 841–851. https://doi.org/10.1002/art.38318

Fert, I., Glatigny, S., Poulain, C., Satumtira, N., Dorris, M. L., Taurog, J. D., & Breban, M. (2008). Correlation between dendritic cell functional defect and spondylarthritis phenotypes in HLA-B27/human β2-microglobulin-transgenic rat lines. *Arthritis and Rheumatism*, *58*(11), 3425–3429. https://doi.org/10.1002/art.24023

Fischer, D., Bieber, T., Li, Y., Elsässer, H. P., & Kissel, T. (1999). A novel non-viral vector for DNA delivery based on low molecular weight, branched polyethylenimine: effect of molecular weight on transfection efficiency and cytotoxicity. *Pharmaceutical Research*, *16*(8), 1273–9. Retrieved from http://www.ncbi.nlm.nih.gov/pubmed/10468031

Förger, F., Villiger, P. M., & Ostensen, M. (2009). Pregnancy in patients with ankylosing spondylitis: do regulatory T cells play a role? *Arthritis and Rheumatism*, *61*(2), 279–283. https://doi.org/10.1002/art.24161

Freifelder, D., & Davison, P. F. (1962). Studies on the sonic degradation of deoxyribonucleic acid. *Biophysical Journal*, *2*, 235–247. https://doi.org/10.1016/S0006-3495(62)86852-0

Fuhrmann, G., Serio, A., Mazo, M., Nair, R., & Stevens, M. M. (2014). Active loading into extracellular vesicles significantly improves the cellular uptake and photodynamic effect of porphyrins. *Journal of Controlled Release*, *205*, 35–44. https://doi.org/10.1016/j.jconrel.2014.11.029

Fujii, K., Hurley, J. H., & Freed, E. O. (2007). Beyond Tsg101: the role of Alix in "ESCRTing" HIV-1. *Nature Reviews. Microbiology*, *5*(12), 912–916. https://doi.org/10.1038/nrmicro1790

Fujita, K., Fukuda, M., Endoh, S., Maru, J., Kato, H., Nakamura, A., … Honda, K. (2016). Pulmonary and pleural inflammation after intratracheal instillation of short single-walled and multi-walled carbon nanotubes. *Toxicology Letters*, *257*, 23–37. https://doi.org/10.1016/j.toxlet.2016.05.025

García-Medel, N., Sanz-bravo, A., Alvarez-Navarro, C., Gómez-Molina, P., Barnea, E., Marcilla, M., … López de Castro, J. A. (2014). Peptide Handling by HLA-B27 Subtypes Influences Their Biological Behavior, Association with Ankylosing Spondylitis and Susceptibility to Endoplasmic Reticulum Aminopeptidase 1 (ERAP1). *Molecular & Cellular Proteomics : MCP*, *13*(12), 3367–80. https://doi.org/10.1074/mcp.M114.039214

García-Medel, N., Sanz-Bravo, A., Van Nguyen, D., Galocha, B., Gómez-Molina, P., Martín-Esteban, A., … de Castro, J. a L. (2012). Functional interaction of the ankylosing spondylitis-associated endoplasmic

reticulum aminopeptidase 1 polymorphism and HLA-B27 in vivo. *Molecular & Cellular Proteomics : MCP*, *11*(11), 1416–29. https://doi.org/10.1074/mcp.M112.019588

Gardiner, C., Vizio, D. Di, Sahoo, S., The, C., Witwer, K. W., Wauben, M., & Hill, A. F. (2016). Techniques used for the isolation and characterization of extracellular vesicles: results of a worldwide survey ´, *1*, 1–6. https://doi.org/10.3402/jev.v5.32945

Gardner, R. G., Swarbrick, G. M., Bays, N. W., Cronin, S. R., Wilhovsky, S., Seelig, L., … Hampton, R. Y. (2000). Endoplasmic reticulum degradation requires lumen to cytosol signaling: Transmembrane control of Hrd1p by Hrd3p. *Journal of Cell Biology*, *151*(1), 69–82. https://doi.org/10.1083/jcb.151.1.69

Gauss, R., Jarosch, E., Sommer, T., & Hirsch, C. (2006). A complex of Yos9p and the HRD ligase integrates endoplasmic reticulum quality control into the degradation machinery. *Nature Cell Biology*, *8*(8), 849–54. https://doi.org/10.1038/ncb1445

Giannotti, E., Trainito, S., Arioli, G., Rucco, V., & Masiero, S. (2014). Effects of physical therapy for the management of patients with ankylosing spondylitis in the biological era. *Clinical Rheumatology*. https://doi.org/10.1007/s10067-014-2647-6

Giltay, E. J., Van Schaardenburg, D., Gooren, L. J. G., Popp-Snijders, C., & Dijkmans, B. A. C. (1999). Androgens and ankylosing spondylitis: A role in the pathogenesis? In *Annals of the New York Academy of Sciences* (Vol. 876, pp. 340–365). https://doi.org/10.1111/j.1749-6632.1999.tb07658.x

Godbey, W. T., Wu, K. K., & Mikos, a G. (1999). Size matters: molecular weight affects the efficiency of poly(ethylenimine) as a gene delivery vehicle. *Journal of Biomedical Materials Research*, *45*(3), 268–75. Retrieved from http://www.ncbi.nlm.nih.gov/pubmed/10397985

Goh, L., & Samanta, a. (2009). A systematic MEDLINE analysis of therapeutic approaches in ankylosing spondylitis. *Rheumatology International*, *29*(10), 1123–35. https://doi.org/10.1007/s00296-009-0973-9

Golder, V., & Schachna, L. (2013). Ankylosing spondylitis: an update. *Australian Family Physician*, *42*(11), 780–4. Retrieved from http://www.ncbi.nlm.nih.gov/pubmed/24217097

Gong, C. (1998). Ultrasound induced cavitation and sonochemical yields. *The Journal of the Acoustical Society of America*, *104*, 2675. https://doi.org/10.1121/1.423851

Grassme, H., Jekle, A., Riehle, A., Schwarz, H., Berger, J., Sandhoff, K., … Gulbins, E. (2001). CD95 Signaling via Ceramide-rich Membrane Rafts. *Journal of Biological Chemistry*, *276*(23), 20589–20596. https://doi.org/10.1074/jbc.M101207200

Guiliano, D., North, H., Panayoitou, E., Campbell, E. C., McHugh, K., Cooke, F., … Antoniou, A. N. (2016). Polymorphisms in the F Pocket of HLA-B27 Subtypes Strongly Impact on Assembly, Chaperone Interactions and Heavy Chain Misfolding. *Arthritis & Rheumatology (Hoboken, N.J.)*, 1–26. https://doi.org/10.1002/art.

Gulbins, E., & Kolesnick, R. (2003). Raft ceramide in molecular medicine. *Oncogene*, *22*(45), 7070–7. https://doi.org/10.1038/sj.onc.1207146

Gulyas, K., Bodnar, N., Nagy, Z., Szamosi, S., Horvath, A., Vancsa, A., … Szanto, S. (2014). Real-life experience with switching TNF-α inhibitors in ankylosing spondylitis. *The European Journal of Health Economics : HEPAC : Health Economics in Prevention and Care*. https://doi.org/10.1007/s10198-014-0598-0

Günther, M., Lipka, J., Malek, A., Gutsch, D., Kreyling, W., & Aigner, A. (2011). Polyethylenimines for RNAi-mediated gene targeting in vivo and siRNA delivery to the lung. *European Journal of Pharmaceutics and Biopharmaceutics : Official Journal of Arbeitsgemeinschaft Für Pharmazeutische Verfahrenstechnik e.V*, *77*(3), 438–49. https://doi.org/10.1016/j.ejpb.2010.11.007

Guo, X., & Huang, L. (2013). Recent Advances in Non-viral Vectors for Gene Delivery. *Accounts of Chemical Research*, *45*(7), 971–979. https://doi.org/10.1021/ar200151m.Recent

Gupta, A., Liberati, T. A., Verhulst, S. J., Main, B. J., Roberts, M. H., Potty, A. G. R., … El-Amin Iii, S. F. (2015). Biocompatibility of single-walled carbon nanotube composites for bone regeneration. *Bone & Joint Research*, *4*(5), 70–77. https://doi.org/10.1302/2046-3758.45.2000382

Hacein-Bey-Abina, S., von Kalle, C., Schmidt, M., McCormack, M. P., Wulffraat, N., Leboulch, P., … Cavazzana-Calvo, M. (2004). LMO2-Associated Clonal T Cell Proliferation in Two Patients after Gene Therapy for SCID-X1. *Science*, *302*, 415–419. https://doi.org/10.1126/science.1088547

Halperin, L., Jung, J., & Michalak, M. (2014). The many functions of the endoplasmic reticulum chaperones and folding enzymes. *IUBMB Life*, *66*(5), 318–326. https://doi.org/10.1002/iub.1272

Hammer, R. E., Maika, S. D., Richardson, J. A., Tang, J. P., & Taurog, J. D. (1990). Spontaneous inflammatory disease in transgenic rats expressing HLA-B27 and human β2m: An animal model of HLA-B27-associated human disorders. *Cell*, *63*(5), 1099–1112. https://doi.org/10.1016/0092-8674(90)90512-D

Haney, M. J., Klyachko, N. L., Zhao, Y., Gupta, R., Plotnikova, E. G., He, Z., … Batrakova, E. V. (2015). Exosomes as drug delivery vehicles for Parkinson's disease therapy. *Journal of Controlled Release*, *207*, 18–30. https://doi.org/10.1016/j.jconrel.2015.03.033

Hemler, M. E. (2005). Tetraspanin functions and associated microdomains. *Nature Reviews. Molecular Cell Biology*, *6*(10), 801–11. https://doi.org/10.1038/nrm1736

Henry, D., L-Y rim, L., Garcia Rodriguez, L. A., Perez Gutthann, S., Carson, J. L., Griffin, M., … Espanol de, C. (1996). Variability in risk of gastrointestinal complications with individual non-steroidal anti-inflammatory drugs: results of a collaborative meta-analysis senior lecturer in clinical pharmacology Lynette L-Y Lim, senior lecturer in biostatistics. *Bmj*, *312*, 1563–6. https://doi.org/10.1136/bmj.312.7046.1563

Herzog, R. W., Cao, O., & Srivastava, A. (2010). Two decades of clinical gene therapy--success is finally mounting. *Discovery Medicine*, *9*(45), 105–111. Retrieved from http://www.ncbi.nlm.nih.gov/pubmed/20193635%5Cnhttp://www.pubmedcentral.nih.gov/articlerender.fcgi?artid=PMC3586794

Heusermann, W., Hean, J., Trojer, D., Steib, E., von Bueren, S., Graff-Meyer, A., … Meisner-Kober, N. C. (2016). Exosomes surf on filopodia to enter cells at endocytic hot spots, traffic within endosomes, and are targeted to the ER. *Journal of Cell Biology*, *213*(2), 173–184. https://doi.org/10.1083/jcb.201506084

Hinz, B., & Brune, K. (2002). Cyclooxygenase-2 — 10 Years Later. *Pharmacology and Experimental Therapeutics*, *300*(2), 367–375.

Hiramatsu, N., Chiang, W.-C., Kurt, T. D., Sigurdson, C. J., & Lin, J. H. (2015). Multiple Mechanisms of Unfolded Protein Response-Induced Cell Death. *The American Journal of Pathology*, *185*(7), 1800–8.

https://doi.org/10.1016/j.ajpath.2015.03.009

Hobel, S., & Aigner, A. (2010). PEI/siRNA-Mediated Gene Knockdown In Vitro and In Vivo. In W.-P. Min & T. Ichim (Eds.), *RNA Interference* (Vol. 623, pp. 283–297). Totowa, NJ: Humana Press. https://doi.org/10.1007/978-1-60761-588-0

Höbel, S., Prinz, R., Malek, A., Urban-Klein, B., Sitterberg, J., Bakowsky, U., … Aigner, A. (2008). Polyethylenimine PEI F25-LMW allows the long-term storage of frozen complexes as fully active reagents in siRNA-mediated gene targeting and DNA delivery. *European Journal of Pharmaceutics and Biopharmaceutics : Official Journal of Arbeitsgemeinschaft Für Pharmazeutische Verfahrenstechnik e.V*, *70*(1), 29–41. https://doi.org/10.1016/j.ejpb.2008.03.014

Hoe, E., Anderson, J., Nathanielsz, J., Toh, Z. Q., Marimla, R., Balloch, A., & Licciardi, P. V. (2017). The contrasting role of Th17 immunity in human health and disease. *Microbiology and Immunology*, (February), 1–24. https://doi.org/10.1111/1348-0421.12471

Hood, J. L., Scott, M. J., & Wickline, S. a. (2013). Maximizing exosome colloidal stability following electroporation. *Analytical Biochemistry*, *448C*, 41–49. https://doi.org/10.1016/j.ab.2013.12.001

Horai, R., Sen, H. N., Caspi, R. R., Horai, R., Sen, H. N., & Caspi, R. R. (2017). Commensal microbiota as a potential trigger of autoimmune uveitis. *Expert Review of Clinical Immunology*, *13*(4), 291–293. https://doi.org/10.1080/1744666X.2017.1288098

Hořejši, V., & Vlček, Č. (1991). Novel structurally distinct family of leucocyte surface glycoproteins including CD9, CD37, CD53 and CD63. *FEBS Letters*, *288*(1–2), 1–4. https://doi.org/10.1016/0014-5793(91)80988-F

Hori, O., Ichinoda, F., Yamaguchi, A., Tamatani, T., Taniguchi, M., Koyama, Y., … Ogawa, S. (2004). Role of Herp in the endoplasmic reticulum stress response. *Genes to Cells*, *9*(5), 457–469. https://doi.org/10.1111/j.1356-9597.2004.00735.x

Huang, K.-H., Kuo, K.-L., Chen, S.-C., Weng, T.-I., Chuang, Y.-T., Tsai, Y.-C., … Liu, S.-H. (2012). Down-regulation of glucose-regulated protein (GRP) 78 potentiates cytotoxic effect of celecoxib in human urothelial carcinoma cells. *PloS One*, *7*(3), e33615. https://doi.org/10.1371/journal.pone.0033615

Hurley, J. H. (2008). ESCRT complexes and the biogenesis of multivesicular bodies. *Current Opinion in Cell Biology*, *20*(1), 4–11. https://doi.org/10.1016/j.ceb.2007.12.002

Inoh, Y., Nagai, M., Matsushita, K., Nakanishi, M., & Furuno, T. (2017). Gene transfection efficiency into dendritic cells is influenced by the size of cationic liposomes/DNA complexes. *European Journal of Pharmaceutical Sciences*, *102*, 230–236. https://doi.org/10.1016/j.ejps.2017.03.023

Iwakura, Y., & Ishigame, H. (2006). The IL-23 / IL-17 axis in inflammation. *The Journal of Clinical Investigation*, *116*(5), 1218–1222. https://doi.org/10.1172/JCI25982.8.

Jethwa, H., & Bowness, P. (2016). The interleukin (IL)-23/IL-17 axis in ankylosing spondylitis: New advances and potentials for treatment. *Clinical and Experimental Immunology*, *183*(1), 30–36. https://doi.org/10.1111/cei.12670

Jimenez-Balderas, F. J., Tapia-Serrano, R., Madero-Cervera, J. I., Murrieta, S., & Mintz, G. (1990). Ovarian function studies in active ankylosing spondylitis in women. Clinical response to estrogen therapy. *The Journal of Rheumatology*, *17*(4), 497–502.

Jo, W., Kim, J., Yoon, J., Jeong, D., Cho, S., Jeong, H., … Park, J. (2014). Large-scale generation of cell-derived nanovesicles. *Nanoscale*, *6*(20), 12056–12064. https://doi.org/10.1039/C4NR02391A

Johnsen, K. B., Gudbergsson, J. M., Skov, M. N., Christiansen, G., Gurevich, L., Moos, T., & Duroux, M. (2016). Evaluation of electroporation-induced adverse effects on adipose-derived stem cell exosomes. *Cytotechnology*, *68*(5), 1–14. https://doi.org/10.1007/s10616-016-9952-7

Jolly, C., & Sattentau, Q. J. (2007). Human Immunodeficiency Virus Type 1 Assembly, Budding, and Cell-Cell Spread in T Cells Take Place in Tetraspanin-Enriched Plasma Membrane Domains. *Journal of Virology*, *81*(15), 7873–7884. https://doi.org/10.1128/JVI.01845-06

Jovanovic, D. V, Di Battista, J. A., Martel-Pelletier, J., Jolicoeur, F. C., He, Y., Zhang, M., … Pelletier, J. P. (1998). IL-17 stimulates the production and expression of proinflammatory cytokines, IL-beta and TNF-alpha, by human macrophages. *Journal of Immunology (Baltimore, Md. : 1950)*, *160*(7), 3513–21. Retrieved from http://www.jimmunol.org/content/160/7/3513.full

Kaiser, J. (2009). B-Thalassemia Treatmeant Succeeds, With a Caveat. *Science*, *326*(5959), 1468–1469. https://doi.org/10.2307/27736612

Kaji, K., & Kudo, A. (2004). The mechanism of sperm-oocyte fusion in mammals. *Reproduction*, *127*(4), 423–429. https://doi.org/10.1530/rep.1.00163

Kalra, H., Simpson, R. J., Ji, H., Aikawa, E., Altevogt, P., Askenase, P., … Mathivanan, S. (2012). Vesiclepedia: A Compendium for Extracellular Vesicles with Continuous Community Annotation. *PLoS Biology*, *10*(12), 8–12. https://doi.org/10.1371/journal.pbio.1001450

Kam, N. W. S., O'Connell, M., Wisdom, J. a, & Dai, H. (2005). Carbon nanotubes as multifunctional biological transporters and near-infrared agents for selective cancer cell destruction. *Proceedings of the National Academy of Sciences of the United States of America*, *102*(33), 11600–5. https://doi.org/10.1073/pnas.0502680102

Karapolat, H., Eyigor, S., Zoghi, M., Akkoc, Y., Kirazli, Y., & Keser, G. (2009). Are swimming or aerobic exercise better than conventional exercise in ankylosing spondylitis patients? A randomized controlled study. *European Journal of Physical and Rehabilitation Medicine*, *45*(4), 449–457.

Kataria, R. K., & Brent, L. H. (2004). Spondyloarthropathies. *American Family Physician*, *69*(12), 2853–2860.

Kelić, S., Levy, S., Suarez, C., & Weinstein, D. E. (2001). CD81 Regulates Neuron-Induced Astrocyte Cell-Cycle Exit. *Molecular and Cellular Neuroscience*, *17*(3), 551–560. https://doi.org/10.1006/mcne.2000.0955

Keller, A. A., Mussbach, F., Breitling, R., Hemmerich, P., Schaefer, B., Lorkowski, S., & Reissmann, S. (2013). Relationships between cargo, cell penetrating peptides and cell type for uptake of non-covalent complexes into live cells. *Pharmaceuticals*, *6*(2), 184–203. https://doi.org/10.3390/ph6020184

Kerr, M. C., & Teasdale, R. D. (2009). Defining macropinocytosis. *Traffic*, *10*(4), 364–371. https://doi.org/10.1111/j.1600-0854.2009.00878.x

Khan, M. A. (2013). Polymorphism of HLA-B27: 105 subtypes currently known. *Current Rheumatology Reports*, *15*(10), 362. https://doi.org/10.1007/s11926-013-0362-y

Khare, S. D., Bull, M. J., Hanson, J., Luthra, H. S., & David, C. S. (1998). Spontaneous inflammatory disease in HLA-B27 transgenic mice is independent of MHC class II molecules: a direct role for B27 heavy chains and

not B27-derived peptides. *Journal of Immunology (Baltimore, Md. : 1950)*, *160*(1), 101–6. Retrieved from http://www.jimmunol.org/content/160/1/101.full

Kichler, a, Leborgne, C., Coeytaux, E., & Danos, O. (2001). Polyethylenimine-mediated gene delivery: a mechanistic study. *The Journal of Gene Medicine*, *3*(2), 135–44. https://doi.org/10.1002/jgm.173

Kim, S., Lee, S., Shin, J., Kim, Y., Evnouchidou, I., Kim, D., … Ahn, K. (2011). Human cytomegalovirus microRNA miR-US4-1 inhibits CD8+ T cell responses by targeting the aminopeptidase ERAP1. *Nature Immunology*.

Kim, S., Lee, S., Shin, J., Kim, Y., Evnouchidou, I., Kim, D., … Ahn, K. (2012). Human cytomegalovirus miRNA-US4-1 inhibits CD 8 Tcell response by targeting the aminopeptidase ERAP1. *Nature Immunology*, *12*(10), 984–991. https://doi.org/10.1038/ni.2097.Human

Kirkham, M., & Parton, R. G. (2005). Clathrin-independent endocytosis: New insights into caveolae and non-caveolar lipid raft carriers. *Biochimica et Biophysica Acta - Molecular Cell Research*, *1745*(3), 273–286. https://doi.org/10.1016/j.bbamcr.2005.06.002

Klyachko, N. L., Haney, M. J., Yuling, Z., Manickam, D. S., Mahajan, V., Suresh, P., … Batrakova, E. V. (2012). Macrophages offer a paradigm switch for CNS delivery of therapeutic proteins. *Nanomedicine*, *29*(6), 997–1003. https://doi.org/10.1016/j.biotechadv.2011.08.021.Secreted

Kokame, K., Agarwal, K. L., Kato, H., & Miyata, T. (2000). Herp, a new ubiquitin-like membrane protein induced by endoplasmic reticulum stress. *Journal of Biological Chemistry*, *275*(42), 32846–32853. https://doi.org/10.1074/jbc.M002063200

Konate, K., Crombez, L., Deshayes, S., Decaffmeyer, M., Thomas, A., Brasseur, R., … Divita, G. (2010). Insight into the cellular uptake mechanism of a secondary amphipathic cell-penetrating peptide for siRNA delivery. *Biochemistry*, *49*(16), 3393–3402. https://doi.org/10.1021/bi901791x

Kooijmans, S. a a, Stremersch, S., Braeckmans, K., De Smedt, S. C., Hendrix, A., Wood, M. J. a, … Vader, P. (2013). Electroporation-induced siRNA precipitation obscures the efficiency of siRNA loading into extracellular vesicles. *Journal of Controlled Release : Official Journal of the Controlled Release Society*, *172*(1), 229–38. https://doi.org/10.1016/j.jconrel.2013.08.014

Kostova, Z., Tsai, Y. C., & Weissman, A. M. (2007). Ubiquitin Ligases, Critical Mediators of Endoplasmic Reticulum Associateed Degradation. *Seminars in Cell & Developmental Biology*, *18*(6), 770–779. https://doi.org/10.1016/j.pestbp.2011.02.012.Investigations

Kurosaki, T., Kodama, Y., Muro, T., Higuchi, N., Nakamura, T., Kitahara, T., … Sasaki, H. (2013). Secure splenic delivery of plasmid DNA and its application to DNA vaccine. *Biological & Pharmaceutical Bulletin*, *36*(11), 1800–6. Retrieved from http://www.ncbi.nlm.nih.gov/pubmed/24189423

Lamichhane, T., Raiker, R., & Jay, S. (2015). Exogenous DNA Loading into Extracellular Vesicles via Electroporation is Size-Dependent and Enables Limited Gene Delivery. *Molecular Pharmaceutics*, *12*(10), 3650–3657. https://doi.org/10.1038/nbt.3121.ChIP-nexus

Laroui, H., Geem, D., Xiao, B., Viennois, E., Rakhya, P., Denning, T., & Merlin, D. (2014). Targeting Intestinal Inflammation With CD98 siRNA/PEI–loaded Nanoparticles. *Molecular Therapy*, *22*(1), 69–80. https://doi.org/10.1038/mt.2013.214

Leitman, J., Shenkman, M., Gofman, Y., Shtern, N. O., Ben-Tal, N., Hendershot, L. M., & Lederkremer, G. Z.

(2014). Herp coordinates compartmentalization and recruitment of HRD1 and misfolded proteins for ERAD. *Molecular Biology of the Cell*, *25*(7), 1050–60. https://doi.org/10.1091/mbc.E13-06-0350

Liao, H.-T., Lin, Y.-F., Tsai, C.-Y., & Chou, C.-T. (2015). Regulatory T cells in ankylosing spondylitis and the response after adalimumab treatment. *Joint Bone Spine*, *82*(6), 423–427. https://doi.org/10.1016/j.jbspin.2015.03.003

Lin, H. Y., Lin, S. E., Chien, S. F., & Chern, M. K. (2011). Electroporation for three commonly used yeast strains for two-hybrid screening experiments. *Analytical Biochemistry*, *416*(1), 117–119. https://doi.org/10.1016/j.ab.2011.04.038

Liu, Y., Li, D., Liu, Z., Zhou, Y., Chu, D., Li, X., … Zhang, C.-Y. (2015). Targeted exosome-mediated delivery of opioid receptor Mu siRNA for the treatment of morphine relapse. *Scientific Reports*, *5*(November), 17543. https://doi.org/10.1038/srep17543

López, M., Bollag, R. J., Yu, J. C., Isales, C. M., & Eroglu, A. (2016). Chemically defined and xeno-free cryopreservation of human adipose-derived stem cells. *PLoS ONE*, *11*(3), 1–15. https://doi.org/10.1371/journal.pone.0152161

Lories, R. J. U., Luyten, F. P., & de Vlam, K. (2009). Mechanisms of new bone formation in spondyloarthritis. *Arthritis Research & Therapy*, *11*(2), 221. https://doi.org/10.1186/ar2642

Lőrincz, Á. M., Timár, C. I., Marosvári, K. A., Veres, D. S., Otrokocsi, L., Kittel, Á., & Ligeti, E. (2014). Effect of storage on physical and functional properties of extracellular vesicles derived from neutrophilic granulocytes. *Journal of Extracellular Vesicles*, *3*, 25465. https://doi.org/10.3402/jev.v3.25465\r25465 [pii]

Lottridge, J. M., Flannery, A. R., Vincelli, J. L., & Stevens, T. H. (2006). Vta1p and Vps46p regulate the membrane association and ATPase activity of Vps4p at the yeast multivesicular body. *Proceedings of the National Academy of Sciences of the United States of America*, *103*(16), 6202–7. https://doi.org/10.1073/pnas.0601712103

Lötvall, J., Hill, A. F., Hochberg, F., Buzás, E. I., Di Vizio, D., Gardiner, C., … Théry, C. (2014). Minimal experimental requirements for definition of extracellular vesicles and their functions: a position statement from the International Society for Extracellular Vesicles. *Journal of Extracellular Vesicles*, *3*, 26913. https://doi.org/http://dx.doi.org/10.3402/jev.v3.26913

Lu, Y. P., Zhang, C., Lv, F. X., Bie, X. M., & Lu, Z. X. (2012). Study on the electro-transformation conditions of improving transformation efficiency for Bacillus subtilis. *Letters in Applied Microbiology*, *55*(1), 9–14. https://doi.org/10.1111/j.1472-765X.2012.03249.x

Mains, P. E., Sulston, I. A., & Wood, W. B. (1990). Dominant maternal-effect mutations causing embryonic lethality in Caenorhabditis elegans. *Genetics*, *125*(2), 351–369. https://doi.org/10.1091/mbc.E05

Martín-Esteban, A., Gómez-Molina, P., Sanz-Bravo, A., & López de Castro, J. a. (2013). Combined effects of ankylosing spondylitis-associated ERAP1 polymorphisms outside the catalytic and peptide-binding sites on the processing of natural HLA-B27 ligands. *The Journal of Biological Chemistry*. https://doi.org/10.1074/jbc.M113.529610

Masi, A. T., & Medsger, T. A. J. (1979). A new look at the epidemiology of ankylosing spondylitis and related

syndromes. *Clinical Orthopaedics and Related Research*, (143), 15–29.

Masi, A. T., Nair, K., Andonian, B. J., Prus, K. M., Kelly, J., Sanchez, J. R., & Henderson, J. (2011). Integrative structural biomechanical concepts of ankylosing spondylitis. *Arthritis*, *2011*, 205904. https://doi.org/10.1155/2011/205904

Mathivanan, S., & Simpson, R. J. (2009). ExoCarta: A compendium of exosomal proteins and RNA. *Proteomics*, *9*(21), 4997–5000. https://doi.org/10.1002/pmic.200900351

Maugars, Y., Mathis, C., Berthelot, J. M., Charlier, C., & Prost, a. (1996). Assessment of the efficacy of sacroiliac corticosteroid injections in spondylarthropathies: a double-blind study. *British Journal of Rheumatology*, *35*(8), 767–70. Retrieved from http://www.ncbi.nlm.nih.gov/pubmed/8761190

Mazurov, D., Barbashova, L., & Filatov, A. (2013). Tetraspanin protein CD9 interacts with metalloprotease CD10 and enhances its release via exosomes. *FEBS Journal*, *280*(5), 1200–1213. https://doi.org/10.1111/febs.12110

McGonagle, D., Stockwin, L., & Isaac, J. (2001). An enthesitis based model for the pathogenesis of spondyloarthropathy. *J Rheumatol*, *28*(10), 2155–2159.

McLaughlin, M., Alloza, I., Quoc, H. P., Scott, C. J., Hirabayashi, Y., & Vandenbroeck, K. (2010). Inhibition of secretion of interleukin (IL)-12/IL-23 family cytokines by 4-trifluoromethyl-celecoxib is coupled to degradation via the endoplasmic reticulum stress protein HERP. *Journal of Biological Chemistry*, *285*(10), 6960–6969. https://doi.org/10.1074/jbc.M109.056614

Mear, J. P., Schreiber, K. L., Münz, C., Zhu, X., Stevanović, S., Rammensee, H. G., … Colbert, R. A. (1999). Misfolding of HLA-B27 as a result of its B pocket suggests a novel mechanism for its role in susceptibility to spondyloarthropathies. *J Immunol*, *163*(12), 6665–6670. Retrieved from http://www.ncbi.nlm.nih.gov/pubmed/10586062

Mei, Y., Pan, F., Gao, J., Ge, R., Duan, Z., Zeng, Z., … Ye, D. (2011). Increased serum IL-17 and IL-23 in the patient with ankylosing spondylitis. *Clinical Rheumatology*, *30*(2), 269–73. https://doi.org/10.1007/s10067-010-1647-4

Miossec, P. (2009). IL-17 and Th17 cells in human inflammatory diseases. *Microbes and Infection*, *11*(5), 625–630. https://doi.org/10.1016/j.micinf.2009.04.003

Mittelbrunn, M., Gutiérrez-Vázquez, C., Villarroya-Beltri, C., González, S., Sánchez-Cabo, F., González, M. Á., … Sánchez-Madrid, F. (2011). Unidirectional transfer of microRNA-loaded exosomes from T cells to antigen-presenting cells. *Nature Communications*, *2*, 282. https://doi.org/10.1038/ncomms1285

Mittelbrunn, M., Yáñez-Mó, M., Sancho, D., Ursa, A., & Sánchez-Madrid, F. (2002). Cutting edge: dynamic redistribution of tetraspanin CD81 at the central zone of the immune synapse in both T lymphocytes and APC. *Journal of Immunology (Baltimore, Md. : 1950)*, *169*(12), 6691–6695. https://doi.org/10.4049/jimmunol.169.12.6691

Miyanishi, M., Tada, K., Koike, M., Uchiyama, Y., Kitamura, T., & Nagata, S. (2007). Identification of Tim4 as a phosphatidylserine receptor. *Nature*, *450*(7168), 435–439. https://doi.org/10.1038/nature06307

Miyazaki, T., Müller, U., & Campbell, K. S. (1997). Normal development but differentially altered proliferative responses of lymphocytes in mice lacking CD81. *EMBO Journal*, *16*(14), 4217–4225.

https://doi.org/10.1093/emboj/16.14.4217

Mizuno, E., Kawahata, K., Okamoto, A., Kitamura, N., & Komada, M. (2004). Association with Hrs Stability Is Required for the Early Endosomal Localisation, Stability, and Function of STAM. *Journal of Biochemistry*, *135*, 385–396. https://doi.org/10.1093/jb/mvhO46

Mohr, J. C., De Pablo, J. J., & Palecek, S. P. (2006). Electroporation of human embryonic stem cells: Small and macromolecule loading and DNA transfection. *Biotechnology Progress*, *22*(3), 825–834. https://doi.org/10.1021/bp0600334

Molinari, M., Galli, C., Piccaluga, V., Pieren, M., & Paganetti, P. (2002). Sequential assistance of molecular chaperones and transient formation of covalent complexes during protein degradation from the ER. *Journal of Cell Biology*, *158*(2), 247–257. https://doi.org/10.1083/jcb.200204122

Molinari, M., & Helenius, A. (2000). Chaperone selection during glycoprotein translocation into the endoplasmic reticulum. *Science*, *288*(5464), 331–333. https://doi.org/10.1126/science.288.5464.331

Momen-Heravi, F., Bala, S., Bukong, T., & Szabo, G. (2014). Exosome-mediated delivery of functionally active miRNA-155 inhibitor to macrophages. *Nanomedicine : Nanotechnology, Biology, and Medicine*, 1–11. https://doi.org/10.1016/j.nano.2014.03.014

Moncur, C. (2003). Ankylosing spondylitis measures. *Arthritis & Rheumatism*, *49*(S5), S197–S209. https://doi.org/10.1002/art.11412

Mörck, B., Pullerits, R., Geijer, M., Bremell, T., & Forsblad-D'Elia, H. (2013). Infliximab dose reduction sustains the clinical treatment effect in active HLAB27 positive ankylosing spondylitis: A two-year pilot study. *Mediators of Inflammation*, *2013*. https://doi.org/10.1155/2013/289845

Morelli, A. E., Larregina, A. T., Shufesky, W. J., Sullivan, M. L. G., Stolz, D. B., Papworth, G. D., … Thomson, A. W. (2004). Endocytosis, intracellular sorting, and processing of exosomes by dendritic cells. *Blood*, *104*(10), 3257–3266. https://doi.org/10.1182/blood-2004-03-0824

Morris, M. C., Deshayes, S., Heitz, F., & Divita, G. (2008). Cell-penetrating peptides: from molecular mechanisms to therapeutics. *Biology of the Cell / under the Auspices of the European Cell Biology Organization*, *100*(4), 201–217. https://doi.org/10.1042/BC20070116

Morris, M. C., Vidal, P., Chaloin, L., Heitz, F., & Divita, G. (1997). A new peptide vector for efficient delivery of oligonucleotides into mammalian cells. *Nucleic Acids Research*, *25*(14), 2730–2736. https://doi.org/10.1093/nar/25.14.2730

Mousavi, S. A., Malerød, L., Berg, T., & Kjeken, R. (2004). Clathrin-dependent endocytosis. *The Biochemical Journal*, *377*(Pt 1), 1–16. https://doi.org/10.1042/BJ20031000

Mulcahy, L. A., Pink, R. C., & Carter, D. R. F. (2014). Routes and mechanisms of extracellular vesicle uptake. *Journal of Extracellular Vesicles*, *3*, 1–14. https://doi.org/10.3402/jev.v3.24641

Müller, J., Triebus, J., Kretzschmar, I., Volkmer, R., & Boisguerin, P. (2012). The agony of choice: How to find a suitable CPP for cargo delivery. *Journal of Peptide Science*, *18*(5), 293–301. https://doi.org/10.1002/psc.2396

Munoz, J. L., Bliss, S. a, Greco, S. J., Ramkissoon, S. H., Ligon, K. L., & Rameshwar, P. (2013). Delivery of Functional Anti-miR-9 by Mesenchymal Stem Cell-derived Exosomes to Glioblastoma Multiforme Cells

Conferred Chemosensitivity. *Molecular Therapy. Nucleic Acids*, *2*(April), e126. https://doi.org/10.1038/mtna.2013.60

Mussauer, H., Sukhorukov, V. L., & Zimmermann, U. (2001). Trehalose improves survival of electrotransfected mammalian cells. *Cytometry*, *45*(3), 161–9. Retrieved from http://www.ncbi.nlm.nih.gov/pubmed/11746084

Mussbach, F., Franke, M., Zoch, A., Schaefer, B., & Reissmann, S. (2011). Transduction of peptides and proteins into live cells by cell penetrating peptides. *Journal of Cellular Biochemistry*, *112*(12), 3824–33. https://doi.org/10.1002/jcb.23313

Nakanishi, K. (2016). Anatomy of RISC: how do small RNAs and chaperones activate Argonaute proteins? *Wiley Interdisciplinary Reviews: RNA*. https://doi.org/10.1002/wrna.1356

Nobezawa, D., Ikeda, S. I., Wada, E., Nagano, T., & Miyata, H. (2017). Directional Transport of a Bead Bound to Lamellipodial Surface Is Driven by Actin Polymerization. *BioMed Research International*, *2017*. https://doi.org/10.1155/2017/7804251

Odorizzi, G. (2006). The multiple personalities of Alix. *Journal of Cell Science*, *119*(Pt 15), 3025–3032. https://doi.org/10.1242/jcs.03072

Ohno, S., Takanashi, M., Sudo, K., Ueda, S., Ishikawa, A., Matsuyama, N., … Kuroda, M. (2013). Systemically Injected Exosomes Targeted to EGFR Deliver Antitumor MicroRNA to Breast Cancer Cells. *Molecular Therapy*, *21*(1), 185–191. https://doi.org/10.1038/mt.2012.180

Okuda-Shimizu, Y., & Hendershot, L. (2007). Characterisation of an ERAD pathway for non-glycosylated BiP substrates which requires Herp, *4*(28), 544–554. https://doi.org/10.1016/j.pestbp.2011.02.012.Investigations

Oral, O., Cıkım, T., Zuvin, M., Unal, O., Yagci-Acar, H., Gozuacik, D., & Koşar, A. (2015). Effect of Varying Magnetic Fields on Targeted Gene Delivery of Nucleic Acid-Based Molecules. *Annals of Biomedical Engineering*. https://doi.org/10.1007/s10439-015-1331-6

Ostensen, M., Romberg, O., & Husby, G. (1982). Ankylosing spondylitis and motherhood. *Arthritis & Rheumatism*, *25*(2), 140–143. https://doi.org/10.1002/art.1780250204

Palm-Apergi, C., Lorents, A., Padari, K., Pooga, M., & Hällbrink, M. (2009). The membrane repair response masks membrane disturbances caused by cell-penetrating peptide uptake. *FASEB Journal : Official Publication of the Federation of American Societies for Experimental Biology*, *23*(1), 214–23. https://doi.org/10.1096/fj.08-110254

Pan, Y., Wang, N., Zhou, Z., Liang, H., Pan, C., Zhu, D., … Zen, K. (2016). Circulating human cytomegalovirus-encoded HCMV-miR-US4-1 as an indicator for predicting the efficacy of IFNα treatment in chronic hepatitis B patients. *Scientific Reports*, *6*(February), 23007. https://doi.org/10.1038/srep23007

Papadia, K., Markoutsa, E., & Antimisiaris, S. G. (2016). How do the physicochemical properties of nanoliposomes affect their interactions with the hCMEC / D3 cellular model of the BBB ? *International Journal of Pharmaceutics*, *509*(1–2), 431–438. https://doi.org/10.1016/j.ijpharm.2016.06.019

Parodi, A. J. (2000). Protein Glucosylation and its Role in Protein Folding, 69–93.

Parolini, I., Federici, C., Raggi, C., Lugini, L., Palleschi, S., De Milito, A., … Fais, S. (2009). Microenvironmental pH

is a key factor for exosome traffic in tumor cells. *The Journal of Biological Chemistry*, *284*(49), 34211–22. https://doi.org/10.1074/jbc.M109.041152

Payton, N. M., Wempe, M. F., Xu, Y., & Anchordoquy, T. J. (2014). Long-term storage of lyophilized liposomal formulations. *Journal of Pharmaceutical Sciences*, *103*(12), 3869–3878. https://doi.org/10.1002/jps.24171

Pepys, M., & Hirschfield, G. (2003). C-reative Protein: a critical update. *Journal of Clinical Investigation*, *111*, 1805–1812. https://doi.org/10.1172/JCI200318921.Introduction

Piper, R. C., & Katzmann, D. J. (2007). Biogenesis and Function of Multivesicular Bodies. *Annual Review of Cell and Developmental Biology*, *23*, 519–547. https://doi.org/10.1146/annurev.cellbio.23.090506.123319.Biogenesis

Pols, M. S., & Klumperman, J. (2009). Trafficking and function of the tetraspanin CD63. *Experimental Cell Research*, *315*(9), 1584–92. https://doi.org/10.1016/j.yexcr.2008.09.020

Pospichalova, V., Svoboda, J., Dave, Z., Kotrbova, A., Kaiser, K., Klemova, D., … Bryja, V. (2015). Simplified protocol for flow cytometry analysis of fluorescently labeled exosomes and microvesicles using dedicated flow cytometer. *Journal of Extracellular Vesicles*, *4*, 25530. https://doi.org/10.3402/jev.v4.25530

Poste, G., Bucana, C., Raz, A., Bucana, C., Bugelski, P., Kirsh, R., & Fidler, I. J. (1982). Analysis of the Fate of Systemically Administered Liposomes and Implications for Their Use in Drug Delivery Analysis of the Fate of Systemically Administered Liposomes and Implications for Their Use in Drug Delivery1, *42*(April), 1412–1422.

Pourgholaminejad, A., Aghdami, N., Baharvand, H., & Moazzeni, S. M. (2016). Is TGF b as an anti-inflammatory cytokine required for differentiation of inflammatory TH 17 cells ? *Journal of Immunotoxicology*, *0*(0), 1–9. https://doi.org/10.1080/1547691X.2016.1193574

Provost, P., Dishart, D., Doucet, J., Frendewey, D., Samuelsson, B., & R??dmark, O. (2002). Ribonuclease activity and RNA binding of recombinant human Dicer. *EMBO Journal*, *21*(21), 5864–5874. https://doi.org/10.1093/emboj/cdf578

Puratchikody, A., Sriram, D., Umamaheswari, A., & Irfan, N. (2016). 3-D structural interactions and quantitative structural toxicity studies of tyrosine derivatives intended for safe potent inflammation treatment. *Chemistry Central Journal*, *10*, 24. https://doi.org/10.1186/s13065-016-0169-9

Pyrko, P., Kardosh, A., Liu, Y.-T., Soriano, N., Xiong, W., Chow, R. H., … Schönthal, A. H. (2007). Calcium-activated endoplasmic reticulum stress as a major component of tumor cell death induced by 2,5-dimethyl-celecoxib, a non-coxib analogue of celecoxib. *Molecular Cancer Therapeutics*, *6*(4), 1262–75. https://doi.org/10.1158/1535-7163.MCT-06-0629

Pyrko, P., Kardosh, A., & Schönthal, A. H. (2008). Celecoxib transiently inhibits cellular protein synthesis. *Biochemical Pharmacology*, *75*(2), 395–404. https://doi.org/10.1016/j.bcp.2007.08.029

Raper, S. E., Chirmule, N., Lee, F. S., Wivel, N. A., Bagg, A., Gao, G. P., … Batshaw, M. L. (2003). Fatal systemic inflammatory response syndrome in a ornithine transcarbamylase deficient patient following adenoviral gene transfer. *Molecular Genetics and Metabolism*, *80*(1–2), 148–158.

https://doi.org/10.1016/j.ymgme.2003.08.016

Reeves, E., Elliott, T., James, E., Edwards, C. J., & Edwards, C. J. (2014). ERAP1 in the pathogenesis of ankylosing spondylitis, 257–269. https://doi.org/10.1007/s12026-014-8576-2

Reich, M., van Swieten, P. F., Sommandas, V., Kraus, M., Fischer, R., Weber, E., … Driessen, C. (2007). Endocytosis targets exogenous material selectively to cathepsin S in live human dendritic cells, while cell-penetrating peptides mediate nonselective transport to cysteine cathepsins. *Journal of Leukocyte Biology*, *81*(4), 990–1001. https://doi.org/10.1189/jlb.1006600

Reveille, J. D. (2015). Biomarkers for diagnosis, monitoring of progression, and treatment responses in ankylosing spondylitis and axial spondyloarthritis. *Clinical Rheumatology*. https://doi.org/10.1007/s10067-015-2949-3

Rezvani Amin, Z., Rahimizadeh, M., Eshghi, H., Dehshahri, A., & Ramezani, M. (2013). The effect of cationic charge density change on transfection efficiency of polyethylenimine. *Iranian Journal of Basic Medical Sciences*, *16*(2), 150–6. Retrieved from http://www.pubmedcentral.nih.gov/articlerender.fcgi?artid=3843858&tool=pmcentrez&rendertype=abstract

Robbins, P. D., & Morelli, A. E. (2014). Regulation of Immune Responses by Extracellular Vesicules. *Nature Immunology*, *14*(3), 195–208. https://doi.org/10.1038/nri3622.Regulation

Robinson, P. C., & Brown, M. a. (2014). Genetics of ankylosing spondylitis. *Molecular Immunology*, *57*(1), 2–11. https://doi.org/10.1016/j.molimm.2013.06.013

Romberg, B., Hennink, W. E., & Storm, G. (2008). Sheddable coatings for long-circulating nanoparticles. *Pharmaceutical Research*, *25*(1), 55–71. https://doi.org/10.1007/s11095-007-9348-7

Rossini, M., Viapiana, O., Adami, S., Idolazzi, L., Fracassi, E., & Gatti, D. (2016). Focal bone involvement in inflammatory arthritis: the role of IL17. *Rheumatology International*, *36*(4), 469–482. https://doi.org/10.1007/s00296-015-3387-x

Rudwaleit, M., Listing, J., Brandt, J., Braun, J., & Sieper, J. (2004). Prediction of a major clinical response (BASDAI 50) to tumour necrosis factor alpha blockers in ankylosing spondylitis. *Annals of the Rheumatic Diseases*, *63*(Basdai 50), 665–670. https://doi.org/10.1136/ard.2003.016386

Rudwaleit, M., van der Heijde, D., Khan, M. A., Braun, J., & Sieper, J. (2004). How to diagnose axial spondyloarthritis early. *Annals of the Rheumatic Diseases*, *63*(5), 535–43. https://doi.org/10.1136/ard.2003.011247

Rysnik, O., McHugh, K., van Duivenvoorde, L., van Tok, M., Guggino, G., Taurog, J., … Bowness, P. (2016). Non-conventional forms of HLA-B27 are expressed in spondyloarthritis joints and gut tissue. *Journal of Autoimmunity*, *70*, 12–21. https://doi.org/10.1016/j.jaut.2016.03.009

Saar, K., Lindgren, M., Hansen, M., Eiríksdóttir, E., Jiang, Y., Rosenthal-Aizman, K., … Langel, Ü. (2005). Cell-penetrating peptides: A comparative membrane toxicity study. *Analytical Biochemistry*, *345*(1), 55–65. https://doi.org/10.1016/j.ab.2005.07.033

Sachse, M., Strous, G. J., & Klumperman, J. (2004). ATPase-deficient hVPS4 impairs formation of internal endosomal vesicles and stabilizes bilayered clathrin coats on endosomal vacuoles. *Journal of Cell Science*,

117(Pt 9), 1699–708. https://doi.org/10.1242/jcs.00998

Sadasivan, B., Lehner, P. J., Ortmann, B., Spies, T., & Cresswell, P. (1996). Roles for calreticulin and a novel glycoprotein, tapasin, in the interaction of MHC class I molecules with TAP. *Immunity*, *5*(2), 103–114. https://doi.org/10.1016/S1074-7613(00)80487-2

Salimzadeh, L., Jaberipour, M., Hosseini, A., & Ghaderi, A. (2013). Non-viral transfection methods optimized for gene delivery to a lung cancer cell line. *Avicenna Journal of Medical Biotechnology*, *5*(2), 68–77. Retrieved from http://www.pubmedcentral.nih.gov/articlerender.fcgi?artid=3689559&tool=pmcentrez&rendertype=abstract

Saric, T., Chang, S.-C. C., Hattori, A., York, I. a, Markant, S., Rock, K. L., … Goldberg, A. L. (2002). An IFN-gamma-induced aminopeptidase in the ER, ERAP1, trims precursors to MHC class I-presented peptides. *Nature Immunology*, *3*(12), 1169–76. https://doi.org/10.1038/ni859

Sartorello, R., Budu, A., Bagnaresi, P., Fernandes, C. a H., Sato, P. M., Bueno, V. B., … Garcia, C. R. S. (2010). In vivo uptake of a haem analogue Zn protoporphyrin IX by the human malaria parasite P. falciparum-infected red blood cells. *Cell Biology International*, *34*(8), 859–865. https://doi.org/10.1042/CBI20090427

Saunderson, S. C., Dunn, A. C., Crocker, P. R., & McLellan, A. D. (2014). CD169 mediates the capture of exosomes in spleen and lymph node. *Blood*, *123*(2), 208–216. https://doi.org/10.1182/blood-2013-03-489732

Schäfer, J., Höbel, S., Bakowsky, U., & Aigner, A. (2010). Liposome-polyethylenimine complexes for enhanced DNA and siRNA delivery. *Biomaterials*, *31*(26), 6892–900. https://doi.org/10.1016/j.biomaterials.2010.05.043

Schey, K. L., Luther, J. M., & Rose, K. L. (2016). Proteomics Characterization of Exosome Cargo. *Methods*, 1–21. https://doi.org/10.1126/scisignal.274pe36.Insulin

Schlosstein, L., Terasaki, P. I., Bluestone, R., & Pearson, C. M. (1973). High Association of an HL-A Antigen, W27, with Ankylosing Spondylitis. *New England Journal of Medicine*, *288*(14), 704–706. https://doi.org/10.1056/NEJM197304052881403

Schönthal, A. H. (2006). Antitumor properties of dimethyl-celecoxib, a derivative of celecoxib that does not inhibit cyclooxygenase-2: implications for glioma therapy. *Neurosurgical Focus*, *20*(4), E21. https://doi.org/10.3171/foc.2006.20.4.14

Schönthal, A. H. (2012). Endoplasmic reticulum stress: its role in disease and novel prospects for therapy. *Scientifica*, *2012*, 857516. https://doi.org/10.6064/2012/857516

Schorey, J. S., & Bhatnagar, S. (2008). Exosome Function: From Tumor Immunology to Pathogen Biology. *Traffic*, *9*(6), 871–881. https://doi.org/10.1007/s11103-011-9767-z.Plastid

Schumacher, T. N., Kantesaria, D. V, Heemels, M. T., Ashton-Rickardt, P. G., Shepherd, J. C., Fruh, K., … Ploegh, H. L. (1994). Peptide length and sequence specificity of the mouse TAP1/TAP2 translocator. *The Journal of Experimental Medicine*, *179*(2), 533–40. https://doi.org/10.1084/jem.179.2.533

Scott, A., Chung, H.-Y., Gonciarz-Swiatek, M., Hill, G. C., Whitby, F. G., Gaspar, J., … Sundquist, W. I. (2005).

Structural and mechanistic studies of VPS4 proteins. *The EMBO Journal*, *24*(20), 3658–3669. https://doi.org/10.1038/sj.emboj.7600818

Seedher, N., & Bhatia, S. (2006). Reversible binding of celecoxib and valdecoxib with human serum albumin using fluorescence spectroscopic technique. *Pharmacological Research*, *54*(2), 77–84. https://doi.org/10.1016/j.phrs.2006.02.008

Segura, E., Guerin, C., Hogg, N., Amigorena, S., & Thery, C. (2007). CD8+ Dendritic Cells Use LFA-1 to Capture MHC-Peptide Complexes from Exosomes In Vivo. *The Journal of Immunology*, *179*(3), 1489–1496. https://doi.org/10.4049/jimmunol.179.3.1489

Shahabipour, F., Barati, N., Johnston, T. P., Derosa, G., Maffioli, P., & Sahebkar, A. (2017). Exosomes: Nanoparticulate Tools for RNA Interference and Drug Delivery. *Journal of Cellular Physiology*, (January), 1660–1668. https://doi.org/10.1002/jcp.25766

Shao, Y., Qi, Y., Huang, Y., Liu, Z., Ma, Y., Guo, X., … Ruan, Q. (2016). Human cytomegalovirus-encoded miR-US4-1 promotes cell apoptosis and benefits discharge of infectious virus particles by targeting QARS. *Journal of Biosciences*, *41*(2), 183–192. https://doi.org/10.1007/s12038-016-9605-1

Sharma, V., Yusuf, M., & Pathak, K. (2014). Nanovesicles for transdermal delivery of felodipine: Development, characterization, and pharmacokinetics. *International Journal of Pharmaceutical Investigation*, *4*(3), 119. https://doi.org/10.4103/2230-973X.138342

Shen, H., Goodall, J. C., & Hill Gaston, J. S. (2009). Frequency and phenotype of peripheral blood Th17 cells in ankylosing spondylitis and rheumatoid arthritis. *Arthritis and Rheumatism*, *60*(6), 1647–56. https://doi.org/10.1002/art.24568

Shtam, T. A., Kovalev, R. A., Varfolomeeva, E. Y., Makarov, E. M., Kil, Y. V, & Filatov, M. V. (2013). Exosomes are natural carriers of exogenous siRNA to human cells in vitro. *Cell Communication and Signaling : CCS*, *11*, 88. https://doi.org/10.1186/1478-811X-11-88

Sieper, J., Rudwaleit, M., Baraliakos, X., Brandt, J., Braun, J., Burgos-Vargas, R., … van der Heijde, D. (2009). The Assessment of SpondyloArthritis international Society (ASAS) handbook: a guide to assess spondyloarthritis. *Annals of the Rheumatic Diseases*, *68 Suppl 2*(May), ii1-44. https://doi.org/10.1136/ard.2008.104018

Sieper, J., van der Heijde, D., Dougados, M., Brown, L. S., Lavie, F., & Pangan, A. L. (2012). Early response to adalimumab predicts long-term remission through 5 years of treatment in patients with ankylosing spondylitis. *Annals of the Rheumatic Diseases*, *71*(5), 700–6. https://doi.org/10.1136/annrheumdis-2011-200358

Simeoni, F., Morris, M. C., Heitz, F., & Divita, G. (2003). Insight into the mechanism of the peptide-based gene delivery system MPG: Implications for delivery of siRNA into mammalian cells. *Nucleic Acids Research*, *31*(11), 2717–2724. https://doi.org/10.1093/nar/gkg385

Simons, K., & Ehehalt, R. (2002). Cholesterol, lipid rafts, and disease. *Journal of Clinical Investigation*, *110*(5), 597–603. https://doi.org/10.1172/JCI200216390

Simonsen, J. B. (2015). A liposomal-based size calibration method for measuring microvesicles by flow cytometry. *Journal of Thrombosis and Haemostasis*, (October 2015), n/a-n/a.

https://doi.org/10.1111/jth.13176

Singh, N., Jenkins, G. J. S. S., Asadi, R., & Doak, S. H. (2010). Potential toxicity of superparamagnetic iron oxide nanoparticles (SPION). *Nano Reviews*, *1*(0), 1–15. https://doi.org/10.3402/nano.v1i0.5358

Slagsvold, T., Aasland, R., Hirano, S., Bache, K. G., Raiborg, C., Trambaiolo, D., … Stenmark, H. (2005). Eap45 in mammalian ESCRT-II binds ubiquitin via a phosphoinositide- interacting GLUE domain. *Journal of Biological Chemistry*, *280*(20), 19600–19606. https://doi.org/10.1074/jbc.M501510200

Smith, J. A., Märker-Hermann, E., & Colbert, R. A. (2006). Pathogenesis of ankylosing spondylitis: Current concepts. *Best Practice and Research: Clinical Rheumatology*, *20*(3), 571–591. https://doi.org/10.1016/j.berh.2006.03.001

So, S., & Lodge, T. P. (2016). Size Control and Fractionation of Ionic Liquid Filled Polymersomes with Glassy and Rubbery Bilayer Membranes. *Langmuir*, *32*(19), 4959–4968. https://doi.org/10.1021/acs.langmuir.6b00946

Sobolewski, C., Rhim, J., Legrand, N., Muller, F., Cerella, C., Mack, F., … Diederich, M. (2015). 2 , 5-Dimethyl-Celecoxib Inhibits Cell Cycle Progression and Induces Apoptosis in Human Leukemia Cells s, 308–328.

Soema, P. C., Willems, G.-J., Jiskoot, W., Amorij, J.-P., & Kersten, G. F. (2015). Predicting the influence of liposomal lipid composition on liposome size, zeta potential and liposome-induced dendritic cell maturation using a design of experiments approach. *European Journal of Pharmaceutics and Biopharmaceutics : Official Journal of Arbeitsgemeinschaft Für Pharmazeutische Verfahrenstechnik e.V*, *94*, 427–35. https://doi.org/10.1016/j.ejpb.2015.06.026

Southerst, D., Dufton, J., & Stern, P. (2012). Multiple Myeloma presenting as sacroiliac joint pain: a case report. *The Journal of the Canadian Chiropractic Association*, *56*(2), 94–101. Retrieved from http://www.pubmedcentral.nih.gov/articlerender.fcgi?artid=3364058&tool=pmcentrez&rendertype=abstract

Steinbach, J. M., Seo, Y.-E., & Saltzman, W. M. (2016). Cell penetrating peptide-modified poly(lactic-co-glycolic acid) nanoparticles with enhanced cell internalization. *Acta Biomaterialia*, *30*, 49–61. https://doi.org/10.1016/j.actbio.2015.11.029

Stoll, M. L. (2011). Interactions of the innate and adaptive arms of the immune system in the pathogenesis of spondyloarthritis. *Clinical and Experimental Rheumatology*, *29*(2), 322–330. https://doi.org/10.1038/jid.2014.371

Stremersch, S., Brans, T., Braeckmans, K., De Smedt, S., & Raemdonck, K. (2017). Nucleic acid loading and fluorescent labeling of isolated extracellular vesicles requires adequate purification. *International Journal of Pharmaceutics*, (April), 0–1. https://doi.org/10.1016/j.ijpharm.2017.10.022

Stuchell, M. D., Garrus, J. E., Müller, B., Stray, K. M., Ghaffarian, S., McKinnon, R., … Sundquist, W. I. (2004). The human endosomal sorting complex required for transport (ESCRT-I) and its role in HIV-1 budding. *Journal of Biological Chemistry*, *279*(34), 36059–36071. https://doi.org/10.1074/jbc.M405226200

Su, M.-J., Aldawsari, H., & Amiji, M. (2016). Pancreatic Cancer Cell Exosome-Mediated Macrophage Reprogramming and the Role of MicroRNAs 155 and 125b2 Transfection using Nanoparticle Delivery Systems. *Scientific Reports*, *6*(July), 30110. https://doi.org/10.1038/srep30110

Sun, Z., Liu, Z., Meng, J., Meng, J., Duan, J., Xie, S., … Yang, X. Da. (2011). Carbon nanotubes enhance cytotoxicity mediated by human lymphocytes in vitro. *PLoS ONE*, *6*(6), 0–7. https://doi.org/10.1371/journal.pone.0021073

Szanto, S., Aleksza, M., Mihaly, E., Lakos, G., Szabo, Z., Vegvari, A., … Szekanecz, Z. (2008). Intracytoplasmic cytokine expression and T cell subset distribution in the peripheral blood of patients with ankylosing spondylitis. *The Journal of Rheumatology*, *35*(12), 2372–2375. https://doi.org/10.3899/jrheum.070839

Szebeni, J., Muggia, F., Gabizon, A., & Barenholz, Y. (2011). Activation of complement by therapeutic liposomes and other lipid excipient-based therapeutic products: Prediction and prevention. *Advanced Drug Delivery Reviews*, *63*(12), 1020–1030. https://doi.org/10.1016/j.addr.2011.06.017

Thompson, P. A., Ashbeck, E. L., Roe, D. J., Fales, L., Buckmeier, J., Wang, F., … Lance, P. (2016). Celecoxib for the Prevention of Colorectal Adenomas: Results of a Suspended Randomized Controlled Trial. *Journal of the National Cancer Institute*, *108*(12), 1–11. https://doi.org/10.1093/jnci/djw151

Todeschini, A. R., & Hakomori, S. (2008). Functional role of glycosphingolipids and gangliosides in control of cell adhesion, motility, and growth, through glycosynaptic microdomains. *Biochimica et Biophysica Acta*, *1780*(3), 421–433. https://doi.org/10.1007/s11103-011-9767-z.Plastid

Toyokuni, S. (1996). Iron-induced carcinogenesis: The role of redox regulation. *Free Radical Biology and Medicine*, *20*(4), 553–566. https://doi.org/10.1016/0891-5849(95)02111-6

Tran, T. M., Satumtira, N., Dorris, M. L., May, E., Wang, A., Furuta, E., & Taurog, J. D. (2004). HLA-B27 in transgenic rats forms disulfide-linked heavy chain oligomers and multimers that bind to the chaperone BiP. *Journal of Immunology (Baltimore, Md. : 1950)*, *172*(8), 5110–9. Retrieved from http://www.ncbi.nlm.nih.gov/pubmed/15067095

Turkcapar, N., Toruner, M., Soykan, I., Aydintug, O. T., Cetinkaya, H., Duzgun, N., … Duman, M. (2006). The prevalence of extraintestinal manifestations and HLA association in patients with inflammatory bowel disease. *Rheumatology International*, *26*(7), 663–668. https://doi.org/10.1007/s00296-005-0044-9

Turner, M. J., Sowders, D. P., DeLay, M. L., Mohapatra, R., Bai, S., Smith, J. A., … Colbert, R. A. (2005). HLA-B27 misfolding in transgenic rats is associated with activation of the unfolded protein response. *J Immunol*, *175*(4), 2438–2448. https://doi.org/175/4/2438 [pii]

Urbano, P. C., Soccol, V. T., Teixeira, V. N., Oliveira, P. G., Filippin, L. I., Bonat, W. H., … Azevedo, V. F. (2015). Effect of pegylated phosphatidylserine-containing liposomes in experimental chronic arthritis. *BMC Pharmacology & Toxicology*, *16*(1), 24. https://doi.org/10.1186/s40360-015-0022-0

Van der Meel, R., Fens, M. H. a M., Vader, P., van Solinge, W. W., Eniola-Adefeso, O., & Schiffelers, R. M. (2014). Extracellular vesicles as drug delivery systems: lessons from the liposome field. *Journal of Controlled Release : Official Journal of the Controlled Release Society*. https://doi.org/10.1016/j.jconrel.2014.07.049

Van der Pol, E., Coumans, F. A. W., Grootemaat, A. E., Gardiner, C., Sargent, I. L., Harrison, P., … Nieuwland, R. (2014). Particle size distribution of exosomes and microvesicles determined by transmission electron microscopy, flow cytometry, nanoparticle tracking analysis, and resistive pulse sensing. *Journal of Thrombosis and Haemostasis*, *12*(7), 1182–1192. https://doi.org/10.1111/jth.12602

Van Der Pol, E., Van Gemert, M. J. C., Sturk, A., Nieuwland, R., & Van Leeuwen, T. G. (2012). Single vs. swarm detection of microparticles and exosomes by flow cytometry. *Journal of Thrombosis and Haemostasis*, *10*(5), 919–930. https://doi.org/10.1111/j.1538-7836.2012.04683.x

van der Vlist, E. J., Nolte-'t Hoen, E. N. M., Stoorvogel, W., Arkesteijn, G. J. a, & Wauben, M. H. M. (2012). Fluorescent labeling of nano-sized vesicles released by cells and subsequent quantitative and qualitative analysis by high-resolution flow cytometry. *Nature Protocols*, *7*(7), 1311–26. https://doi.org/10.1038/nprot.2012.065

Van Dommelen, S. M., Vader, P., Lakhal, S., Kooijmans, S. a a, van Solinge, W. W., Wood, M. J. a, & Schiffelers, R. M. (2012). Microvesicles and exosomes: opportunities for cell-derived membrane vesicles in drug delivery. *Journal of Controlled Release : Official Journal of the Controlled Release Society*, *161*(2), 635–44. https://doi.org/10.1016/j.jconrel.2011.11.021

Vassilakos, A., Cohen-doyle, M. F., Peterson, P. A., Jackson, M. R., & Williams, D. B. (1996). The molecular chaperone calnexin facilitates folding and assembly of class I histocompatibility molecules. *Embo J*, *15*(7), 1495–506. Retrieved from http://www.pubmedcentral.nih.gov/articlerender.fcgi?artid=450057&tool=pmcentrez&rendertype=abstract

Villarroya-Beltri, C., Gutiérrez-Vázquez, C., Sánchez-Cabo, F., Pérez-Hernández, D., Vázquez, J., Martin-Cofreces, N., … Sánchez-Madrid, F. (2013). Sumoylated hnRNPA2B1 controls the sorting of miRNAs into exosomes through binding to specific motifs. *Nature Communications*, *4*, 2980. https://doi.org/10.1038/ncomms3980

Vlassov, A. V., Magdaleno, S., Setterquist, R., & Conrad, R. (2012). Exosomes: Current knowledge of their composition, biological functions, and diagnostic and therapeutic potentials. *Biochimica et Biophysica Acta - General Subjects*, *1820*(7), 940–948. https://doi.org/10.1016/j.bbagen.2012.03.017

Volpe, E., Servant, N., Zollinger, R., Bogiatzi, S. I., Hupé, P., Barillot, E., & Soumelis, V. (2008). A critical function for transforming growth factor-beta, interleukin 23 and proinflammatory cytokines in driving and modulating human T(H)-17 responses. *Nature Immunology*, *9*(6), 650–7. https://doi.org/10.1038/ni.1613

Wahajuddin, & Arora, S. (2012). Superparamagnetic iron oxide nanoparticles: Magnetic nanoplatforms as drug carriers. *International Journal of Nanomedicine*, *7*, 3445–3471. https://doi.org/10.2147/IJN.S30320

Wanders, A., Heijde, D. Van Der, Landewé, R., Béhier, J.-M., Calin, A., Olivieri, I., … Dougados, M. (2005). Nonsteroidal antiinflammatory drugs reduce radiographic progression in patients with ankylosing spondylitis: a randomized clinical trial. *Arthritis and Rheumatism*, *52*(6), 1756–1765. https://doi.org/10.1002/art.21054

Wang, Y., Li, Y.-P., Paulson, C., Shao, J.-Z., Zhang, X., Wu, M., & Chen, W. (2014). Wnt and the Wnt signaling pathway in bone development and disease. *Front Biosci*, *19*, 379–407. https://doi.org/10.1016/j.immuni.2010.12.017.Two-stage

Ward, M. M., & Kuzis, S. (2002). Medication toxicity among patients with ankylosing spondylitis. *Arthritis and Rheumatism*, *47*(3), 234–41. https://doi.org/10.1002/art.10399

Warner, T. D., Giuliano, F., Vojnovic, I., Bukasa, A., Mitchell, J. A., & Vane, J. R. (1999). Nonsteroid drug

selectivities for cyclo-oxygenase-1 rather than cyclo-oxygenase-2 are associated with human gastrointestinal toxicity: a full in vitro analysis. *Proceedings of the National Academy of Sciences of the United States of America*, *96*(13), 7563–8. https://doi.org/10.1073/pnas.96.13.7563

Widder, K. J., Senyei, A. E., & Ranney, D. F. (1979). Magnetically Responsive Microspheres and Other Carriers for the Biophysical Targeting of Antitumor Agents. *Advances in Pharmacology*, *16*(C), 213–271. https://doi.org/10.1016/S1054-3589(08)60246-X

Williams, R. L., & Urbé, S. (2007). The emerging shape of the ESCRT machinery. *Nature Reviews. Molecular Cell Biology*, *8*(5), 355–68. https://doi.org/10.1038/nrm2162

Wilson, N. J., Boniface, K., Chan, J. R., McKenzie, B. S., Blumenschein, W. M., Mattson, J. D., … de Waal Malefyt, R. (2007). Development, cytokine profile and function of human interleukin 17-producing helper T cells. *Nature Immunology*, *8*(9), 950–957. https://doi.org/10.1038/ni1497

Wong-Baeza, I., Ridley, A., Shaw, J., Hatano, H., Rysnik, O., McHugh, K., … Kollnberger, S. (2013). KIR3DL2 binds to HLA-B27 dimers and free H chains more strongly than other HLA class I and promotes the expansion of T cells in ankylosing spondylitis. *Journal of Immunology (Baltimore, Md. : 1950)*, *190*(7), 3216–24. https://doi.org/10.4049/jimmunol.1202926

WTCCC, & TASC. (2007). Association scan of 14,500 nsSNPs in four common diseases identifies variants involved in autoimmunity. *Nature Genetics*, *39*(11), 1329–1337. https://doi.org/10.1038/ng.2007.17.Association

Wu, X., Tan, Y., Mao, H., & Zhang, M. (2010). Toxic effects of iron oxide nanoparticles on human umbilical vein endothelial cells. *International Journal of Nanomedicine*, *5*(1), 385–399.

Xiao, R., Wilkinson, B., Solovyov, A., Winther, J. R., Holmgren, A., Lundström-Ljung, J., & Gilbert, H. F. (2004). The contributions of protein bisulfide isomerase and its homologues to oxidative protein folding in the yeast endoplasmic reticulum. *Journal of Biological Chemistry*, *279*(48), 49780–49786. https://doi.org/10.1074/jbc.M409210200

Yousaf, N., Low, W. Y., Onipinla, A., Mein, C., Caulfield, M., Munroe, P. B., & Chernajovsky, Y. (2015). Differences between disease-associated endoplasmic reticulum aminopeptidase 1 (ERAP1) isoforms in cellular expression, interactions with tumour necrosis factor receptor 1 (TNF-R1) and regulation by cytokines. *Clinical and Experimental Immunology*, *180*(2), 289–304. https://doi.org/10.1111/cei.12575

Yuana, Y., Jiang, L., Lammertink, B. H. A., Vader, P., Deckers, R., Bos, C., … Moonen, C. T. (2017). Microbubbles-assisted ultrasound triggers the release of extracellular vesicles. *International Journal of Molecular Sciences*, *18*(8). https://doi.org/10.3390/ijms18081610

Zambrano-Zaragoza, J. F., Agraz-Cibrian, J. M., González-Reyes, C., Durán-Avelar, M. D. J., & Vibanco-Pérez, N. (2013). Ankylosing spondylitis: from cells to genes. *International Journal of Inflammation*, *2013*, 501653. https://doi.org/10.1155/2013/501653

Zeeshan, H., Lee, G., Kim, H.-R., & Chae, H.-J. (2016). Endoplasmic Reticulum Stress and Associated ROS. *International Journal of Molecular Sciences*, *17*(3), 327. https://doi.org/10.3390/ijms17030327

Zeineddine, D., Papadimou, E., Chebli, K., Gineste, M., Liu, J., Grey, C., … Pucéat, M. (2006). Oct-3/4 Dose Dependently Regulates Specification of Embryonic Stem Cells toward a Cardiac Lineage and Early Heart

Development. *Developmental Cell*, *11*(4), 535–546. https://doi.org/10.1016/j.devcel.2006.07.013

Zeng, Y., Yi, R., & Cullen, B. R. (2005). Recognition and cleavage of primary microRNA precursors by the nuclear processing enzyme Drosha. *The EMBO Journal*, *24*(1), 138–48. https://doi.org/10.1038/sj.emboj.7600491

Zhang, Z., Yang, X., Zhang, Y., Zeng, B., Wang, S., Zhu, T., … Yang, R. (2006). Delivery of telomerase reverse transcriptase small interfering RNA in complex with positively charged single-walled carbon nanotubes suppresses tumor growth. *Clinical Cancer Research*, *12*(16), 4933–4939. https://doi.org/10.1158/1078-0432.CCR-05-2831

Zhao, Y., Haney, M. J., Gupta, R., Bohnsack, J. P., He, Z., Kabanov, A. V., & Batrakova, E. V. (2014). GDNF-Transfected Macrophages Produce Potent Neuroprotective Effects in Parkinson's Disease Mouse Model. *PLoS ONE*, *9*(9), e106867. https://doi.org/10.1371/journal.pone.0106867

Zhou, R., Horai, R., Mattapallil, M., & Caspi, R. R. (2011). A new look at immune privilege of the eye: dual role for the vision-related molecule, retinoic acid. *J Immunol*, *187*(15), 4170–4177. https://doi.org/10.1038/jid.2014.371